Influence of BMP signaling on neural crest cells during heart outflow tract septation

Jean-François Darrigrand

Thèse de doctorat de Sorbonne Université

Ecole doctorale Complexité du Vivant, ED 515
Spécialité: Biologie du développement

Présentée et soutenue publiquement au Centre de Recherche en Myologie
le 18 Mars 2019, par Jean-François Darrigrand
Pour obtenir le grade de docteur de Sorbonne Université

Influence of BMP signaling on neural crest cells during heart outflow tract septation

---

Devant un jury composé de:

- Stéphane ZAFFRAN	Rapporteur
- Luc PARDANAUD	Rapporteur
- Onnik AGBULUT	Examinateur
- Sigolène MEILHAC	Examinatrice
- Sophie CREUZET	Examinatrice
- Vanessa RIBES	Invitée
- Bruno CADOT	Directeur de thèse

Contents

Table of Figures 6

Résumé 8

I. INTRODUCTION 15

Foreword 16

I.1 Evolution and early development of the cardiovascular system 17

I.1.1 How and why did the cardiovascular system evolve? 17

Evolutionary origin and diversity of cardiovascular systems 17

The chambered heart is composed of complementary segments 19

The cardiovascular evolution was influenced by homeothermy and terrestrial life conditions 19

I.1.2 The emergence of cardiovascular progenitors during gastrulation 21

Cardiogenic progenitors specification at early embryonic stages 21

Formation of a cardiogenic field in the mesoderm: the cardiac crescent 23

I.1.3 Formation and morphogenesis of the heart tube 25

Chambered heart emergence requires heart tube elongation and looping 25

Early evidences of a second cardiogenic field adding to the primary linear heart tube 25

Specification and deployment of the second heart field 26

Regionalization of the heart and segregation of the heart field lineages 28

Heterogeneity in the second heart field enables asymmetry appearance in the heart structure 29

Clonal relation of the second heart field with the facial skeletal muscle 31

Regulatory signals tuning SHF deployment and interaction with the neural crest cells and other pharyngeal progenitors 32

I.2 Neural Crest Cells origin, specification and contribution to heart development 33
I.2.1 NCCs specification and migration along the rostrocaudal axis of the embryo..... 33
NCCs emergence and specification 33
Neural crest cells epithelial-to-mesenchymal transition (EMT) and migration 35
NCCs axial diversity..... 36
Fate restriction along the anteroposterior axis..... 37
A complex GRN sequence underlies the differential axial fates of NCCs..... 38
Timing of emigration and migratory behaviors..... 40
Regulatory interactions and molecular control during NCCs migration 41
Cell-Cell interactions and signaling on the way to the homing niche 42
I.2.2 The evolution of the vertebrate circulatory system is linked to NCCs 43
The cardiac NCCs evolution..... 43
The cardiac NCCs discovery..... 45
The cardiac NCCs path to outflow tract septation 47
A complex dialogue exist between cardiac NCCs and the other cell-types composing the outflow tract..... 48
I.2.3 NCCs dialogue with the outflow environment drives OFT septation and valve formation..... 49
NCCs and SHF deployment are regulated by paracrine and autocrine signals 49
NCCs remodelling of the OFT 54
Regulation of Sema3c expression in NCCs and NCCs differentiation in smooth muscle..... 55
NCCs contribution to arterial valve development..... 56
Regulatory pathways controlling heart valve development 57
Heterogeneity of the cardiac NCCs and function in valve formation 57
Cardiac NCCs differentiation in vascular smooth muscle 58
I.2.4 Many human heart malformations present arterial pole defects linked to NCCs dysfunction..... 59
Human arterial pole malformations..... 59
Human syndromes likely involving NCCs function defects 61

I.3 Role and mechanism of BMP signaling, a master regulator of gene expression, cell specification and morphogenesis 64

I.3.1 BMP signaling, an evolutionary innovation serving multicellular organization 64

I.3.2 Protein phosphatases, and specifically the phosphatase called Dullard, play a fundamental regulatory role in BMP signaling 66

Activation of BMP signaling 67

Non-canonical BMP signaling 68

Regulation of the Smad signaling cycle in canonical BMP signaling 68

Pattern of Smad binding to the genome 70

Phosphatases regulatory function in the BMP pathway 70

Phosphatases act on BMP receptors to modulate R-Smad activity 72

Dullard regulatory function in Xenopus, Drosophila and Mice 73

I.3.3 The spatiotemporal control of BMP signaling during embryonic development 74

The competence of receiving cells determines the signaling output 75

The regionalisation and specification of cells is ruled by morphogen gradients 75

Complex gene regulatory networks integrate signaling inputs 78

II. MATERIALS & METHODS 80

Cell culture and transfection 81

Mouse strains 81

Immunohistochemistry 81

2D imaging, analysis and quantification 83

3D imaging and image analysis 83

In situ hybridisation 83

Tissue dissociation and FACS sorting 84

Single-Cell gene expression 84

Bioinformatic analysis 85

Statistical analysis 85

III. RESULTS 88

Aim of the project 89

III.1 Effect of Dullard on BMP signaling activity 90

III.1.1 In vitro experiments confirm the regulatory function of Dullard on BMP signaling 90

III.1.2 Cre-Lox recombination efficiently suppress Dullard expression in neural crest cells (NCCs) 91

III.1.3 Increase in NCCs graded response to BMP signals upon *Dullard* deletion 93

III.2 Phenotypic impact of BMP signaling overactivation in cardiac NCCs 95

III.2.1 Mutant NCCs do not present defects of migration, survival or proliferation in the developping OFT 96

III.2.2 Dullard deletion in the NCCs causes malformation of the great arteries and embryonic death 99

III.3 Attempt of phenotypic rescue of *Dullard* mutants using a BMP signaling inhibiting drug . 102

III.4 Single cell transcriptomic analysis of OFT progenitors 104

III.4.1 Validation of the single-cell transcriptional analysis 104

III.4.2 *Dullard* regulates NCCs mesenchymal state and Sema3c expression 105

III.5 Impact of BMP signaling overactivation on NCCs behavior and myocardial progenitors differentiation 109

III.5.1 *Sema3c* overexpression is associated with increased NCCs condensation to the endocardium 109

III.5.2 Overactivation of BMP signaling in NCCs induces asymmetrical differentiation of the distal subpulmonary myocardium 112

IV. DISCUSSION 115

References 126

Table of Figures

Introduction

Figure 1 – Evolution of heart structures 18
Figure 2 – Temporal and morphological representation of the heart fields and during the heart tube formation process 24
Figure 3 – Regionalization of the heart and identification of diverse cardiogenic lineages 27
Figure 4 – Early steps of cardiovascular progenitor specification and lineage commitment during mouse development 29
Figure 5 – Induction, specification and delamination of the NCCs 34
Figure 6 – NCCs heterogeneity along the anteroposterior axis 37
Figure 7 – Cranial-specific gene regulatory network provides ectomesenchymal potential 39
Figure 8 – Mechanisms driving the collective migration of NCCs 43
Figure 9 – Cardiac NCCs path to outflow tract (OFT) septation 46
Figure 10 – Development and myocardialization of the OFT 49
Figure 11- Regulation of SHF deployment in the OFT 52
Figure 12 – Heterogeneity of the SHF at the arterial pole of the heart. 54
Figure 13- Ventral schematic view of the arterial tree formation 59
Figure 14 – A variety of malformations can affect the arterial pole of the heart in humans. 60
Figure 15 - Structural features of the TGFβ-Smad signaling pathway.. 65
Figure 16 - Different types of determinants impact the transcriptional response of cells to TGFβ signals.. 66
Figure 17 – Structure and function of the domains of R-Smads. 69
Figure 18 – Regulatory functions of protein phosphatases on BMP signaling transduction and duration 71
Figure 19 – Degree of conservation of the Dullard phosphatase 72
Figure 20 - Establishment of morphogens gradients 76
Figure 21 – Negative feddback loops induce the adaptation of the receiving cell to the morphogen signals. 77
Figure 22 – Two types of interactions are combined in gene regulatory networks: the feed-forward and the cross-repressions motifs 79

Results

Figure 23 – Dullard inhibits the BMP-mediated phosphorylation of Smad1,5,8 *in vitro*. 91
Figure 24 - Pattern of recombination driven by *Pax3* or *Wnt1* loci in the heart OFT 92
Figure 25 - Level of expression of *Dullard* in the progenitors composing control and mutant OFT 93
Figure 26 - Dullard regulates the cardiac NCCs response to myocardial BMP signals. A. Schematic view of OFT septation with the different stages of NCCs ingression 95
Figure 27- Imaging of the NCCs colonization in the heart OFT at E11.5-E12 97

Figure 28- Quantification of the cardiac NCCs (NCCs) number, proliferation and apoptosis. 98
Figure 29- Quantification of mutant embryos recovered alive along the gestation period. 100
Figure 30 – Measurement of the OFT transversal area. 100
Figure 31 – Dullard deletion in neural crest cells causes asymmetric and premature OFT septation 101
Figure 32 – Analysis of the BMP signaling activity in NCCs of LDN treated and non-treated embryos, and the resulting OFT phenotype 103
Figure 33 - Single cell transcriptional analysis of OFT progenitors at E11.5 105
Figure 34 – Unsupervised hierchical clustering of *Wnt1^{Cre}; Dullard$^{+/Flox}$* and *Wnt1^{Cre}; Dullard$^{Flox/Flox}$* NCCs 107
Figure 35 – Diffusion map and gene expression levels in NCCs clusters 108
Figure 36 –NCCs compaction and orientation to the endocardium in cardiac cushions 110
Figure 37 – Analysis of *Sema3C* expression pattern in control and mutant NCCs along the OFT axis. 112
Figure 38 – Asymmetric positioning of the differentiating subpulmonary myocardium at the OFT distal level 114

Discussion

Figure 39 – Proposed model for the molecular cues driving the spatiotemporal septation of the OFT. 119

“ Quand on cherche reprit Siddharta, il arrive facilement que nos yeux ne voient que l’objet de nos recherches ; on ne trouve rien parce qu’ils sont inaccessibles à autre chose, parce qu’on s’est fixé un but à atteindre et qu’on est entièrement possédé par ce but. Qui dit chercher, dit avoir un but. Mais trouver, c’est être libre, c’est être ouvert à tout, c’est n’avoir aucun but déterminé. Toi, vénérable, tu es peut-être en effet un chercheur; mais le but que tu as devant les yeux et que tu essaies d’atteindre, t’empêche justement de voir ce qui est tout proche de toi. ” [1]

[1] Herman Hesse - Siddharta

Title:

Influence of BMP signaling on neural crest cells during heart outflow tract septation

Summary:

The heart outflow tract (OFT) is originally a solitary tube, which is septated into the aortic and pulmonary artery (Pa) during embryonic development. This morphogenesis is regulated by the cardiac neural crest cells (cNCC), which colonize the OFT and condense towards the endocardium, triggering its rupture and the fromation of the two arteries. Investigations to identify the molecular cues controlling cNCC behaviour in the OFT mesenchyme have established the importance of the Bone Morphogenic Proteins (BMP). However, little is known on the molecular cascades triggered by BMP signaling responsible for the cNCC mediated OFT septation.

To get insights into these molecular cascades, we decided to dissect the role of Dullard, a perinuclear phosphatase uncovered as a BMP intracellular signaling inhibitor, during OFT morphogenesis. Our results show that deletion of *Dullard* in the cNCC increases BMP intracellular signaling, leading to premature and asymmetric septation of the OFT, Pa obstruction and embryonic death. This BMP overactivation in the cNCC triggers the downregulation of mesenchymal markers and the upregulation of a cytokine called *Sema3c*, which in turn results in premature cNCC compaction at the endocardium. In addition, asymmetric differentiation of the distal subpulmonary myocardium contributes to asymmetrical rupture of the endocardium and Pa obstruction. Finally, our data converge to a model whereby graded BMP activity and *Sema3c* expression in the cNCC along the OFT axis set the tempo of OFT septation from its distal to its proximal regions. Hence, our findings reveal that fine tuning of BMP signaling levels in cNCC orchestrate OFT septation in time and space.

Keywords:

Neural crest cells, Heart, Outflow tract, BMP signaling, Sema3c, Dullard

Titre:

Influence des signaux BMP sur les cellules de crête neurale durant la septation de la voie d'éjection cardiaque

Résumé:

La voie d'éjection cardiaque (VEC) est initialement un tube unique, qui se divise ensuite en artère aorte (Ao) et pulmonaire (Pa) au cours du développement embryonnaire. Cette morphogenèse est régulée par les cellules de crête neurale (CCN) qui colonisent la VEC et se condensent le long de l'endocarde, entraînant sa rupture et la formation des Ao et Pa. Des recherches ont montré que les Bone Morphogenetic Proteins (BMP) contrôlent le comportement des CCN durant ce processus. Cependant, les cascades moléculaires impliquées sont méconnues.

Afin de mieux comprendre ces cascades moléculaires nous avons étudié le rôle de Dullard, une phosphatase identifiée comme inhibiteur intracellulaire de la voie BMP, au cours de la morphogenèse de la VEC. Nos résultats montrent que la délétion de Dullard dans les CCN augmente la signalisation BMP dans ces cellules, induit une septation asymmétrique et prématurée de la VEC, l'obstruction de Pa et la mort embryonnaire. Cette suractivation de la voie BMP dans les CCN entraîne la diminution de leurs marqueurs mésenchymateux et augmente l'expression d'une cytokine appelée *Sema3c*, qui elle-même induit une compaction prématurée des CCN à l'endocarde. En parallèle, la différentiation asymmétrique du myocarde sous-pulmonaire entraîne la rupture asymmétrique de l'endocarde et l'obstruction de Pa. Enfin, nos résultats montrent qu'un gradient d'activation de la voie BMP et d'expression de *Sema3c* dans les CCN le long de l'axe de la VEC régule sa septation disto-proximale. Ainsi, nous mettons en évidence que la régulation des BMP dans les CCN orchestre spatiotemporellement la septation de la VEC.

Mots-clés:

Cellules de crête neurale, Coeur, Voie d'éjection cardiaque, Signalisation BMP, Dullard, Sema3c

Remerciements

Je souhaite tout d'abord remercier Luc Pardanaud et Stéphane Zaffran pour avoir accepté d'être rapporteur de mon manuscrit de thèse ainsi que Onnik Agbulut, Sophie Creuzet et Sigolène Meilhac, pour avoir accepté d'évaluer mon travail de thèse en qualité de rapporteur.trice.s.

Je voudrais également chaleureusement remercier mon directeur de thèse, Bruno Cadot, pour m'avoir encadré et supporté pendant ces années de thèse, pour m'avoir donné l'opportunité de travailler sur un projet de thèse qui m'a passionné malgré des débuts incertains, et pour avoir été ouvert à mes idées, qui ont parfois pu être farfelues. Je le remercie également de m'avoir donné l'opportunité de participer à des conférences à l'internationale et de suivre de nombreuses formations au sein ou en dehors du champ académique. De même, je tiens à remercier Vanessa Ribes dont les conseils et l'expertise ont été de vrais atouts pour l'aboutissement de mon travail de thèse, mais également pour son optimisme inaltérable et pour sa passion contagieuse.

Merci à Glenda Comai avec qui j'ai eu le plaisir de collaborer au cours de mon projet de thèse, avec qui j'ai eu de très intéressantes discussions sur les crêtes neurales et le développement embryonnaire. Merci aussi à Pauline Martinez que j'ai eu le plaisir d'encadrer en stage de Master et à qui je souhaite bonne chance dans sa nouvelle carrière viticole. Enfin, je remercie Mariana Valente pour tous les moments passé ensemble au cours de nos expériences, notamment les journées à rallonge à l'Institut Pasteur ; sans son aide et son calme il aurait été difficile d'obtenir des résultats aussi intéressants.

Je tiens à remercier les équipes de Marc Bitoun et Edgar Gomes avec qui j'ai passé des réunions riches en découvertes et discussions scientifiques. Merci également à Lidia Dollé pour avoir su gérer mes nombreuses demandes administratives.

Mon doctorat ne saurait avoir été une expérience aussi agréable sans les nombreuses personnes que j'ai rencontrées au sein de l'Institut de Myologie. Je remercie tout particulièrement Petra et Valérie qui m'ont pris sous leur aile à mes débuts et avec qui j'ai passé d'excellents moments dans mais surtout en dehors du laboratoire. Merci à mes amis de l'association La Myocoop', Jordan, Mélanie et Elsa, dont la création et la gestion fut, il faut bien le dire, une aventure presqu'aussi trépidante que celle du doctorat. J'espère que cette association pourra continuer d'accompagner les chercheurs de l'Institut à l'avenir. De même, j'adresse de chaleureux remerciements aux nombreux autres valeureux participants aux évènements de La MyoCoop', sans qui les afterworks, les soirées jeux de société et la Fête de la science auraient été des expériences beaucoup moins sympathiques : Fanny, Cloé, Gaelle, Francesco, Nicolas, Lorenzo, Magdalena, Blanca, Astrid, Margot, Michel, Julie, Déborah et Justine.

Merci à l'équipe de Maria-Grazia, autrement appelée Team 6 ou La famille, pour m'avoir fait une place dans leur univers haut-en-couleur ainsi que pour leur sens de la fête et des pauses goûter, je me souviendrai. Une pensée particulière pour Mathilde, Aurore, Stéphanie et Benoit et une dédicace toute spéciale à Jordan et Thibaut qui ont su établir une atmosphère de travail chaleureuse et « studieuse » dans le bureau, ainsi que Francesco et Nicolas pour leurs blagues, Massiré et Julie pour leur calme et Cécile pour son aide et son impressionnante capacité de géolocalisation de tout objet dans l'institut.

Mon expérience en tant que thésard n'aurait pas été la même sans le soutien de mes « amis de toujours ». Merci à mes amies Paige et Tiphaine, rencontrées à l'étranger et avec qui j'ai passé des moments si mémorables en Amérique et en France. Merci également à mes chers amis de lycée, de prépa et de l'Agro pour nos weekends, nos voyages, nos discussions et nos aventures sans cesse réinventées : Laure, Julie, Chloé, Alice, Louise, Marion, Morgane, Candice et Violette. Merci particulièrement à la bande des petits cochons toujours aussi soudée et motivante: Claire, Clémence, Clément, Sandrine, Edouard, à mes amis de longue date Antoine et Florent, et à Aubin pour sa présence.

Enfin, je souhaite remercier ma famille pour m'avoir donné les moyens d'entreprendre cette thèse dans les meilleurs conditions, pour les repas du dimanche et les fêtes de famille, ainsi que pour leur soutien et leur confiance indéfectible. Une pensée toute spéciale à ma grand-mère, qui ne pourra pas assister à ma soutenance.

Résumé

Le cœur est le premier organe qui se forme durant le développement embryonnaire. Sa morphogénèse repose sur la coordination de différents types cellulaires qui interagissent entre eux ainsi qu'avec leur environnement afin de produire la structure tridimensionnelle complexe qui le caractérise. Deux paramètres majeurs rentrent en jeu dans ce processus morphogénétique: la spécification cellulaire, qui correspond à l'acquisition par les cellules embryonnaires, originellement pluripotentes, d'une identité propre, et la migration cellulaire, qui permet aux cellules de migrer en bon nombre et au bon moment dans le tissu où leur fonction est requise. Ces propriétés cellulaires permettent la mise en place d'un organe cardiaque fonctionnel, nécéssaire à l'oxygénation et à la nutrition des autres organes. Le cœur est composé de différents segments qui possèdent des fonctions complémentaires. L'alignement et la connexion de ces segments sont des paramètres particulièrement sensibles. La complexité de la structure tridimensionnelle du cœur et de sa connexion avec le système vasculaire font que les malformations cardiaques sont les malformations les plus couramment observées à la naissance (avec une prévalence de 1%) (Hoffman, 1995; Srivastava and Olson, 2000). La voie d'éjection cardiaque (VEC), qui permet l'éjection du sang vers les poumons et les autres organes, est particulièrement touchée par ces malformations. Elles comprennent entre autres les anomalies des valves et des grands vaisseaux ainsi que les défauts de séparation des ventricules. Les régulations moléculaires qui permettent la mise en place de la VEC sont nombreuses et complexes, ce qui rend très difficile l'établissement des causes génétiques des malformations qui la touche. L'étude des voix de signalisation cellulaires et du comportement des types cellulaires impliqués est donc un intense sujet de recherche.

Durant le développement embryonnaire, la VEC est originellement un tube unique qui se divise en deux pour générer l'aorte (Ao) et l'artère pulmonaire (Pa), ainsi que leurs valves respectives (Brickner et al., 2000). Ce processus morphogénétique est orchestré dans le temps et dans l'espace par les progéniteurs du myocarde, de l'endocarde, ainsi que les cellules de crête neurale (CCNs) qui migrent depuis le tube neural vers la VEC (Jain et al., 2011; Kelly, 2012). Les CCNs colonisent les coussins cardiaques qui bordent le lumen de la VEC et jouent un rôle crucial dans la septation du tube. De nombreuses expériences d'ablation des CCNs ont en effet abouti à une absence de septation de la VEC (Bockman et al., 1987; Hutson and Kirby, 2010). Ce type de malformation couramment observée chez l'homme est létal si aucune chirurgie n'est pratiquée sur le nouveau-né. En effet elle entraîne le mélange du sang oxygéné et non-oxygéné, aussi appelé cyanose, et cause une trop faible oxygénation des organes.

La septation de la VEC repose sur l'expansion de coussins cardiaques positionnés de chaque côté du lumen (Person et al., 2005). Cette expansion est permise par l'ingression des CCNs à partir du jour de gestation 9.5 chez la souris. Les CCNs convergent ensuite vers l'endocarde ce qui induit sa rupture, la fusion des coussins cardiaques et donc la genèse de l'aorte et de l'artère pulmonaire (Plein et al., 2015; Waldo et al., 1998). Les signaux moléculaires qui contrôlent le comportement des CCNs dans la VEC et permettent sa septation sont mal connus (Keyte and Hutson, 2012). Différentes études ont montré l'importance des signaux Bone Morphogenic

Proteins (BMPs) sur les CCNs, signaux sécrétés par la couche de myocarde qui entoure la VEC (Jiao et al., 2003; Liu et al., 2004; McCulley et al., 2008; Stottmann et al., 2004; Tang et al., 2010). Affecter les signaux BMP induit une malformation de la VEC ayant des caractéristiques proches de celles causée par l'ablation des CCNs. Ces résultats indiquent que les BMPs jouent vraisemblablement un rôle primordial dans les CCNs durant la septation de la VEC. Cependant, les cascades moléculaires déclenchées par les BMPs et qui régissent le comportement des CCNs durant la septation, ainsi que le comportement des CCNs elles-mêmes, sont mal compris.

Afin de répondre à ces questions nous avons décidé d'étudier le rôle d'une protéine inhibitrice des BMPs dans les CCNs, Dullard. Bien que son mécanisme d'action soit toujours débattu, il a été montré que Dullard est capable de réguler l'activité de la voie des BMPs chez la drosophile, le xénope et la souris (Sakaguchi et al., 2013; Satow et al., 2006; Urrutia et al., 2016). Cette protéine, très conservée au cours de l'évolution, diminue les niveaux de phosphorylations des Smad1,5,8, qui sont les effecteurs canoniques de la voie des BMPs. Nos résultats montrent que la délétion de Dullard dans les CCNs par recombinaison Cre-Lox entraîne une hausse des niveaux de phosphorylation des Smad1,5,8 et donc de l'activité de la voie des BMPs dans ces cellules. Grâce à ce modèle, nous avons donc pu étudier l'influence des BMPs durant la septation de la VEC. Tout d'abord, une analyse phénotypique poussée a montré que le gain-de-fonction des BMPs dans les NCCs entraîne une septation prématurée et asymétrique de la VEC, aboutissant à une atrophie de l'artère pulmonaire et à la mort embryonnaire. Pour mieux comprendre la cause moléculaire de cette malformation nous avons effectué une analyse sur cellules uniques et analysé la signature transcriptomique des progéniteurs de la VEC et plus particulièrement des CCNs. Nous avons montré que la sur-activation des BMPs induit la diminution de l'expression de marqueurs mésenchymateux (*Snai2*, *Twist1*, *Cdh2*, *Mmp14)* dans les CCNs ainsi que l'augmentation de *Sema3c*, une chemokine impliquée dans la migration cellulaire. Nous observons que la surexpression de *Sema3c* induit la compaction prématurée des CCNs vers l'endocarde, ce qui corrobore la transition des CCNs vers des états épithéliaux. De plus, nos résultats dévoilent que l'activation graduelle de la voie BMP dans les CCNs positionnées le long de la VEC entraîne la formation d'un gradient d'expression de *Sema3c*. Le niveau de *Sema3c* étant lié à la convergence des CCNs et à la septation de la VEC, nos résultats décrivent le mécanisme moléculaire régulant la septation dite « en fermeture Eclair » de la VEC qui génère les artères aorte et pulmonaire au cours du développement. Enfin, nous montrons que la septation asymétrique de la VEC dans les embryons mutants est corrélée à la différentiation asymétrique du myocarde sous-pulmonaire. Ces résultats suggèrent une interaction privilégiée des CCNs avec le lignage du myocarde sous-pulmonaire via *Sema3c.* Cela corrobore l'idée que les CCNs et ce sous-lignage du myocarde ont co-évolué lors de la genèse de la circulation pulmonaire chez les vertébrés.

I. INTRODUCTION

Foreword

Organ morphogenesis involves multipotent progenitor cells, which drive the morphogenetic processes in the organ-forming region. These progenitors specify and differentiate depending on their lineage and on their signaling environment. Specification is the first step of differentiation. At this stage, the progenitors' commitment to a cell fate can still be reversed. Two opposite visions exist concerning progenitors commitment during organogenesis, which actually complement each other in most cases of organ development. The mosaic model describes an organogenesis driven by cells fate, where specification is only determined by cell lineage. On the contrary, the regulative model conceives organogenesis as driven by tissues external cues, like signaling gradients, which specify progenitors in three dimensions along the different body axes. In addition to progenitors' specification, organogenesis requires progenitors' migration to the organ-forming region and their proper interaction with the surrounding tissues. The precise migration of embryonic progenitors at the right place and at the right time is essential to coordinate the formation of the organ. Defects in progenitors migration often lead to severe developmental defects (Kurosaka and Kashina, 2008). Remarkably, the heart is the first organ formed during organogenesis, which implies multiple critical and time-sensitive steps. This complexity makes the heart prone to malformations, which are the most common causes of developmental birth defects in humans (Kloesel et al., 2016).

The heart has a very complex structure, where diverse segments play complementary roles for the chambered pump to function efficiently and provide high-pressure blood flow. Unlike other organs with repetitive substructures (like lungs or liver), the proper alignment and connection of all segments in three dimensions is needed and highly sensitive to miscoordination between cell-types. Therefore many questions arise. Are all parts of the heart derived from a single progenitor lineage? If not, how do different lineages specify and interact in time and space to generate the mature heart structure? And finally, what type of signaling cues coordinate the behavior and specification of the progenitors during heart morpogenesis?

I.1 Evolution and early development of the cardiovascular system

I.1.1 How and why did the cardiovascular system evolve?

Evolutionary origin and diversity of cardiovascular systems

To survive and reproduce, all higher organisms need an efficient system of distribution of nutrients and oxygen combined with an efficient excretion of metabolic wastes. As soon as organisms went from small clusters of cells to more complex organizations, diffusion of molecules did not reach the required efficiency to reach cells survival. Circulatory systems emerged as cell arrangements able to support fluid movement and reduce the functional diffusion distance that nutrients, gases, and metabolic wastes must traverse. Thus, circulatory systems evolved from simple molecules diffusion in the intercellular space to complex networks of vessels tailored to supply the unique architecture of tissues and organs. In these complex architectures, the fluid flow can be regulated to go preferentially to one tissue or another depending on the organism metabolic needs. It is generally agreed that the vascular system first appeared over 600 million years ago as an evolutionary advantage in a bilaterian ancestor. Later on, vertebrates gained a new-type of cell-lining called endothelium, which probably appeared about 540–510 million years ago to optimize flow dynamics and barrier function in comparison with the simple matrix lining of invertebrates (Monahan-Earley et al., 2013). The word “heart” describes any segment of the circulation system that contracts and pumps blood in opposition to systems where blood is only propelled by pulsatile vessels. Evidences suggest that the heart structure evolved by addition of new segments to a primitive peristaltic pump (Simões-Costa et al., 2005) (Figure 1A, page 18). In its primitive linear form, the directional flow was achieved thanks to a peristaltic wave of contraction and to the presence of unidirectional valves. However, peristaltic pumps lack effective coordination between the fluid entering and leaving the contractile region. In vertebrates, the word “heart” rather describes a chambered, non-linear pump, composed of an inflow and an outflow segment with synchronized contractility. Thus, evolution has followed a transition from single-layered tubes with poor contractility and low electrical conductivity to more sophisticated pumps with fast-conducting and well-contracting muscular chambers, ensuring high pressure and high cardiac output (Šolc, 2007).

In the diversity of organisms, fluid circulation can be opened, as observed in the peripheral circulation of insects and worms, where hemolymph flows in the interstitial space before being taken back by venous collectors (Bettex et al., 2014). Open circulations are of low resistance explaining why no high-discharge pumps are needed in these organizations, where primitive peristaltic pumps are sufficient. Moreover, an open circulation implies a big volume of circulating fluid (20-50% of body weight) and low velocity. It limits the size of the

organism because interstitial diffusion is only efficient over short distances. Some accessory hearts can be added in species with open circulations to accelerate the flow during physical activity because tubular aortic hearts are too weak for this task (Bettex et al., 2014).

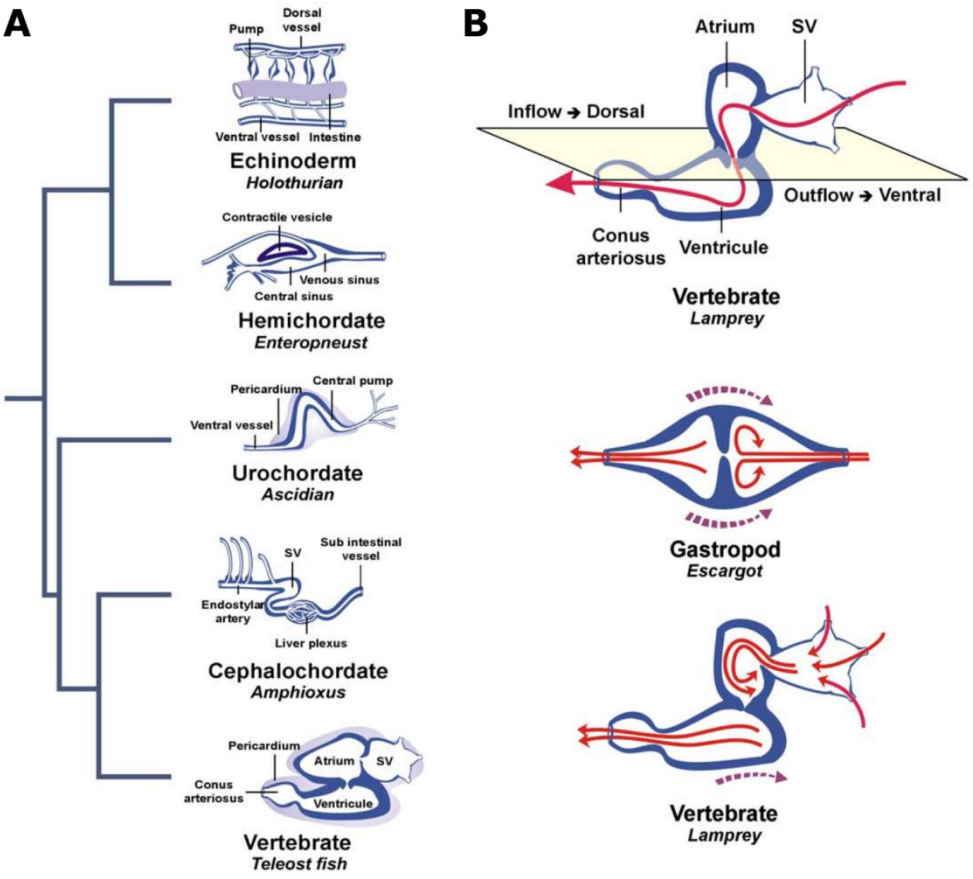

Figure 1 – Evolution of heart structures. Heart structures have evolved and gained in complexity to reach high standards in terms of contractility regulation, blood pressure and cardiac output. **A**. Evolution of the heart shape, went from linear tubes with poor contractility to nonlinear muscular chambers with synchronized contractility. **B**. The vertebrate heart has seen a critical shape transition in comparison with the gastropod heart. In fact, its inflow and outflow tracts are positionned on different planes. In the inflow tract, this creates a vortex that minimizes energy loss, while in the outflow tract, the ventricular recoil does not prevent but assist inflow because the ventricule is positionned on different plane (Adapted from (Simões-Costa et al., 2005)).

The chambered heart is composed of complementary segments

All vertebrates and cephalopods present closed circulation systems. This configuration allows fluid to flow faster and further via arteries, veins and capillaries delineated by endothelial cells. A higher efficiency of the pump is required in this configuration and has been achieved by developing conducting systems with pacemaking activity. In fact, pumps of closed systems are composed of contractile myocytes but also of differentiated conduction systems ensuring periodicity of the contraction and preventing reverse blood flow. Specific segments of fast-conduction (atria and ventricles), separated by low-conduction regions (inflow region, atrioventricular region and outflow region), emerged to provide the time sequence of contraction needed in chambered hearts (Christoffels and Moorman, 2009).

Segments devoted to two hemodynamics functions compose the vertebrate's hearts, one to receive blood flow upstream (inflow), and one to pump it downstream (outflow). The emergence of different dorso-ventral planes for inflow and outflow segments and the separation of these segments by valves presented a critical gain in hemodynamics efficiency (Figure 1, page 18). On the contrary, primitive linear peristaltic pumps are in straight line with vessels and therefore are characterized by high energy dissipation caused by distension of downstream segments, stream reflection, and potential retrograde flow. In these systems, inflow and outflow chambers are placed on the same plane, so flow entering symmetrically the atrium reflects away from the atrioventricular valve, which decreases mechanical efficiency (Figure 1, page 18). Plus, ventricular recoil against the atrium prevents its efficient filling when the ventricle pulse the flow out in the outflow tract (dotted lines) (Xavier-Neto et al., 2012). The heart of vertebrates resolved these problems by placing the inflow and outflow chambers at an almost right angle and on different planes. This "S-shape" arrangement establishes asymmetrical vortexing streams in the atrium directed towards the valve, reducing dissipation of energy and increasing cardiac output. The ventricular recoil is placed on a different plane than the atrial chamber and thus assists inflow rather than preventing it (Simões-Costa et al., 2005).

The cardiovascular evolution was influenced by homeothermy and terrestrial life conditions

The transition from an aquatic to a terrestrial life exposed animals to gravitational forces and forced them to adapt to gaseous oxygen exchanges. Organisms had to limit water loss and therefore lost skin breathing because it causes high evaporation. They also had to gain internalized gas-exchange structures with a large surface area in connection with the circulatory system. A crucial evolutionary breakthrough is believed to be associated with body temperature regulation. In fact, while homeothermic animals possess a fully formed conducting system, cold-blooded animals do not (Šolc, 2007). Another aspect of heart

evolution is the apparition of two separate circulatory systems. As the respiratory exchange shifted from the gills to the lungs, a vascular system rearrangement occurred. It transformed a single-loop branchial arch system into a double-loop pulmonary and systemic circulation. The double circulation system supports a differential pressure blood flow: sending low-pressure blood flow to lungs and high-pressure to the rest of the body. This arrangement prevents mixing of arterial and venous blood in species where separation is not total, and thus optimizes oxygen intake. Moreover, high pressure in the pulmonary system would be incompatible with efficient oxygen intake and would lacerate the lungs. On the contrary, high pressure in the systemic circulation ensures full oxygenation of animals muscles especially in the case of big animals with high level of activity. The double-pressure circulation also emerged to support efficient blood flow even under the influence of gravitation. Hence, the double-pressure circulation solved the limitations preventing vertebrates to colonize lands and allowed them to gain a full terrestrial lifestyle. Accordingly, it is believed to have enabled their body growth over time. Shreds of evidence suggest that reptiles, which evolved thick skin against water loss and for body protection, were the first vertebrates to rely entirely on lungs for gas exchange (Bettex et al., 2014). Interestingly, the ability to separate pulmonary and systemic circulations is thought to have evolved independently in mammals and birds/reptile, showing the importance of this circulatory evolution for full terrestrial colonization (Monahan-Earley et al., 2013).

Very interestingly, the degree of separation of the dual circulations correlates with the proportion of lifetime spent out of water (except for the thick-skin reptiles). The fish heart has a single circulation with a unique atrial chamber connected to a ventricle. Amphibians, which have a semi-terrestrial life, gained higher but not complete separation with two atria connected to one ventricle. As for the reptiles, they show a wide spectrum of heart anatomical features ranging for three-chambered hearts (turtles and most snakes) to four-chamber heart (crocodiles), correlating with their activity levels. Birds and terrestrial mammals, which are warm-blooded animals, present a complete separation of the pulmonary and systemic circulations thanks to a full septation of the heart outflow tract and ventricles. In addition, their heart and lungs are anatomically close together to minimize loss of pressure along vessels in the low-pressure pulmonary circulation.

In sum, to reach high pressure and circulatory efficiency, closed circulations with contractile pumps are the most common circulatory solutions found in the animal kingdom. However, it might represent an evolutionary trade-off. In fact, the advantages of closing the blood circulation are balanced by the disadvantages of possible occurrences of atherosclerotic lesions.

I.1.2 The emergence of cardiovascular progenitors during gastrulation

Cardiogenic progenitors specification at early embryonic stages

Early after uterine implantation, the germ disc is composed of two layers: the epiblast and the hypoblast. A transient groove appears in the epiblast, called the primitive streak, which enables the ingression of the epiblast cells in between the two pre-existing germ layers. The embryonic disk then presents three newly formed germ layers: the endoderm, the mesoderm, and the ectoderm. The mesoderm gives rise to almost all the different lineages that comprise the mature heart: the cardiomyocytes, the vascular cells, the smooth muscle cells and the pacemaker cells. As cardiovascular progenitors are almost exclusively derived from mesodermal progenitors, the cardiac specification can be traced back to mesoderm formation. In that respect, heart development begins at gastrulation. During gastrulation, the cardiovascular progenitors progress through the primitive streak, which is posteriorly localized in the germ disk, and move anteriorly to reach the anterior lateral mesoderm postionned on either side of the midline under the headfolds (Garcia-Martinez and Schoenwolf, 1993).
But what is driving the cardiovascular lineage specification and regional segregation during gastrulation? The earliest known sign of cardiovascular development is the transient expression of *Fgf8* and *Mesp1*, a basic helix-loop-helix transcription factor, in the primitive streak (Saga et al., 1996). Genetic lineage tracing experiments have shown that the population of *Mesp1* expressing cells contain most future cardiac progenitors (Saga et al., 1999). Only a subset of cells forming the interventricular septum and outflow tract septum is not linked to the Mesp1 lineage but derive from the ectoderm-derived neural crest cells (Kitajima et al., 2006). Mesp1-positive cells also give rise to endocardial cells of the aorta and brain, to some muscle of the neck and head, as well as to part of the liver (Buckingham et al., 2005; Devine et al., 2014; Lescroart et al., 2014).

Strikingly, loss-of-function of *Mesp1* leads to defects in mesoderm ingression through the primitive streak. *Mesp1* knockout embryos show dramatic early heart tube malformation (e.g. cardia bifida) due to defects in cardiac mesoderm migration to the ventral midline, although mesodermal cells are able to exit the primitive streak (Saga et al., 1999). On the contrary, in the *Mesp1/2* double-knockout embryos, abnormal accumulation of cells in the primitive streak suggests that mesodermal cells are unable to exit the primitive streak, causing a total absence of heart development (Kitajima et al., 2000). Thus, Mesp1 and Mesp2 seem to play a redundant function in controlling the exit of mesoderm progenitors from the primitive streak, but their functions later diverge in following developmental stages. Mesp1 regulates the specification of cardiovascular progenitors while Mesp2 influences somite formation. An interesting study from Chiapparo and colleagues showed that Mesp2 and Mesp1 have a very similar transcriptional activity, equally promoting target

genes implicated in cardiovascular specification and differentiation, as well as EMT (Chiapparo et al., 2016). However, Mesp1 but not Mesp2, promotes oriented cell migration via the induction of unique target genes *RasGRP3* and *Prickle1*.

The question then is: what possible factors could be triggering the expression of *Mesp1* in the early steps of gastrulation, hereby initiating the first step of cardiac specification?
The specification and behavior of the primitive streak is in fact regulated by multiple signaling pathways, namely Wnt, Nodal and BMP (Tam et al., 2006). Interestingly, Wnt signaling seems to play a paradoxical and time-dependent function during cardiac field specification and differentiation. Wnt signaling positively induces *Mesp1* expression and germ layer induction during gastrulation. Thus, Wnt is required for cardiac mesoderm formation, but it later acts as an inhibitor of cardiac differentiation that has to be turned down to enable heart formation. In other words, Wnt signaling regulation is biphasic, promoting early steps of cardiogenesis while inhibiting the later ones (Lindsley et al., 2006; Ueno et al., 2007).

How is the expression of *Mesp1* able to specify mesoderm cells into a cardiogenic lineage? And does it have a cell-autonomous role? Once *Mesp1* is expressed during gastrulation, it rapidly activates and represses sets of genes forming a gene regulatory network. Transcriptional profiling has indeed shown that Mesp1 represses genes promoting endoderm cell fate while activating key cardiovascular differentiation factors such as *Nkx2-5*, *Gata4*, *Hand2*, and *Mef2c* (Bondue and Blanpain, 2010; Bondue et al., 2008; Lindsley et al., 2008). A key insight into the influence of the expression of *Mesp1* on the mesoderm was gained from *Mesp1* gain-of-function experiments. These experiments showed that *Mesp1* gain-of-function is sufficient to induce the ectopic formation of cardiomyocytes in vivo and the cardiovascular differentiation of embryonic stem cells in vitro. In addition to embryonic stem cells differentiation into the different types of cardiomyocytes composing the mature heart (atrial, ventricular, pacemaker like), Mesp1 was also shown to induce endothelial and smooth muscle fates. Thus, Mesp1 is considered to be the key regulator of cardiovascular progenitors specification and the earliest marker of the cardiogenic field (Bondue et al., 2008; David et al., 2008; Lindsley et al., 2008).

Importantly, continuous expression of *Mesp1* is deleterious for cardiac differentiation. Its expression has to be transient, which is in accordance with the biphasic regulation of Wnt signaling aforementioned (Bondue et al., 2008). Another interesting point is that *Mesp1* key cardiovascular potency might be specific of primitive streak cells. In fact, the expression of *Mesp1* alone is not able to direct other progenitors into the cardiovascular lineage. Forced expression of *Mesp1* in fibroblasts does not induce cardiovascular specification, whereas a combination of downstream key cardiogenic factors (Gata4, Mef2c, Tbx5 and Smarcd3) efficiently reprogram these fibroblasts in cardiomyocytes like cells (Ieda et al., 2010; Takeuchi and Bruneau, 2009). To conclude, *Mesp1* expression can be seen as a

transcriptional priming required for the exit of the pluripotent state and enabling the activation of the downstream gene regulatory network responsible of cardiac specification.

Formation of a cardiogenic field in the mesoderm: the cardiac crescent

After leaving the primitive streak, the Mesp1-positive cardiovascular progenitors migrate in a semi-circular fashion and assume residence in the anterior lateral plate mesoderm. They regionalize in paired left and right precardiac fields on both sides of the midline. This pattern is called the cardiac crescent (Kelly and Buckingham, 2002). Dorsoventrally, the cardiovascular progenitors are positioned in the splanchnic mesoderm. This "primary cardiac field" contains the cells with the potency to form myocardium but also the endocardium and smooth muscle cells (Rawles, 1943). At this point, the ventral folding of the embryo initiates the convergence of the splanchnic mesoderm from both sides towards the ventral midline (Figure 2, page 24). Two populations arise in the splanchnic mesoderm. The presumptive endocardial cells segregate by EMT to form endocardial primordia. These primordia will form the endocardium, the inner-lining of the heart in continuity with the vessels (Milgrom-Hoffman et al., 2011). The remaining bilateral splanchnic mesoderm fuses at the ventral midline under the head folds and forms the myocardium of the primary heart tube (Abu-Issa and Kirby, 2007; Hosseini et al., 2017). When the paired myocardial primordia are still fusing, cardiac pulsations begin. The appearance of the Ncx-1 sodium-calcium exchange pump enables first contractions while rhythmicity is later orchestrated by the sinus venosus (Linask et al. 2001). Polarized waves of muscle contraction through the tube ensure directional blood-flow even though the pump is still valve-less.

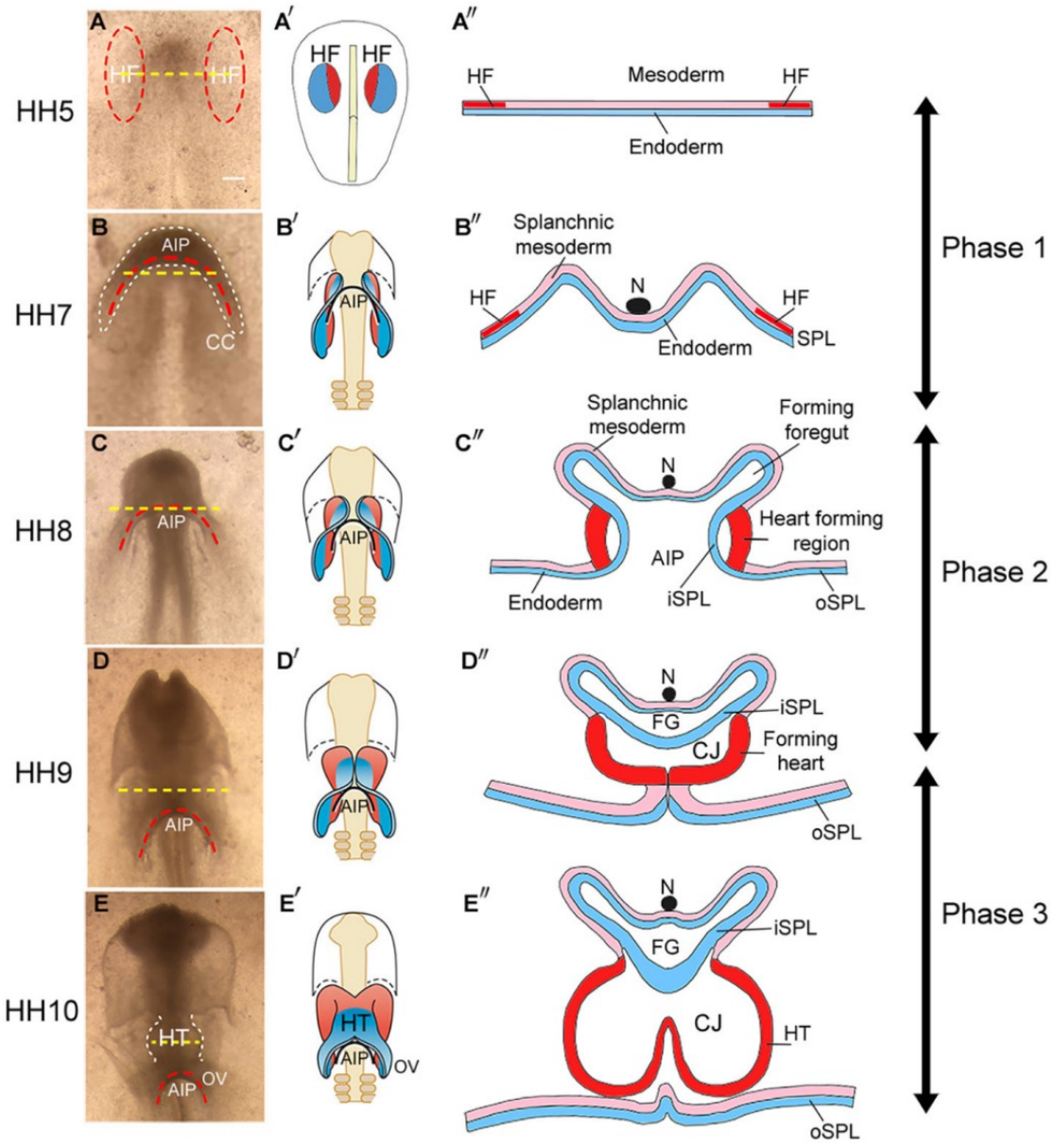

Figure 2 – Temporal and morphological representation of the heart fields and of the heart tube formation process. (**A-E**) Brightfield images of chick embryo (ventral view). Schematic interpretation of the folding of the heart fields from a ventral perspective (**A'-E'**), and through crossections (**A"-E"**). Red dashed lines indicate s in **A** heart fields and anterior intestinal portal (AIP) in **B-E**. **CC**, cardiac crescent; **CJ**, cardiac jelly; **FG**, foregut; **HT**, heart tube; **iSPL**, **oSPL**, inner, outer splanchnopleure; **N**, notochord; **OV**, omphalomesenteric vein. (Image from (Hosseini et al., 2017)).

I.1.3 Formation and morphogenesis of the heart tube

Chambered heart emergence requires heart tube elongation and looping

Initial cardiac contractions are happening in a myocardium that is actually still open dorsally. The myocardium is in continuity with the overlying medial splanchnic mesoderm and in contact with the overlying foregut endoderm (Figure 2, page 24). The linking structure between the differentiated myocardium and the medial splanchnic mesoderm is called mesocardium, which is in fact supporting the heart tube in the pericardial cavity. At this point, the initial growth of the linear tube is driven by addition of splanchnic mesodermal progenitors on its entire length. However, to allow formation of the three dimensional chambered heart observed in mammals and more generaly vertebrates, the tube needs to go through a process called looping. Looping consists in the rightwards folding of the tube on itself. The tube is freed from part of its dorsal attachment; in fact the mesocardium breaks along its anterior-posterior length but remains attached at both extremities of the tube. The anterior pole will give rise to the arterial pole of the heart, and the posterior pole to the venous one (Kelly and Buckingham, 2002). Thus, the rightward looping and the elongation of the heart tube are happening concomitantly. But what are the cues regulating the heart looping process? In the 1990s the origin of the myocardial progenitors participating in the looping of the tube was uncertain. It was not clear if progenitors forming the looping heart were coming only from the linear heart tube territory or from“extracardiac”regions.

Early evidences of a second cardiogenic field adding to the primary linear heart tube

First pieces of evidences to support the existence of a second lineage of progenitor cells were given by the observation of myocardial progenitors ingressing and differentiating at the arterial pole of the tube (de la Cruz et al., 1977; Virágh and Challice, 1973). That same year, three groups published evidences confirming the existence of novel sources of cardiovascular progenitors coming from the overlying pharyngeal mesoderm. They identified overlapping progenitors populations contributing to the elongation of the outflow tract at the arterial pole of the tube (Kelly et al., 2001; Mjaatvedt et al., 2001; Waldo et al., 2001). These overlapping heart-forming fields located in the pharyngeal mesoderm were actually regrouped in a single population called the secondary heart field (SHF), in opposition with the first heart field (FHF) forming the primary linear heart tube and derived from the cardiac crescent.

Before entering the tube poles, SHF progenitors proliferate in the dorsal pericardial wall, where they express the cardiogenic markers such as *Nkx2.5*, *Gata4* and *Hnk1*. They later specify and differentiate progressively while ingressing in the looping tube. Although first

described in the arterial pole of the heart, ingression of the second heart field is also happening at the venous pole of the heart, coming from the posterior part of the SHF (Galli et al., 2008) (Figure 3, page 27). SHF progenitors are characterized by two spatio-temporal core properties: their continued proliferation in the pharyngeal mesoderm and their delayed differentiation compared to the primary heart field (Kelly et al., 2014; Mesbah et al., 2012). In sum, the current view is that heart morphogenesis is supported by two lineages, the first and second heart fields. The first, immediately differentiating into myocardial cells, would play a primitive role of pump and scaffold allowing the deployment of the second, which later differentiates while ingressing at the arterial and venous poles.

Historically, two complementary approaches were used to study the contribution of progenitor populations to heart morphogenesis. The first one is the prospective lineage tracing (mostly using genetic Cre-Lox recombination), which establishes the correspondence between a precursor population expressing a given marker at one stage of development, for example *Mesp1* during gastrulation, with the fate and regionalisation of the progeny at later stages of development. The second approach is called retrospective lineage analysis, where a spontaneous low-frequency recombination in a single cell is used to study the fate and regionalization of its clonal progeny. More simply, the difference between both approaches is the scale of the study envisionned, either a whole population lineage analysis or a single-cell clonal analysis.

Specification and deployment of the second heart field

The SHF lineage was historically visualized thanks to the prospective genetic lineage tracing of SHF markers such as Fgf10 and Isl1 (Cai et al., 2003; Kelly et al., 2001). Second waves of lineage tracing experiments were performed using Isl1-Cre lines and more sensitive reporters to minimize the historical variability in Cre-Lox recombination efficiency (Ma et al., 2008; Sun et al., 2007). These experiments were highly informative to unravel gene function in the SHF and refine the SHF contribution to heart segments. They showed that SHF originates as a bilateral population in the splanchnic mesoderm but is placed medially to the first cardiac crescent. The medial-lateral patterning axis of the early embryonic splanchnic mesoderm is thus associated with the arterial-venous gradial contribution to the mature heart. Once still in the pharyngeal mesoderm at the dorsal side of the tube, SHF progenitors are controlled by a dynamic signaling environment pushing them to proliferate. First, SHF progenitors express growth factors such as *Fgf8* and *Fgf10*, and transcription factors such as *Isl1*, *Tbx1*, *Prdm1* and *Six1* (Cai et al., 2003; Chen et al., 2009; Ilagan et al., 2006; Kelly et al., 2001; Xu et al., 2004). These markers are only transiently expressed and soon downregulated when differentiation starts as progenitors approach the primary heart tube poles. Loss-of-function of *Fgf8/10* and *Tbx1* induce dramatic SHF development defects, especially in the outflow tract region (Théveniau-Ruissy et al., 2008; Watanabe et al., 2010). The SHF location moves anteriorly as the heart is displaced away from the head folds and

towards the pharyngeal arches. Accordingly, the environmental cues change and cardiac specification of the progenitors starts, characterized by the expression of *Nkx2.5*, *Gata4* and *Mef2c* (Verzi et al., 2005; Waldo et al., 2001).

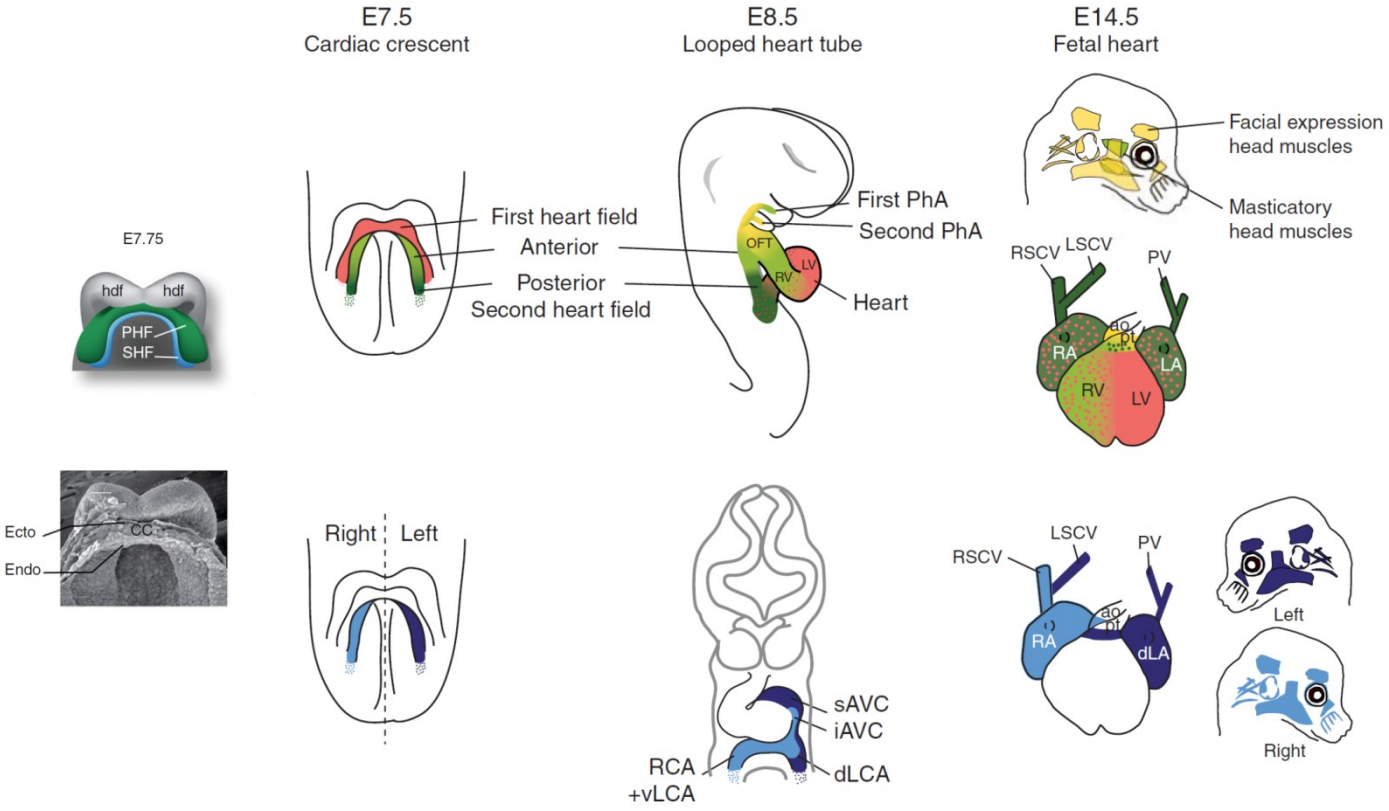

Figure 3 – Regionalization of the heart and identification of diverse cardiogenic lineages. The heart is a complex 3D structure, which derives from heterogeneous cardiac lineages. These lineages contribute to specific heart segments depending on their antero-posterior and right-left origin. First (red) and second (green) heart fields and anterior (pale green/yellow) or posterior (dark green) subdomains of the second heart field are shown at different stages of heart and head development. Regions of the heart with a dual origin are shown with colored dots. Left (dark blue)/right (pale blue) derivatives of the second heart field, also show right and left facial expression muscles in the head. ao, aorta; iAVC, inferior atrioventricular canal; sAVC, superior atrioventricular canal; E, embryonic day; LA, left atrium; dLA, dorsal left atrium; dLCA, dorsal left common atrium; vLCA, ventral left common atrium; LSCV, left superior caval vein; LV, left ventricle; OFT, outflow tract; PhA, pharyngeal arches; pt, pulmonary trunk; PV, pulmonary vein; RA, right atrium; RCA, right common atrium; RSCV, right superior caval vein; RV, right ventricle. (Adapted from (Meilhac et al., 2014; Moon, 2008)).

Regionalization of the heart and segregation of the heart field lineages

Meilhac and colleagues successfully used retrospective lineage analysis to confirm that two lineages corresponding to the FHF and SHF segregate and give rise to different segments of the heart (Meilhac et al., 2004). The analysis of clones size from the FHF and SHF suggest early segregation from a common precursor pool, which is presumably the Mesp1 population observed during gastrulation. This analysis also corroborated the fact that the SHF ingresses by both poles of the heart and contributes to the outflow tract, inflow tract, right ventricle and atria segments. Concerning the first heart field, it seemingly contributes to the left ventricle myocardium but also to a minor part of the atria and right ventricle (Lescroart et al., 2014; Zaffran et al., 2004). Hence, the cardiac crescent and early heart tube contribute for the most part to the left ventricular myocardium. As Hcn4 is an early marker of the cardiac crescent, $Hcn4^{Cre}$ genetic tracing was performed and showed labeling mainly in the left ventricle and myocardial lineage, especially contributing to the conduction system (Liang et al., 2013; Später et al., 2013). Although retrospective clonal analysis suggested the existence of a common progenitor pool for both heart fields, the timing of the lineage segregation remained unclear. Temporal clonal analysis shows an absence of overlap among the future FHF and SHF in the Mesp1 original population, suggesting that the common progenitor of all cardiac progenitors arise actually in the epiblast before gastrulation (Lescroart et al., 2014). Mesp1 progenitors actually consist of two temporally distinct pools of progenitors, which will be sequentially restricted to either the FHF or the SHF: the early *Mesp1* expressing progenitors contributing to the FHF, the later *Mesp1* expressing progenitors contributing to the SHF. Hence, Mesp1 marks unspecifically the two distinct cardiovascular progenitor fields. Although molecularly very similar, single cell transcriptomic profiling of Mesp1 progenitors at early and late stage of *Mesp1* expression showed that these two populations present different transcriptional profiles with key markers expressed in one or the other (Lescroart et al., 2014). The same study on deficient *Mesp1* CPs showed that *Mesp1* expression is necessary for progenitors to exit the epiblast expression programm and lose pluripotency (Lescroart et al., 2018).

The analysis of the localization of clones from the FHF or SHF, combined with their expression of cell-type specific markers, allowed to assess the fate restriction of single Mesp1 progenitors descendancy. Interestingly, while FHF clones are unipotent and differentiate into cardiomyocytes and endocardial cells, SHF clones can be either unipotent or bipotent, differentiating in cardiomyocytes, endocardial cells or smooth muscle cells (Figure 4, page 29). Another interesting point highlighted by the study is the fragmentation rates of clones. Clones composed of endocardial cells show more dispersion in the heart segments they contribute to,compared to those composed of cardiomyocytes (Lescroart et al., 2014).

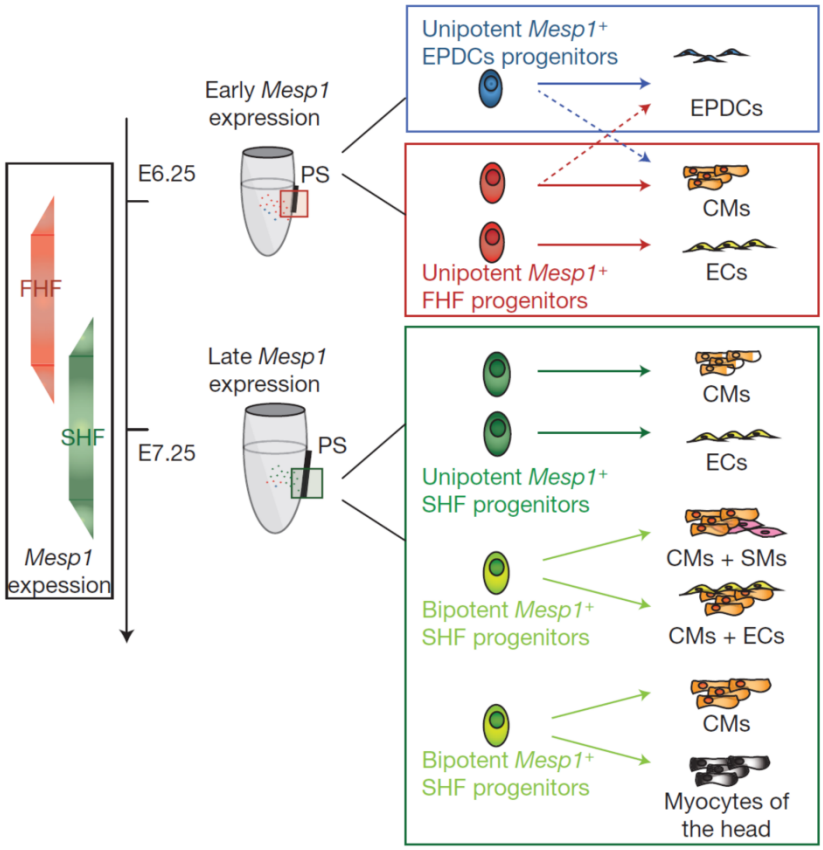

Figure 4 – Early steps of cardiovascular progenitor specification and lineage commitment during mouse development. Sequential specification of Mesp1 progenitors shows the existence of temporally distinct Mesp1 progenitors that contribute to the heart development. Mesp1 progenitors first give rise to the FHF (in red) and then to the SHF (in green) progenitors with an overlapping expression of *Mesp1* in the two populations at E6.75. FHF progenitors are unipotent and give rise to either CMs or ECs. SHF progenitors are either unipotent or bipotent. Epicardial and EPDCs arise as an independent Mesp1-derived lineage at the early time points. PS: primitive streak. (Image and legend from (Lescroart et al., 2014)).

Heterogeneity in the second heart field enables asymmetry appearance in the heart structure

The fact that SHF progenitors are contributing to a great diversity of segments in the mature heart suggests that the SHF progenitor pool is heterogeneous. Yet, the spatiotemporal specification and patterning of a diversity of SHF subpopulations remains poorly understood. The diversity in SHF progenitors is underlined by the difference in its anterior-posterior regionalization. In fact, the SHF ingresses by both arterial and venous poles in the primary heart tube but contributes to functionally different segments on both sides. The anterior region of the SHF contributes to the right ventricle and great and OFT, whereas the posterior region contributes to the atria and inflow tract. These two components of the SHF are called the anterior and posterior heart fields and their lineage boundary is still poorly defined. Interestingly, the posterior region of the SHF is characterized by *Isl1* expression as the rest of the SHF, but lacks anterior SHF markers as Fgf8/10. In addition, it is characterized

by *Tbx5* expression, which is required for its contribution to the venous pole (Bruneau et al., 2001; Xie et al., 2012). *Tbx1*, the major candidate gene for the DiGeorge syndrome, is expressed in the pharyngeal endoderm, ectoderm and mesoderm, where it regulates the balance between proliferation and differentiation (Chen et al., 2009). *Tbx1* was shown to be required for the deployment and segregation of the posterior SHF to the venous pole and arterial subpulmonary myocardium. Clonal analysis shows indeed that Tbx1-derived clones contribute to both poles of the heart suggesting that local signaling must induce their divergence (Lescroart et al., 2010; Rana et al., 2014). *Tbx1* is required for the Hoxb1-positive progenitors from the posterior SHF to give rise to the future subpulmonary myocardium (Rana et al., 2014). This Tbx1 dependent contribution to the pulmonary trunk myocardium is critical for arterial pole development and septation (Bajolle et al., 2008; Théveniau-Ruissy et al., 2008; Xu et al., 2004). Retinoic acid signaling has also been shown to be crucial in anteroposterior patterning and in defining the posterior boundary of the SHF (Ryckebusch et al., 2008; Sirbu et al., 2008). Retinoic acid signaling acts upstream of *Hox* genes and hereby defines sub-domains in the SHF. It regulates different combinations of *Hox* genes expression, which triggers spatially seggregated domains that contribute differentially to the proximodistal patterning of the OFT and atria (Bertrand et al., 2011). Hence, specific markers of anterior versus posterior SHF lineages exist, enabling isolation of these populations, namely Fgf10 to mark the anterior SHF and Hoxb1 and Tbx5 for the posterior SHF (Rana et al., 2014). Recent single-cell transcriptomic analysis of cardiovascular progenitors reasserted this lineage segregation between anterior SHF and posterior SHF (Lescroart et al., 2018).

To add a third dimension to the previously described dorso-ventral and anteroposterior heart patterning, one can wonder about the determination of a left-right asymmetry in the heart. In fact, rightward heart looping is the first morphological sign of bilateral asymmetry during heart development, and more broadly during embryonic development. Looping is critical for the proper alignment of cardiac segments and the establishment of the double-circulation. This process happens concomitantly with heart tube elongation, suggesting that the two might be linked. To support this view, recent *in vivo* and *in silico* results demonstrate that the asymmetric ingression of cardiovascular precursors at both poles of the tube is responsible for looping (Garrec et al., 2017). At the molecular level, the left-specific program in the lateral plate mesoderm is driven by Nodal and its downstream target *Pitx2*. The specific expression of *Pitx2* in the left primary heart field confers left identity to heart segments at the arterial and venous poles of the heart tube (Campione et al., 2001; Galli et al., 2008; Liu et al., 2002). Combination of retrospective clonal analysis and DiI labeling enabled the identification of left/right derivatives from the posterior heart field and suggest that right and left progenitors diverge before first and second heart fields (Domínguez et al., 2012).

Clonal relation of the second heart field with the facial skeletal muscle

Very interestingly, recent results gained from retrospective clonal analysis have revealed a common lineage origin between craniofacial skeletal muscles and SHF derived myocardium (Lescroart et al., 2010). This demonstrates that the SHF and branchiomeric skeletal muscles share a closer lineage relationship than SHF with the FHF. The Isl1 expressing pharyngeal mesoderm is thus a bipotent myogenic lineage composed of presumptive myocardial and skeletal muscle progenitors. Segregation of these lineages is observed in the first two branchial arches; the myogenic determinants *MyoD* and *Myf5* are expressed in the more proximal region, whereas SHF markers are expressed distally (Nathan et al., 2008). Lineage trees inferred from the retrospective clonal analysis data can predict lineage relationships inbetween specific head muscles and heart segments. The results highlight that the head and heart structures deriving from the same pharyngeal arch mesoderm are most closely related. In fact, anterior head muscles deriving from the first pharyngeal arch are more closely related to right ventricle myocardium, whereas facial expression muscles deriving from the second pharyngeal arch are more closely related to the outflow tract myocardium at the base of the great arteries. This is in link with the posterior movement of the arterial pole during pharyngeal morphogenesis (Lescroart et al., 2010; Meilhac et al., 2014) (Figure 3, page 27).

In addition, compelling evolutive perspective came from the study of *Ciona intestinalis*, a widely used model to study early heart tube formation. Ancestors skeletal muscle progenitors expressing *Isl1* would have been assimilated into the heart during vertebrate evolution (Stolfi et al., 2010). In fact, in *Ciona intestinalis* Isl1 progenitors close to the cardiogenic field only show skeletal muscle fate, suggesting that they were later incorporated in a newly evolved cardiac field, the SHF. The SHF has also been identified in other vertebrate species with partial septation, suggesting that SHF was first incorporated to the heart in order to increase the heart structure, rather than to drive septation. Moreover, as divided circulations evolved in vertebrates, the differentiation delay and proliferative capacity provided by the SHF must have allowed for the elongation of the heart tube and the addition of new segments necessary to build heart chambers. Perturbation of SHF deployment leads to a wide spectrum of congenital heart defects ranging from failure of heart tube extension, to misalignment of the heart segments. But what signaling cues are regulating SHF deployment to the primary heart tube and SHF fate determination?

Regulatory signals tuning SHF deployment and interaction with the neural crest cells and other pharyngeal progenitors

As described when a second cardiogenic lineage was shown to contribute to heart development, the SHF is positioned in the overlying pharyngeal mesoderm. The SHF differentiation is precisely regulated when progenitors approach their sites of deployment on the primary linear heart scaffold, namely the anterior and posterior poles of the heart tube. This deployment requires a complex interaction between the different tissues and cell-types composing the pharyngeal mesoderm environment. A complex array of extracellular signals defines the niche of the SHF in the pharyngeal region. A dialogue is established between the SHF and the different cell-types composing the niche: the adjacent pharyngeal endoderm, the overlying pharyngeal ectoderm as well as another migrating cell-type, the neural crest cells (Figure 9, page 46). Paracrine signals between this diversity of cell-types, and autocrine signals of the pharyngeal mesoderm, are regulating SHF progenitors behavior, proliferation and differentiation. As previously mentioned, the SHF is in fact characterized by a precisely time-sequenced development, with continued proliferation in the pharyngeal mesoderm, followed by induced differentiation when ingressing in the heart tube. The neural crest cells specification and paracrine signalling was shown to be crucial to enable proper SHF deployment and heart morphogenesis. To investigate further the interactions occuring between neural crest cells and the SHF, we thereafter describe the lineage origin and specification of neural crest cells (NCCs).

I.2 Neural Crest Cells origin, specification and contribution to heart development

I.2.1 NCCs specification and migration along the rostrocaudal axis of the embryo

NCCs emergence and specification

Neural crest cells are remarkable early embryonic progenitor cells characterized by their incredible migratory capacities and their multipotency. They were first described in 1868 by Wilhelm Hes, as being formed in the ectoderm but contributing externally to sensory glia. This was, in developmental biology, the first realization that tissue formation could include contributions of migrating cells and was not only of stationary progenitors. The second important realization was that the NCCs, which are of ectodermal origin, could generate mesoderm cell-types (Platt, 1894)(Katschenlo 1888). This challenged the law according to which the three germ layers were determining mutually exclusive cell fates with no overlap. Hence, the NCCs are often considered as a 'fourth germ layer' due to their developmental plasticity and remarkable ability to give rise to both ectodermal and mesenchymal-like derivatives (Hall, 2000). In fact, neural crest cells give rise to an outstandingly wide range of derivatives. On the one hand they contribute to cell-types considered as "ectoderm-related": namely, the sensory and autonomic neurons of the peripheral system, Schwann cells, ganglionic glia, and melanocytes (Ayer-Le Lievre and Le Douarin, 1982). On the other hand, they also contribute to "mesoderm-related" cell-types: namely, the craniofacial skeleton and cartilage, the connective tissues of neck glands (parathyroid, thyroid, *etc*…) and the walls of the great arteries. This second type of lineage is grouped under the name of ectomesenchyme, because it encompasses mesenchymal cell-types derived from the NCCs, which is of ectodermal origin.

The initiation of the neural crest development starts at gastrulation and results in the establishment of a defined domain in the ectoderm, called the neural plate border. This domain is positioned between the neural plate and the future epidermal ectoderm (also called non-neural ectoderm) (Figure 5, page 34). Presumptive NCCs are thus induced at the border between future neural and non neural-ectoderm. As neurulation begins, these cells come to lie in the elevating neural folds, which is where the name "crescent" came from. As the neural tube closes, nascent neural crest cells reside at its dorsal aspect, and subsequently delaminate. The delamination of the NCCs is actually a well-studied process of epithelial-to-mesenchymal transition (EMT), characterized by the loss of cell-cell adhesion and cytoskeletal rearrangements. This is followed by NCCs acquisition of migratory capacities supported by the expression of new proteins (cell-surface receptors, metalloproteases and adhesion molecules), enabling these cells to sense and migrate along stereotypical trajectories to reach their final destination localized all over the embryo.

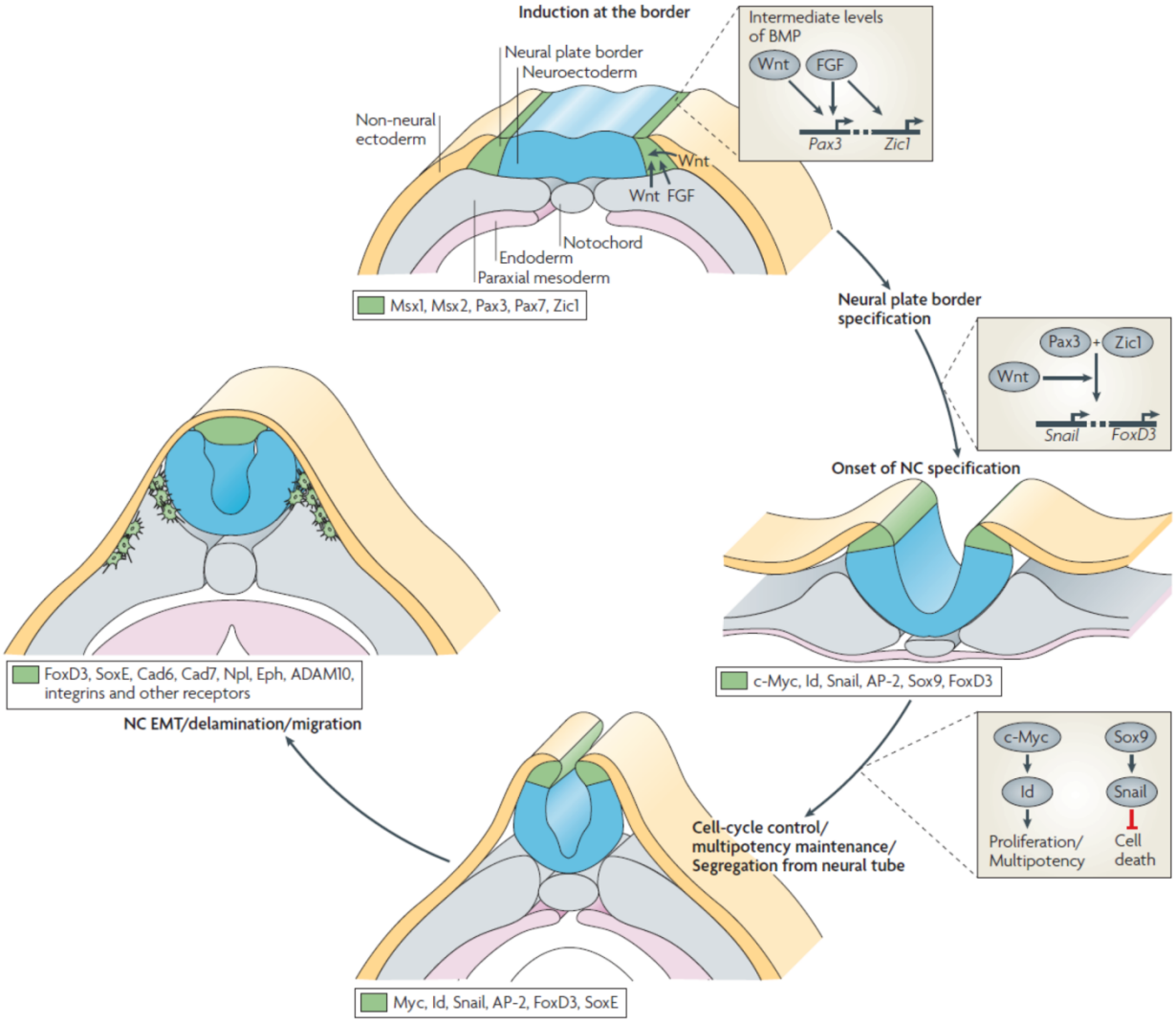

Figure 5 – Induction, specification and delamination of the NCCs. The induction of neural crest cells (NCCs) starts as a specific domain called Neural Plate Border (NPB), generated inbetween the neuroectoderm and the non-neural ectoderm. Signals including FGF from the underlying mesoderm and Wnts from mesoderm and adjacent non-neural ectoderm induce the expression of NPB specifier genes, such as *Pax3* and *Zic1*. This induction requires intermediate levels of BMP signaling. In turn, Pax3 and Zic1 up-regulate trigger NCCs specification by upregulating NCCs specifier genes such as *Snail* and *FoxD3* in the neural folds. Expression of these early NCC specifiers in the NCC precursor population segregates them from the dorsal neuroepithelium, as these genes control cell proliferation, delamination and the onset of the epithelial to mesenchymal transition (EMT). Subsquently, NCCs start delaminating and migrating away from the neural folds. To that extent, genes like *FoxD3* and *Sox10* control the expression of downstream effector genes such as type II cadherin, cadherin-7 (*Cad7*), matrix metalloproteases (*Adam10*), integrins, neuropilins (*Npl*), *Eph* and other transmembrane receptors. These observations have been primarily derived from work in *Xenopus laevis* and as such may not uniformly apply to other organisms (Image from (Sauka-Spengler and Bronner-Fraser, 2008).

The progenitor pool composing the neural plate border (NPB) is heterogeneous and apart from NCCs also generates the ectodermal placodes, epidermal cells, roof plate cells and sensory neurons of the central nervous system (Groves and LaBonne, 2014; Simões-Costa and Bronner, 2015). The usual model poses that signals between the neural plate and non-

neural ectoderm are inducing the establishment of the neural plate border. This induction of the neural plate border takes place concomitantly with the more lateral neural induction. It is therefore believed that redundant signaling cues are regulating both processes. In fact, genes characterizing NPB induction, called NPB specifiers genes, are initially expressed in territories which include neural and epidermis prospective domains. After induction of the specifier genes, the second step is a cross-repression process where boundaries between the various domains are sharpened and become mutually exclusive. The interactions between neural and non-neural transcription factors lead to the definition of the neural plate progenitor domain in the area of intermediate levels of WNT and BMP activity (Groves and LaBonne, 2014) (Figure 5, page 34). FGF and Notch signaling are also involved in the sharpening of the neural plate domain. Yet, the expression of NPB specifier genes is not homogeneous in the domain. This fact might later take part in the generation of the different subpopulations derived from the NPB. Nonetheless, the global domain is usually defined by the expression of *Pax3/7*, *Dlx3/5*, *Gbx2*, *Zic1*, *Tfap2*, *Msx1*, *Gata2/3*, *Foxi1/2* and *Hairy2* (Betancur et al., 2010; Khudyakov and Bronner-Fraser, 2009; Meulemans and Bronner-Fraser, 2004; Nichane et al., 2008). Cross-regulations between outer neural genes and inner NPB specifiers actually establish regionalized domains and a sharp boundary separating NCCs from the CNS progenitors. But how are the NCCs physically segregating in the NPB from the other lineages? The key function gained by NCCs is the ability to undergo EMT and become a migratory cell-type. However, they have to remain undifferentiated until they reach their multitude of final niches. NCCs premigratory specification requires the expression of *FoxD3*, *Ets1* and *Snai1/2* regulated by the NBP aforementioned specifiers, notably *Pax3/7*, *Msx1* and *Zic1* (Figure 5, page 34). Concomitantly, the presumptive placodal domain characterized by the expression of other specifier genes (*Six1*, *Eya1/2*, *Irx1*) is established laterally to the NCCs. Particular specifier genes of the NCCs and placodal progenitors respectively inhibit each other, and morphogens like Wnt signals seem to take part in this restriction process. Despite the expression of specific markers, the fate of the progenitors is not yet fixed, but this new transcriptional state of the NCCs initiates a structural transformation leading to EMT and delamination from the neural tube.

Neural crest cells epithelial-to-mesenchymal transition (EMT) and migration

The EMT is a drastic transcriptional turn point, which requires the precise control of hundreds of genes. The transcription factors described as NCCs specifiers take part in the molecular machinery responsible of the cell structural remodeling during EMT. EMT can be seen as two sequential steps, the first one being delamination from the neural tube and the second one being cells dispersion. First, delamination from the epithelium requires changes in cells adhesive properties, which is supported by a change in the cadherins expressed at the cell surface. This transition is demonstrated by the repression of the epithelial-specific type 1 Cadherins (*Ncad*, *Ecad* and *Cad6b*), which are replaced by the type 2 Cadherins

(*Cad11* and *Cad7*). The transcriptional repressors Snai1/2 and their co-effector phosphorylated-Sox9, are key in the downregulation of type 1 cadherins (Coles et al., 2007; Liu et al., 2013). Interestingly, a discrepancy appears between type 1 cadherins: while Cad6b is required for the loss of adhesion within the epithelium structure, E-Cad regulates the adhesion of the NCCs themselves in aggregates after delamination. Furthermore, Twist and Zeb2 appear to be transcriptional regulators of E-Cad expression and are required for the NCCS dispersion phase (Powell et al., 2013). Apart from cell-adhesion, the surrounding niche of the epithelium has also to go through drastic changes. For this to happen, NCCs gain the ability to secrete metalloproteinases and ADAM proteins, which are able to degrade the basement membrane. The expression of these proteins seems also to be regulated by Snai1/2 and Zeb2 (Simões-Costa and Bronner, 2015). Concerning their migratory capacities, which will be described later on in more depth, NCCs undergo cytoskeletal rearrangements in part mediated by Rho-GTPase (Clay and Halloran, 2010).

NCCs axial diversity

NCCs are formed all along the rostrocaudal axis of the neural tube, from the forebrain to the tail. Their apparent uniformity masks the heterogeneity of the subpopulations characterized by their axial origins (Figure 6, page 32). A nomenclature of four distinct subpopulations of NCCs has been established. The cranial subpopulation encompasses cells from the forebrain to the 6th rhombomere, the vagal from the first to the 7th somite, the trunk from the 8th to the 24th somite, and the sacral cells are posterior to the 24th somite. These subpopulations show specific migratory trajectories, specific gene expression profile and specific differentiation potential. The wide range of derivatives that can be generated from NCCs streams were uncovered thanks to classical embryology experiments including ablations, heterotopic transplantations, dye-labeling and genetic lineage tracing (Ayer-Le Lievre and Le Douarin, 1982; Wagner, 1990). The main contributions of each NCCs subpopulation are described in (Figure 6, page 32).

Cranial NCCs give rise to craniofacial skeleton, cranial ganglia, odontoblasts and thyroid cells. Vagal NCCs generate enteric ganglia and smooth muscle cells (notably in the outflow tract septum). Trunk NCCs give rise to the dorsal root ganglia, sympathetic ganglia and adrenal medulla. And finally sacral NCCs generate enteric ganglia and sympathetic ganglia.

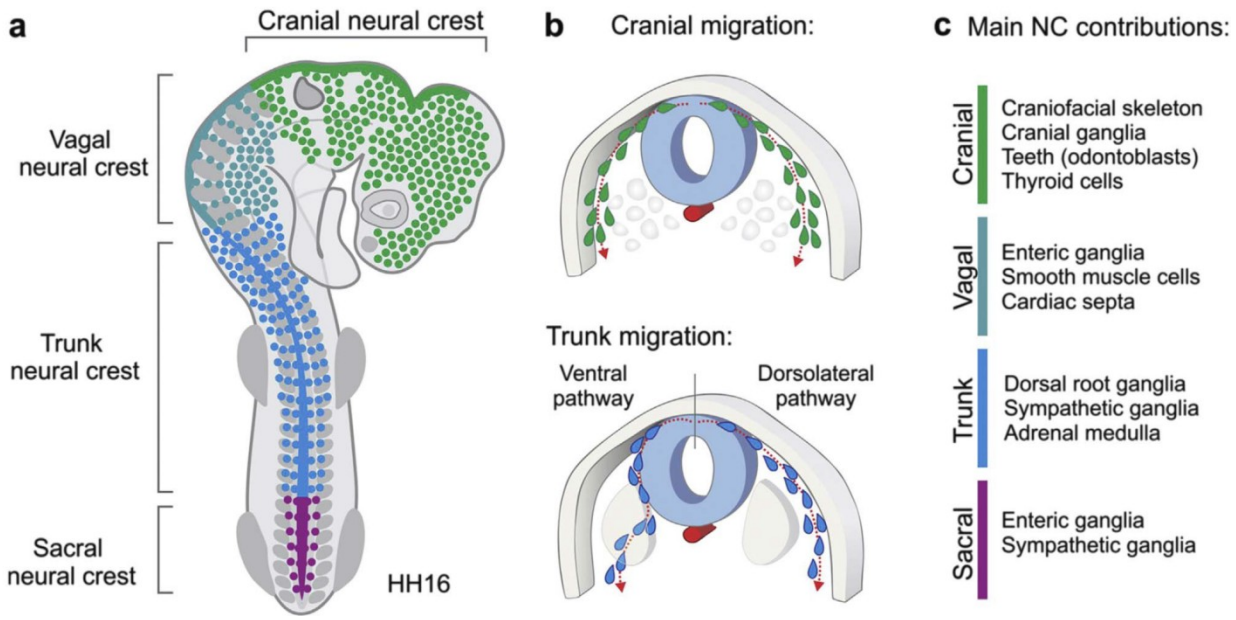

Figure 6 – NCCs heterogeneity along the anteroposterior axis. **a.** Representation of the axial-specific NCCs subpopulations in a chick embryo. The cranial subpopulation encompass cells from the forebrain to the 6th rhombomere, the vagal from the first to the 7th somite, the trunk from the 8th to the 24th somite, and the sacral cells are posterior to the 24th somite. These subpopulations show specific migratory trajectories, specific gene expression profile and specific differentiation potential. **b.** Differences are observed in migratory patterns among NCCs subpopulations. The cranial NCCs migrate dorsolaterally, whereas the trunk NCCs, which are localized adjacent to the developing somites, can take either a dorsolateral or a ventral path of migration. **c.** The different NCCs subpopulations give rise to an incredible variety of derivatives, which may be specific to a given subpopulation. For example, cranial NCCs generate the craniofacial skeleton and is the only subpopulation possessing ectomesenchymal potential in amniotes (Image from (Rothstein et al., 2018)).

Fate restriction along the anteroposterior axis

One can wonder if the diversity of lineages and fates granted to NCCs is coming from axial specific environmental cues or on the contrary from original cell-intrinsic differences. The results of NCCs grafts to different axial levels, called heterotopic transplantations, have proven the large plasticity of NCCs. NCCs are able to gain the fate characterizing the hosting niches positioned at different axial levels. For instance, transplanted cranial or vagal NCCs are able to differentiate in trunk derivatives (i.e. neurons, glia and pigment cells) when grafted at trunk axial levels. Likewise, trunk NCCs are able to differentiate in vagal derivatives like enteric ganglia when they are grafted at vagal levels (Douarin et al., 2004; Le Douarin and Teillet, 1974; Rothstein et al., 2018). On the other hand, heterotopic transplantations have shown through the years a trend of restriction in NCCs fates along the anteroposterior axis (Douarin et al., 2004; Kirby, 1989; Lwigale et al., 2004). In fact, although each axial subpopulation shows a wide range of derivatives, it seems that some mesenchymal fates are unique to NCCs originating from the two anterior most streams, the

cranial and vagal streams. For example and very remarkably, trunk NCCs are unable to generate cartilage and bone, which are specific derivatives of cranial NCCs (Lwigale et al., 2004; Nakamura and Lievre, 1982). Taken together, these results draw a peculiar portrait of NCCs potential, where NCCs originating from all axial levels are able to differentiate into neural cell-types and melanocytes, but only specific axial levels can prime NCCs to differentiate into mesenchymal cell-types. The general view is that NCCs plasticity is progressively restricted in the caudal direction, with cranial NCCs being able to generate almost all NCCs derived cell-types, and trunk/sacral NCCs fewer cell-types (Lwigale et al., 2004).

On a very interesting note, the anterior vagal NCCs, named cardiac NCCs, contribute to the cardiovascular development. Although they belong to the vagal subpopulation, they seem unable to contribute to the craniofacial structures when transplanted at the cranial level (Lwigale et al., 2004). Moreover, their unique ability to differentiate in smooth muscle and tune heart outflow tract septation is inaccessible to NCCs from other axial levels, even trunk NCCs (Kirby, 1989). This suggests that cardiac NCCs have diverged from the other NCCs subpopulations during evolution and acquired a unique ability to contribute to cardiovascular development.

A complex GRN sequence underlies the differential axial fates of NCCs

What are the gene regulatory networks underlying the differential NCCs specification along the anteroposterior axis? As explained earlier in this introduction, NCCs development is regulated by a sequence of transcriptional modules (Rothstein et al., 2018) (Figure 7, page 39). The first module is established by Wnt, FGF and BMP signals in the neural tube environment. They induce neural plate border (NPB) identity, marked notably by expression of genes like *Msx1*, *Pax7* and *Zic1*. In turn, these NPB specific genes cooperate to drive the induction of a second module. This second module regulates neural crest specification and is characterized by markers as *FoxD3*, *Sox10* and *Ets1*. Later on, a third module is engaged, inducing NCCs EMT and migration. Although this chain of modules is commonly presented as the GRN responsible for general NCC development, increasing evidences support the hypothesis of axial-specific NCCs specification program. This discrepancy in NCCs specification process along the anteroposterior axis could explain the variability in fate potential, notably the inability of trunk NCCs to give rise to bone and cartilage.

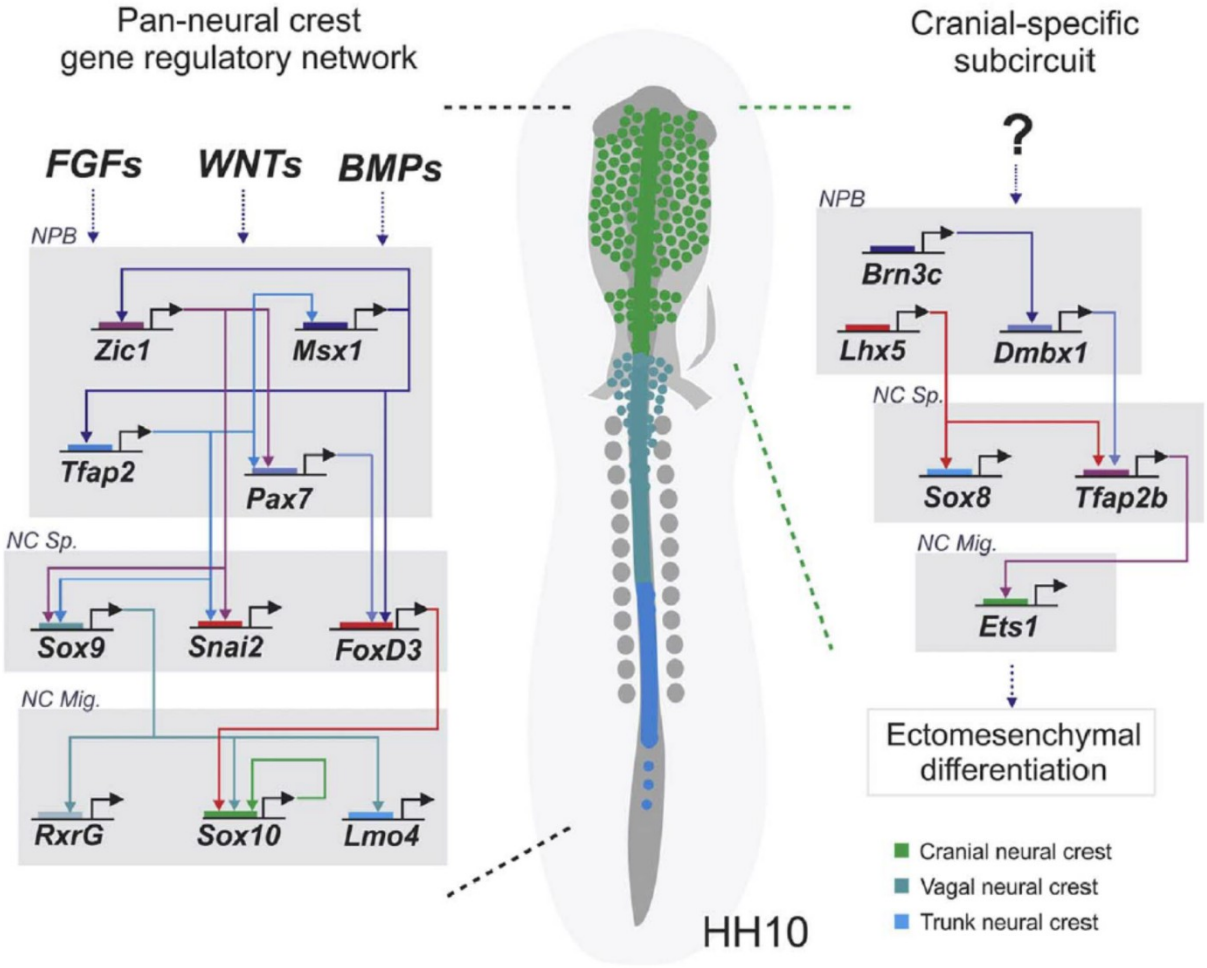

Figure 7 – Cranial-specific gene regulatory network provides ectomesenchymal potential. Cranial NCCs generate craniofacial skeleton, which is an axial-specific feature as it is the only subpopulation possessing ectomesenchymal potential in amniotes. This figure highlights the specificity of the cranial-specific gene regulatory network that supports ectomesenchymal differentiation. NPB: Neural Plate Border; NC Sp: Neural Crest Specification; NC. Mig: Neural Crest Migration (Image from (Rothstein et al., 2018)).

First, although expression of NCCs specifier genes like *sox10* and *FoxD3* can seem redundant at all axial levels, their expression is in fact regulated by different enhancers in the cranial and trunk NCCs (Betancur et al., 2010; Martik and Bronner, 2017; Simões-Costa et al., 2012). The fact that cranial and trunk NCCs need the activation of axial specific enhancers to undergo similar stages of specification could be explained by the heterogeneity of environmental signals at different axial levels. In fact, NCCs progenitors in the head and trunk are exposed to different retinoic acid, FGF and Wnt signals and show variable *Hox* genes expression (Trainor and Krumlauf, 2000). Anterior cranial NCCs are negative for Hox gene expression whereas more posterior NCCs populations (as cranial, vagal and trunk NCCs) are positive. The unique plasticity of anterior cranial NCCs, which allows them to generate ectomesenchyme, is linked to the absence of *Hox* genes expression. In contrast, posterior populations require *Hox* genes expression to properly differentiate (Creuzet et al.,

2002; Helms et al., 2005; Minoux et al., 2009). These axial specific discrepancies highlight that the general GRN proposed to rule NCC differentiation is in fact characterized by axial-specific sub-circuits. Simoes and Bronner recently uncovered a remarkable cranial-specific subcircuit composed of three transcription factors: *Ets1*, *Sox8* and *Tfap2b*. The expression of these factors in trunk NCCs is sufficient to reprogram these cells and give them the cranial-specific ability to generate cartilage (Simoes-Costa and Bronner, 2016). Thus, the generation of same cell-types by NCCs coming from different axial levels actually hides different specification routes.

Timing of emigration and migratory behaviors

An intriguing question is the timing of NCCs streams emigration from the neural tube. Is there a time-sequence among the different streams or are they all emigrating concomitantly? In chick embryos, trunk NCCs delaminate first at the most rostral level and delamination proceeds sequentially towards the caudal region. Nonetheless, there can be a significant variability among species regarding the timing of NCCs emigration. For example at the cranial level, birds NCCs emigrate as neural plate fusion occurs, whereas in mice they start emigrating earlier, when the neural plate is still open. This suggests that neural tube closure and NCCs delamination are functionally uncoupled (Copp et al., 2003). Then stands the question of trajectories after delamination. In fact, the pattern of NCCs emigration is very different at different axial levels. Even in the cranial category itself, while NCCs from the forebrain and midbrain undergo a massive delamination forming a continuous mesenchymal stream, cells from the hindbrain follow segmented trajectories forming three streams emanating from different rhombomere levels. These distinct streams sequentially colonize the three first pharyngeal arches and generate respectively, the jawbone, malleus and incus bones of the middle ear in the first pharyngeal arch, the hyoid bone and stapes bones of the ear in the second pharyngeal arch, and the thyroid and parathyroid in the third pharyngeal arch. Concerning the trunk NCCs, they consistently delaminate after neural tube closure in all species and show a progressive dripping pattern, different from the continuous wave observed for cranial NCCs (Davidson and Keller, 1999; Duband, 2010; Erickson and Weston, 1983; Kalcheim and Burstyn-Cohen, 2003). Like the caudal cranial NCCs, the trunks NCCs mostly migrate following well-defined and segmented streams. Different routes are thus created. At first, trunk NCCs favor a ventral unsegmented pathway between the neural tube and the early somites. Later on, as somite maturation occurs, NCCs gain segmented trajectories, passing through the anterior half of somites (in the sclerotome and along the dermomyotome basement membrane) (Erickson and Weston, 1983; Kuriyama and Mayor, 2008). The segmented streams are delimited by signals and physical barriers emanating from the somites and the neural tube. Another route is taken dorsolaterally between the ectoderm and the dermomyotome. While NCCs from the ventral pathway will give rise to the dorsal root ganglia, sympathetic ganglia and glial cells, NCCs from the dorsolateral pathway generate melanocytes (Douarin and Kalcheim, 1999; Vermeren et al., 2003).

Regulatory interactions and molecular control during NCCs migration

Although an axial specific priming of NCCs, induced by *Hox* and *Ephrin* genes pattern of expression might exist, the general view is that NCCs are plastic and respond to environmental cues while migrating, which explains how they form the stereotypical and robust trajectories observed *in vivo* (Theveneau and Mayor, 2012). Experiments have shown indeed that grafted NCCs gain the specific trajectory of the NCCs of their axial hosting niche, which convincingly demonstrates NCCs plasticity (Douarin et al., 2004). Two families of signaling molecules have been shown to participate in establishing NCCs trajectories by preventing entry in untargeted areas, thus refining NCCs pathways. Ephrins and semaphorins, respectively binding to ephrin receptors and neuropilin receptors, can induce the collapse of cell protrusions and therefore inhibit migration (Mellott and Burke, 2008). Results suggest that the different streams of NCCS express distinct ephrins and that their surrounding tissues express complementary receptors. This NCCs-tissue complementarity guides the NCCs, preventing the different streams of NCCs to intermingle and invade untargeted regions (Baker and Antin, 2003; Smith et al., 1997). In fact, impairing ephrins can lead to defect in NCCs stream segregation. Likewise, when semaphorin signaling is affected, NCCs invade traditionally NCCs-free areas (Gammill et al., 2006; Osborne et al., 2005; Yu and Moens, 2005). NCCs express Neuropilin 1 and Neuropilin 2, which are responsible for the binding of semaphorin ligands. Neuropilins associate with co-receptors of the plexin family, which in turn trigger the intracellular signaling (Eickholt, 2008). Interestingly, neuropilins can also play a receptor function for VEGF signaling, where the co-receptor function is played by VEGF receptors (McLennan et al., 2010). This dual signaling involvement of neuropilins might explain why NCCs are able to invade semaphorin class-3 positive pharyngeal arches, whereas the semaphorin class-3 are potent inhibitor of NCCs migration at more dorsal locations (Gammill et al., 2007). This could be due to a loss of sensitivity of neuropilins to semaphorins at the advantage of VEGF signaling. Remarkably, the negative regulation of class-3 semaphorins ensuring proper segregation of NCCs streams, is followed by a positive regulation attracting cardiac NCCs to the outflow tract region (Plein et al., 2015; Toyofuku et al., 2008). Hence, these results suggest that the neuropilin receptors can switch their engagement to signaling pathways and may segregate either to VEGF receptors or neuropilin receptors depending on environmental cues.

In terms of positive cues that tune NCCs behavior during migration, two types of molecules stand out: the chemoattractants signaling to NCCs and attracting them to homing tissues, and the permissive factors facilitating their motion in the extracellular matrix. FGF, VEGF and PDGF growth factors were shown to be involved in NCCs migration but it is not yet clear if their play permissive or chemoattractant roles in NCCs environment (Richarte et al., 2007). For example, while FGFs seem to play a non-cell autonomous permissive role during NCCs migration to the second pharyngeal arch, they also act as a chemoattractants as cardiac NCCs approach the heart outflow tract (Sato et al., 2011; Trokovic et al., 2004). NCCs

trajectories are also restrained by physical barriers. In fact, while some extracellular proteins as laminins and fibronectins create permissive paths for NCCs, other components of the extracellular matrix are playing restraining roles. They participate in creating nonpermissive environments aside NCCs trajectories comparable to railings. For example, F-spondin and Versicans are involved in proper NCCs stream establishment by creating non-permissive environments along NCCs paths (Debby-Brafman et al., 1999; Dutt et al., 2006).

Cell-Cell interactions and signaling on the way to the homing niche

It was observed that migrating NCCs keep long and short-range cell communication while migrating. They are mostly engaged in chains rather than migrating individually and it is known that cells in chains have a higher directionality (Kulesa and Fraser, 1998; Teddy and Kulesa, 2004). The Mayor group and others have elegantly refined the mechanisms responsible for NCCs collective migration. This migration is both coordinated and cooperative, and thus implies NCCs interactions. The first mechanism uncovered was Contact Inhibition of Locomotion (CIL), that is to say, the process whereby cells making contact repolarize away from one another and separate (Abercrombie and Dunn, 1975; Carmona-Fontaine et al., 2008) (Figure 8, page 43). CIL is mediated by the Wnt non-canonical pathway, also called Planar Cell Polarity (PCP) pathway, which signals through N-Cadherin. In fact, the polarity of cellsis mediated by the axis of RhoA-Rac1 localization in the cells. Cell contacts create transient N-Cadherin binding, inversing the cell polarity and pushing cells apart. In other words, upon collison, NCCs retract their protrusions and repolarizes in the opposite direction. But this cannot be the sole existing mechanism ruling NCCs migration, otherwise NCCs would keep moving apart and would never create well-patterned streams. Co-attraction is the second mechanism uncovered in Xenopus that allows NCCs to remain as a chain by secreting and positively responding to the chemoattractant C3a (Carmona-Fontaine et al., 2011) (Figure 8, page 43). Thanks to this mutual attraction, NCCs are migrating towards regions of higher NCCs density, which prevents uncontrolled dispersion of the NCCs and maintains NNCs streams integrity. Thus, negative short-range interactions and positive long-range interactions give a polarity to the NCCs stream. The third mechanism, called confinement, is obtained thanks to the physical barriers like Versican and other negative signals mentioned above. Acting as railways, confinement enhances directional collective NCCs migration (Szabó et al., 2016) (Figure 8, page 43). In summary, these observations highlight that migrating NCCs take decisions based upon the signals emitted by their environment but also that their ability to respond is tuned by co-interactions with NCCs. The mechanisms supporting directional NCCs migration have been mostly described in cranial *Xenopus* NCCs, which questions whether we should yet generalize this vision to the trunk NCCs of other species.

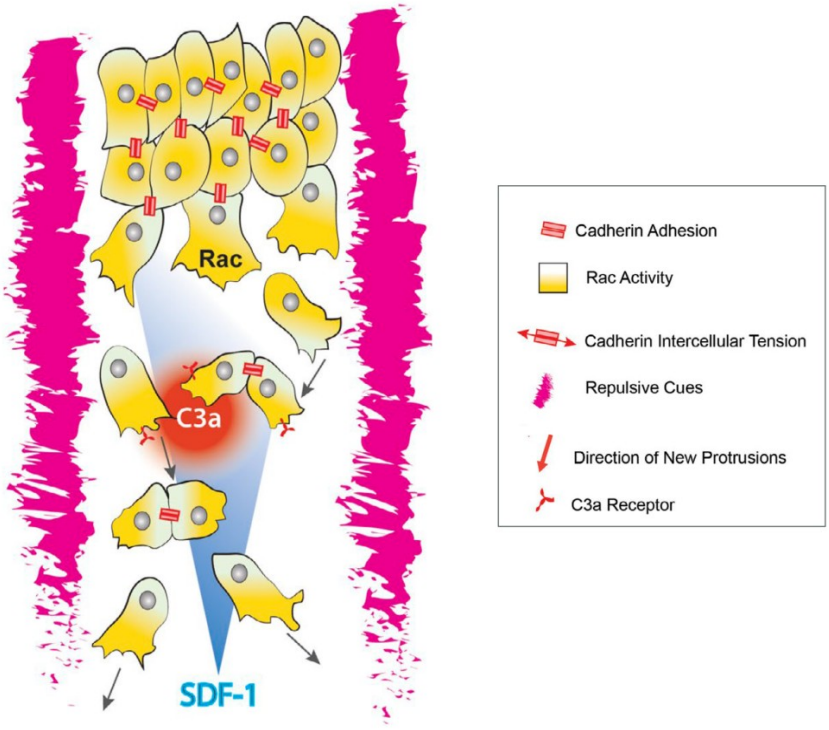

Figure 8 – Mechanisms driving the collective migration of NCCs. First, Contact inhibition of locomotion (CIL) describes a phenomenon where NCCs making contact repolarize away from one another and migrate appart. It promotes formation of large protrusions in cells at the front of the group because of polarized Rac1 activity, leading to monolayering and cell dispersion. Second, the confinment parameter encompass the repulsive cues that surround NCCs streams (such as Versican, Ephrins and Semaphorins) that restrict NCCs migration in a limited space and therefore favors cell–cell interactions. In addition, co-attraction comes from the autocrine signaling of NCCs through the C3a chemokine and C3aR receptor. This opposes cell dispersion by attracting NCCs toward one another and ensures NCCs stream integrity. Finally, a gradient of the chemokine SDF-1 confers directionality to the migrating collective (Adapted from (Scarpa and Mayor, 2016)).

I.2.2 The evolution of the vertebrate circulatory system is linked to NCCs

The cardiac NCCs evolution

At the evolutionary timescale, the current vision is that the appearance of NCCs provided a key advantage in the emergence of vertebrates from protochordates (Gans and Northcutt, 1983). This transition was characterized by the acquisition of facial and skeletal tissues (Ayer-Le Lievre and Le Douarin, 1982). The ectomesenchyme derived from the NCCs supposedly enabled the remodeling of the chordate head and enabled the transition from the filter-feeding strategy of swarm-like creatures to the more active-feeding of predatory vertebrates. Hence, NCCs widened the evolutionary prospects of the newly evolved vertebrate species compared to the simpler chordates. *Amphioxus* is an interesting model species because vertebrates are thought to have evolved from such a cephalochordate (Le

Douarin and Dupin, 2012; Meulemans and Bronner-Fraser, 2004). Interestingly, *Amphioxus* do not have NCCs, which appears to confirm that NCCs were a vertebrate innovation. Although parts of the NCCs specifier genes and paracrine signals are observed in *Amphioxus* and other chordates, many are lacking such as *Snail2*. This corroborates the idea that new levels of regulation in gene regulatory networks co-opted the emergence of NCCs during vertebrate evolution (Yu et al., 2008). On the other hand, the study of early vertebrate fossils revealed an astonishing fact. Early in vertebrate evolution and transiently during evolution, NCCs have provided vertebrates with an ectoderm-derived exoskeletal protection covering their whole bodies. Progressively, this exoskeleton disappeared to give room to an endoskeleton derived from the somitic sclerotome that characterizes current vertebrates. The origin of the skeletal support of vertebrate bodies thus shifted from an ectodermal to a mesodermal origin. However, the rostral part of the NCCs-derived exoskeleton remained at the cranial level and today provides vertebrate species with a skull. This rostral exoskeleton surely played a crucial role in vertebrates evolution by protecting their brains (Dupin and Sommer, 2012; Le Douarin and Dupin, 2012; Smith, 1991; Smith and Hall, 1990).

By adapting to a terrestrial lifestyle, vertebrate species went through a transition from respiration supported by gills to respiration supported by internal structures, the lungs. In aquatic species like fishes, blood is oxygenated by flowing through the gills, a bilateral capillary network interrupting the six branchial arch arteries. As terrestrial vertebrate became exclusively air-breathing, critical modifications were brought to the branchial arches region. In fact, this region did not have to support the bilateral gills structure anymore and the pharyngeal arteries were remodelled to form a double-circulation system perfectly connected to the heart. Concomitantly, the skeletal and muscular elements of the gills were re-purposed to neck pharyngeal structures (Keyte et al., 2014). It is still visible in amphibians development, where larvae possess gills, which transform into internal vasculature during embryonic development (DeLong, 1962). This metamorphosis goes through a remodelling of the pharyngeal arteries also observed in other vertebrates. NCCs played a determinant role in the remodelling of the great arteries. A specific stream of NCCs termed the cardiac NCCs emerged and its primary function was most likely to remodel and reinforce branchial arch arteries by providing smooth muscle tunics to these arteries (Bergwerff et al., 1998; Lee and Saint-Jeannet, 2011). The general assumption in the field is that, after having been recruited to the pharyngeal region, cardiac NCCs were then further attracted to the outflow region of the heart. In fact, the ventral aspect of the pharyngeal arches lies in close proximity to the heart outflow tract. In the outflow tract region, NCCs have the key function of supporting outflow tract septation, providing birds and mammals with a fully separated double circulation materialised by the formation of aortic and pulmonary arteries (Keyte et al., 2014). Interestingly in *Xenopus*, cardiac NCCs seem never to enter the outflow tract but remain in the pharyngeal region. This suggests that outflow tract septation is an evolutionary trait acquired by higher vertebrates (birds and mammals), the selective

pressure of gaining a double circulation enabling their terrestrial invasion (Chin et al., 2012; Lee and Saint-Jeannet, 2011).

The cardiac NCCs discovery

The crucial need of cardiac NCCs for proper double circulation development and outflow tract septation was first recognized in 1983 by M. Kirby (Kirby et al., 1983). In fact, experiments of NCCs ablation between the mid-otic placode and the third somite show persistent truncus arteriosus (i.e. unseptated outflow tract), which was the first proof of NCCs involvement in the outflow tract septation process. The ablation experiments also resulted in abnormal myocardial function and defects in pharyngeal arch arteries (PAA) formation. Hence, the subpopulation of NCCs delaminating between the mid-otic placode and third somite was termed cardiac NCCs although they not only contribute to the development of the arterial pole of the heart, but also to the pharyngeal arteries remodelling and reinforcement (Bockman et al., 1987). Interestingly, a recent study uncovered the cardiac contribution of a second more anterior pre-otic NCCs population (Arima et al., 2012). This population, described in birds and mice, seems to contribute to the smooth muscle of the later forming coronary arteries.

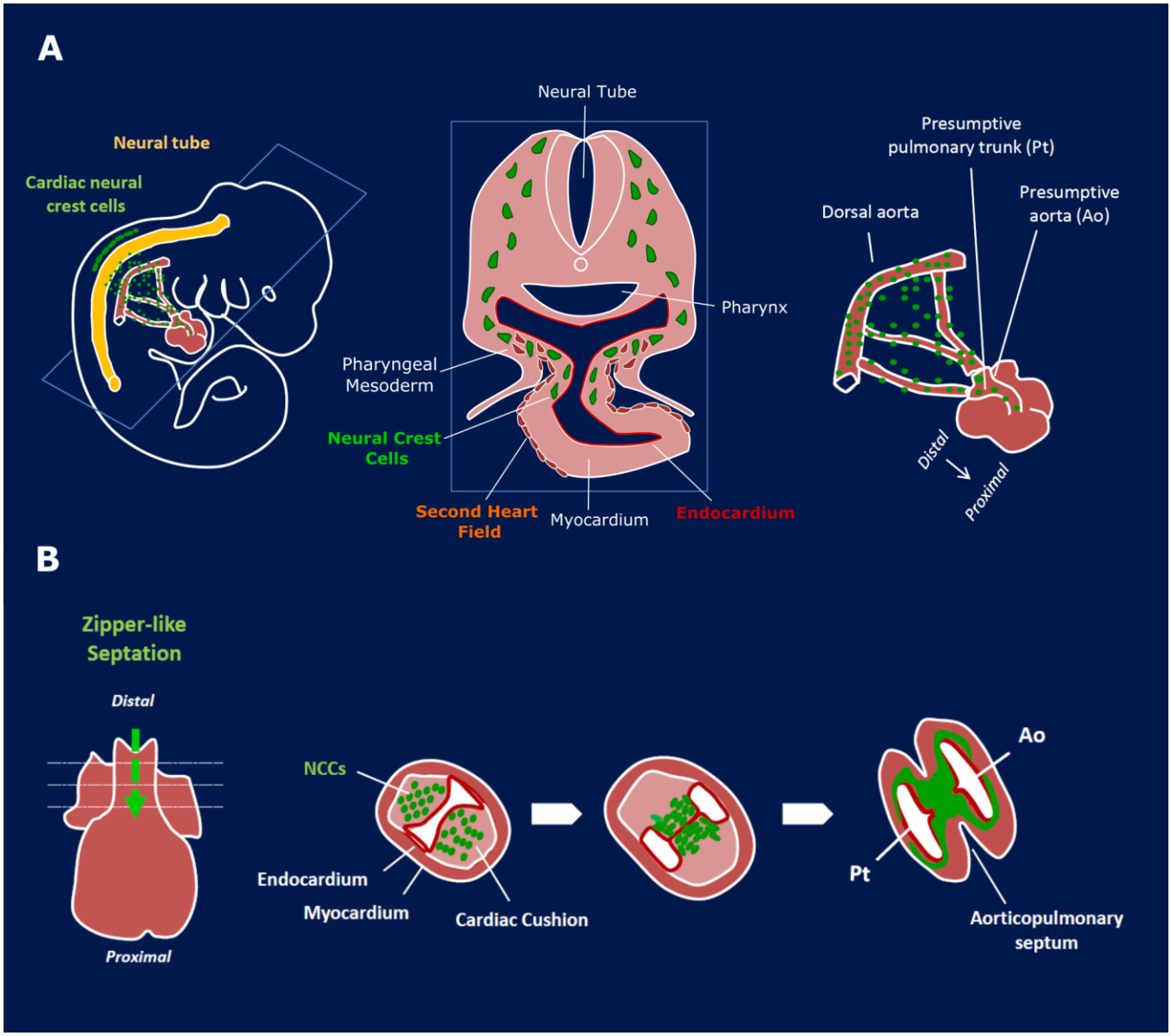

Figure 9 – Cardiac NCCs path to outflow tract (OFT) septation. **A.** The cardiac stream of NCCs delaminates from the neural tube and NCCs migrate to the circumpharyngeal region, where they receive signals from the surrounding pharyngeal layers (endoderm, ectoderm and mesoderm). The second heart field (SHF) derives from the pharyngeal mesoderm, ingress and elongates the primary heart tube. Subsequently, the NCCs colonize the OFT cardiac cushions. **B.** At E10.5 in mice, the NCCs are postionned in the cardiac cushions between the outer myocardium and inner endocardium. OFT septation starts at the distal OFT level with the convergence of the NCCs towards the endocardium. This phenomenon triggers the breakdown of the inner endocardium, the fusion of the cardiac cushions and the separation of the aorta from the pulmonary artery. The newly formed aortico-pulmonary septum is strenghtened by the NCCs-dependent ingrowth of myocardium. The sepation process spans the whole length of the OFT in a zipper-like, distal to proximal fashion, to ultimately fuse with the ventricular septum, and allow complete separation of the systemic and pulmonary circulations at birth.

The cardiac NCCs path to outflow tract septation

Cardiac NCCs delaminate from the dorsal neural tube at approximately E8.5 in mice and migrate ventrally to accumulate in the circumpharyngeal ridge (Figure 9, page 46) (Hutson and Kirby, 2010; Kuratani and Kirby, 1992). They later migrate further through the pharyngeal mesoderm (between the pharyngeal ectoderm and endoderm) to reach the pharyngeal arches three, four and six. In the arches, they proliferate and participate to the arch arteries remodelling. In fact, the pharyngeal arch arteries are first formed as symmetric pairs of vessels connecting the aortic sac and the dorsal aortas. Later, some arteries segments regress to finally reach the asymmetric double circulation of birds and mammals. For example, the third arch arteries give rise to the common carotids, one of the fourth arch artery give rise to the aorta, whereas the fifth arch arteries regress and the sixth generate the pulmonary arteries (Anderson et al., 2016). While some NCCs remain in the pharyngeal area, a subset of NCCs migrate into the heart outflow tract (Figure 9, page 46). Around E10, they invade the outflow tract swellings, called cardiac cushions, filled with extracellular matrix of endocardial origin. These cushions are positioned along the tube, on both sides of the endocardium. Hence, NCCs form two lateral columns positioned in the two cushions spanning the tube length from the distal to the proximal end, the proximal end being attached to the right ventricle. After colonizing the cardiac cushions, NCCs condensate towards the endocardium that delineates the tube lumen. This NCCs condensation process is thought to trigger the rupture of the endocardium and the fusion of the cardiac cushions (Plein et al., 2015; Waldo et al., 1998). At E11.5 the distal lumen is divided in two. NCCs are positioned centrally between the two newly formed tubes and form the so-called aorticopulmonary septation complex. This complex is consolidated on the sides by myocardial ingrowth, a process called myocardialization, giving rise to the muscular septum separating the pulmonary and systemic circulations (van den Hoff and Moorman, 2005; van den Hoff et al., 1999). Hence, the aorticopulmonary complex divides the common arterial trunk into the aortic and pulmonary trunks. This process happens in a zipper-like fashion from the distal to the proximal end of the tube. Because distally this septation starts between the fourth and sixth arch arteries, which respectively generate the aorta and the pulmonary arteries, the aorticopulmonary complex is perfectly positioned to divide the systemic and pulmonary circulations. More proximally, the leading edge of the septum eventually attaches to the interventricular septum, enabling the connection of the aorta and pulmonary artery to the ventricles. The outflow tract septum is spiraling in a 180° rotation from the distal to the proximal level. This enables the proper alignment of the great arteries with their respective ventricles (Bajolle et al., 2006; Lomonico et al., 1986).

A complex dialogue exist between cardiac NCCs and the other cell-types composing the outflow tract

The septation of the outflow tract requires a complex temporal and spatial coordination of three main cell types. The second heart field (SHF) myocardial progenitors constitute the outer-ring of the OFT, the endocardial progenitors (ECs) delineate the inner lumen, and the neural crest cells (NCCs) form most of the cardiac cushion mesenchyme, at least at the distal level. All three cell types operate movements in the developing OFT. ECs go through an EMT process colonizing the cardiac cushions, SHF progenitors add to the primitive tube to elongate it and allow chambers formation, and the NCCs colonize the cardiac cushions and trigger the septation process. All these cell-types signal to each other. In fact, experiments affecting one cell type can lead to anomalies of behavior of the others. For example, specific gene deletions in the SHF that impair proper myocardium differentiation, affected SHF signaling to the NCCs, leading to defects in NCCs attraction and OFT septation failure (High et al., 2009). On the other hand, cardiac NCCs play a key role for SHF development before entering the OFT. Their signaling is in fact required for the OFT deployment and heart tube elongation (Waldo et al., 2005). This raises the very intriguing question of SHF and NCCs co-evolution. The general view is that SHF evolved to allow the morphogenesis of a longer heart tube able to fold and form extra chambers. On the other hand, the NCCs would have evolved to support outflow tract septation and thus connect the chambered heart with a properly divided circulation (Keyte and Hutson, 2012). A cross-species comparison in vertebrates has unraveled consistency in the outflow tract composition in myocardium and smooth muscle during evolution. The study suggests that the outflow tract is invariably constituted of three distinct segments in vertebrates. It is layered from the proximal to the distal level, with a distal smooth muscle component called truncus, a proximal myocardial component called conus, and a middle component constituted of both cell-types (Grimes et al., 2010). The SHF forms a continuum of differentiation, first differentiating in myocardium for the major part of the OFT and then in smooth muscle (van den Hoff et al., 1999) (Figure 10, page 49). Hence, after that the SHF evolution elongated the outflow, the distal smooth muscle outflow tract, gained the ability to attract the NCCs from the pharyngeal region to the heart (Grimes et al., 2010).

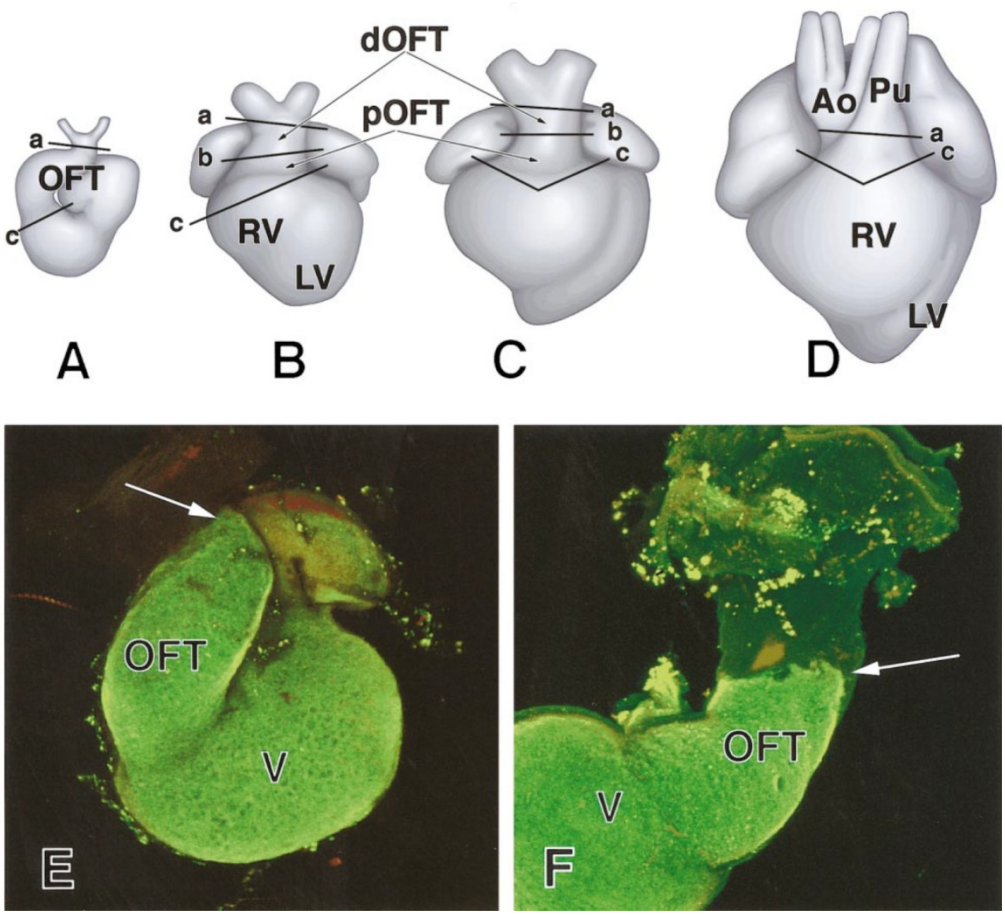

Figure 10 – Development and myocardialization of the OFT (here chick embryos). **A-D.** Cartoons of embryonic chick hearts. **E-F.** Isolated chicken hearts at stages HH21 (**E**) and HH26 (**F**) processed for whole-mount immunofluorescence using the monoclonal antibody MF20 against myosin heavy chain and imaged using scanning laser confocal microscopy. The arrow in **E** indicates the distal boundary of the myocardial OFT close to the junction with the aortic sac. The arrow in **F** indicates how this boundary has shifted as a result of differential fate of the SHF, first differentiating in myocardium and then in smooth muscle as its addition to the heart tube proceeds. pOFT, proximal OFT; dOFT, distal OFT; Ao, aorta; LV, left ventricle; RV, right ventricle; V, ventricle (Image and legend from (van den Hoff et al., 1999)).

I.2.3 NCCs dialogue with the outflow environment drives OFT septation and valve formation

NCCs and SHF deployment are regulated by paracrine and autocrine signals

Phylogeny informs ontogeny. We previously described how NCCs and SHF lineages very likely co-evolved and respectively provided the vertebrate heart with chambers and a septated outflow tract. These two progenitor populations interact through a complex dialogue, first in the pharyngeal region, and later in the outflow region. The specific SHF properties of continued proliferation in the pharyngeal mesoderm and delayed differentiation in the OFT, are regulated by the NCCs and other environmental cues.

Reciprocally, NCCs migration and contribution to the arterial pole of the heart are tuned by SHF paracrine signals and other environmental cues. The environmental signals sensed by the SHF and NCCs in the OFT are numerous: self autocrine signals, paracrine signals from endocardial cells or pharyngeal endoderm and ectoderm, as well as mechanical stress caused by blood flow and outflow contraction. These signals regulate a diversity of transcription factors in the responding progenitors, which in turn regulate their behavior, survival, proliferation and differentiation.

A first family of growth factors impacting outflow tract progenitors is the FGF family. In the pharyngeal region, Fgf3, Fgf8 and Fgf10 are secreted by pharyngeal endoderm, mesoderm and ectoderm (Aggarwal et al., 2006). But what is the influence of the Fgf signals on SHF progenitors? Fgf10 was the first known marker of the SHF, therefore potentially acting as an autocrine signaling on the SHF (Kelly et al., 2001). SHF deployment occurs normally in Fgf10 null embryos yet Fgf10 deletion increases the severity of the defects in embryos where Fgf8 was also deleted in the cardiac mesoderm (Marguerie et al., 2006; Watanabe et al., 2010). In fact, the specific deletion of Fgf8 in the cardiac mesoderm resulted in decreased proliferation and survival of SHF progenitors and defects in its contribution to outflow tract elongation (Ilagan et al., 2006). Fgf8 is thus considered as the major Fgf ligand regulating SHF proliferation by acting on Erk intracellular signaling (Tirosh-Finkel et al., 2010). Interestingly, Fgf8 plays an autocrine signaling role on SHF progenitors, which is critical for SHF contribution to the OFT and thus tube elongation. Notch, Wnt and Hedgehog signaling act upstream of FGF signaling. They regulate major cardiogenic transcription factors as Isl1 and Tbx1. In turn, these transcription factors control FGF ligand expression (and antagonize BMP and RA signaling)(Garg et al., 2001; High et al., 2009; Roberts et al., 2005; Vitelli et al., 2002; Xu et al., 2004). In sum, Isl1 and Tbx1 play a central integrating function for sensing the paracrine and autocrine cues and control FGF secretion responsible of SHF differentiation (Figure 11, page 52).

What are the effects of such FGF signals on NCCs? Fgf8 signals are chemotactic for NCCs and attract them to the pharyngeal region. Indeed, when Fgf8 is overexpressed in the pharyngeal region, greater numbers of NCCs migrate and colonize more quickly the arches (Sato et al., 2011). In the wild type condition, when NCCs enter the arches, Fgf8 is expressed at high levels in the pharyngeal endoderm and ectoderm, and at lower levels in the SHF generating splanchnic mesoderm. Fgf8 signaling to the NCCs appears required for NCCs survival. In fact, specifically deleting Fgf8 or generating hypomorphic mutants showed abnormal apoptosis of the NCCs (Abu-Issa et al., 2002; Frank et al., 2002; Macatee et al., 2003). Reciprocally, NCCs also act on FGF signaling. In fact, NCCs ablation causes an increase in Fgf8 expression in the pharyngeal area, linked with overproliferation of the SHF in this area. Thus, NCCs play a role of buffer for FGF signals by secreting a still unknown inhibitor of Fgf8 expression, primordial to limit SHF proliferation (Hutson et al., 2006; Tang et al., 2010). Remarkably, inhibiting FGF partly rescues OFT development (its alignment but not its

septation) in embryos ablated for NCCs (Hutson et al., 2006). To conclude, the FGF8 signaling pathway has multiple roles on NCCs survival and migration, as well as on SHF proliferation and addition to the developing outflow tract. The emergence of this pathway must have represented a key step towards septation of the cardiac outflow tract during evolution (Keyte et al., 2014).

The notion of synexpression groups identifies sets of genes that share a similar spatial expression pattern, are simultaneously regulated, and are involved in the same biological process (Tirosh-Finkel et al., 2010). Tirosh-Finkel *et al.* show in chick embryos that members of the FGF synexpression group (*Fgf3/8/18/19*, *Sprouty2*, *Pea3*, *Erm*, *Sef*) and BMP synexpression group (*Bambi*, *Smad6*, *BmprII*) are expressed in a mutually exclusive way in the dorsal pharyngeal area for FGF, versus the ventral pharyngeal area close to the heart tube for BMP. In fact, BMP signals are secreted more ventrally by the SHF-derived myocardium located in the outflow tract. These BMP signals (Bmp2/4/6/7) are sensed by NCCs and SHF progenitors at later stages of migration when approaching the distal heart tube (Jiao et al., 2003; Jones et al., 1991, 1991; Kaartinen et al., 2004; Kim et al., 2001; Liu et al., 2004; McCulley et al., 2008) (Figure 11, page 52). In opposition to Fgf8 causing SHF proliferation, BMP signals are known to drive SHF differentiation (Hutson et al., 2010; Tirosh-Finkel et al., 2010). Waldo et al. showed that blocking BMP signaling inhibited SHF differentiation and identified BMP signals secreted by the outflow myocardium as attracting SHF to the elongating outflow tract (Waldo et al., 2001). In addition, deleting *Bmp4* in the SHF up-regulates SHF proliferation (Liu et al., 2004). As regards the pathway regulation, Isl1 and Tbx1 TFs control BMP ligand expression, while BMP signaling downregulates *Isl1* expression in the SHF (Fulcoli et al., 2009; Yang et al., 2006). FGF signaling itself upregulates *Bmp4* expression in the outflow tract myocardium, thus triggering its own downregulation (Zhang et al., 2010). Similarly, Nkx2.5 brakes BMP signaling, which itself is necessary for *Nkx2.5* expression, creating a negative feedback loop (Prall et al., 2007). Pro-differentiation BMP signals are thus inducing a switch of state for SHF progenitors. The SHF progenitor pool is expanding under the influence of FGF signals in the pharyngeal area, but start differentiating while approaching the heart tube under the influence of BMP signals. The differentiation of cardiomyocytes is characterized by an increase in sarcomeric organization and electrophysiological maturation, both required for emergence of contractions (Martin-Puig et al., 2008; Tirosh-Finkel et al., 2010). This translates into an induction of myofibrillar gene expression in the pharyngeal SHF, as Myosins heavy chains, troponin C, and tropomyosin. Additionally, Retinoic acid and noncanonical Wnt signaling have also been shown to regulate SHF deployment. While Retinoic acid has been shown to regulate the anteroposterior regionalization of the SHF by modulating cardiogenic specifier genes (Ryckebusch et al., 2008; Sirbu et al., 2008). Concerning the PCP pathway (non canonical Wnt), Wnt5a and Wnt11 have been shown to up-regulate SHF differentiation (Schleiffarth et al., 2007; Zhou et al., 2007).

In sum, the presence of NCCs adds a layer of regulation to SHF differentiation. As mentioned previously, signals from the NCCs brake FGF expression in the SHF. Thus NCCs regulate the balance between pro-proliferation FGF signals and pro-differentiation BMP signals (Figure 11, page 52). Moreover, it is believed that BMP signals enhance the paracrine action of NCCs on SHF. In fact, BMP gain-of-function experiments in chick NCCs induces *Msx1* and *Msx2* expression and decreases FGF ligand expression and FGF signaling (Tirosh-Finkel et al., 2010). In parallel, BMP signaling also modulates the proliferative effect of hedgehog signaling in the SHF (Dyer et al., 2010).

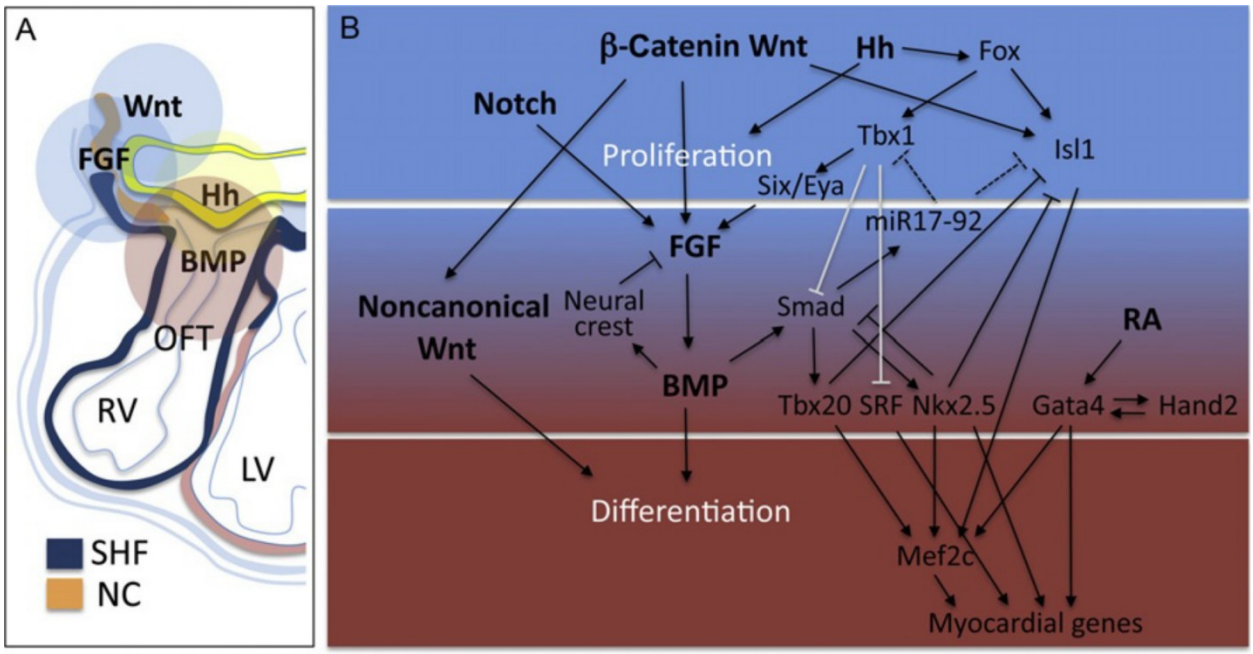

Figure 11- Regulation of SHF deployment in the OFT. It is regulated by paracrine and autocrine signals, which are integrated by complex gene regulatory networks. **A.** Cartoon showing zones of Wnt, fibroblast growth factor (FGF), Hedgehog (Hh), and bone morphogenetic protein (BMP) signaling at the arterial pole of the mouse heart. **B.** Representation showing the network of major signaling pathways and regulatory genes regulating SHF development. The differentiation process is presented from the top (proliferating progenitor cells) to the bottom (differentiated cardiomyocytes). At the top, we can observe in central position Isl1 and Tbx1 transcription factors regulating the proliferative progenitor state. In the middle, the FGF/BMP antagonism has a pivotal role in controlling the balance between proliferation and differentiation of SHF progenitors. LV: left ventricle; RV: right ventricle; OFT: outflow tract; SHF: second heart field; NC, neural crest cells. Gray lines, direct protein interactions; dotted lines, microRNA silencing (Figure from (Kelly, 2012)).

NCCs do not only inhibit SHF proliferation in the dorsal pharyngeal area, they also actively trigger the outflow tract septation process when they reach the ventral pharyngeal area and cardiac cushions (Kirby et al., 1983). BMP signaling is required for NCCs to play their part in OFT septation. Multiple NCCs specific conditional loss-of-function of BMP signaling were performed either by deletion of BMP receptors or intracellular Smad effectors. Deleting BMP receptor IA in mouse using the NCCs specific Wnt1Cre leads to hypoplastic cushions,

absence of outflow tract septation (i.e. persistent truncus arteriosus) and mid-gestation embryonic death due to acute heart failure (Stottmann et al., 2004). A shorter outflow tract was also observed in link with reduced SHF proliferation and thus reduced tract elongation. It was also shown that the cardiac cushions derived from the NCCs play a critical valve-like function before septation (Nomura-Kitabayashi et al., 2009). This function is impaired in embryos with impaired BMP signaling in the NCCs, causing a retrograde blood flow during diastole. The hypoplasia and shortening of the cardiac cushions show that BMP signaling in NCCs is crucial for their contribution to the cardiac cushions. In a complementary manner, Jia et al. observed a severe OFT cushions hypoplasia and OFT septation failure by deleting *Smad4* in the NCCs (Jia et al., 2007). Interestingly, they show that intracellular blocking of BMP signalling causes a strong decrease in *Semaphorin-3c* (*Sema3c*) and PlexinA2 expression, suggesting that Semaphorin paracrine signals might be important during OFT septation.

At the anterior pole of the heart where lies the OFT, the presumptive aortic and pulmonary myocardia are developmentally distinct (Bajolle et al., 2008; Bertrand et al., 2011; Rochais et al., 2009; Théveniau-Ruissy et al., 2008) (Figure 12, page 54). Prior to addition to the outflow tract, the SHF localized in the pharyngeal region is pre-patterned in discrete myocardial subdomains that respectively add to the superior and inferior wall of the outflow tract and later to the base of the aorta and pulmonary artery (Keyte et al., 2014). The correct ingression of both subpopulations is crucial for the correct elongation and rotation of the OFT and subsequent alignment of the great arteries with the ventricles. Hence, the outflow tract myocardium derives from different anteroposterior subpopulations of SHF. More specifically, the subpulmonary myocardium derives from both anterior and posterior SHF while the subaortic myocardium seems to exclusively derive from the anterior SHF (Domínguez et al., 2012; Rana et al., 2014). *Tbx1* has been shown to be required for the deployment and segregation of the posterior SHF to the subpulmonary myocardium. In fact, the expression of *Tbx1* is required for the posterior, Hoxb1-positive, SHF to contribute to the subpulmonary myocardium (Domínguez et al., 2012; Rana et al., 2014). *Tbx1*$^{-/-}$ embryos have a missing or reduced subpulmonary myocardial domain causing traits characteristic of the Tetralogy of Fallot (Figure 14D, page 60). Furthermore, the reduction or absence of the subpulmonary myocardial domain leads to defect in cardiac NCCs ingression in the outflow tract and persistent truncus arteriosus, suggesting that subpulmonary myocardium is particularly involved in NCCs attraction to the OFT cushions. Very interestingly, Rana et al. showed that the future subpulmonary myocardium is characterized by a specific transcriptomic signature. Most of the genes enriched in this presumptive subpulmonary domain, and thus absent in *Tbx1*-/- mutant embryos, are linked to NCCs migration and attraction. Among the featured genes lie *Sema3c*, which was already known as a marker of subpulmonary myocardium as well as a chemoattractant of NCCs. *Nrp2*, the coreceptor of Sema3c, as well as *Barx1* and *Dlx2* also mark subpulmonary myocardium (Bajolle et al., 2006; Rana et al., 2014). As previously mentioned, Sema3c signals secreted by the outflow

tract myocardium are responsible for NCCS chemoattraction to the outflow tract. This signalling is required for outflow tract septation, as underlined by the persistent truncus arteriosus phenotype observed in *Sema3c* conditional or full knockout embryos (Feiner et al., 2001; Gitler et al., 2004; Plein et al., 2015). From an evolutionary point of view, the emergence of a Tbx1 regulation of Sema3c expression is very intriguing. It may have represented a turning point in the dialogue between SHF and NCCs, SHF gaining the ability to attract NCCs to the OFT, enabling OFT septation and providing a divided circulation to the embryos. Although the Sema3c attraction of NCCs to the OFT represents an attractive possibility, recent results question this hypothesis. In fact, Plein et al showed that a NCCs specific deletion of the receptors of Sema3c, Nrp1/2, did not prevent the NCCs from colonizing the cardiac cushions and trigger OFT septation (Plein et al., 2015).

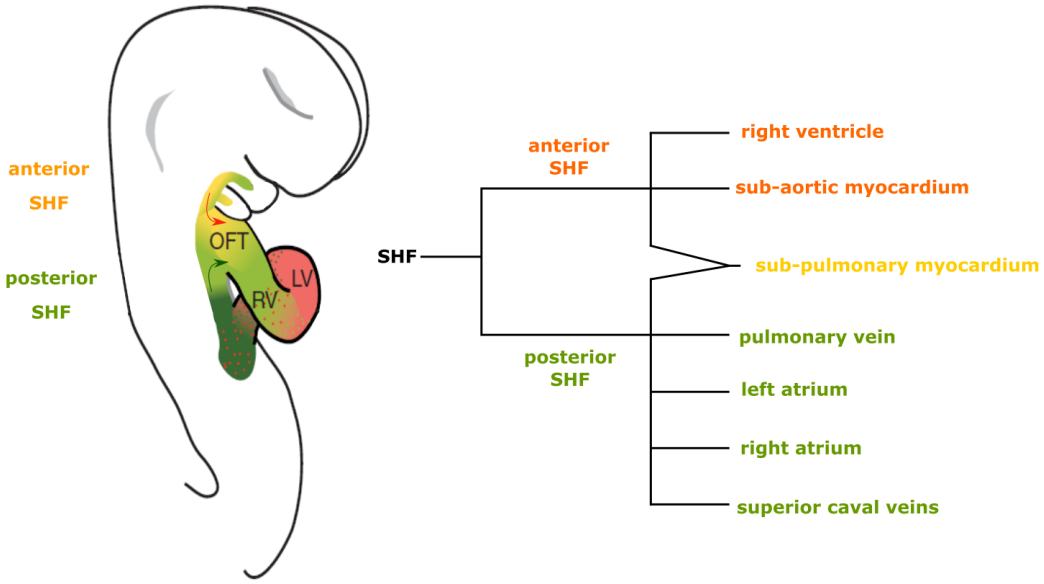

Figure 12 – Heterogeneity of the SHF at the arterial pole of the heart. At the arterial pole of the elongating heart tube, heterogeneity exists in the SHF contributing to the great arteries and to the right ventricle. In fact, both anterior and posterior SHF contribute to the tube elongation at the arterial pole. Interestingly, while the sub-aortic myocardium only derives from the anterior SHF, the sub-pulmonary myocardium has a dual lineage contribution from the anterior and posterior SHF. Hence, discrete myocardial subdomains respectively add to the superior and inferior wall of the outflow tract and subsequently seggregate between the the aorta and pulmonary artery (Adapted from (Meilhac et al., 2014)).

NCCs remodelling of the OFT

What is the specific role of cardiac NCCs during outflow tract septation? Recent results have unraveled molecular programs specifically regulating NCCs migration and function. Together with results ruling out the chemoattractive function of Sema3c to NCCs, Plein et al. showed that cardiac NCCs themselves actually secrete Sema3c signals in the cardiac cushions (Plein et al., 2015). The expression of *Sema3c* by the NCCs localized in the cardiac cushions is

corroborated by earlier studies (Brown et al., 2001; Feiner et al., 2001). We can conclude from these studies that the Sema3c signals orchestrate the dialogue between the endocardium, the NCCs and the OFT myocardium. Plein et al. results demonstrate that the expression of *Nrp1* in the endocardium, but not in the NCCs, is required for OFT septation. Moreover, they claim that the NCCs-derived Sema3c would signal through endocardial-Nrp1 to drive EMT of the endocardial cells, probably facilitating the rupture of the endocardium and the fusion of the cardiac cushions. Complementary to the weakening of the endocardium, the Sema3c-Nrp1 signaling seems to be required for the convergence of the NCCs towards the endocardium (Plein et al., 2015). This central convergence of the cardiac NCCs leads to the fusion of the bilateral columns of NCCs disto-proximally in a zipper-like fashion (Figure 9, page 46). On the other hand, NCCs-derived Sema3c signals are also signaling to the myocardium. In the myocardialization process, during which myocardial ingrowth strengthens the newly formed septum, myocardial cells follow centrally the NCCs converging towards the endocardium. Disrupting the convergence of the NCCs by deleting *Sema3c* in the NCCS leads to the downregulation of myocardilization, myocardial cells remaining in proximity to the laterally mislocalized NCCs (Plein et al., 2015). Even though Nrp1 also acts as a receptor for VegfA and was suggested to be involved in outflow tract remodeling, embryos with impaired VegfA-Nrp1 signaling show proper outflow septation (Plein et al., 2015; Stankunas et al., 2010). Plxnd1, a co-receptor of Nrp1, appears to be involved in the Sema3c-Nrp1 signal transduction in endocardial cells (Zhang et al., 2009). Taken together, all these results show that the essential Nrp1 receptor function is localized in endocardial cells and respond to NCCs-derived Sema3c to orchestrate outflow tract septation.

Regulation of Sema3c expression in NCCs and NCCs differentiation in smooth muscle

Cardiac NCCs start expressing *Sema3c* when colonizing the cardiac cushions at the distal part of the outflow tract. *Sema3c* expression is observed in the cardiac NCCs at E11.5 (Brown et al., 2001; Feiner et al., 2001; Plein et al., 2015). Fgf8 signals from the pharyngeal mesoderm, which inhibits SHF differentiation, have also recently been shown to downregulate the expression of *Sema3c* in the NCCs (Kodo et al., 2017). The Fgf8 inhibition of Sema3c seems to act intracellularly through ERK signaling. In fact, inhibiting ERK signaling in Fgf-stimulated NCCs caused an upregulation of *Sema3c* (Kodo et al., 2017). Moreover, *Sema3c* overexpression in cardiac NCCs primary cultures trigger NCCs aggregation (Kodo et al., 2017). Hence, the opposition between pharyngeal and outflow tract signals to control SHF maturation seems likewise to balance NCCs differentiation, or at least their ability to express *Sema3c*, while they migrate from the pharyngeal to the OFT territories.

Gata6, a member of the zinc finger family of transcription factors, has been described as an activator of *Sema3c* expression in the cardiac NCCs (Kodo et al., 2009; Lepore et al., 2006). Remarkably, Gata6 also regulates the expression of *Plxna2*, a co-receptor for the

semaphorin-3 and semaphorin-6 families. The phenotype observed in embryos with NCCs specific deletion of *Gata6* recapitulates the phenotypes described in the NCCs specific deletion of *Sema3c*, that is, OFT septation and alignment defects (Lepore et al., 2006). In humans, similarly to mice, *GATA6* mutations were associated with persistent truncus arteriosus conditions (Kodo et al., 2009). It is noteworthy that the intercellular signaling regulating *Gata6* expression in the cardiac NCCs remains unknown. Interestingly, although first evidence suggested a regulatory function of *Gata6* for NCCs differentiation in smooth muscle, a second study showed that the specific deletion of Gata6 in the NCCs did not impair their differentiation (Lepore et al., 2006). This results suggest that no impairment of smooth muscle NCCs differentiation should be involved in the OFT malformations observed in embryos with *Sema3c* or *Gata6* NCCs specific deletions. Rather, these defects should be caused by a lack of paracrine signals from the NCCs, and thus failure to orchestrate the coordination between the endocardium, myocardium and NCCs supporting OFT development.

NCCs contribution to arterial valve development

While playing a crucial role during OFT septation, NCCs also contribute to the formation and patterning of the arterial valves (de Lange et al., 2004; Lincoln et al., 2004; Nakamura et al., 2006; Odelin et al., 2018). The specific contribution of the NCCs to the arterial valves distinguishes the arterial valves from the atrioventricular valves. Fate mapping experiments have shown that NCCs are important contributors to the arterial valve primordium at E12.5 as the valve primordia are forming, but also at subsequent maturation stages. The formation of the arterial valves is in fact a remodelling of the cardiac cushions at a specific intermediate level of the OFT. This is where the junction between the distal septated OFT and the proximal conotruncus is happening. Above this level, the great arteries will ultimately be positioned, whereas under this level will lie the ventricular roots of the great arteries. Both arterial valves (aortic and pulmonary) are tricuspid. They derive in part from the NCCs, which contribute predominantly to the right and left leaflets of the valves, making reduced contribution to the non-coronary leaflets of the aortic and pulmonary valves (Jiang et al., 2000; Phillips et al., 2013). It is well established that the NCCs are not the unique mesenchymal contributors of the valves. Endocardial cells also represent a significant source of progenitors of the cardiac cushions mesenchyme along the outflow tract length and specifically at the level of valve formation. The endocardial contribution occurs through an EMT process and seems to be more significant at proximal OFT levels compared at the distal ones (Eisenberg and Markwald, 1995; Person et al., 2005). A point of inconsistency in the litterature is the survival of the NCCs in the arterial valves during embryogenesis. Whereas first fate mapping studies claimed that the ultimate contribution of NCCs was not significant in late embryos, recent studies show that the NCCs lineage represent a major part of the valves mesenchyme at late gestation stages (Jain et al., 2011; Jiang et al., 2000; Odelin et al., 2018; Phillips et al., 2013). This raises the question of the NCCs fate after valvulogenesis and

whether they undergo apoptosis or limited proliferation during late arterial maturation. In fact, some studies report significant NCCs apoptosis in arterial valves during late gestation (Jain et al., 2011; Poelmann and Gittenberger-de Groot, 2005; Zhang et al., 2010).

Regulatory pathways controlling heart valve development

Endocardial cells (ECs) contribute to valve leaflets by undergoing EMT and NCCs via migration. In the OFT, ECs and NCCs proliferate. Cell proliferation in the valve primordia is regulated by multiple signaling pathways. While Wnt/B-catenin, TGFBs, BMPs and Fgf4 are described as potent inducers of mesenchymal cell proliferation, EGF inhibits this process (Chen et al., 2000; Combs and Yutzey, 2009; McCulley et al., 2008; Person et al., 2005; Sugi et al., 2004; Zhao et al., 2007). Apart from cell proliferation, cardiac cushions and valve primordia grow by continued extracellular matrix (ECM) synthesis. Cardiac cushion ECM provides the physical support to mesenchymal cells behavior and cardiac cushions remodeling. Hence, the expression of proteins composing the ECM has to be tightly regulated. BMP and FGF signals have been shown to take part in the maturation of the arterial valves and in the diversification of the precursor cells composing it. In fact, on one side BMP signals promote cartilage-related *Sox9* and *Aggrecan* expression. On the other, FGF promotes tendon-related scleraxis and tenascin expression (Lincoln et al., 2006; Zhao et al., 2007). The multiple studies that have started unraveling the complex regulation of proliferation in valve primordia have not yet been able to discriminate between NCCs versus ECs specific regulatory effects. While we can assume that the regulatory pathways aforementioned affect similarly both lineages, doubts subsist.

Heterogeneity of the cardiac NCCs and function in valve formation

Very interestingly, recent results pave the way to the study of heterogeneity in NCCs that contribute to the arterial valves. NCCs of the Krox20 lineage (specifically emerging from the rhombomere r5 and r6 levels) seem to contribute specifically to the insertion zone of the valve leaflets and to the interleaflet triangle (Odelin et al., 2018). Deletion of *Krox20* causes increased NCCs migration from r6 and hyperplasia of the arterial valves, suggesting that the r5 NCCs stream provides important informations for proper arterial valvulogenesis. The precise role of the NCCs in arterial valves formation still remains open to debate. Some first clues emerged recently from the work of Philips *et al*. Their results suggest that, at the level of valve formation in the OFT, the correct aggregation and positioning of the NCCs is fundamental for the emergence of valve primordia (Phillips et al., 2013). In the context of OFT remodelling, components of the non-canonical Wnt signaling, such as *Vangl2*, *Wnt11*, *Dvl2*, *RhoA* and *Rock1/2*, are expressed in different cell-types. They orchestrate the complementary cell movements that remodel the cardiac cushions, notably NCCs condensation and myocardialization (Phillips et al., 2005, 2013). Likewise, the deletion in the

NCCs of proteins involved in cell-cell adhesion or cell adhesion to the extracellular matrix (ECM) impair the ability of cardiac NCCs to pattern the great arteries and the OFT. For example, N-Cadherin and Integrin-linked kinase (ILK) mutants present persistent truncus arteriosus, highlighting the importance of tissue-tissue interaction and of NCCs interaction with their environment to support the heart arterial pole development (Arnold et al., 2013; Luo et al., 2006).

Cardiac NCCs differentiation in vascular smooth muscle

Apart from arterial valve patterning, the ultimate fate of the cardiac NCCs is to form the smooth muscle lining of the pharyngeal, coronary and great arteries as well as to contribute to the cardiac conduction system (Arima et al., 2012; Jiang et al., 2000; Nakamura et al., 2006). The vascular remodelling at the arterial pole of the heart is similar in humans and mice; it is complex and asymmetric (Chen et al., 2015; Moon, 2008). In fact, the paired pharyngeal arteries are formed sequentially and some of their segments disintegrate to eventually form the vertebrate arterial tree (Figure 13, page 59). In mice, the left and right fourth arch arteries give rise respectively to the aortic arch and a segment of the subclavian arteries, the right sixth disappears and the left six persists to generate the ductus arteriosus (closing at birth). The development of vascular smooth muscle around the bilateral arch arteries is thought to reinforce and prevent the premature regression of these vessels, as well as to facilitate the asymmetrical remodelling. The NCCs extensively contribute to the vascular smooth muscle of the ductus arteriosus, the aorta, the aortic arch and the carotid arteries, but not to the dorsal aorta, subclavian arteries and neither to the emerging pulmonary arteries (Jiang et al., 2000). Notch signaling emanates from the vascular endothelium and plays a critical role in regulating NCCs differentiation in smooth muscle. In fact, the inhibition of Notch signaling results in the loss of smooth muscle markers in the developing aortic arch arteries (High and Epstein, 2008; High et al., 2007). The transduction of Notch signals from the endocardium to the NCCs is mediated by the specific extracellular matrix surrounding the arteries, notably rich in Fibronectin (Chen et al., 2015; Wang and Astrof, 2016). Moreover, the remodelling of the arterial tree seems to be orchestrated by localized apoptosis, mediated by TGFβ signaling and metalloproteinase specific expression (Camenisch et al., 2002; Molin et al., 2003; Poelmann and Gittenberger-de Groot, 2005). Finally, pulsatility and shear stress in the vessels, which is dependent on the fluid flow inside the vessels, are known environmental factors regulating gene expression and apoptosis (Dijke et al., 2012; Egorova et al., 2011; Poelmann and Gittenberger-de Groot, 2005). However, the precise role played by the cardiac NCCs (and their smooth muscle specification) during the processes of arterial remodeling it is still unclear.

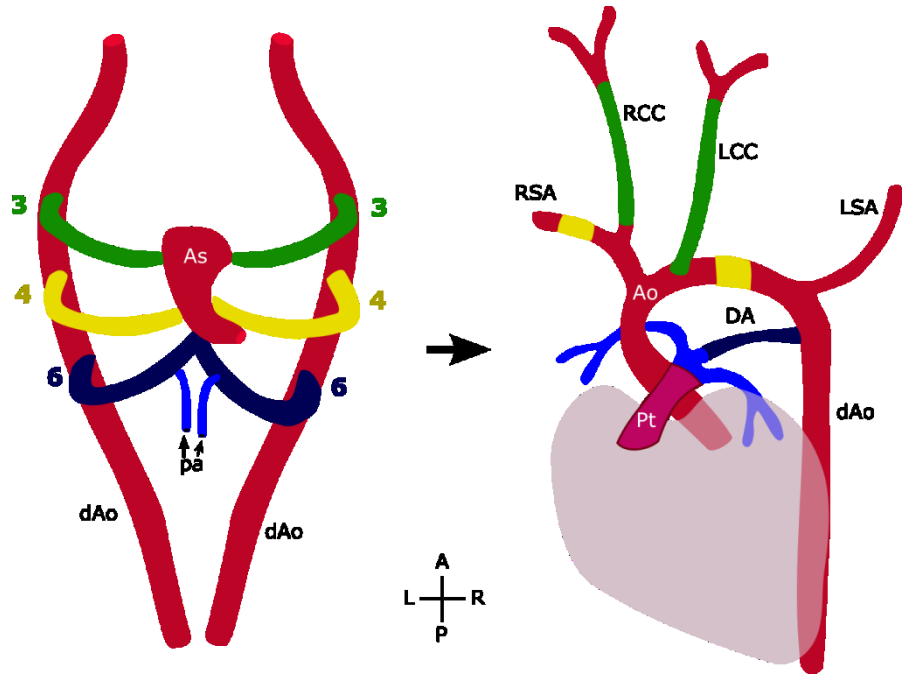

Figure 13- Ventral schematic view of the arterial tree formation. The pharyngeal arch arteries are formed sequentially and connect the two dorsal aorta (dAo) with the aortic sac (As). The 1st and 2nd paired arteries regress very rapidly while the 3rd contributes respectively to the right and left common carotid arteries (RCC and LCC). The right 4th pharyngeal artery forms part of the right subclavian artery (RSA) and the left 4th pharyngeal artery forms the central part of the aortic arch. The left distal part of the 6th PAA forms the ductus arteriosus (DA), which is a shunt between the pulmonary and systemic circulations that exist only during fetal life to bypass the non-functional lungs and closes at birth. A-P, Antero-Posterior; L-R, Left-Right.

I.2.4 Many human heart malformations present arterial pole defects linked to NCCs dysfunction

Human arterial pole malformations

Congenital heart defects (CHDs) represent 20% of spontaneous abortions, 10 % of stillbirths and affect 1% of newborn babies (Hoffman, 1995; Srivastava and Olson, 2000). A majority of CHDs present an impaired development of the cardiac OFT region, which is critical for the correct connection of the systemic and pulmonary circulations with the chambered heart. In humans, CHDs encompass a wide spectrum of malformations that usually affect a combination of heart segments. As we are interested in NCCs contribution to the heart, we focus here on CHDs characterized by defects in OFT formation. Mouse models are key tools to understand the etiology of arterial pole malformations, since they allow the thorough study of OFT progenitors lineage and behavioral defects. We can artificially subdivide OFT malformations in two types, although many human syndromes are a combination of both subcategories. On the one hand, the shape of the OFT itself can be affected by defects in

elongation, rotation and alignment with the ventricles. On the other, OFT septation and valvulogenesis arise from defectuous remodelling of the cardiac cushions. These second type of defects in septum formation and valvulogenesis are the most common type of congenital heart defects seen in humans (Hoffman and Kaplan, 2002).

Disrupted rotation and elongation of the outflow tract during the septation process causes abnormal positioning of the great arteries relative to the ventricles. This is materialized by congenital heart defects such as complete transposition of the great arteries (Figure 14B, page 60) or double outlet right ventricle (Figure 14C, page 60) (Moon, 2008). The circulation arising from the faulty morphogenesis of the great arteries is nonfunctional and most often leads to death at birth. Indeed, the phenotype of great arteries transposition does not establish a serial circulation but two parallel circulations. The oxygenated blood flows back and forth between the left ventricle and the lungs in a closed loop, while deoxygenated blood circulates in the systemic circuit. This vascular system is viable at fetal stages when shunts exist between systemic and pulmonary circulations but is rapidly fatal at birth when shunts close. Regarding the double outlet right ventricle condition, both great arteries emerge from the right ventricle. It is associated with ventricular septal defects forming a postnatal shunt with blood draining from the left ventricle to the right. Without treatment, prognosis is poor due to severe cyanosis at birth. Finally, Tetralogy of Fallot is the most common form of cyanotic CHD with approximately 1 in 4000 live birth (Botto et al., 2003). It is characterized by four features: a ventricular septal defect, right ventricular hypertrophy, pulmonary artery stenosis and overriding aorta (where the aorta is misaligned and is positioned over the ventricular septal defect) (Kloesel et al., 2016) (Figure 14D, page 60). The tetralogy of Fallot can occur sporadically but is mainly associated to the DiGeorge Syndrome, which will be described thereafter.

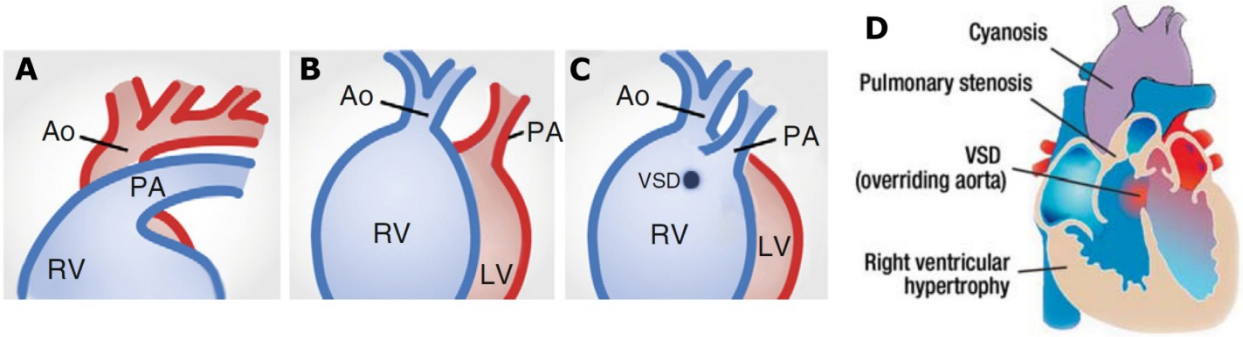

Figure 14 – A variety of malformations can affect the arterial pole of the heart in humans. They can result from faulty rotation or alignment of the outflow tract with the ventricles during heart morphogenesis. Here are some schematic representations showing the positions of the great arteries relative to the ventricles. **A.** Normal situation. **B.** Complete transposition of the great arteries. **C.** Double outlet right ventricule with ventricular septal defect. **D.** The tetralogy of Fallot is characterized by a combination of features: interventricular communication, also known as a ventricular septal defect (VSD), with the aorta overriding the ventricular septum (overriding aorta), obstruction of the right ventricular outflow tract (pulmonary stenosis), and right ventricular hypertrophy. Ao, aorta; PA, pulmonary artery; RV and LV, right and left ventricles; VSD, ventricular septal defect (Adapted from (Diller et al., 2011; Moon, 2008)).

The proper septation of the heart segments is fundamental. In fact the serial circulation, going via the lungs, from the systemic venous to the systemic arterial circuits, is only possible if all segments of the heart are well septated. Impaired OFT septation presents a spectrum of severity. It ranges from total absence of septation, called persistent truncus arteriosus, to small ventricular septal defect where the proximal OFT septum is not attached to the ventricular septum (Figure 14D). Consequently to these defects, mixing of oxygenated and deoxygenated blood occurs and this mixed blood circulates in systemic, pulmonary, and coronary circulations. This leads to symptoms of cyanosis and possible heart failure (Moon, 2008). After OFT septation, valve morphogenesis occurs in the vicinity of the newly formed great arteries and is also crucial for blood circulation. Valves are in fact dynamic septa preventing retrograde blood flow and coordinating the sequential filling and emptying of the heart segments. Their function can be affected by stenosis, as in the case of bicuspid aortic valves. Bicuspid aortic valve have an incidence positioned between 0,4% to 2,25% of the overall population depending on the studies (Kloesel et al., 2016). Aortic valves stenosis can prevent valves from opening fully, reducing blood flow ejection to the circulatory system, or prevent them to close hermetically, causing blood flow regurgitation into the left ventricle. This decrease in the pumping function of the heart causes inadequate tissue perfusion followed by organ damage and potential death in absence of treatment. NCCs play a crucial role in the arterial pole development and are a subject of intense research to better understand the etiology of CHDs presenting OFT malformations.

Human syndromes likely involving NCCs function defects

The DiGeorge syndrome, Charge syndrome, Alagille syndrome and Fetal Alcohol syndrome are examples of human heart malformations where the arterial pole of the heart is affected and where NCCs function is thought to be altered. DiGeorge syndrome phenocopies in many aspects the cardiac NCCs ablation experiments done in chick and mouse, and thus is thought to be caused by NCCs disfunction. This syndrome has been linked to a microdeletion in the chromosome 22q11. Haploinsufficiency for chromosome 22q11 is the most common microdeletion thus far detected in humans. DiGeorge syndrome presents a constellation of craniofacial, cardiovascular and glandular phenotypes, tissues to which NCCs contribute. Concerning the cardiovascular part of the syndrome, it is characterized by a spectrum of features: human patients suffer from tetralogy of Fallot, persistent truncus arteriosus, double-outlet right ventricle or aortic arch interruption of type B. *Tbx1* has been identified at the microdeletion site as a critical player in the observed phenotype caused by the syndrome. Its function during cardiogenesis was previously mentioned in this introduction and does not seem to play a cell-autonomous role in NCCs, where it is not expressed. Rather, as *Tbx1* is expressed in the SHF, its expression is thought crucial for SHF deployment and for the establishment of a dialogue between SHF and NCCs (Hutson et al., 2006, 2010; Moon, 2008). Although the 22q11 deletion is detected in many patients diagnosed with DiGeorge syndrome, the severity of the phenotypes varies among patients

with the 22q11 deletion. Besides, some patients affected by the syndrome do not present a deletion or mutation in *Tbx1*. This suggests that other genetic or epigenetic cues are at play in the etiology of the syndrome (Hutson et al., 2010; Moon, 2008). Another syndrome, called the Charge syndrome, present a phenotypic basis comparable to the DiGeorge Syndrome but with additional features, such as malformation of the foregut, kidney and reproductive organs. Microdeletions on the chromosome 8q12 or mutations in the chromodomain helicase DNA binding protein (CDH7) have been linked to the etiology of the syndrome (Aramaki et al., 2006; Jongmans et al., 2006).

Similarly, the Alagille syndrome is a multisystemic disorder often characterized by heart malformations. Pulmonary valve stenosis and pulmonary arteries stenosis are the most common heart defects observed. It is an autosomal dominant disorder characterized by a variable severity and is linked to the impairment of the Notch signaling pathway. In fact, many patients present mutations in the JAGGED1 ligand of NOTCH receptors (Oda et al., 1997). As mentionned previously, Notch signaling is thought to regulate the differentiation of the NCCs into smooth muscle at the arterial pole, which is crucial for arterial tree patterning. However, the etiology of the syndrome is also surely due to defects in other lineages than the NCCs. Indeed, Notch signaling has also been described as an important regulator of endocardial cells EMT in the cardiac cushions, and of BMP/TGFβ signaling activity in the myocardium (Garside et al., 2013).

Finally, environmental factors can also be taken responsible for the genesis of arterial pole defects, and are potentially in link with faulty regionalization and specification of the cardiac NCCs. Fetal exposure to alcohol during heart development stages where NCCs contribute to the arterial pole are linked with defects reminiscent of those observed in DiGeorge syndrome (Sulik et al., 1986). Epidemiological studies demonstrate that mothers that consume alcohol once or more per week during early stages of embryonic development, present a 2- to -2.5 fold chance increase to give birth to newborns presenting OFT malformations (Carmichael et al., 2003; Hutson and Kirby, 2010). Ethanol exposure can have different detrimental effects on cells survival, specification and behavior. It can lead to cell death in the NCCs due toxicity at the cellular level (Hassler and Moran, 1986). Conversely, ethanol also plays an antagonistic role against Vitamin A, impacting Retinoic Acid (RA) signaling, and thus gene expression, progenitor lineages regionalization and specification (Yelin et al., 2005; Zachman and Grummer, 1998). In fact, as previously mentioned RA alters the regional specification of SHF progenitors and NCCs, probably leading to aberrant contributions to the cardiac segments. It was reported that mice embryos exposed to RA present complete transposition of the great arteries, and that chick embryos present outflow alignment defects (Bouman et al., 1995; Nakajima et al., 1996). As for other CHDs, it is difficult to link the observed phenotype with a dysfunction in a specific progenitor lineage. Their roles during arterial pole formation are complementary and impacting one is very likely impacting the others, with which a continuous dialogue is established during the

morphogenetic processes. In sum, impacting NCCs induces defects in SHF deployment during outflow lengthening, and conversely, impacting SHF leads to faulty regionalization of the NCCs. The expansion of tissue-specific and time-dependant gene deletion, now possibly coupled with single-cell analysis, will enable to unveil the complex dialog established between SHF, NCCs and endocardial progenitors during the arterial pole formation of the heart. We have seen that BMP signaling is implicated in key progenitors specification steps and morphogenetic events during arterial pole formation. But how does this morphogen signaling function at the cellular level?

I.3 Role and mechanism of BMP signaling, a master regulator of gene expression, cell specification and morphogenesis

I.3.1 BMP signaling, an evolutionary innovation serving multicellular organization

The emergence of multicellular organisms went hand in hand with the appearance of extracellular signals, called cytokines, which govern cells interactions. Cytokines provide animal cells with a versatile means of regulating embryonic development, of ensuring tissue homeostasis and regeneration, while the malfunction of cytokines causes severe diseases and embryonic death. The TGFβ family is one family of cytokines, whose emergence was concomitant with the appearance of the first known animal species (Huminiecki et al., 2009). The TGFβ pathway is essentially composed of a variety of extracellular ligands, binding to type I and II receptors, which activate nuclear trnascriptional effectors, called the Smads components. The Smads include the receptor-regulated R-Smads, which interact with a unique central Co-Smad, Smad4, and possibly with two Inhibitory I-Smads. Upon ligand stimulation, complexes formed by R-Smads and Co-Smad translocate to the nucleus where they bind to the genome and regulate target genes expression. This chain of interactions forms a sensitive pathway, which enables cells to respond and adapt to a changing environment. The core components of the TGFβ signaling pathway have been found in the genome of all metazoans sequenced to date (Macias et al., 2015). Their sequences present a high degree of conservation, suggesting that the function and regulatory logic of the TGFβ pathway remained intact across evolution. The general view is that, as animal diversity and complexity increased during evolution, TGFβ ligands, receptors, and Smads diversified as well to provide sufficient regulatory adaptation. As a matter of fact, while the *Nematoda* and *Cnidaria phila* have four Smads (two R-Smads, one Co-Smad, and one I-Smad), vertebrates have eight (five R-Smads, one Co-Smad, two I-Smads).

The secreted TGFβ ligands are dimers of subunits linked by a disulfide bond and their dimerization is essential for receptor activation. They bind to specific membrane receptors, which are serine/threonine kinases belonging to two distinct subfamilies, the type I and II TGFβ receptors. The ligand-receptor interaction forms a complex including two type I and two type II receptors. This interaction triggers the phosphorylation of type-I receptor by the type-II receptor subunit at multiple N-terminally located serine and threonine residues. This activates the type I receptor which in turn, recruits and phosphorylates R-Smads at a specific C-terminal Ser-X-Ser motif. This process results in signal transduction (Figure 15, page 65).
The Smads components are composed of two globular domains (MH1 and MH2) connected by a linker region. The MH1 and MH2 domains have complementary functions. The MH1 domain binds to DNA to mediate its function of transcriptional regulation, whereas the MH2 domain is a region of protein-protein interaction. It interacts with numerous players, such as the above mentioned membrane receptors, but also cytoplasmic anchor proteins, DNA-

binding cofactors and chromatin modifiers. Finally, the linker region is an integrative entry point that binds to regulators of the pathway. It undergoes two cycles of phosphorylation as the Smad-Complex reaches the nucleus. First, CDK8/9 phosphorylations favor the interaction with cofactors and thus maximize the transcriptional action of the Smad-complex (Alarcón et al., 2009). Second, GSK3 phosphorylation decreases the linker domain affinity for cofactors but favors binding with E3 ubiquitin ligases and subsequent proteasomal degradation (Aragón et al., 2011; Fuentealba et al., 2007).

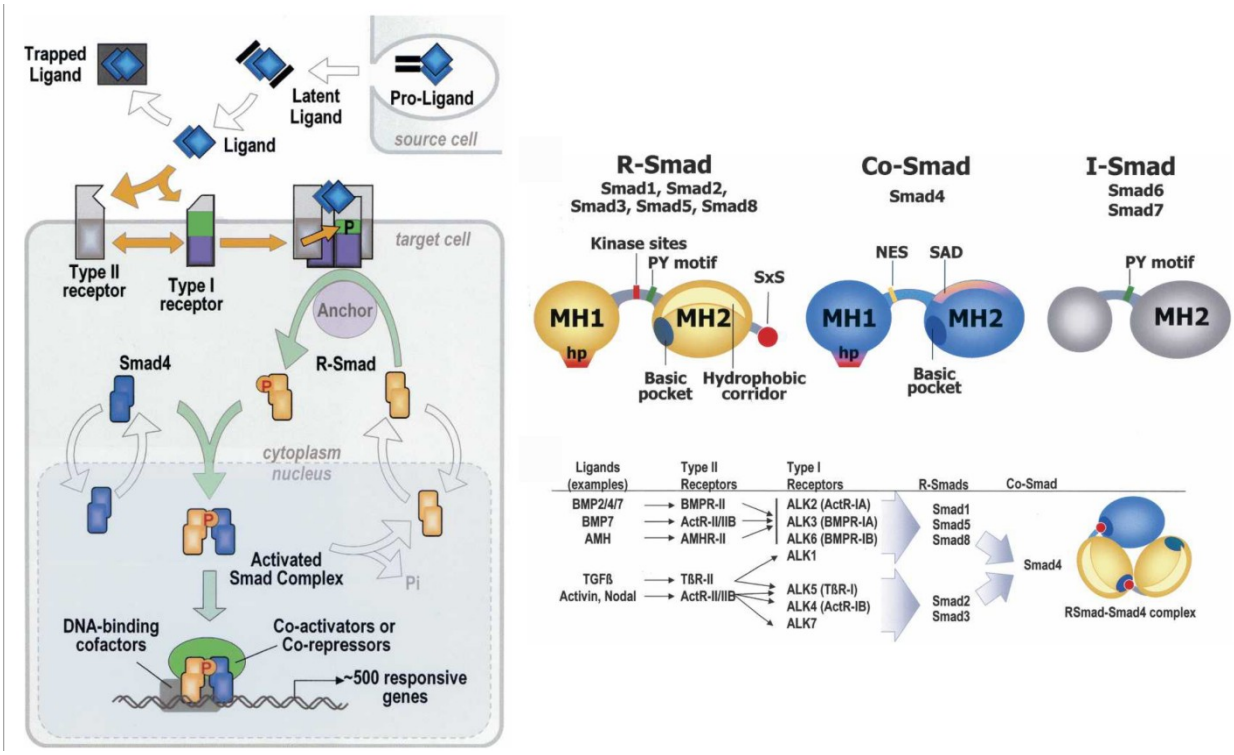

Figure 15 - Structural features of the TGFβ-Smad signaling pathway. TGFβ ligands are secreted as inactive dimeric propeptides that, after activation by convertases, can bind to membrane TGFβ receptor complexes (type I and II hetero-tetramers). TGFβ ligands can be inactivated extracellularly by occluding factors. Type I TGFβ receptor is phosphorylated at a GS domain by type II, which creates a docking site for regulated Smad porteins (R-Smads). Whereas at basal state Rsmads and Smad4 undergo constant cytoplasmic shuttling, the activation of type I receptor enable Rsmad presentation by Anchor proteins and phosphorylation at the C-terminal pS-X-pS domain. Phosphorylated R-Smads interact with Smad4 and form Smad complexes that accumulate in the nucleus, where they bind to DNA. Rsmad-Smad4 complexes interact with DNA-binding cofactors that confer gene selectivity, and with transcriptional co-activators or co-repressors to regulate target genes expression (Adapted from (Massagué et al., 2005)).

The specificity of TGFβ signaling comes from the combination of ligands and receptors activated in a given cellular context. The TGFβ family is generally decomposed in two subfamilies (i) the TGFβ branch, acting through the TGFβ, nodal, activin and myostatin receptors and activating Smad2 and 3 and (ii) the BMP branch that acts through BMP and anti-Müllerian receptors and activates Smad1, 5 and 8. In this introduction, we will thereafter focus on the BMP branch of the TGFβ family (Figure 15, page 65).

The first hint of BMP's signaling function was given at the time of its discovery, in the mid-1960s, when its pro-osteogenic capacity was observed (Urist, 1965). Yet, it rapidly became obvious that the influence of BMP signaling could be different, or even opposite, given the cellular environment and the cell-type receiving the signal. The effect of BMP on cell cycle, survival, proliferation, growth, extracellular matrix production, and differentiation is mediated by positive or negative gene regulations. The number of target genes activated by BMP signaling can range from just a few in ES cells, to hundreds in differentiated cells (Trompouki et al., 2011). In a given environment, the cell's response to BMP will be driven by the nature, abundance, and activity of the extracellular and intracellular BMP signaling components. Four types of determinants mediate the cell transcriptional response: the accessibility of the BMP ligands and BMP receptors for binding, the regulation of Smad-complex activation, the transcriptional impact of Smad depending on its interaction with various transcription cofactors and chromatin remodelers, and finally, the cell epigenetic status in its given environment (Massagué, 2012) (Figure 16 ,page 66).

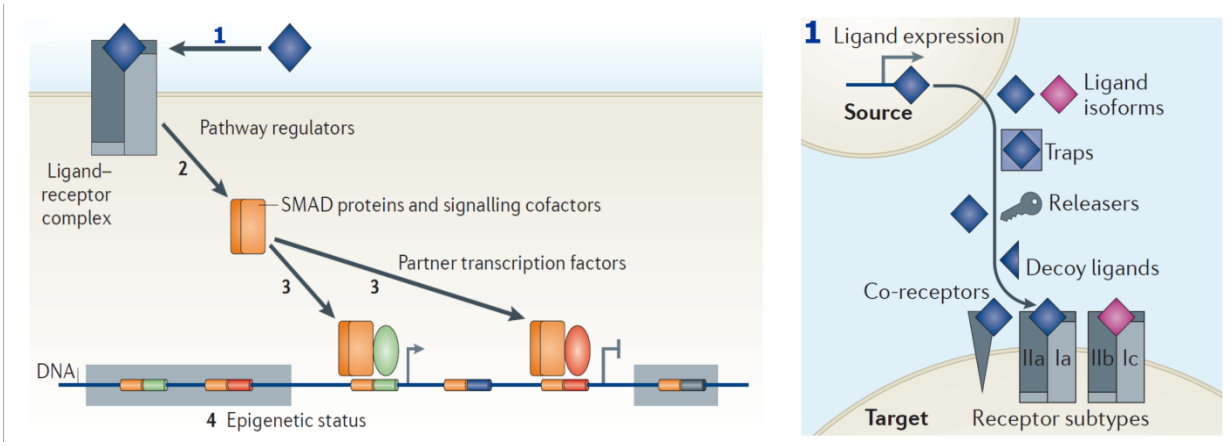

Figure 16 - Different types of determinants impact the transcriptional response of cells to TGFβ signals. Extracellularly, many proteins determine the efficiency of signal transduction by regulating the access of TGFβ ligands to signalling receptors (1). Intracellularly, other factors regulate the TGFβ receptors activation and accessibility to SMAD proteins and signalling cofactors (2). In addition, transcription factors and chromatin modifiers that interact with activated SMAD proteins specify what genes will be targeted by the signal transduction and whether they will be positively or negatively regulated (3). Finally, the epigenetic state of the cell determines if target genes are in an 'open' chromatin region (represented by absence of shade) and thus accessible to Smad complexes (4) (Adapted from (Massagué, 2012)) .

I.3.2 Protein phosphatases, and specifically the phosphatase called Dullard, play a fundamental regulatory role in BMP signaling

Activation of BMP signaling

More than 15 BMP ligands have been described to date and they can be categorized in three subgroups based on their amino acid sequences and phylogeny. Hence, BMP2/4, BMP5/6/7/8, BMP9/10, and BMP12/13/14 can be considered as subgroups (Wang et al., 2014). These ligands are first synthesized as dimeric precursor proteins. Convertases cleave the precursors andrelease active ligands that can be secreted (Dubois et al., 1995). The diffusion of BMP ligands is extensively regulated by extracellular factors. In fact, there are many extracellular variables at play to modulate the intensity of BMP activation prior to intracellular transduction. The level of ligand secretion by the cells at the source is an obvious first variable. Also, antagonist effectors such as Noggin and Gremlin inhibit the diffusion of BMP ligands by either occluding the BMP receptors or binding to the BMP ligands (Hsu et al., 1998; Piccolo et al., 1996). Adding up to this regulation, some releaser proteins mediate the spatiotemporal liberation of BMP ligands from trapping proteins. Finally, decoy ligands and accessory receptors also impact the extent of BMP stimulation in responsive cells (Higashihori et al., 2008) (Figure 16, page 66).

At the membrane, BMP pathway activation is mediated by the combination of ligand and receptor subtypes, which present different affinities. The ligand-receptor binding induces the formation of a hetero-tetrameric receptor complex with two type I and two type II BMP receptors. Type I receptors, which are constitutive serine/threonine kinases, are activators that phosphorylate the type II receptors. Type II receptors are signal propagators activating R-Smads. Three receptors are known as type I BMP receptors: Type 1A BMP receptor (BMPR-1A or ALK3), type 1B BMP receptor (BMPR-1B or ALK6), and type 1A activin receptor (ACVR-1A or ALK2). In a similar manner, three type II receptors have been described: type 2 BMP receptor (BMPR-2), type 2 activin receptor (ACVR-2A), and type 2B activin receptor (ACVR-2B). While BMPR-1A, BMPR-1B, and BMPR-2 are specific to BMPs, ActR-1A, ActR-2A, and ActR-2B are shared with Nodal and Activins ligands (Massagué, 2012) (Figure 15, page 65).

Non-canonical BMP signaling

Although the main transduction pathway of BMP signals is operated via a cascade of phosphorylation activating the translocation of Smad components to the nucleus, different pathways have been described. For example, the BMPR2 receptor can directly bind to LIM kinase 1, which increases actin filaments stability by inhibiting cofilin (Foletta et al., 2003). Moreover, Smad proteins have supplementary functions besides their transcriptional regulation. They can be involved in miRNA maturation, as testified by their implication in miR-21 biogenesis during vascular smooth muscles differentiation (Davis et al., 2008).

Regulation of the Smad signaling cycle in canonical BMP signaling

Intracellularly, the receptor type II mediates BMP signaling transduction by phosphorylating the R-Smads (Smad1, 5 or 8) at their C-terminal Ser-X-Ser motif (Bruce and Sapkota, 2012). This creates an acidic knob enabling Smad4 binding to the MH2 domain of R-Smads. Interestingly, trimers with two R-Smad and one Smad4 are thought to be the main form of Smad complex shuttling between the cytoplasm and the nucleus (Massagué et al., 2005). Prior to activation, Smad proteins can cycle back and forth through nucleopores but when they form R-Smad-Smad4 complexes, the contribution of import and export factors is required for nuclear translocation (Hill, 2009). Once in the nucleus, the R-Smad-Smad4 complexes interact with transcription cofactors and chromatin remodelers to regulate target gene recognition and transcription. Through their MH1 domain, BMP activated Smads bind to GC-rich and CAGAC regions also called Smad binding elements (Morikawa et al., 2011) (Figure 17, page 69). The Smad linker region, located between the MH1 and MH2 domains, is a point of entry for cues regulating Smad transcriptional activity. It contains several Ser/Thr residues that are phosphorylated by various kinases in response to regulatory stimuli (Morikawa et al., 2013). In sum, two types of phosphorylation events have been described: first at the C-terminal Ser-X-Ser motif by type I receptor kinases, and second in the linker-region by multiple proline-directed kinases targeting Ser/Thr residues (Bruce and Sapkota, 2012) (Figure 17, page 69).

Once Smads are engaged in transcriptional regulation, their linker region is phosphorylated by cyclin-dependent kinases (CDK8 and CDK9), creating binding sites for the WW domains of YAP, which supports Smad transcriptional action (Alarcón et al., 2009). On the same domain, subsequent glycogen synthase kinase 3 (GSK3) phosphorylation, switches off Yap binding but favors the binding of a Smad specific E3 ubiquitin ligase, called Smurf1, which targets Smad to proteasomal degradation (Alarcón et al., 2009; Aragón et al., 2011; Fuentealba et al., 2007).

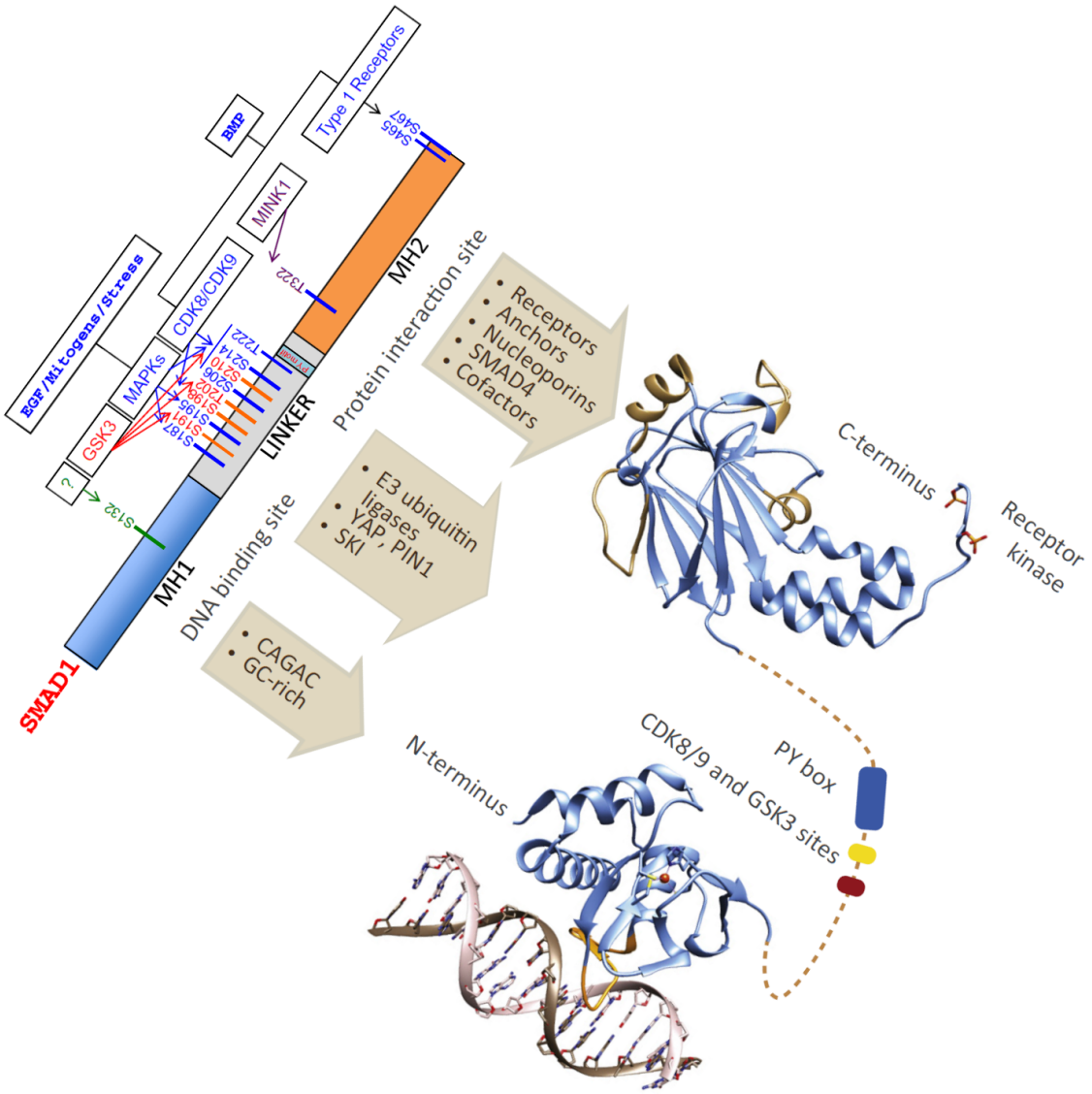

Figure 17 – Structure and function of the domains of R-Smads. R-Smads are composed of three distinct domains, which present Serine/Threonine residues that can be phosphorylated. The MH1-domain is the DNA-binding domain; the MH2 is the protein-binding domain, whereas the Linker domain is site of regulatory integration. This domain is sensitive to the regulatory influence of the many kinases and phosphatases, since it presents a high number of phospho-residues. Hyper-phosphorylation of the Linker region triggers R-Smad degradation through the action of E3 ubiquitin ligases. The activation of R-Smad by Type I receptor kinase is mediated via the phosphorylation of S465 and S467 in the MH2 C-terminus (Adapted from (Bruce and Sapkota, 2012; Macias et al., 2015)).

Moreover, the linker region is integrating inputs from other growth factors and stress signals. As an example, mitogen-activated protein kinases (MAPKs), which are downstream effectors of FGF and EGF signaling, can phosphorylate CDK target sites (Aubin et al., 2004). On the contrary, GSK3 can be inhibited by Wnt signaling, and thus provides a possible entry point for cooperation between Wnt and BMP signaling (Fuentealba et al., 2007). In sum, the reversible phosphorylation state of the R-Smad linker region, mediated by protein kinases and phosphatases is a key variable in Smad transcriptional activity. R-Smad are mandatory for mediating a cellular response to BMP ligands and consequently represent key regulatory targets.

Pattern of Smad binding to the genome

Smad binding elements are numerous throughout the genome, yet a majority of them are not occupied. This suggests that the DNA sequence of the Smad binding elements alone is not sufficient to trigger Smad binding and that additional regulatory mechanisms are at play. In fact, Smad complexes have a relatively low binding affinity with DNA, and therefore are bound to interact with a wide variety of cofactors to enhance their binding affinity. These cofactors cooperatively regulate Smads binding pattern to the genome and thus orchestrate the expression of a panel of target genes (Morikawa et al., 2013). The general view is that two complementary mechanisms determine the binding patterns of Smads to the genome. First, cell-type specific pioneer transcription factors modulate the local chromatin structure and thus Smad binding sites accessibility (Zaret and Carroll, 2011). Fairly recent results indicate that the Smad1/5 binding pattern characterizing endothelial cells is predetermined by the contextual landscape of chromatin accessibility (Morikawa et al., 2011). Second, the context-dependent Smad co-factors specifically strengthen the affinity between Smad and DNA. It has been shown that lineage specific transcription factors, such as C/EBPa in the myeloid lineage and Gata1 in the erythroid lineage, restrict Smad1 binding to lineage-specific genes (Trompouki et al., 2011)

Phosphatases regulatory function in the BMP pathway

The phosphorylation and dephosphorylation of proteins is a fundamental mechanism of regulation of signaling transduction. Smad proteins are a perfect illustration of this concept since their degradation and nucleocytoplasmic shuttling is regulated by the action of kinase and phosphatase proteins on both their linker and MH2 domains. Interestingly, there are far more kinases described in the human genome (approximately 518) compared to phosphatases (approximately 147), which suggests a lower substrate specificity for phosphatases (Alonso et al., 2004; Bruce and Sapkota, 2012). All reported phosphorylation sites of R-Smads are Ser/Thr residues. Therefore, serine-threonine phosphatases are the major focus of researches aiming at unraveling the phosphatases regulatory influence on R-Smads shuttling and stability. R-Smads dephosphorylation can be operated by a number of

different Ser/Thr phosphatases (Figure 18, page 71). On the one hand, the C-terminal phosphatases 1-3 (SCP1-3), the protein phosphatase magnesium-dependent 1A (PPM1A), and the pyruvate dehydrogenase phosphatase (PDP) have been described as potent BMP terminating signals by dephosphorylating of the MH2 domain of Smad1/5 (Chen et al., 2006; Duan et al., 2006; Knockaert et al., 2006; Kokabu et al., 2010). Although promising, none of these phosphatases regulatory mechanisms have yet been confirmed in mouse models. SCP1-3 phosphatases have mainly been described to be nuclear, whereas PDP is mitochondrial and PPM1A location is rather cytoplasmic.

Besides the MH2 phosphorylation, the linker region phosphorylation is also a prominent regulatory input for Smad activity. In addition to their action on the MH2 domain, it was shown that SCP1-3 phosphatases also dephosphorylate the Smad-1 Linker region (Knockaert et al., 2006). Hence, SCP1-3 seems to play a key regulatory function by being able to target both Linker and MH2 domains of Smad1, in this way resetting Smad1 activity to the baseline. However, there is heterogeneity in the kinetics of phosphorylation and dephosphorylation of the Linker region Ser/Thr residues, which points out that more detailed studies are needed on the substrate specificity and kinetics of SCPs and other unknown phosphatases.

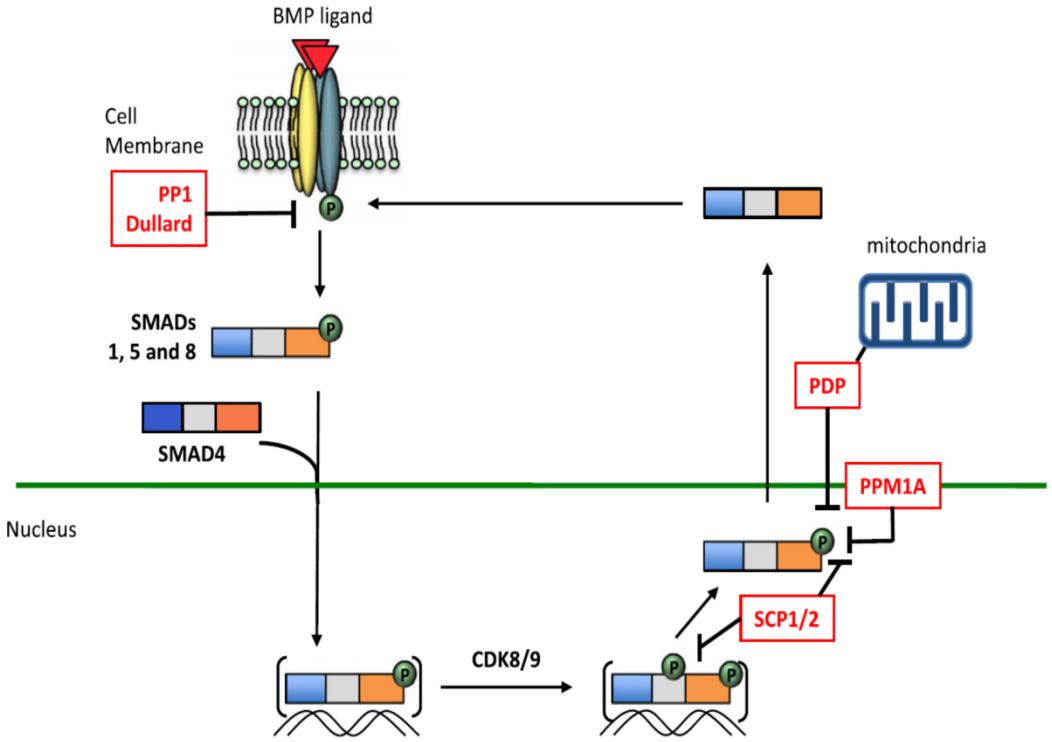

Figure 18 – Regulatory functions of protein phosphatases on BMP signaling transduction and duration. R-Smad activation and transcriptional influence are regulated by the phosphorylation state of the Ser/Thr residues localized on its MH2 and Linker domains. Multiple phosphatases, acting in the cytoplasm or in the nucleus, have been shown to regulate the phospho-residues phosphorylation dynamics, thus tuning R-Smad activation, shuttling and the duration of the transcriptional regulation before R-Smad degradation (Adapted from (Bruce and Sapkota, 2012)).

Phosphatases act on BMP receptors to modulate R-Smad activity

The BMP receptors state of phosphorylation is also a key variable regarding pathway activation. The type I BMP receptors are regulated by degradation and dephosphorylation, which can efficiently terminate signaling. Their degradation involves the E3 ubiquitin ligases and the negative regulatory feedback of the I-Smads (Smad6 and Smad7) (Massagué et al., 2005). Phosphatases are thought to play a key regulatory role in BMP receptors degradation and dephosphorylation, although very few have been described to date. From the PPP phosphatase family, PP1 has been reported to function as a type I TGFβ/BMP receptor phosphatase in endothelial cells (Valdimarsdottir et al., 2006). Another phosphatase, from the FCP family and called Dullard (Ctdnep1), was demonstrated to interact with BMP receptors (Satow et al., 2006). Very interestingly, Dullard belongs to the same FCP family of Ser/Thr phosphatase as SCP1-3, characterized by a DLDET active site in their C-terminal domain (Kim et al., 2007). In contrast to SCP, Dullard possesses a N-terminal transmembrane domain that directs it to the extranuclear and ER membranes (Kim et al., 2007; Satow et al., 2006). Like the rest of the FCP subfamily, Dullard is highly conserved although its N-terminal amino-acid sequence is quite divergent. In fact in yeast, the human DULLARD can functionally rescue the phenotype induced by the deletion of its yeast homolog, Nem1 (Kim et al., 2007) (Figure 19, page 72).

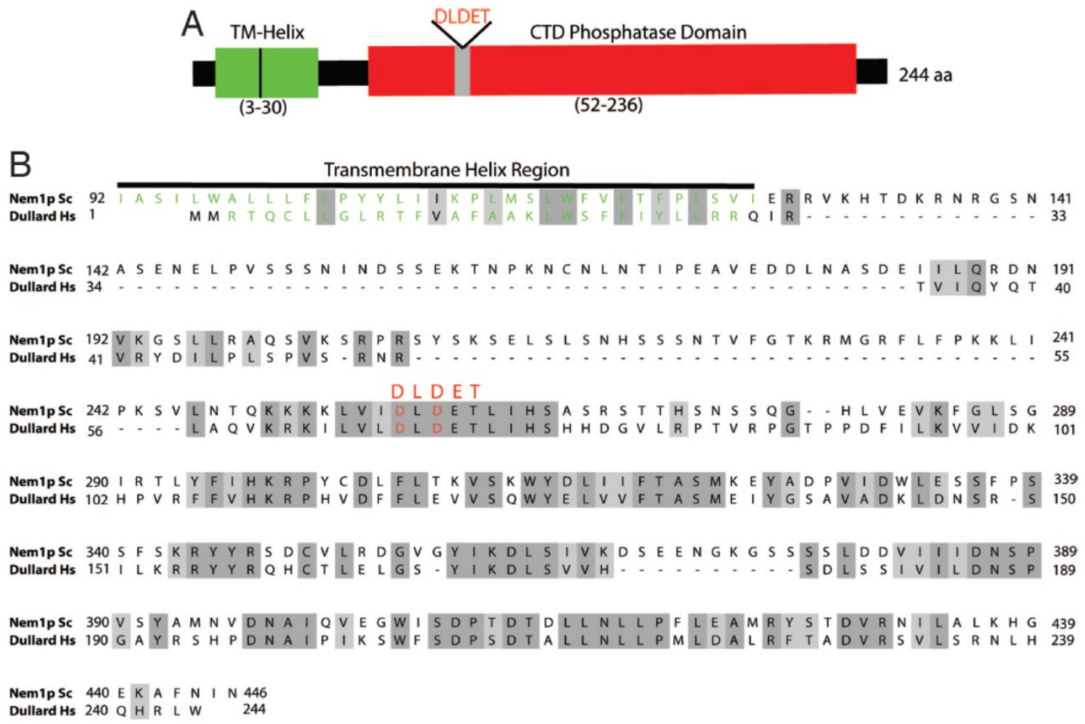

Figure 19 – Degree of conservation of the Dullard phosphatase. The protein phosphatase Dullard presents a high degree of conservation with its yeast ortholog Nem1, as testified by the homology of sequence in the CTD phosphatase domain (in red). The DLDET catalytic signature is characteristic of the FCP family of phosphatases. In contrast, the transmembrane-helix domain (in green) is much less conserved (Adapted from (Kim et al., 2007)).

The ultimate test to confirm the regulatory role of a Ser/Thr phosphatase on R-Smad activation is to validate the phosphatase activity in transgenic mouse models. Until now, Dullard is the only phosphatase among the aforementioned ones, whose function in BMP signaling regulation has been confirmed in mice (Sakaguchi et al., 2013). Yet, Dullard's mode of action remains poorly understood. While first results in mammalian cells suggest that Dullard regulates BMP signaling by interacting with the BMP receptors, recent evidences in *Drosophila* convincingly show that Dullard directly binds to Mad, the *Drosophila* R-Smad homolog (Urrutia et al., 2016). Very interestingly, this last study demonstrates that the activity of the Dullard phosphatase depends on its C-terminal catalytic domain, which is reminiscent of the SCP1-3 phosphatases, for it is able to dephosphorylate both MH2 and Linker phospho-residues. Hence, by acting on both domains, Dullard would act on R-Smad activity and stability. A major difference between SCPs and Dullard is their localization since SCPs are nuclear whereas Dullard is perinuclear. This difference of localization might dissociate temporally their regulatory actions during Smad shuttling, with Dullard acting extranuclearly on R-Smad complexes formation, and SCP1-3 acting intranuclearly on R-Smad transcriptional regulation.

Dullard regulatory function in Xenopus, Drosophila and Mice

Historically, *Dullard* was first identified as a gene expressed in neural tissues, branchial regions and pronephroi during early *Xenopus* development (Satow et al., 2002). Inhibition of *Dullard* by morpholino injection in *Xenopus* embryos showed that Dullard was essential for neural development, and Dullard overexpression led to cell apoptosis. Later on, Satow et al. presented the first evidences of Dullard regulatory function on BMP signaling (Satow et al., 2006). Their experiments performed on *Xenopus* caps showed that Dullard, through its phosphatase activity, was inhibiting the phosphorylation of the downstream effectors of BMP signaling (Smad1,5,8) but not of Smad2 and Mapk, respectively downstream effectors of TGFβ and FGF signaling. Conversely, knocking-down *Dullard* expression upregulated the phosphorylation levels of Smad1,5,8 and the expression of BMP target genes (*Msx1*, *Bambi*, *Xvent-1*). Interestingly, overexpressing Dullard in the same system caused a significant decrease in BMPRII protein level (Satow et al., 2006). Satow *et al.* complemented this analysis with experiments on mammalian cells, on which they were able to show that Dullard interacts with BMP receptors and promote BMPRII proteasomal degradation as well as BMPRI dephosphorylation. However, the binding of Dullard to the BMP receptors was observed by overexpressing both Dullard and the BMP receptors, which could have led to artefactual binding.

In mice, a lacZ and flox transgenic lines were generated to study the expression pattern and function of Dullard in mammals (Hayata et al., 2015; Sakaguchi et al., 2013; Tanaka et al., 2013). Dullard appeared to be expressed in the ectoderm and mesoderm, but not in the

definitive endoderm of E7.5 embryos (Tanaka et al., 2013). However, it is ubiquitously expressed in E11.5 embryos (Hayata et al., 2015). Cre-Lox recombination of the exon2-3 of *Dullard* validated the negative regulation of Dullard on BMP signaling during nephron postnatal maintenance (Tanaka et al., 2013). In fact, the specific impairment of Dullard's function in nephron progenitors caused enhanced BMP signaling, in link with severe nephron loss and postnatal death (Sakaguchi et al., 2013). Intrigingly, results from Tanaka *et al.* highlighted that E7.5 Dullard$^{-/-}$ embryos present impaired primordial germ cells development due to Wnt signalling dysregulation, although this phenotype might just be due to a developmental delay (Tanaka et al., 2013). In addition, Dullard has been involved in the regulation of TGF-β signaling during endochondral ossification (Hayata et al., 2015). Recently, experiments, inducing Cre mediated recombination of *Dullard* in adult ovaries, showed that Dullard was also regulating BMP signaling in this context (Hayata et al., 2018). All together, the characterization of Dullard's function shows a clear impact on BMP signaling regulation although it might affect other signaling pathways in a yet unknown manner.

In addition and as previously mentioned, Dullard was shown to function as a BMP terminating regulator in *Drosophila,* where it directly binds and dephosphorylates the Smad component (Urrutia et al., 2016). In sum, Dullard seems to possess a conserved regulatory function on BMP signaling in all Deuterostome species examined so far. Whether it acts both at the BMP receptor and Smad levels in mammals remains to be clearly extablished.

I.3.3 The spatiotemporal control of BMP signaling during embryonic development

Now focusing at the tissue-level, we describe the implication of BMP signaling in morphogenesis during the different stages of embryonic development. Because morphogens such as BMPs are diffusible factors, they form gradients that influence the fates of neighboring cells. In fact, cells neighboring an induction zone read morphogen gradients in a threshold-dependent manner, which induces distinct cellular responses, and thus the patterning of forming tissues. In other words, morphogen gradients provide cells with positional information that is used to form patterns of distinct cell types. Because tissue patterning has to be tightly constrained to provide the organism with functional organs, morphogen gradients are generated and stabilized by molecular feedback circuits. This ensures appropriate cell-types production at the right time, at the right place and in good quantities (Bier and Robertis, 2015). The output of a formed morphogen gradient in a given tissue depends on three main parameters: the competence of the receiving cells, the extraordinarily diverse molecular mechanisms regulating the dynamics of morphogen distribution, and last, the nature of the transcriptional network integrating the levels and duration of morphogen signals (Sagner and Briscoe, 2017).

The competence of receiving cells determines the signaling output

First, the differential competence of receiving cells can modulate their response to BMP signals. The cell competence is not solely regulated by the total loss of capacity of signal transducers, since this would only lead to ON or OFF response state. In fact, this would not match with the finely tuned signaling outputs observed during morphogenesis. This is achieved thanks to context-dependent receptors, downstream signal transducers, transcriptional factors and chromatin modifiers (Sagner and Briscoe, 2017). An interesting example of context-dependent receptor expression is observed during neural tube development, where a sequential action of BMP receptors occurs in the neural precursors. At first, the neural precursors only express BMPR1a, which integrates BMP signals and triggers cell proliferation but also subsequent BMPR1b expression. In turn, integration of BMP signals through BMPR1b leads to cell cycle arrest and differentiation (Panchision et al., 2001). Moreover, the competence of receiving cells can also be modulated by BMP downstream cofactors, such as transcriptional effectors, recruited to varying chromatin regions according to the environment. For instance in progenitor cells, the proper interpretation of Shh and BMP signals that trigger neural specification, relies on the presence of the neural specific SoxB transcription factors. In fact, genes induced in a SoxB1-dependent manner constitute a gene regulatory network acting in *Cis* to favor neural competency and constrain regionally gene expression (Oosterveen et al., 2013). At last, epigenetic modifications can mediate the competence of cells over long time periods compared to gene regulatory networks. Epigenetic repressor complexes, by modulating chromatin condensation, mediate the accessibility of regulatory motifs. This control is particularly important since epigenetic modifications can confer cell-state maintenance and memory. Very interestingly, the epigenetic modifications have different durations depending on their nature and thus provide variable memory timescales (Bintu et al., 2016).

The regionalisation and specification of cells is ruled by morphogen gradients

Extracellularly, the dynamics of morphogen concentration regulate cell fate decisions and lineage diversification during tissue morphogenesis. The signals vary both spatially and temporally. Their variability can arise from spatial displacement of the morphogens source or simply from temporal fluctuation in morphogens or counteractors production rate. The concentration of morphogens in a cell environment is regulated by its rate of production, its rate of clearance, its speed of diffusion and degradation, and the potency of possible counteractors. Yet, the simple concentration of morphogens is not the only information perceived by receiving cells. It goes hand in hand with other properties of the signal, such as the fold change in signal levels, the duration of the signal over a certain threshold, the accumulation of signal over time, or the number and frequency of oscillations (Sagner and Briscoe, 2017).

Interestingly, a linear morphogen gradient can have a linear output in the tissues or on the contrary establish stable and distinct territories of gene expression. The first step is for the tissue to build a continuous gradient of morphogen. For example, the formation of a stable BMP gradient can be based on a two-factor system, a BMP and an antagonist signal. This is what is observed during *Xenopus* dorsoventral patterning, where the pair of activator (BMP) and inhibitor (Chordin) morphogens originate from the same source. The activator stimulates its own production as well as the one of the inhibitor, which in turn represses the activator. This establishes a stable gradient because Chordin diffuses more rapidly than BMPs and terminates BMP signaling away from the source (Figure 20, page 76) (Plouhinec et al., 2013). Secondly comes the question of the output generated by a stable morphogen gradient. On the one hand it can give rise to a linear output. With regards to BMP signaling, this is illustrated during *Drosophila* wing disc development, where the BMP ligand concentration is translated into a similarly shaped BMP activity gradient, encoded in the phosphorylation state of Smad (Bollenbach et al., 2008). On the contrary, a stable gradient can generate discrete gene expression territories, possibly leading to the segregation of different cell-lineages in space. To this end, some pathway intrinsic regulatory feedback loops have to decouple the direct connection between the morphogen concentrations as input, from the pathway output.

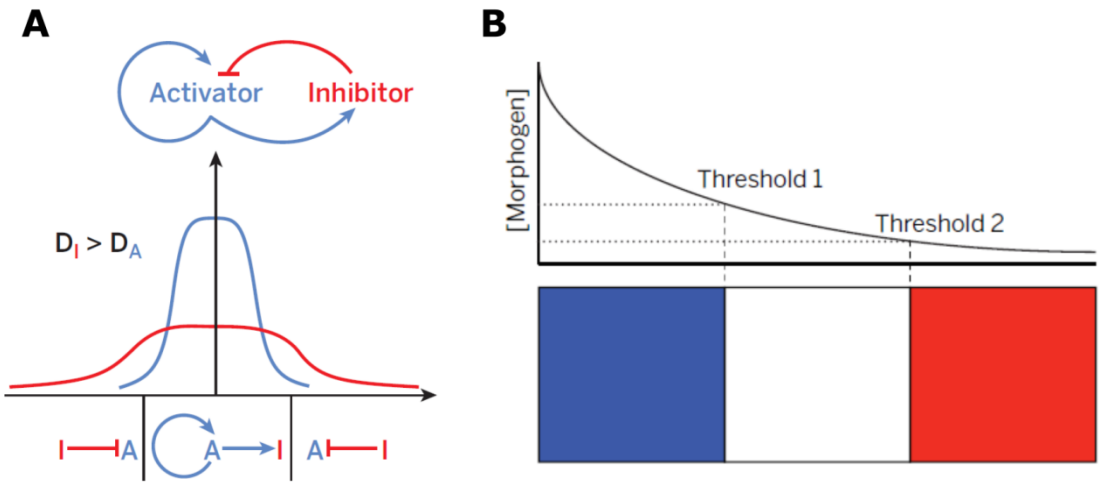

Figure 20 - **Establishment of morphogens gradients**. First, gradients can be established and stabilized cues that regulate morphogens concentration in space and time, as in for the example in **A**. Second, the response of the receiving cell depends on inner regulatory feedback loops that integrate the signals. A positive feedback loop can translate a continuous graded input into a step-like interpretation at the transcriptional level, here shown in **B** with the 'French Flag Model'. This enables the regionalisation of distinct gene express domains and potentially, lineage diversification (Adapted from (Bier and Robertis, 2015)).

First of all, positive feedbacks can translate a linear signal into a cellular step-like response. In such a feedback mechanism, high levels of signals further activate the pathway whereas low levels inhibit it, thus creating a signaling threshold (Figure 20, page 76). In BMP signaling, such a mechanism has been proposed to occur during *Drosophila* dorsoventral patterning. Wang and Ferguson showed that in a first time-sequence, a BMP gradient is established and initiates a positive feedback loop that promotes ligand binding. The strength of ligand-binding depends on the history of BMP signalling strength, which varied along the BMP gradient. This mechanism leads to two-stable states of BMP-receptor interactions that are segregated in space, with high BMP intracellular activity in dorsal-most cells and low in lateral cells (Wang and Ferguson, 2005).

In a complementary manner, a variety of negative feedback loops exist and result in the adaptation of receiving cells to the morphogen signals. For example, BMP signaling promotes the expression of inhibitors of its own transduction cascade, namely Smad6 and Smad7 (Ishida et al., 2000). Smad6 and Smad7 serve as decoys interfering with Smad-receptor or Smad-Smad interactions. Smad6 competes with Smad4 for interaction with the receptor-activated Smad1, while Smad7 binds to the BMP receptors in competition with R-Smads (Hata et al., 1998; Nakao et al., 1997). The higher the signaling input, the more inhibitor is produced, forcing the system to continuously increase signaling input (ligand concentration) to maintain a stable level of output. Accordingly, negative feedback loops can trigger the termination of response to ligands despite the presence of the ligands extracellularly. Besides, it provides a means for measuring the duration of signaling and its dynamics. Such an adaptive system has been described for TGFβ signaling, where Smad4 translocation to the nucleus is only transient. And thus well-spaced ligand pulses combine additively and outbest a slow and continuous increase in ligand concentration (Sorre et al., 2014) (Figure 21, page 77).

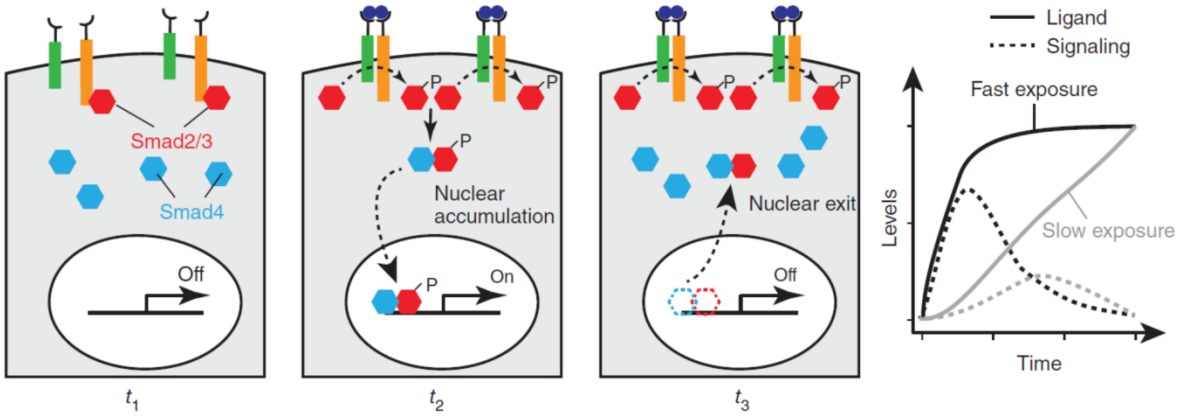

Figure 21 – Negative feddback loops induce the adaptation of the receiving cell to the morphogen signals. The rapid termination of the DNA binding capacity of Rsmad-Smad4 complexes shortens their transcriptional regulation. Adaptation of cells result in a stable output from continuous increase in signal concentration. In contrast, very dynamic changes in signal exposure reach high level of output and enable the reuse of the same morphogen (Image from (Sagner and Briscoe, 2017)) .

Complex gene regulatory networks integrate signaling inputs

Morphogen signaling triggers differential activation of target genes that are part of gene regulatory networks (GRN). The GRNs are providing cells with robust and divisive interpretations of signals, which results in stable gene expression domains. The morphogen signals acts as stimuli for cells that respond depending on the combination of their lineage-specific TFs and chromatin modifiers.

Basically, two types of interactions are combined in the building of GRNs, the feed-forward and the cross-repressions motifs (Figure 22A, page 79). The feed-forward loops integrate morphogen signals by triggering self-enhancing cascades of gene expression. The expression of genes induced at the end of the cascade depends on the expression of the upstream genes, and thus on signal duration. This mechanism is fundamental to stabilize gene expression domains regionally. Such a regulatory motif is described for the BMP-dependent induction of zen, and subsequently of Race and C15, in *Drosophila* (Xu et al., 2005). In contrast to this gene interaction motif, the cross-repression motifs consist in the induction by the same signal of two transcriptional factors that repress each other (cf. TF1 and TF2 in Figure 22B). Mutual cross-repression results in the formation of a signaling threshold at a certain distance of the morphogen source, where TF2 repression takes over TF1. This mechanism efficiently forms a sharp spatial boundary. The region closely located to the source is characterized by a specific gene expression domain, which distinguishes it from the region further away. Initiated by the antagonist functions of TF1 and TF2, this enables to convert linear gradients into binary expressions domains, which efficiently creates linneage segregation (Sagner and Briscoe, 2017). Of particular interest for this introduction, the neural crest cells induction process is a good example of a complex gene regulatory network integrating cross-repression motifs. In fact, during neural crest cells induction, the interactions between neural and non-neural transcription factors leads to the definition of an intermediate domain, called the neural plate progenitor (NPB) domain, which is subsequently stabilized by cross-repression between NPB-specific and neural-specific TFs (Simões-Costa and Bronner, 2015).

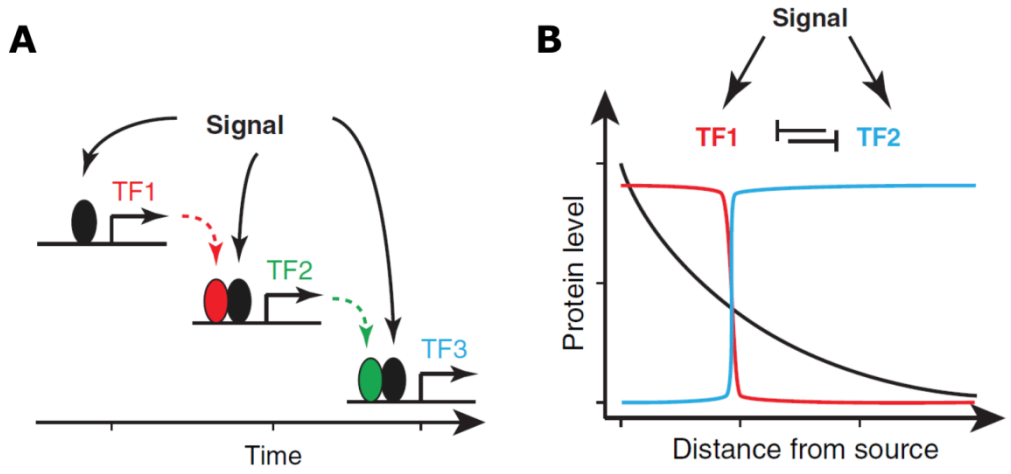

Figure 22 – Two types of interactions are combined in gene regulatory networks: the feed-forward and the cross-repressions motifs. A. Feed-forward loops integrate morphogens signals by triggering self-enhancing cascades of gene expression, which is fundamental for the stabilization of gene expression domains in space and time. **B. C**ross-repression motifs can form sharp boundaries in cells responding to a same morphogen. This is achieved through the action of transcriptional factors that repress each other and take over their couterpart depending on the morphogen concentration (Adapted from (Sagner and Briscoe, 2017)).

II. MATERIALS & METHODS

Cell culture and transfection

The immortalized myogenic C2C12 cell line was cultivated in a humidified incubator at 37°C/5% CO2, in growth medium (DMEM, 4.5g/L, D-glucose, 4mM L-glutamine, 1mM sodium pyruvate, 10% fetal calf serum). Plasmid transfection was performed using Lipofectamine 2000 (Life Technologies). 24 hours after transfection, BMP2 recombinant human protein (Thermo Fisher Scientific, #PHC7145) was applied for 1h on cells. Cells were then fixed with 4% paraformaldehyde (Electron Microscopy Science, #15710S) and immunostained with the phospho-Smad1,5,8 antibody. Or, cells were washed once with PBS, collected with PBS 1% SDS and passed through Qiashredder columns (Qiagen) to disrupt nuclei acids. Proteins extracts were then processed for Western blotting.

Mouse strains

All animal experiments were approved by the Animal Ethics Committee of Sorbonne University. We used the mouse strains described in the following papers with their MGI IDs: *Dullard*$^{flox/flox}$ (Sakaguchi et al., 2013), *Pax3*^{Cre} ((Engleka et al., 2005), MGI: 3573783), *Wnt1*^{Cre} ((Danielian et al., 1998), MGI:2386570), *Rosa26Rtdtomato* ((Muzumdar et al., 2007){Citation}, MGI: 3716464), and *C57BL/6JRj* (Janvier Labs).
Genotyping was performed with the following primers:

- Amplification of the Wildtype *Dullard* allele (210 bp):
  - Dullard WT Forward1 : 5'-CTGCAGGTGGTAATAGACAAACAC-3
  - Dullard WT Reverse1 : 5'-CTGTTCATTT AGAGAACCCCAACTA-3'

- Amplification of the floxed *Dullard* allele (573 bp):
  - Dullard WT Forward1 : 5'-CTGCAGGTGGTAATAGACAAACAC-3'
  - Dullard Flox Reverse2 : 5'-CTGTCCATCTGCACGAGACT-3'

- Amplification of the Cre allele (700bp) :
  - Forward : 5'-GTCCAATTTACTGACCGT ACACC-3'
  - Reverse : 5'-GTTATTCGG ATCATCAGCTAC ACC-3'

Immunohistochemistry

Mouse embryos were collected at embryonic day 11.5 (E11.5), noon of the day of vaginal plug observation being considered as E0.5. Embryos were dissected in cold PBS (4°c), incubated 5min in 200mM KCl to stop heart beating and fixed for 2 to 3 hours in 4% PFA at 4°c. They were cryoprotected by equilibration in 20% sucrose overnight at 4°c, embedded in OCT the following day and kept at -80°c. Cryosections were performed at 12µm thickness.
Sections were let to dry 10 min at room temperature upon withdrawal from the -80°c freezer and rehydrated for 10min in PBS. They were permeabilized 10min in PBS/0.5% Triton, rinsed in PBS and incubated for 1h in a blocking buffer (5% goat serum in PBS). The cryosections were then incubated overnight at 4°c in primary antibody solution diluted in blocking buffer (1% BSA in PBS). On the following day, they were washed multiple times in

PBS and incubated 1h in the secondary antibody solution, diluted in blocking buffer (1% BSA in PBS).

Whole-mount immunostainings were performed on whole embryos for Lightsheet microscopy and on micro-dissected OFT regions from PFA-fixed embryos for confocal microscopy.
Whole embryos were cleared following the 3Disco protocol, immunostained and imaged by Lightsheet microscopy. We followed the protocol detailed in (Belle et al., 2014) with minor changes. The first phase of sample treatment was a sequence of dehydratation, bleaching and rehydratation achieved by incubating them in solutions of increasing MetOH concentration to reach 100% MetOH concentration, then transfering them in MetOH+6% H_2O_2 and sequentially rehydrating them in H_2O. Blocking was performed by incubating the samples in PBSGT (1xPBS, 0.2% gelatin, 0.5% Triton, 0.5% saponin) for 2-3 days with rotation at RT. In the following steps, samples were incubated at 37°C in antibody solutions to increase antibody penetration in tissues. Primary antibody incubation lasted 7 days in PBSGT +10mg/ml saponin, after wish 1 day of thorough washing in PBS +0.5% Triton was performed. Then, samples were incubated overnight in secondary antibody (diluted in in PBSGT +10mg/ml saponin) and rinsed again for one extra day. Finally, we cleared the samples by incubating samples overnight in 50% Tetrahydrofuran (THF) and sequentially increasing concentration of THF to 100% by steps of 1-2h. Finally we transferred the samples in Dichloromethane for 30min and Benzyl ether until samples became transparent.

For 3D confocal microscopy, micro-dissected OFTs were immunostained, clarified and acquired following the protocol described in (Gopalakrishnan et al., 2015) with some adjustments. OFTs of E11.5 and E12 embryos were micro-dissected from embryos fixed for 2-3 hours in PFA (4%). Samples were blocked for 1h in blocking buffer (3% goat serum, 1% BSA, 0.5% Triton-100X, 1XPBS) at 4°C. The samples were then incubated for 5-7 days in primary antibody diluted in blocking buffer, at 4°C on a roller. After rinsing the samples multiple times in PBS +0,1% Tween20X for 1-2h, they were incubated in secondary antibody diluted in blocking buffer for 3-4 days. Last, the samples were deshydrated in MetOH and cleared with BABB solution (Yokomizo et al., 2012).

The primary antibodies used on cryosections include the following: GFP (chicken, Aves Labs, GFP-1020, 1/500), Pecam (rat monoclonal, Santa-Cruz Biotechnology, sc-18916, 1/200), Phospho-Smad1,8,9 (rabbit monoclonal, Cell Signaling Technology, 13820S, 1/500), MyHC (mouse monoclonal, DSHB, MF20,1/300), Smooth Muscle Actin (mouse monoclonal, Sigma-Aldrich, A2547, 1/300), Phospho-Histone H3 (rabbit monoclonal, Cell Signaling Technology, 9701, 1/500), Cleaved Caspase-3 (rabbit monoclonal, Cell Signaling Technology, Asp175, 1/500).

2D imaging, analysis and quantification

Images of immunostainings on cryosections were acquired using the following system: a Nikon Ti2 equipped with a motorized stage and a Yokogawa CSU-W1 spinning disk head coupled with a Prime 95sCMOs camera (Photometrics) driven by Metamorph (Molecular Devices).

Images were assembled and analyzed using Fiji (Schindelin et al., 2012). Quantification of phospho-Smad1,5,8 staining intensity in the NCCs (GFP^+) was achieved by creating Region of Interest (ROI) encompassing GFP^+ areas and measuring the "mean value" in these ROI.

Measures of NCCs distance and orientation to the endocardium were performed using Metamorph (Molecular Devices). The coordinates of the endocardium endpoints were registered to create an axis of reference and all NCCs nuclei were pointed to register the coordinates of their longest axis. Thus, each NCCs nucleus was represented spatially by its longest axis. From these data we inferred the centroid coordinates of the NCCs nuclei and calculated their distances as well as the angles formed by the NCCs nuclei axis with the endocardium axis.

3D imaging and image analysis

3D Lightsheet imaging was achieved by using an ultramicroscope and the supplied software from LaVision BioTec. The light sheet was generated by a laser (wavelength 488 or 561 nm, Coherent Sapphire Laser, LaVision BioTec) and two cylindrical lenses. A binocular stereomicroscope (MXV10, Olympus) with a 23 objective (MVPLAPO, Olympus) was used at different magnifications (1.63, 43, 53, and 6.33). Samples were placed in the imaging reservoir filled with DBE and illuminated from the side by the laser light. Images were acquired with a PCO Edge SCMOS CCD camera (2,560 3 2,160 pixel size, LaVision BioTec) with a step size between each image fixed at 2 mm. The acquisition varied depending on the number of lasers used to generate and focus the light sheet, one side or two sides depending on the image rendering (Belle et al., 2014).

3D acquisition of BABB cleared samples was done using LSM 700 laser-scanning confocal microscope and ZEN software (Carl Zeiss). 16 bit mosaic images were acquired as Z-stacks with a Plan-Apochromat 10x/0.45 objective (digital zoom 1.5) using a 7um z-interval. Volume-3D rendering of the z-stack series was performed in Imaris software (Bitplane). All images were assembled in Adobe Photoshop and InDesign (Adobe Systems).

In situ hybridisation

PFA fixed cryosections were let to dry and incubated overnight at 69°C with the Digoxigenin-labeled RNA probe targeting Sema3c mRNA, diluted in hybridisation buffer (1x Salt, 50% deionised formamide, 10% dextran sulphate, tRNA (1mg/ml), 1X Denhardt's in H_2O). The Sema3c probe was kindly provided by the lab of S. Zaffran (Bajolle et al., 2006). On the

following day sections were washed multiple times in SSC 1x, 50% formamide, 0,1% Tween, as well as in MABT. After 1h of blocking, slides were incubated 1h at RT in anti-digoxigenine antibody (Roche, 1/3000) diluted in MABT. Slides were washed multiple times in MABT for 1h. Finally, the staining was revealed with NTMT (NBT 4.5µl/ml, BCIP 3.5µl/ml) until colour reaction reached satisfying levels, after which the staining was fixed in PFA 1%.

Tissue dissociation and FACS sorting

Mouse embryos were collected at E11.5 and placed in HBSS +1% FBS (HBSS +/+, Invitrogen) during the duration of genotyping. Then, OFTs were micro-dissected under the stereomicroscope and dissociated by 15min incubation in collagenase (0.1mg/ml in H_2O, C2139 Sigma). Subsequently, we virougorously pipetted the solution until no pieces of tissues were left to see by examination under the stereomicroscope. HBSS +10% FBS was added to the cells medium to stop the enzymatic reaction. OFTs cells suspensions were centrifugated and resuspended in HBSS +1% FBS before following up with the FACS antibody staining procedure. The panel of conjugated antibodies used for FACS included Ter119 Pe-Cy7 (Erythroid Cells, anti-mouse, Sony, Catalog No. 1181110, 1/300), CD45 APC-Cy7 (Rat anti-mouse, BD Pharmingen, Catalog No. 557659, 1/300), CD31 APC (Rat anti-mouse, BD Pharmingen, Clone MEC 13.3 Catalog No. 561814, 1/300), diluted in HBSS (1% FBS). Cells were centrifugated and resuspended in antibody solution for a 25min incubation period (4°C in the dark). Before acquisition, cells were washed several times, filtered (Fisher cell strainer, 70µm mesh) and 7AAD PE-Cy7 (1/800) was added in the cells suspension to exclude dead cells.

Cells were sorted in a BD FACSAria™ III directly into 96-well plates loaded with RT-STA reaction mix (CellsDirect™ One-Step qRTPCR Kit, Invitrogen, according to the manufacturer's procedures) and 0.2x specific TaqMan ® Assay mix (see Table1 page 82 for assays list). For single cell sorting a control-well with 20 cells was consistently realized.

Single-Cell gene expression

Cells were sorted in 96-well qPCR plates in 9 µl of a CellsDirect One-Step quantitative RT-PCR Kit (Life Technologies), containing mixtures of diluted primers (0.05× final concentration). Preamplified cDNA was obtained after reverse transcription (15 min at 40°C, 15 min at 50°C and 15 min at 60°C), and preamplification (22 cycles: 15 s at 95°C and 4 min at 60°C), and diluted 1:5 in TE pH8 Buffer (Ambion), as described in (Perchet et al., 2018). Sample mix was as follows: diluted cDNA (2.9 µl), Sample Loading Reagent (0.29 µl; Fluidigm), TaqMan Universal PCR Master Mix (3.3 µl; Applied Biosystem), or Solaris quantitative PCR Low ROX Master Mix (3.3 µl; GE Dharmacon). The assay mix was as follows: Assay Loading Reagent (2.5 µl; Fluidigm) and TaqMan (2.5 µl; Applied Biosystem). A 48.48 dynamic array integrated fluidic circuit (IFC; Fluidigm) was primed with control line fluid, and the chip was loaded with assays (TaqMan) and samples using an HX IFC controller (Fluidigm). The experiments were run on a Biomark (Fluidigm) for amplification and

detection (2 min at 50°C, 10 min for TaqMan reagents or 15 min for Solaris reagents at 95°C, 40 cycles: 15 s at 95°C and 60 s at 60°C).

Quantification of *Dullard* expression was performed with a FAM-MGB custom Taqman® made assay with the following primers and probe sequences.

query_L1	*GCAGATCCGCACGGTAATTC*
query_R1	*GTTTCGTCCAGATCCAGCAC*
query_P1	*CCCGGAATCGCCTAGCCCAGGT*

Bioinformatic analysis

The analytic framework used followed the one described in (Perchet et al., 2018). For visualisation of the single cell multiplex qPCR, done on 44 genes, we generated a heatmap using the pHeatmap (v1.0.10) R package (v3.2.2).

Statistical analysis

Statistical analysis was performed with the Student's t-test or Mann-Whitney test depending on normality. The analysis was performed using Prism Software (GraphPad). Statistical significance is represented as follows: ***$p < 0.001$. All results are shown as mean ± standard deviation.

Table 1 - List of TaqMan® gene expression assays (20x, Life Technologies) used for single-cell qPCRs experiments.

Gene Symbol	Gene ID	Dye	Assay ID
Nkx2-5	18091	FAM-MGB	Mm01309813_s1
Myh6	17888	FAM-MGB	Mm00440359_m1
Gja1	14609	FAM-MGB	Mm00439105_m1
Acta2	11475	FAM-MGB	Mm01546133_m1
Myh11	17880	FAM-MGB	Mm00443013_m1
Snai2	20583	FAM-MGB	Mm00441531_m1
Twist1	22160	FAM-MGB	Mm04208233_g1
Postn	50706	FAM-MGB	Mm00450111_m1
Kdr	16542	FAM-MGB	Mm01222421_m1
Flt1	14254	FAM-MGB	Mm01210866_m1
Nfatc1	18018	FAM-MGB	Mm00479445_m1
Tek	21687	FAM-MGB	Mm00443243_m1
Fn1	14268	FAM-MGB	Mm01256744_m1
Tbx1	21380	FAM-MGB	Mm00448949_m1
Isl1	16392	FAM-MGB	Mm00517585_m1
Tcf21	21412	FAM-MGB	Mm00448961_m1
Wt1	22431	FAM-MGB	Mm01337048_m1
Ctdnep1	67181	FAM-MGB	Mm00835314_g1
Bmp4	12159	FAM-MGB	Mm00432087_m1
Id1	15901	FAM-MGB	Mm00775963_g1
Id2	15902	FAM-MGB	Mm00711781_m1
Msx1	17701	FAM-MGB	Mm00440330_m1
Msx2	17702	FAM-MGB	Mm00442992_m1
Six2	20472	FAM-MGB	Mm03003557_s1
Sema3c	20348	FAM-MGB	Mm00443121_m1

Nrp1	18186	FAM-MGB	Mm00435379_m1
Plxna2	18845	FAM-MGB	Mm00801930_m1
Plxnd1	67784	FAM-MGB	Mm01184367_m1
Hspg2	15530	FAM-MGB	Mm01181173_g1
sox9	20682	FAM-MGB	Mm00448840_m1
Acan	11595	FAM-MGB	Mm00545794_m1
Col2a1	12824	FAM-MGB	Mm01309565_m1
Mmp14	17387	FAM-MGB	Mm00485054_m1
Mmp2	17390	FAM-MGB	Mm00439498_m1
Adamts1	11504	FAM-MGB	Mm01344169_m1
Adamts5	23794	FAM-MGB	Mm00478620_m1
Cdh2	12558	FAM-MGB	Mm01162497_m1
Cdh5	12562	FAM-MGB	Mm00486938_m1
RhoA	11848	FAM-MGB	Mm00834507_g1
Rac1	19353	FAM-MGB	Mm01201653_mH
Klf2	16598	FAM-MGB	Mm00500486_g1
Gapdh	14433	FAM-MGB	Mm99999915_g1
Hprt	15452	FAM-MGB	Mm03024075_m1
Actb	11461	FAM-MGB	Mm02619580_g1
Vim	22352	FAM-MGB	Mm01333430_m1
Vegfa	22339	FAM-MGB	Mm00437306_m1
Stat3	20848	FAM-MGB	Mm01219775_m1

III. RESULTS

Aim of the project

The formation of the great arteries and their connection to the heart is a fascinating morphogenetic process that establishes the systemic circulation in the fetus, and prepares the pulmonary circulation for postnatal life. In humans, many congenital malformations affect the arterial pole of the heart. Yet, the molecular and cellular mechanisms underpinning their etiology are numerous and probably cross-interfering. This complexity makes their understanding difficult. In the heart outflow tract (OFT) a variety of cell types interact in a tightly coordinated manner to drive OFT septation and generate the two great arteries connected to the heart ventricles. Myocardial and endocardial progenitors, as well as neural crest cells (NCCs) coming from the neural tube, compose the niche that orchestrate the remodeling of the OFT. Many studies have shown that the NCCs recruitment to the OFT is a mandatory cellular event to OFT septation. It becomes clearer that this recruitment was a key evolutionary step that supported OFT septation and consequently the emergence of a pulmonary circulation. However, the functions of NCCs during OFT septation and the nature of their interaction with the surrounding progenitors remains poorly understood. At the molecular level, many signaling pathways are involved in the regulation of OFT remodeling, amongst which BMP signaling stands as a major player. It was shown that blocking BMP signaling results in a reduced contribution of NCCs to the OFT mesenchyme, which prevents OFT sepation. Yet, the influence of BMP signaling on the NCCs during septation is not known. In order to investigate the function of NCCs during OFT sepation and the regulation operated by BMP signaling, we aimed at creating a gain-of-function (GOF) model, with increased BMP signaling in the cardiac NCCs. Deleting Dullard, a phosphatase described as a negative regulator of BMP signaling, was recently shown to be an effective approach to obtain such a GOF model in mice (Hayata et al., 2018; Sakaguchi et al., 2013). Hence, we investigated the phenotypes caused by the loss of this protein in NCCs. We first evaluated the levels of BMP intracellular signaling, using immunostaining for the activated forms of Smad. Then, we characterized with immuno-histological approaches the morphology of the OFT and the great arteries. Performing single-cell transcriptional analysis, we assessed the effects of BMP signaling overactivation on the transcriptional signature of NCCs and of other progenitors composing the OFT niche. This screen brought us to reevaluate the cell behaviors in the OFT and re-analyze the pattern of distribution of key regulator of cell-cell communication. This allowed us to correlate gene expression domains with the spatial organization of the tissue, and thus observe the effect of BMP signaling on NCCs behavior, as well as the non cell-autonomous effect notably on myocardial progenitors.

III.1 Effect of Dullard on BMP signaling activity

III.1.1 In vitro experiments confirm the regulatory function of Dullard on BMP signaling

The Dullard protein is a phosphatase composed of a C-teminal catalytic domain and a N-terminal transmembrane domain (Kim et al., 2007). This phosphatase was described as a potent inhibitor of BMP signaling in xenopus, drosophila and mice (Sakaguchi et al., 2013; Satow et al., 2006; Urrutia et al., 2016). To validate Dullard inhibitory effect on BMP signals activation, we performed in vitro experiments using the myogenic cell line C2C12. We transfected C2C12 cells with GFP as a control, the wildtype Dullard or a version of Dullard carrying a phosphatase-dead domain (D67E), and exposed the cells for one hour to BMP2. In order to quantify the activation of BMP signaling we made use of an antibody recognizing the phosphorylated forms of Smad1,5,8 (phosphor-Smad1,5,8), which are the activated forms of the downstream BMP transducers Smad1,5,8. Western Blots were performed on treated cells and showed a strong decrease of Sma1,5,8 phosphorylation levels in cells transfected with Dullard (Figure 23A, page 91). In addition, cells transfected with the D67E Dullard mutated form retained phosphorylation levels comparable to controls. To complement this analysis we examined the intensity of the phospho-Smad1,5,8 immunostaining in C2C12 and quantified the number of positive cells per condition (Figure 23B, page 91). While Dullard transfection significantly reduced the percentage of cells positive for phospho-Smad1,5,8, cells transfected with the mutated form of Dullard (D67E) presented a percentage of cells comparable to control cells. Hence, our results confirmed that Dullard, through its catalytic domain, inhibits the BMP-mediated phosphorylation of Smad1,5,8 *in vitro*.

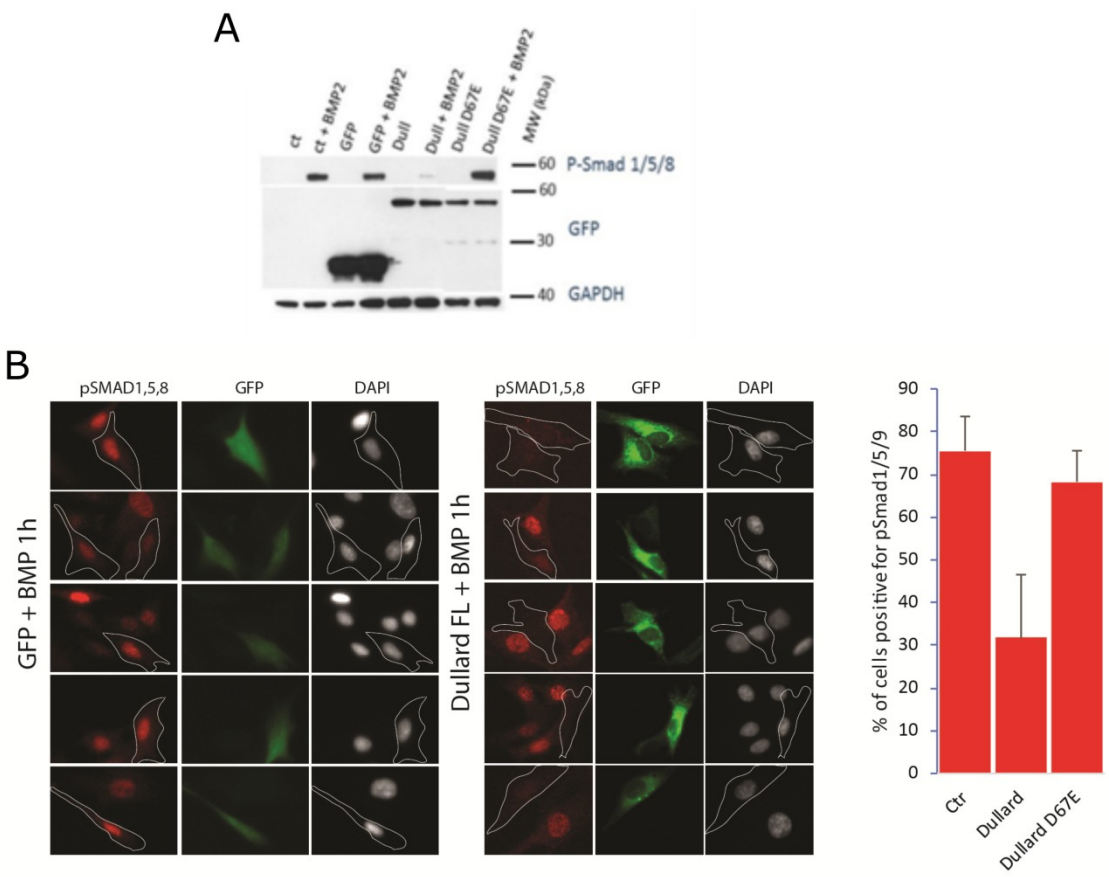

Figure 23 – Dullard inhibits the BMP-mediated phosphorylation of Smad1,5,8 *in vitro*. A. Western blot showing the phosphorylation levels of Smad1,5,8 in the muscle cell line C2C12 after exposure to BMP2 for 1H. Cells transfected with Dullard (Dull) do not show any phosphorylation of Smad1,5,8 whereas a mutation in the phosphatase-dead domain (D67E) retains this phosphorylation. **B.** A similar result was obtained by immunofluorescence, showing that only cells transfected with Dullard lose the nuclear phospho-Smad1,5,8 staining. On the Right: A quantification of three different experiments was performed on transfected cells.

III.1.2 Cre-Lox recombination efficiently suppress Dullard expression in neural crest cells (NCCs)

The NCCs delaminate from the dorsal neural tube between the mid-otic placode and the third somite - and migrate through the pharyngeal mesoderm to reach the developing heart outflow tract (OFT). There, they enlarge the cardiac cushions, which is mandatory for the initiation of OFT septation (Hutson and Kirby, 2010; Jiang et al., 2000; Snider et al., 2007).

We used mice carrying floxed versions of the *Dullard* allele (Sakaguchi et al., 2013) and expressing the Cre recombinase under either the *Pax3* or *Wnt1* loci, which are activated within the pre-delaminating NCCs (Danielian et al., 1998; Engleka et al., 2005). We also used the reporter allele *Rosa26mTmG* to monitor cells that had been recombined by the Cre drivers (Muzumdar et al., 2007). The pattern of cell recombination in the OFT, both in

presence or absence of Dullard in embryos carrying either Cre drivers, matches previous lineage analyses of NCCs colonizing cardiac cushions (Figure 24, page 92) (Brown et al., 2001; Jiang et al., 2000).

In addition, we wanted to make sure that Dullard was expressed in control cardiac NCCs, and that Cre-Lox recombination was an efficient strategy to suppress Dullard expression in mutant NCCs. To address this question we dissected OFT of E11.5 *Wnt1^{Cre}; Dullad$^{Flox/+}$; R26^{mTmG}* and *Wnt1^{Cre}; Dullard$^{Flox/Flox}$; R26^{mTmG}* embryos and sorted the GFP+ NCCs as well as CD31+ endocardium and all other tomato positive progenitors (named RFP^{+}) (Figure 33A, page 105). We performed single-cell RT-qPCR to quantify Dullard expression and observed that Dullard is expressed in the different populations composing the OFT and is specifically suppressed in mutant *Wnt1^{Cre}; Dullard$^{Flox/Flox}$; R26^{mTmG}* GFP^{+} NCCs, thus validating the knock-out approach (Figure 25, page 93).

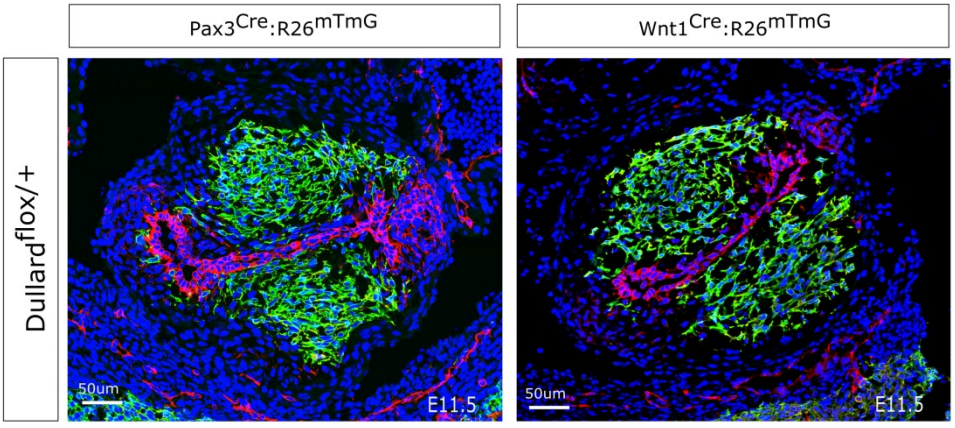

Figure 24 - **Pattern of recombination driven by *Pax3* or *Wnt1* loci in the heart OFT**. OFT transversal section of E11.5 *Pax3Cre; Dullard$^{Flox/+}$; R26^{mTmG}* and *Wnt1^{Cre}; Dullard$^{Flox/+}$; R26^{mTmG}* embryos showing in green GFP+ NCCs in the cardiac cushions, visualized using the *Rosa26Rtdtomato* reporter. *Wnt1^{Cre}* and *Pax3^{Cre}* mouse driver lines present the same pattern of colonization of the OFT.

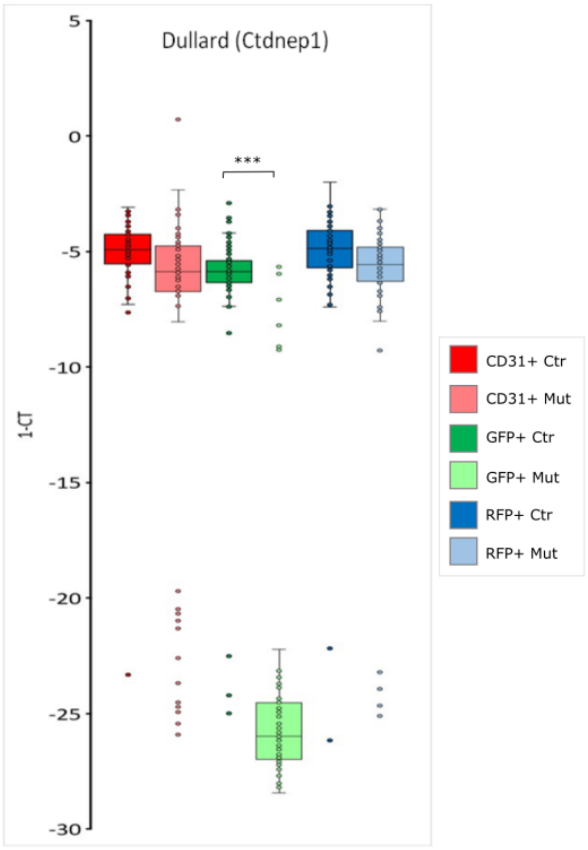

Figure 25 - Level of expression of *Dullard* in the progenitors composing control and mutant OFT. Inversed Ct value for GFP^{+} NCCs, CD31^{+} (endocardium progenitors) and RFP^{+} (other progenitors of the OFT) from *Wnt1^{Cre}; Dullard$^{Flox/+}$; R26^{mTmG}* (Ctr) and *Wnt1^{Cre}:Dullard$^{Fllox/Flox}$; R26^{mTmG}* (Mut) embryos *(Student's T-test, P-value < 0.001)*.

III.1.3 Increase in NCCs graded response to BMP signals upon *Dullard* deletion

BMP signals (BMP2/4/6/7) have been described to be secreted by the OFT outer-ring of myocardium (Jia et al., 2007; Jiao et al., 2003; Jones et al., 1991; Liu et al., 2004; Zhang et al., 2010). NCCs ablation and experiments of BMP loss-of-function in the NCCs both lead to the formation of hypoplastic cushions and absence of OFT septation (Bockman et al., 1987; Jia et al., 2007; Stottmann et al., 2004; Tang et al., 2010). This supports a model whereby fine tuning of BMP levels mainly within NCCs is necessary for proper OFT septation. Yet, the molecular mechanism tuning BMP levels in the NCCs remains to be established. Moreover, we have very little insights on how this signaling influences the NCCs behavior underpinning OFT remodelling.

We first examined if *Dullard* deletion in the NCCs was cell-autonomously upregulating BMP signaling in the NCCs. To this end, we immunolabelled phospho-Smad1,5,8 on serial cryosections positioned 50-60µm apart along the OFT axis at E11.5 (Figure26B, page 95). This method (used in (Tozer et al., 2013)) enabled us to quantify the spatial response of the cardiac NCCs to BMPs signals as they progress from the distal to the proximal OFT levels. Reminiscent of the time-dependent colonization, quantifications revealed variations of phospho-Smad levels, which were more elevated proximally than distally along the OFT axis (Figure 26C, page 95). Furthermore, whatever the levels along the OFT axis, there was a striking increase in Smads phosphorylation in both $Pax3^{Cre}$ and $Wnt1^{Cre}$; $Dullard^{Flox/Flox}$ mutant NCCs compared to heterozygous control NCCs (Figure26B, page 95). All together these results show (i) that *Dullard* deletion in the cardiac NCCs leads to a gain-of-function of BMP signaling in these cells and (ii) that a gradient of BMP signaling activity is established along NCCs colonizing the OFT. We conclude that Dullard is not absolutely required for the establishment of a gradient of BMP response in NCCs along the OFT axis, although it necessary for a tight regulation of its magnitude.

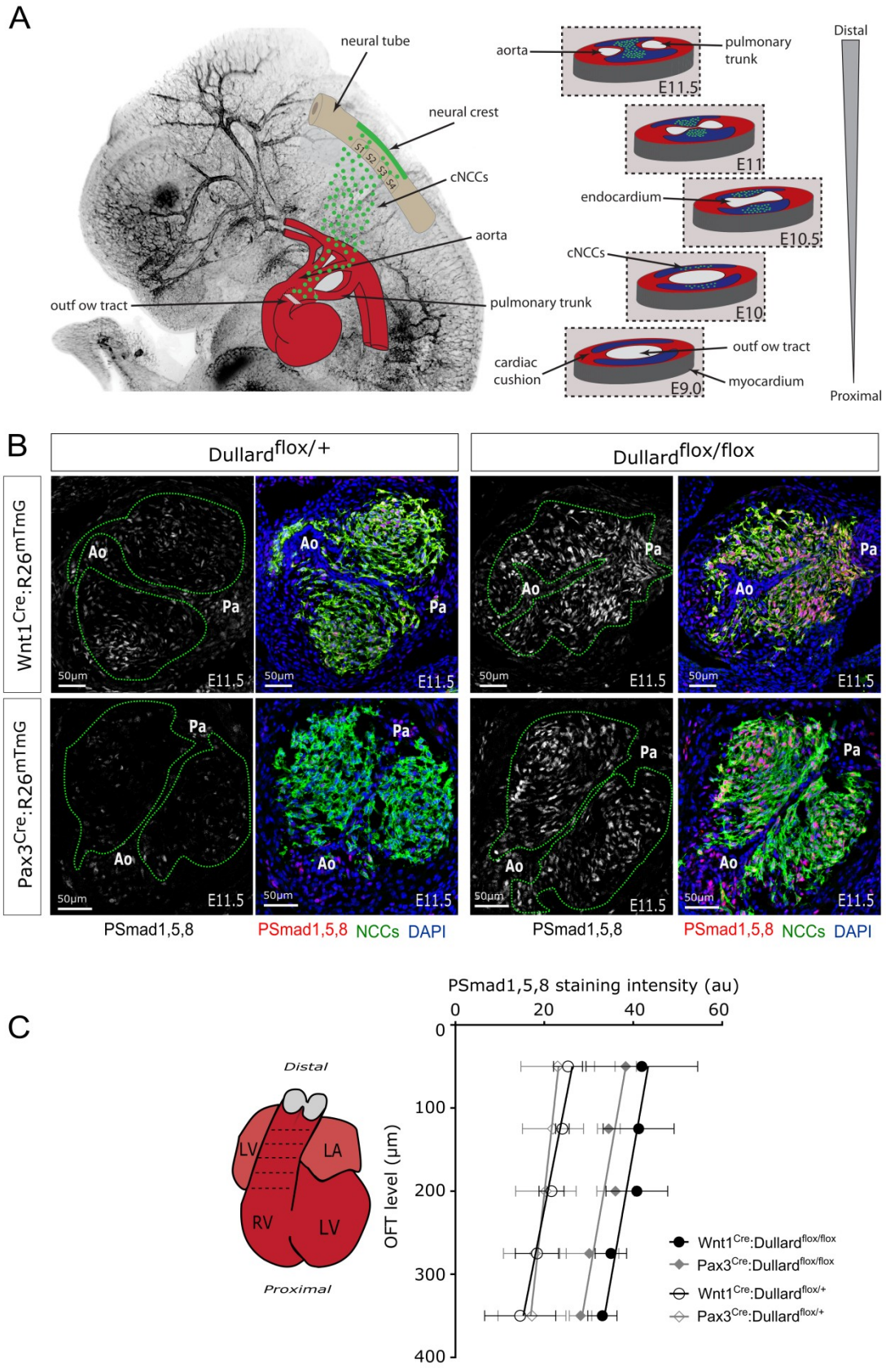

Figure 26 - Dullard regulates the cardiac NCCs response to myocardial BMP signals. **A**. Schematic view of OFT septation with the different stages of NCCs ingression. A drawing of NCCs (in green) migrating from the neural tube towards the heart (in red) has been superimposed to a E11.5 embryo stained for Pecam and imaged by

light sheet microscopy. On the right, schematic transversal sections of OFT at different embryonic stages show the colonization of the cardiac cushions by NCCs that results in the septation of the OFT into the aorta and pulmonary trunk. At E11.5, all the stages of septation can be visualized along the OFT distal to proximal axis. **B.** Transversal sections of OFT from E11.5 *Wnt1^{Cre}/Pax3^{Cre};Dullard$^{Flox/+}$;R26^{mTmG}* and *Wnt1^{Cre}/Pax3^{Cre};Dullard$^{Flox/Flox}$;R26^{mTmG}* embryos stained for phospho-Smad1,5,8. Because the embryos have a *Rosa26Rtdtomato* reporter knock-in, recombined NCCs are GFP^{+} (in green). We observe a strong increase in the phospho-Smad1,5,8 signal intensity in *Wnt1^{Cre}/Pax3^{Cre};Dullard$^{Flox/Flox}$* NCCs. **C.** Graph presenting the intensity of phospho-Smad1,5,8 staining in *Wnt1^{Cre}/Pax3^{Cre};Dullard$^{Flox/+}$* and *Wnt1^{Cre}/Pax3^{Cre};Dullard$^{Flox/Flox}$* embryos at different levels along the OFT distal to proximal axis. A gradient of BMP signaling activity is established in the NCCs positionned along the OFT axis and its magnitude is increased in *Wnt1^{Cre}/Pax3^{Cre};Dullard$^{Flox/Flox}$* embryos. Ao, Aorta; Pa, pulmonary artery.

III.2 Phenotypic impact of BMP signaling overactivation in cardiac NCCs

III.2.1 Mutant NCCs do not present defects of migration, survival or proliferation in the developping OFT

Specifically deleting genes involved in BMP signaling in NCCs was shown to cause NCCs migratory defects, resulting in cardiac malformations (High et al., 2007; Jia et al., 2007, 2007; Stottmann et al., 2004; Tang et al., 2010). We thus used confocal and lightsheet microscopy to study both in 2D and 3D the colonization of NCCs in the OFT. Our observations pointed out that *Wnt1^{Cre}/Pax3^{Cre};Dullard$^{Flox/Flox}$* NCCs colonized the OFT in a similar pattern compared to *Wnt1^{Cre}/Pax3^{Cre};Dullard$^{Flox/+}$* and had reached proximal OFT levels by E11.5 (Figure 27, page 97). In addition, malformations linked to NCCs dysfunction can be due to decreased number of NCCs reaching their final destination (Kaartinen et al., 2004; Tang et al., 2010). Quantifications at E11.5 of the number of GFP-positive NCCs on distal, medial and proximal transversal OFT sections did not reveal any difference between control and mutant NCCs numbers (Figure 28A, page 93). Last, some publications described intense NCCs apoptosis in the OFT of wiltype and mutant embryos (Abu-Issa et al., 2002; Macatee et al., 2003; Poelmann and Gittenberger-de Groot, 2005; Poelmann et al., 1998). Yet, cardiac NCCs with *Dullard* deletion did not present any significant difference in their rate of proliferation and apoptosis at E11.5 (Figure 28B, 28C, page 93). Hence, we concluded that Dullard is not required for NCCs migration nor for their amplification and survival in the OFT niche.

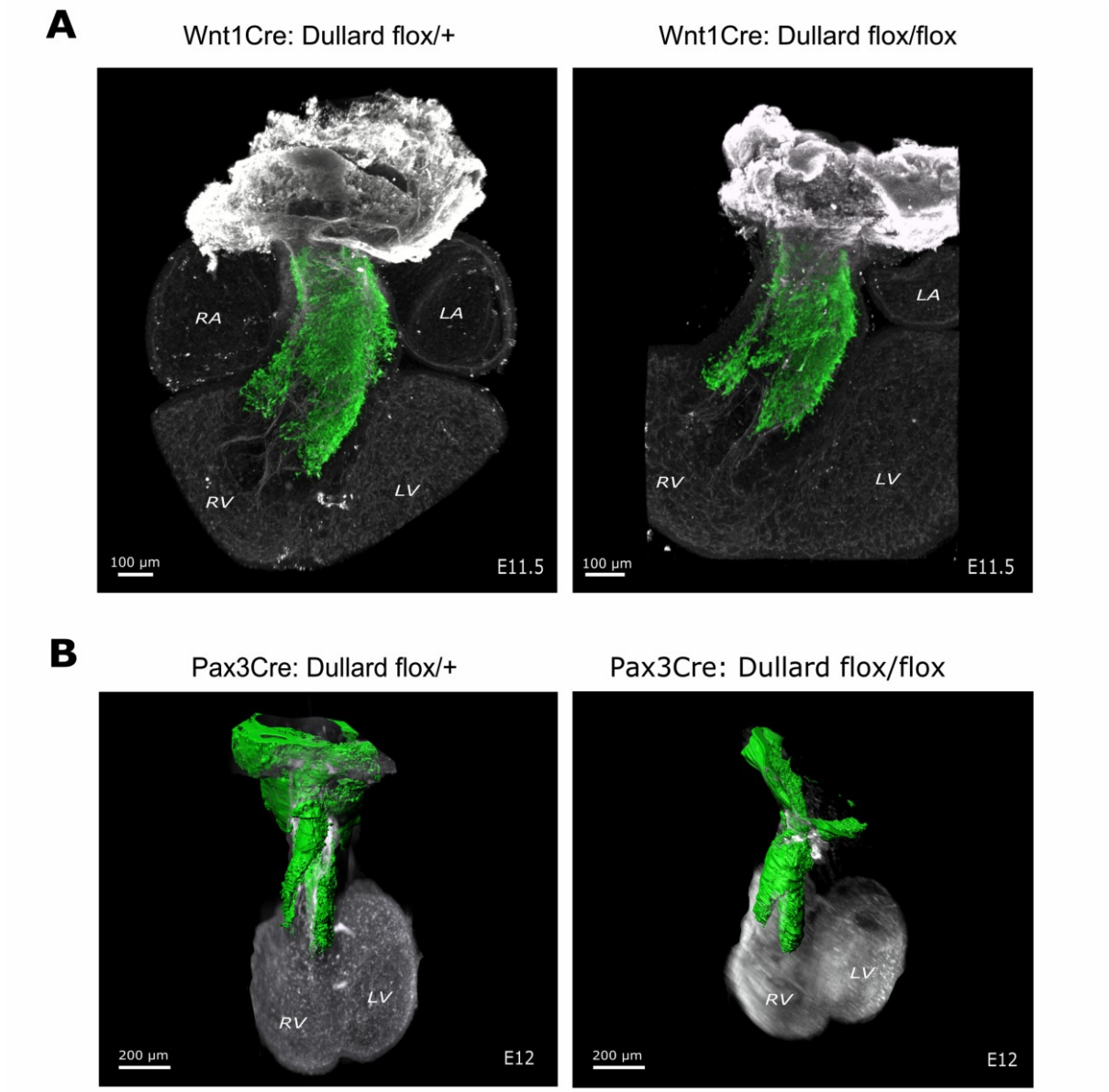

Figure 27- Imaging of the NCCs colonization in the heart OFT at E11.5-E12. **A.** Confocal acquisition of *Wnt1^{Cre};Dullard$^{Flox/+}$;R26^{mTmG}* and *Wnt1^{Cre};Dullard$^{Flox/Flox}$;R26^{mTmG}* E11.5 OFT after BABB clearing. GFP+ NCCs are represented in green and Pecam+ endocardium in white. **B.** Three dimentionnal rendering of a lightsheet acquisition of *Pax3^{Cre};Dullard$^{Flox/+}$;R26^{mTmG}* and *Pax3^{Cre};Dullard$^{Flox/Flox}$;R26^{mTmG}* OFT after 3Disco clearing. No defect in the colonization of the NCCs in the OFT was observed. RA, Right Atrium; LA, Left atrium; RV, Right ventricle; LV, Left Ventricle.

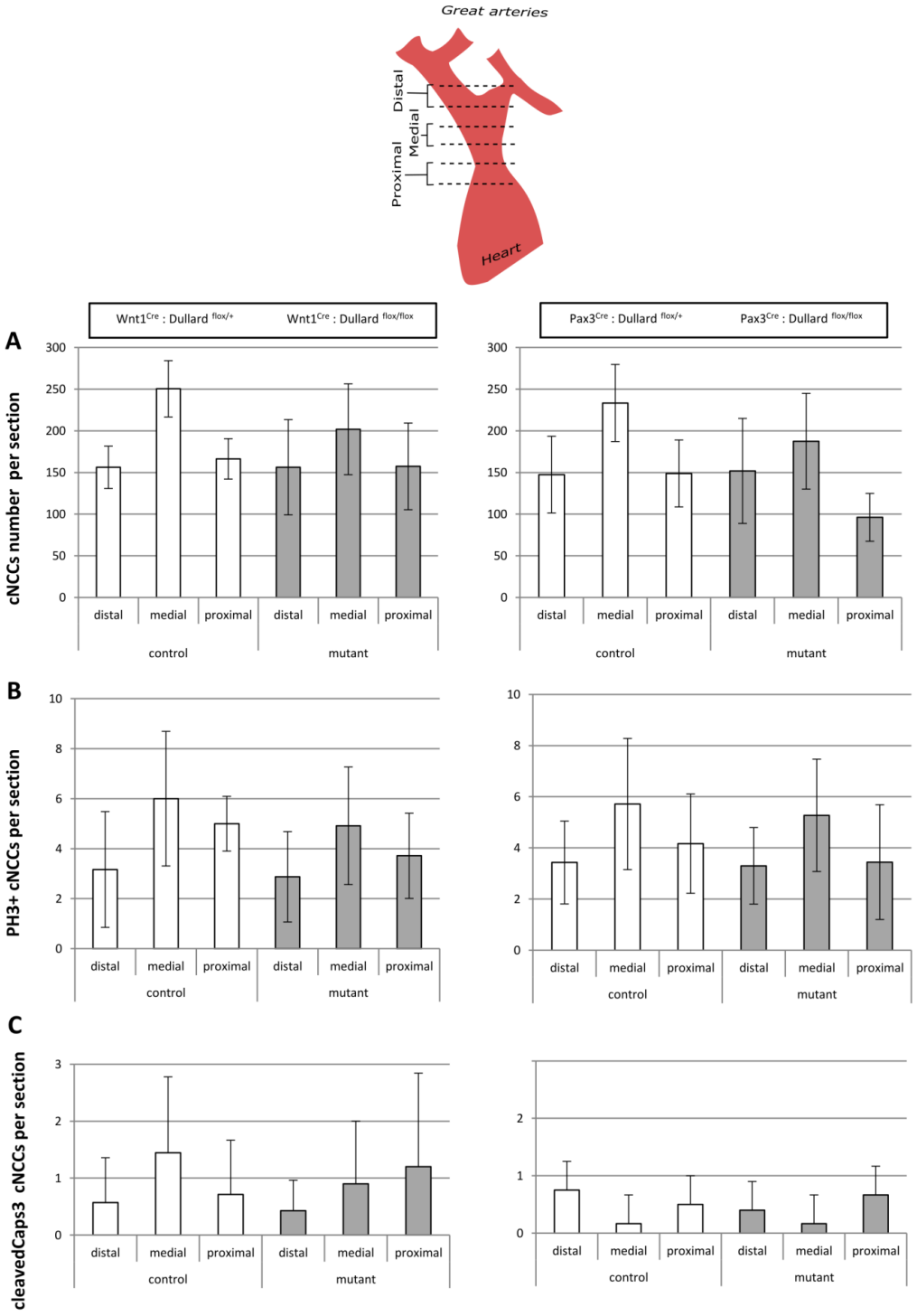

Figure 28- Quantification of the cardiac NCCs (NCCs) number, proliferation and apoptosis. Quantifications were performed in *Pax3/Wnt1^{Cre};Dullar$^{+/Flox}$* and *Pax3/Wnt1^{Cre};Dullard$^{Flox/Flox}$* embryos, on transversal sections positionned along the distal to proximal axis of the OFT. Scheme of OFT levels categorized in three levels, Distal (away from the heart ventricles), Medial and Proximal (close to the heart ventricles). **A.** Quantification of the number of NCCs per axial category shows a similar distribution in control and mutant embryos. **B.** Quantification of the number of NCCs positive for PH3 (marker of G2 or mitotic phases) per axial category shows a similar distribution in control and mutant embryos. **C.** Quantification of the number of NCCs positive for cleaved-Caspase3 (marker of apoptosis) per axial category shows no significant difference in control and mutant embryos.

III.2.2 Dullard deletion in the NCCs causes malformation of the great arteries and embryonic death

The absence of Dullard was embryonically lethal in both *Pax3^{Cre}* and *Wnt1^{Cre}* mice lines. In fact, while *Pax3^{Cre}/Wnt1^{Cre}; Dullard$^{Flox/Flox}$* embryos were recovered at the expected mendelian ratio of 25% before E12.5, this ratio dropped below 10% afterwards (Figure 29, page 100). Such early lethality is often caused by cardiovascular defects during embryonic development. Moreover, the NCCs post-migratory behavior in the cardiac cushions has been shown critical for the proper formation of the aorticopulmonary septum and great arteries (Phillips et al., 2013; Plein et al., 2015). We thus examined the heart septation status of *Pax3^{Cre}/Wnt1^{Cre}; Dullard$^{Flox/Flox}$* embryos. A first morphological analysis revealed that, although non-significant, E11.5 mutant OFTs tended to have smaller transversal areas (Figure 30, page 100). Then, using 3D Lightsheet microscopy and staining the great arteries using Pecam as marker, we consistently observed a malformation of the forming great arteries, characterized by a strong atrophy of the emerging pulmonary artery (Pa) (Figure 31A, page 101).

To examine what morphogenetic dysfunction was driving such a cardiovascular defect, we performed immunostainings on OFT transversal sections (Figure 31B, page 101). At distal levels, the OFT of control embryos displayed symmetrical septation and formation of great arteries similar in size. In contrast, *Pax3^{Cre}/Wnt1^{Cre}; Dullar$^{Fllox/Flox}$* embryos exhibited an asymmetric breakdown of the endocardium on the pulmonary side and obstruction of the Pa. The contact between the endocardium and the subpulmonary myocardium was impaired at proximal/ medial levels whereas it retained its integrity at similar levels in controls. The specific region of the subpulmonary myocardium to which the endocardium attaches is positively stained by Pecam, an adhesion protein, suggesting that it is not a structure of myocardial lineage but rather the presumptive pulmonary valve intercalated-cushion (PV-IC) described by (Mifflin et al., 2018). Hence, while the endocardium joined the PV-IC at medial levels in control OFT, endocardium had already broken down and was pushed on the aortic side in mutant OFT. This demonstrates that the OFT septation is not only asymmetric but also premature in *Pax3^{Cre}/Wnt1^{Cre}; Dullard$^{Flox/Flox}$* embryos.

In sum, our results showed that BMP upregulation in the cardiac NCCs does not seem to impact the ability of the NCCs to colonize the OFT but rather caused a post-migratory phenotype. In fact, the deletion of *Dullard* in the cardiac NCCs caused an asymmetric and premature OFT septation, which provides an explanation for the early lethality of Dullard mutants, probably caused by haemodynamics complications associated to faulty aorta remodelling and Pa obstruction. Moreover, we showed that Dullard plays a pivotal role during NCCs-mediated OFT septation through the modulation of BMP signalling.

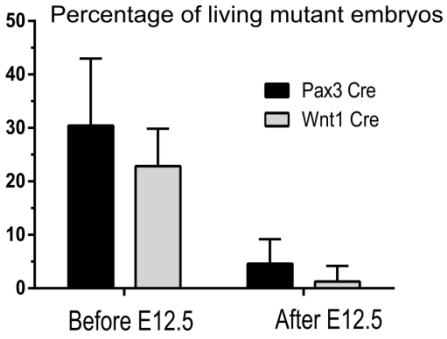

Figure 29- Quantification of mutant embryos recovered alive along the gestation period. Quantification was performed on both *Pax3*^{Cre}*;Dullard*$^{Flox/Flox}$ and *Wnt1*^{Cre}*;Dullard*$^{Flox/Flox}$embryos. A drastic shift occurs around E12.5. After this gestational stage, the percentage of recovered mutant embryos alife drops from an expected Mendelian ratio of 25%, to below 10 %.

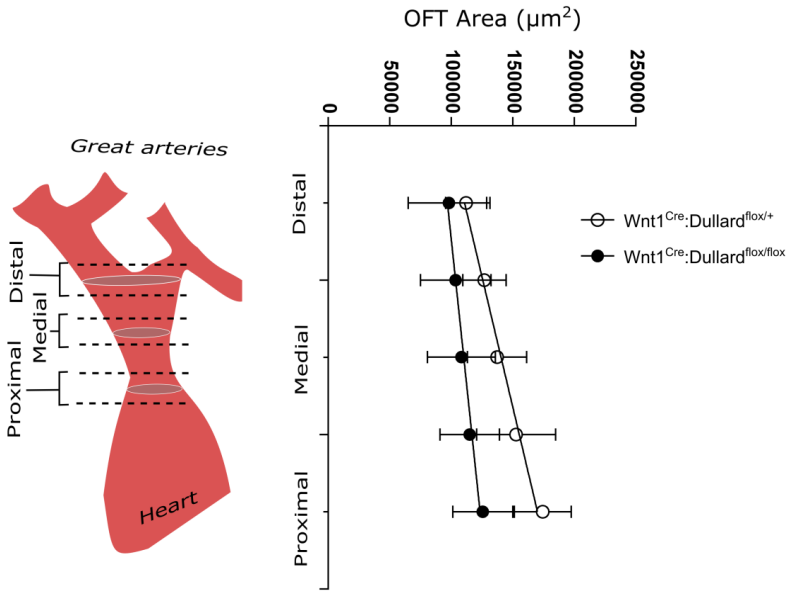

Figure 30 – Measurement of the OFT transversal area. Quantification was performed along the distal to proximal axis in *Wnt1*^{Cre}*;Dullard*$^{Flox/+}$ and *Wnt1*^{Cre}*;Dullard*$^{Flox/Flox}$ embryos at E11.5. Although not significant, there is a tendency for mutant OFT to present a smaller transversal area.

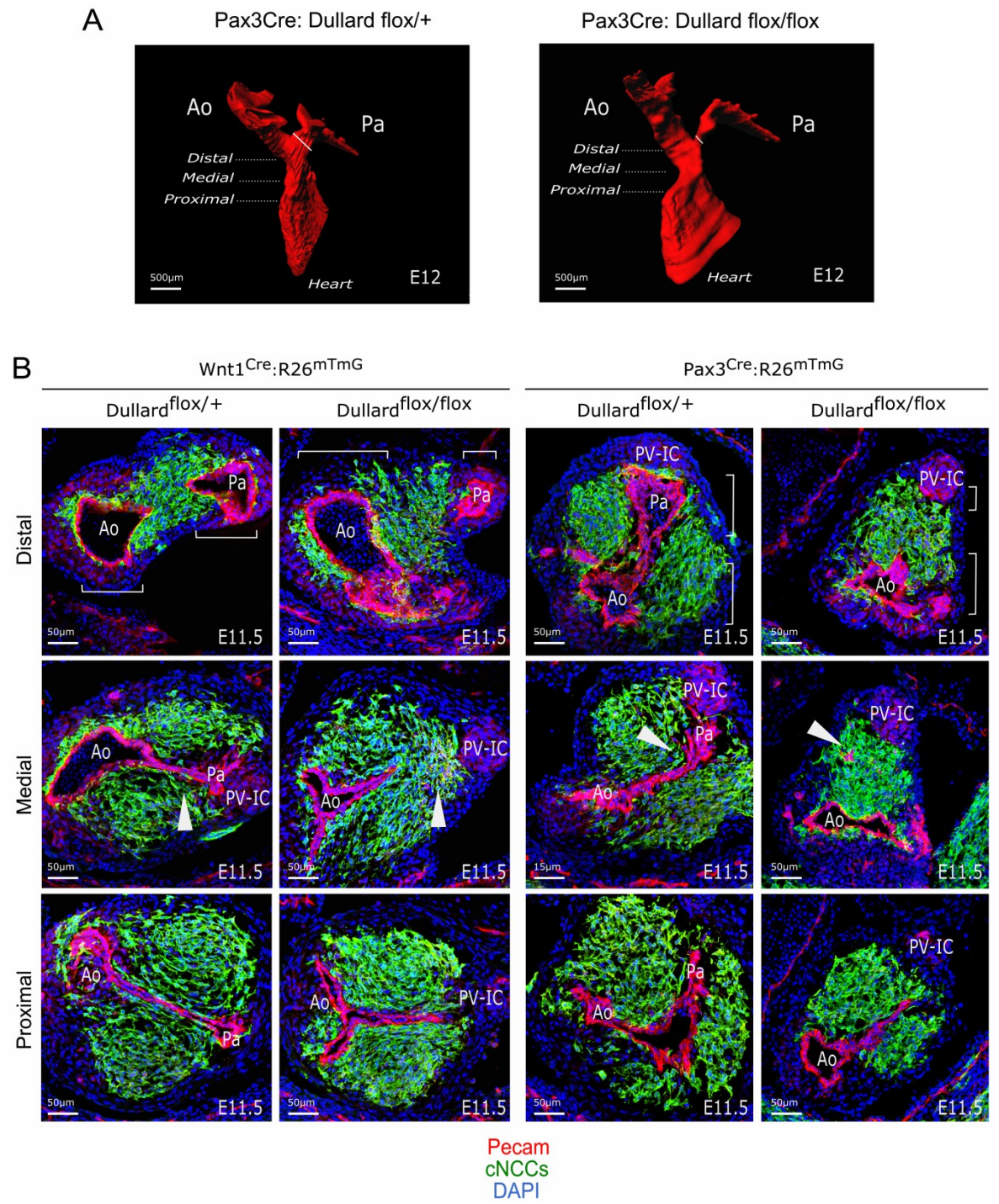

Figure 31 – Dullard deletion in neural crest cells causes asymmetric and premature OFT septation. 3D and 2D imaging of the OFT at E11.5/E12, highlight a stricking defect in the great arteries formation and OFT septation process. **A.** Three-dimensional rendering of the OFT of *Pax3^{Cre}; Dullard$^{Flox/+}$* and *Pax3^{Cre}; Dullard$^{Flox/Flox}$* E11.5 embryos, stained with Pecam antibody and acquired by lightsheet imaging after 3Disco clearing. We observe a strong atrophy of the pulmonary artery in the mutant embryo (oblique white line). **B.** Serial sections of *Wnt1^{Cre}/Pax3^{Cre};Dullard$^{Flox/+}$;R26^{mTmG}* and *Wnt1^{Cre}/Pax3^{Cre};Dullard$^{Flox/Flox}$;R26^{mTmG}* OFT at distal, medial and proximal levels stained for Pecam (red) and GFP (green). At more proximal levels, we observe that the endocardium of mutant *Wnt1^{Cre}/Pax3^{Cre}; Dullard$^{Flox/Flox}$* embryos detaches from the presumptive PV-IC (located in the subpulmonary myocardial wall). At medial and distal levels the endocardium is pushed by converging NCCs towards the aortic side and we see obstructed Pa at distal *Wnt1^{Cre}; Dullard$^{Flox/Flox}$* OFT. In contrast control *Wnt1^{Cre}/Pax3^{Cre}; Dullard^{+Flox+}* embryos present symmetrical breakdown of the endocardium at distal levels, demonstrating that the septation process is happening prematurely in mutant embryos. Lines highlight the

asymmetry between the Ao and Pa poles. Arrowheads show the ruptured endocardium in mutant embryos contrasting with its unruptured state in controls. Pa, Pulmonary artery; Ao, Aorta; PV-IC: Pulmonary valve intercalated-cushion.

III.3 Attempt of phenotypic rescue of *Dullard* mutants using a BMP signaling inhibiting drug

We showed that the specific knock-out of *Dullard* in NCCs triggers an over-activation of BMP signaling in the NCCs, leading to faulty OFT septation and malformation of the great arteries. Following-up on these results, we wanted to investigate whether the heart malformations displayed by mutant embryos was caused only by Dullard's influence on BMP signaling or whether other developmental signaling pathways were impaired. To answer that question, we set out to perform a rescue experiment to lower down the levels of BMP activity in Dullard mutant embryos and assess the resulting OFT morphology. LDN-193189 (LDN) is an inhibitor of BMP type I receptors ALK2 and ALK3, which is commonly used to inhibit BMP signaling *in vitro* and *in vivo* (Sakaguchi et al., 2013; Sanvitale et al., 2013). The drug was dispensed via one intraperitoneal injection of the pregnant females at E10.5. The injections were first performed at a $2.5mg.kg^{-1}$ LDN concentration but preliminary results showed no improvement of the mutant OFT morphology. Because the drug was diluted in DMSO as a vehicle, we chose for toxicity reasons not to increase the LDN concentration above a 20% concentration threshold. Therefore, the whole experiment was performed with injections of LDN at a concentration of $6mg.kg^{-1}$ (with a final DMSO concentration of 17%).

We used the approach presented in III.1.3 to look for a decrease in BMP signaling activity in cardiac NCCs of embryos treated with LDN. We performed immune-labeling of phospho-smad1,5,8 and quantified the staining intensity along the OFT axis in E11.5 embryos Figure 32A, page 103). Surprisingly, we observed no significant difference in the staining intensity between LDN and vehicle treated embryos whatever their genotypes. Hence, we concluded that the treatment was not efficiently inhibiting BMP signaling activity, neither in $Wnt1^{Cre};Dullard^{Flox/+}$ nor in $Wnt1^{Cre};Dullard^{Flox/Flox}$ NCCs. Accordingly, no phenotypic improvement was noted at the tissue level. All the analyzed E11.5 mutant embryos, treated with LDN or with the drug vehicle (17% DMSO), presented a strong asymmetry of OFT septation characterized by a detachment of the endocardium from the PV-IC Figure 32B, page 103). We concluded that the chosen drug strategy was not efficient and did not allow assessing the effect of a rescue of BMP signaling on the cardiovascular phenotype of *Dullard* mutant embryos. Nevertheless, quantification of BMP signaling intensity in the LDN and vehicle treated NCCs confirmed the significant increase of BMP signaling in mutant NCCs compared to controls, as well as the distal to proximal gradient of BMP signaling activity described in (Figure 26).

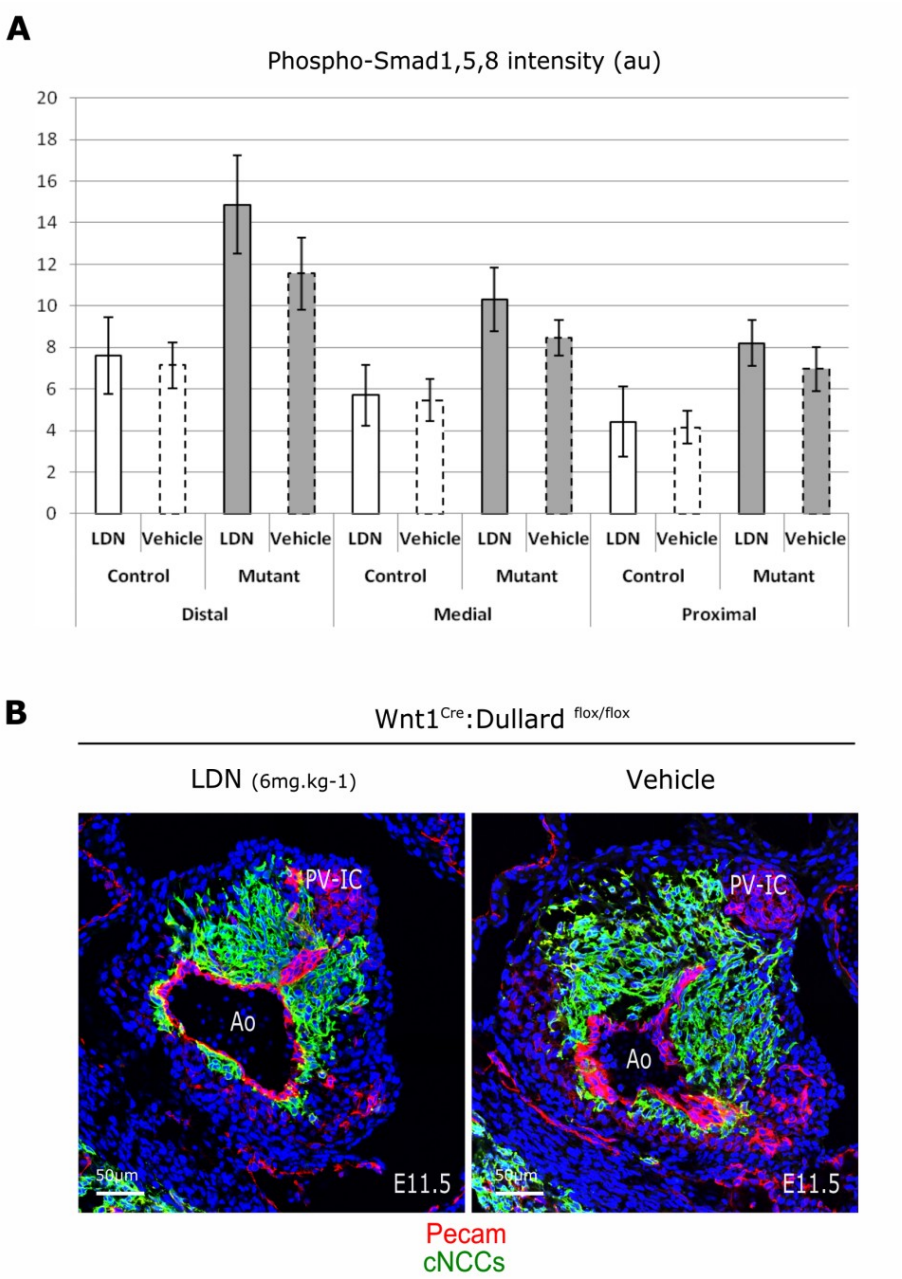

Figure 32 – Analysis of the BMP signaling activity in NCCs of LDN treated and non-treated embryos, and the resulting OFT phenotype. **A.** Quantification of the phospho-Smad1,5,8 staining intensity along the OFT distal to proximal axis of treated and non-treated $Wnt1^{Cre}$;$Dullard^{Flox/+}$ (control) and $Wnt1^{Cre}$;$Dullard^{Flox/Flox}$ (mutant) embryos. No significant decrease of staining intensity is observed in the trated embryos. **B.** Transversal section of treated and non-treated $Wnt1^{Cre}$;$Dullard^{Flox/Flox}$ (mutant) distal OFTs, showing no improvement of the OFT septation defect. 6/6 LDN and 4/4 vehicle treated mutant embryos present the distinctive phenotype of asymmetric OFT septation with pulmonary obstruction described in III.2.2.

III.4 Single cell transcriptomic analysis of OFT progenitors

III.4.1 Validation of the single-cell transcriptional analysis

We set out to decipher the molecular basis of the defective OFT remodeling observed in *Pax3^{Cre}/Wnt1^{Cre}; Dullard$^{Flox/Flox}$* embryos. To address this question, we micro-dissected E11.5 *Wnt1^{Cre}; Dullard$^{+/Flox}$; R26^{mTmG}* and *Wnt1^{Cre}; Dullard$^{Flox/Flox}$; R26^{mTmG}* OFT and sorted the NCCs (GFP^{+}) and the endocardial progenitors (CD31^{+}) from the other types of OFT progenitors (RFP^{+}) (Figure 33A, page 105). We then performed single cell RT-qPCR on 44 genes implicated in epithelial-mesenchymal transition (EMT), migration and/or specification of OFT progenitors (Table 1, page 86). Ct values extracted from the Biomark chips were normalized using those obtained for *Actb* and *Gapdh* house-keeping genes (Figure 33B, page 105). We next performed an unsupervised clustering of all progenitors present in *Wnt1Cre; Dullard$^{+/Flox}$* and *Wnt1Cre; Dullard$^{Flox/Flox}$* OFT according to the molecular signature defined by the expression of our 44 genes of interest. This method allowed to segregate the distinct OFT progenitor subtypes from each other (Figure 33C, page 105). Indeed, out of the 6 populations of cells clustered by this method, the Pop.1 regrouped endocardial cells, all positive for the endocardial markers*, Flt1*, *Kdr, Nfatc* and *Tek,* and the Pop.5 encompassed the epicardial cells, marked by *Tcf21* and *Wt1*. Importantly, these two populations contained both cells derived from *Wnt1Cre; Dullard$^{+/Flox}$* and *Wnt1Cre; Dullard$^{Flox/Flox}$* OFT. In contrast, the NCCs coming from *Wnt1Cre; Dullard$^{+/Flox}$* and *Wnt1Cre; Dullard$^{Flox/Flox}$* OFT segregated in distinct populations. The control NCCs were found in Pop.2, while most mutant NCCs were in Pop.4 and 6 for mutant NCCs. This indicated that Dullard loss induced drastic effect on the transcriptional state of NCCs, and had little impact on the other progenitor cell-types.

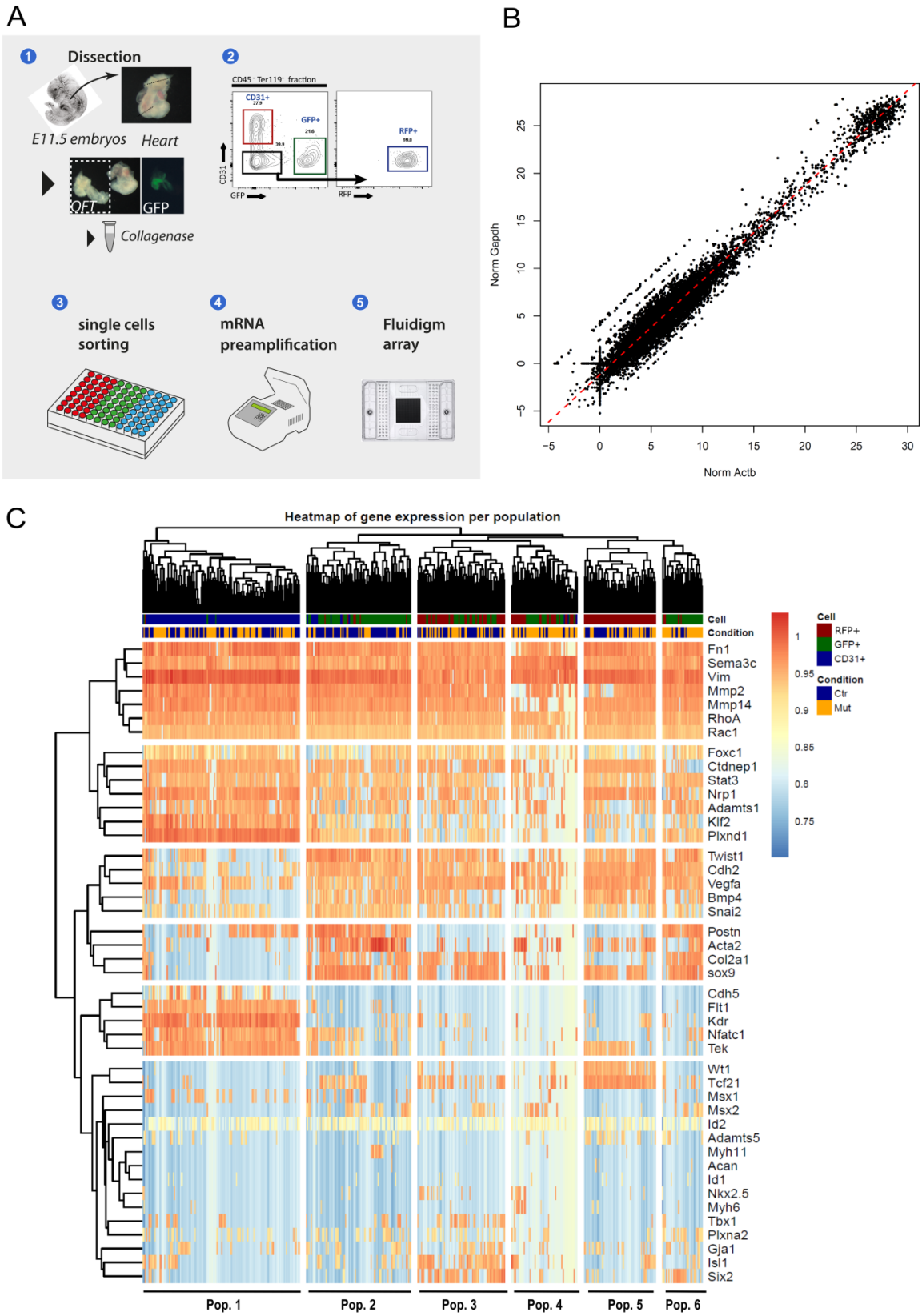

Figure 33 - Single cell transcriptional analysis of OFT progenitors at E11.5. A. Scheme of the experimental approach to perform single cell RT-qPCR. Using Facs sorting, we could isolate three types of cells from E11.5 *Wnt1*^{Cre}*; Dullar*$^{+/Flox}$*;R26*^{mTmG} and *Wnt1*^{Cre}*; Dullard*$^{Flox/Flox}$*;R26*^{mTmG} OFT: CD31 positive cells (endocardium), GFP positive cells (cNCC) and RFP positive cells (pericardium, myocardium and toher progenitors). mRNAs from

each cells were then reverse transcripted in DNA and analyzed with a Fluidigm microchip on a Biomark apparatus. **B.** Graph showing the linear regression between *Actb* and *Gapdh* Ct values **C.** Unsupervised clustering heatmap of the all the OFT progenitors from *Wnt1^{Cre}; Dullard$^{+/Flox}$;R26^{mTmG}* (Ctr) and *Wnt1^{Cre}; Dullard$^{Flox/Flox}$;R26^{mTmG}* (Mut) based on gene expression level of genes included in our panel. Six different populations can be discriminated, among which the endocardial (pop. 1), the pericardial (pop. 5) progenitors.

III.4.2 *Dullard* regulates NCCs mesenchymal state and Sema3c expression

We next decided to identify the transcriptomic changes underpinning the segregation between mutant and control NCCs. By performing unsupervised hierarchical clustering on NCCs we observed that the transcriptional state of control NCCs was variable and that three big classes of cells could be defined (Pop1-3) (Figure 34, page 107). Diffusion maps indicated a continuum of cells going from Pop1 to Pop3, suggesting a development path between these 3 classes of cells (Figure 35, page 108). The comparison of control to mutant NCCs revealed that *Dullard* mutant cells were also found in Pop1 and 2, and thus that Dullard deletion did not impact the path between these transcriptional signatures. Conversely, barely any mutant NCCs clustered with the pop3 control cells. This population of cells presented an upregulation of smooth muscle specification markers *Myh11* and *Acta2* compared to others, indicating their commitment towards a smooth muscle fate, later involved in septum strengthening and maintaining arteries shape. The absence of this population in mutant NCCs highlighted a defect of specification towards smooth muscle fates of *Dullard* mutated NCCs. Furthermore, mutant NCCs clustered together and specifically in Pop4 and even more strongly in Pop5 (28% of mutant versus 3.95% of control NCCs). This Pop5 showed low levels of the mesenchymal markers *Snai2, Twist1, Cdh2, Mmp14, Rac1* and high levels of the epithelial marker *Cdh5,* suggesting that mutant NCCs transitioned towards epithelial-like states. In addition, this population was characterized by higher levels of *Sema3c* expression, a chemokine implicated in cells migration, and lower expression of its receptors *Nrp1* and *Plxnd1*. Cells in Pop4 were reminiscent of those in pop5, although the fold change in the levels of mesenchymal genes, *Cdh5* and *Sema3c* compared to the levels found in control NCCs, was less pronounced than in Pop5. Overall, this analysis confirmed that *Dullard* expression can affect the transcriptional state of NCCs through an overactivation of the BMP signaling, and can induce changes reminiscent of a mesenchymal-epithelial transition, which may alters cell-cell communication properties via Sema3c signaling.

We performed similar analyses on the RFP$^+$ and CD31$^+$ progenitors to investigate what non-cell autonomous effect had *Dullard* deletion in the NCCs on other cell types composing the OFT niche. While we did not any see significant effect on RFP$^+$ progenitors, CD31$^+$ sorted from *Wnt1^{Cre}; Dullard$^{Flox/Flox}$* OFT presented a significant decrease in the expression of *Twist1*, *Fn1* and *Tek*. In sum, our results suggest that *Dullard* deletion in NCCs mainly

affected cell-autonomously the NCCs by changing their mesenchymal properties, and had a very limited impact on the transcriptional signature of the other OFT progenitors.

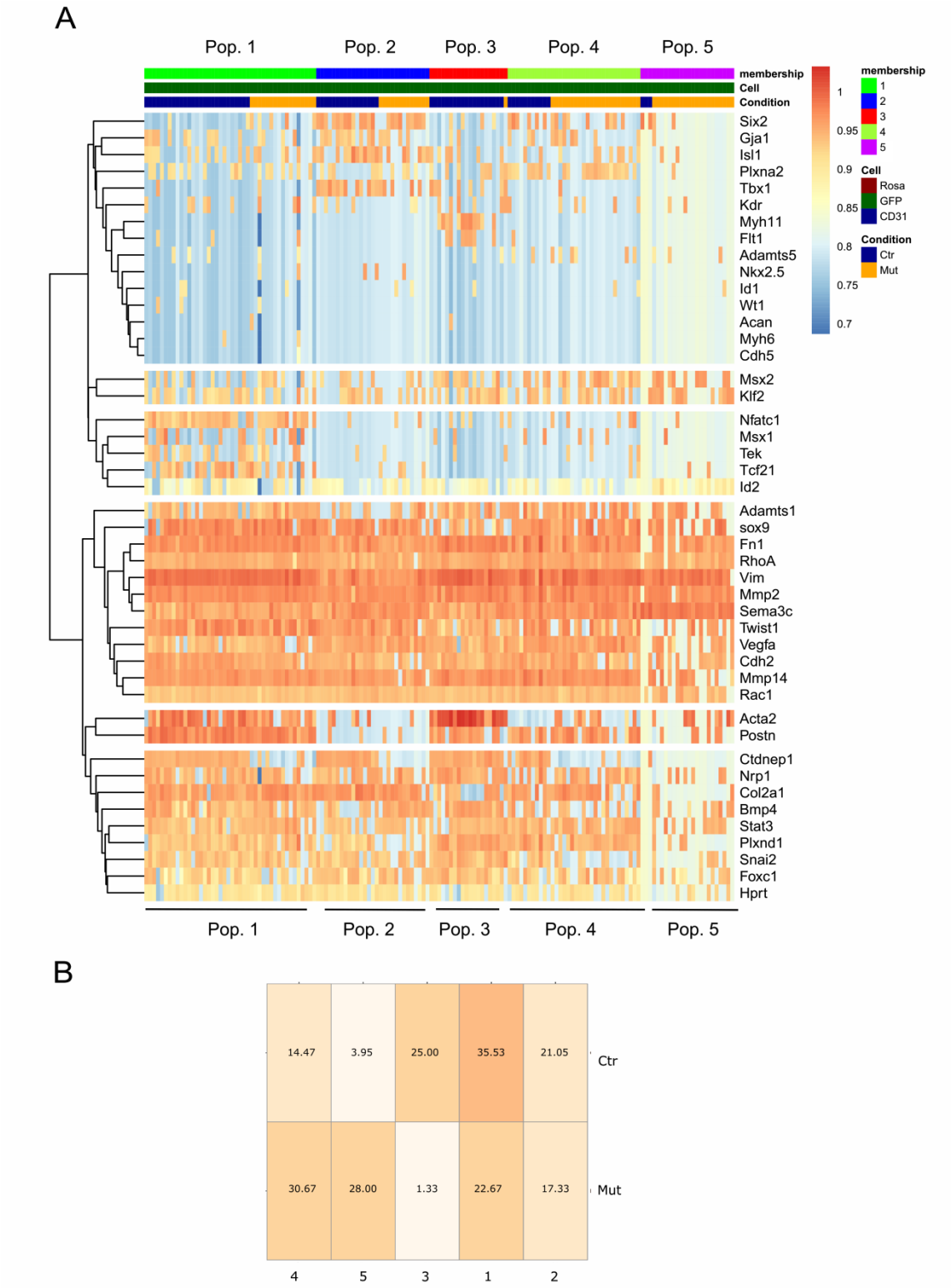

Figure 34 – Unsupervised hierchical clustering of *Wnt1^{Cre}; Dullard$^{+/Flox}$* and *Wnt1^{Cre}; Dullard$^{Flox/Flox}$* NCCs. A. Heatmap of gene expression in the control and mutant NCCs obtained by hierarchical clustering of NCCs in five populations showing distinct transcriptional signatures. **B.** Percentage of control and mutant NCCs in each cluster of cells.

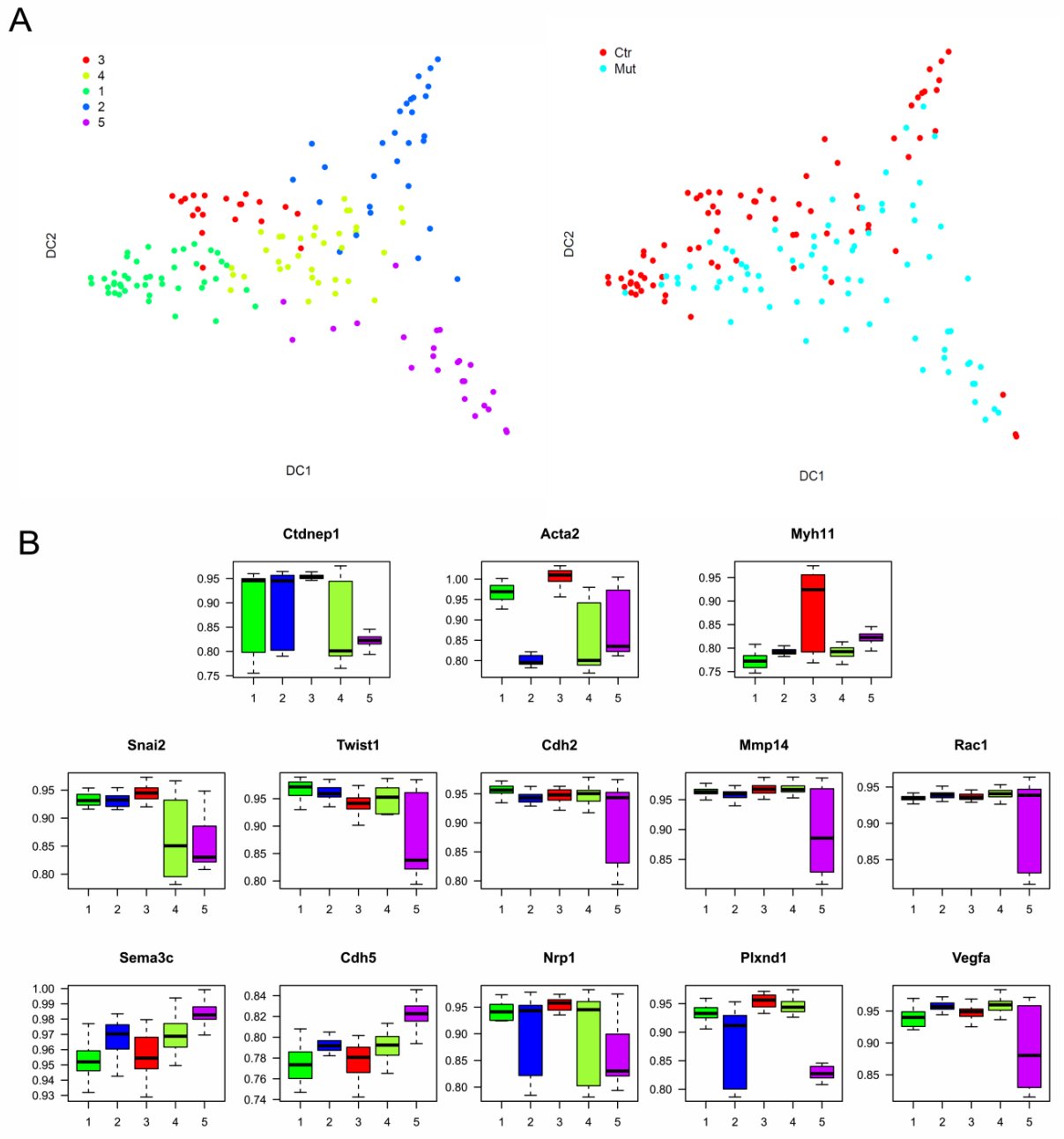

Figure 35 – Diffusion map and gene expression levels in NCCs clusters. A. Diffusion map of the NCCs according to their cluster of appartenance and their genotype (Ctr: *Wnt1*^{Cre}*; Dullard*$^{+/Flox}$ and Mut: *Wnt1*^{Cre}*; Dullard*$^{Flox/Flox}$). The diffusion components (DC) are composed the genes presented in B. **B.** Boxplot representation of the gene expression level differentially expressed between NCCs clusters.

III.5 Impact of BMP signaling overactivation on NCCs behavior and myocardial progenitors differentiation

III.5.1 *Sema3c* overexpression is associated with increased NCCs condensation to the endocardium

During the formation of the aortico-pulmonary septum, NCCs are characterized by different movements that encompass convergence towards the endocardium and perpendicular reorientation relative to the endocardium (Luo et al., 2006; Phillips et al., 2005, 2013; Plein et al., 2015). We thus investigated if the specific alterations in the transcriptome of *Wnt1*^{Cre}*; Dullard*$^{Flox/Flox}$ compared to *Wnt1*^{Cre}*; Dullard*$^{+/Flox}$ NCCs translated into discrete traits in their behavior.

First, by using a nuclear staining, we compared the condensation pattern of control and mutant NCCs towards the endocardium, at levels where the endocardium was not yet ruptured. In control embryos, NCCs at the proximity of the endocardium were scattered and exhibited elongated nuclei, whereas NCCs located away from the endocardium harbored a rounded nuclear shape and a high density (Figure 36A, page 110). In mutant embryos, the population of loosely compacted NCCs by the sides of the endocardium was poorly visible, suggesting a compaction of the NCCs on the endocardium. To quantify these observations, we measured both the shortest distance between NCCs nuclei and the endocardium, as well as between each NCCs nuclei (Figure 36B, page 110). *Wnt1*^{Cre}*; Dullard*$^{Flox/Flox}$ NCCs presented a significant decrease in distance to the endocardium and to their closest neighbor when compared to the *Wnt1*^{Cre}*; Dullard*$^{+/Flox}$ NCCs. Hence, in absence of *Dullard,* mutant NCCs were more aggregated to each other and closer to the endocardium than controls, which is consistent with the elevated levels of adhesive markers (*Cdh5*) and lower mesenchymal genes (*Snai2, Twist1, Cdh2, Mmp14*) described in III.4.

In addition, we examined the relative orientation of the NCCs nuclei relative to the endocardium, which is a good read-out of NCCs orientation to the endocardium. It appeared significantly different between control and mutant NCCs. We thus monitored the angles formed by the NCCs nuclei longest axis and the endocardium axis, and plotted it in a [0°,90°] referential (Figure 36C, page 110). While in control embryos, most NCCs nuclei stood parallel to the endocardium, in Dullard mutants this orientation preference was not as clear, and instead, a significantly higher percentage of NCCs presented nuclei standing perpendicular to the endocardium (Figure 36C, page 110).

Hence, in absence of *Dullard* expression, the aggregation of NCCs, their convergence towards the endocardium and their orientation relative to the endocardium are enhanced compared to control cells. Altogether, these data corroborate the idea of a premature

septation in mutant embryos and demonstrate that *Dullard* participates in the NCCs morphogenetic properties, which are involved in OFT septation.

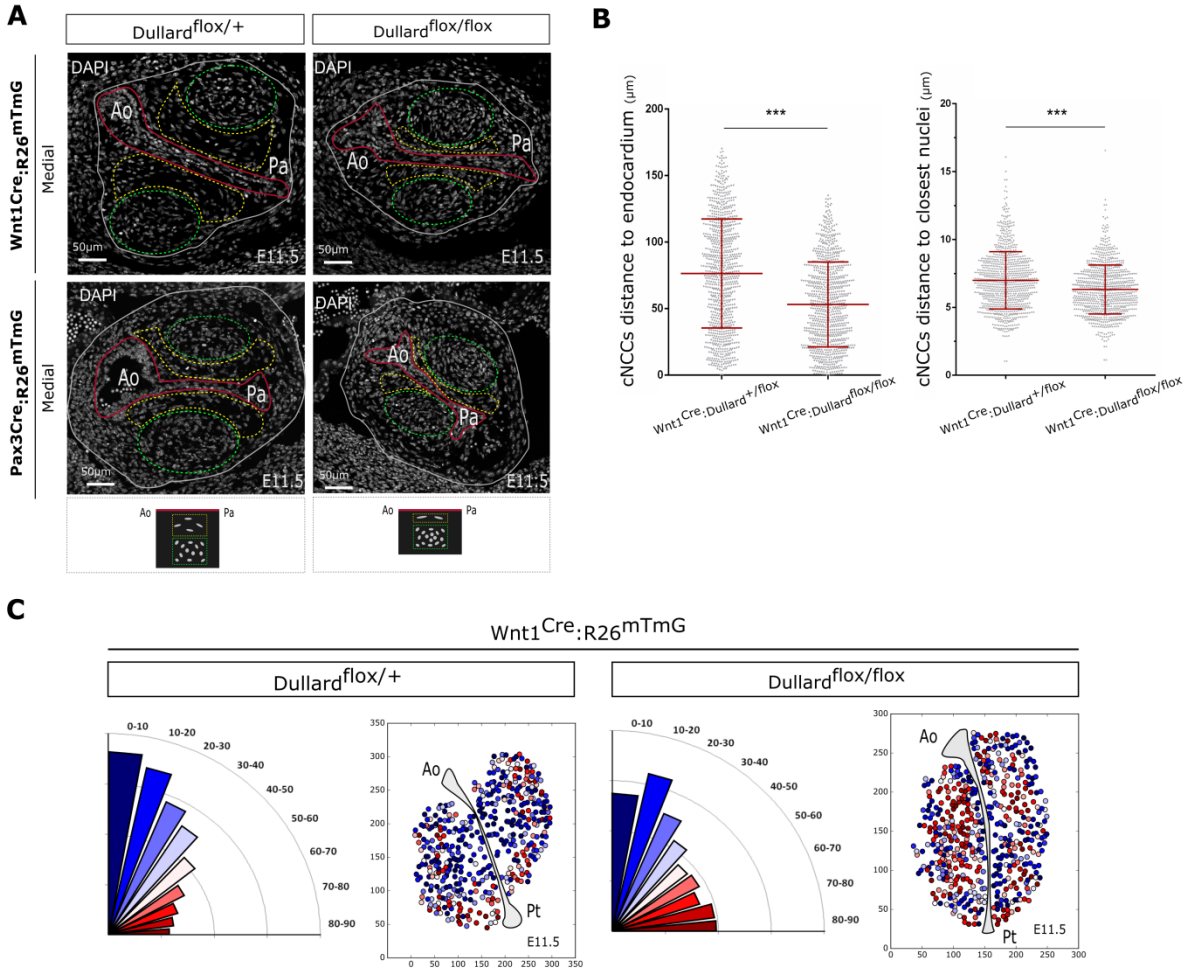

Figure 36 –NCCs compaction and orientation to the endocardium in cardiac cushions. Analysis performed at located at medial/proximal OFT levels. **A.** Transversal sections of medial OFT levels stained with DAPI. The endocardium is delineated with a red line. The NCCs are positionned in areas with high nuclear density and rounded nuclear shape (delineated in green dotted line) and in areas of low density and elongated nuclear shape (delineated in yellow dotted line). We note that in *Pax3^{Cre}/Wnt1^{Cre};Dullard$^{Flox/Flox}$* embryos, the NCCs regions of high density and rounded nuclear shape are closer to the endocardium compared to control in *Pax3^{Cre}/Wnt1^{Cre};Dullard$^{+/Flox}$*, and that the areas of low NCCs density decreased in size. **B.** Measure of the distance of NCCs nuclei to the endocardium, and to the closest neighboring NCCs nuclei, in *Wnt1^{Cre};Dullard$^{+/Flox}$* embryos and *Wnt1^{Cre};Dullard$^{Flox/Flox}$* embryos Quantification shows that mutant NCCs are positionned closer to the endocardium and are closer to each other, highligthing an increase in NCCs convergence and condensation to the endocardium (*respectively 6 and 5 embryos analysed per genotype; Mann-Whitney Test, P-value<0.001*). **C.** Left: Measure, in *Wnt1^{Cre}; Dullard$^{Flox/Flox}$* and *Wnt1^{Cre}; Dullard$^{+/Flox}$* cardiac cushions, of the angles formed by NCCs nuclei longest axis relative to the endocardial axis, and plotted in a [0;90°] referential (blue represents angles parallel to the endocardium, and red represents angles perpendicular to the endocardium). On the side is shown a color-coded visualization of the orientation of NCCs to the endocardium according to their position in the cushion in one representative embryo. We observe a significant increase in perpendicular orientations of mutant NCCs to the endocardium, mostly localized in the middle of the cushion, which in contrast present parallel orientations in control embryos (*respectively 6 and 5 embryos analysed per genotype; Mann-Whitney Test, P-value<0.001*).

Sema3C stands as a cue involved in NCCs convergence towards the endocardium and was the top-upregulated gene in our single-cell transcriptional analysis (Plein et al., 2015). In a second approach complementing our transcriptional results, we analyzed the distribution of expression of *Sema3c* in the cardiac cushions by *in situ* hybridization (ISH). ISH experiments performed on OFT serial sections confirmed the increase in *Sema3c* expression in $Wnt1^{Cre};Dullar^{Fllox/Flox}$ NCCs (Figure 37, page 112). Accordingly, we observed a similar increase in *Sema3c* expression in the $Pax3^{Cre}$ model. Besides, the *Sema3C* expression territories increased distally forming a gradient along the OFT axis of both control and mutant embryos, parallel to the previously described gradient of BMP signaling activity. Hence, Sema3c expression correlated in its strength and in its spatial distribution with BMP signaling activation.

Moreover, in the distal region, Sema3c expression territories converged towards the endocardium and thus associated with areas of highest NCCs condensation (Figure 37, page 112). This stands in good line with the transcriptional signature of NCCs that present both an increase in *Sema3c* expression and in genes supporting transition towards epithelial-like states. Altogether, our results highlight a BMP-regulated gradient of *Sema3c* expression, established along the OFT by the NCCs, which drives the spatiotemporal convergence of the NCCs to the endocardium and subsequent breakdown. Interestingly, the spatiotemporal progress of OFT septation was often compared to a zipper that separates the aorta and the pulmonary artery from the distal to the proximal end of the OFT (Hutson and Kirby, 2007). Our results thus provide a molecular basis for the zipper-like septation of the OFT.

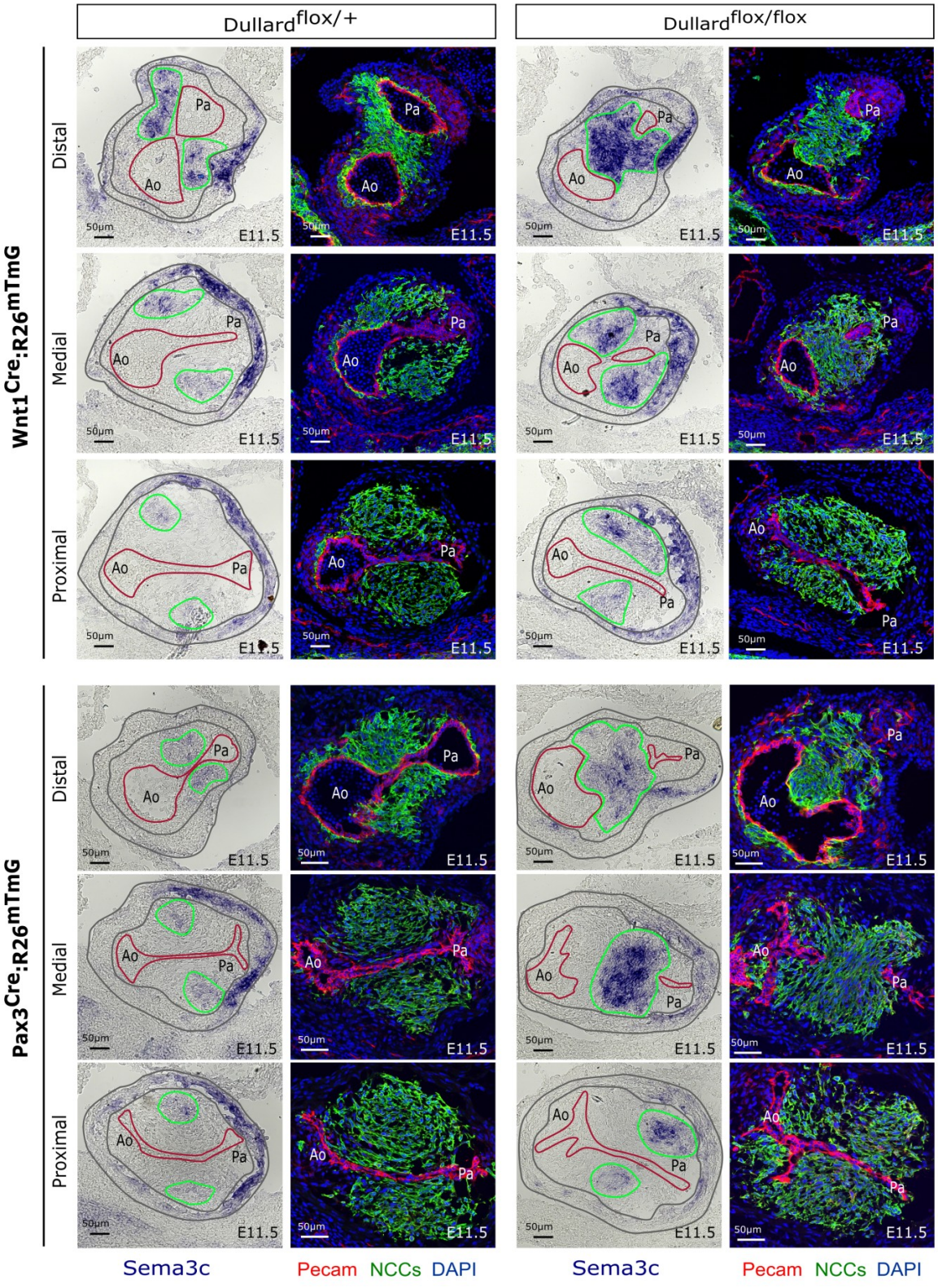

Figure 37 – Analysis of *Sema3C* expression pattern in control and mutant NCCs along the OFT axis. Sema3C ISH and Pecam/GFP immunostainings of transversal OFT sections along its distal to proximal axis, from the indicated genotypes. The areas of *Sema3C* expression are delineated in green, the endocardium in red and the myocardium in grey. Sema3c positive areas are highly increased in the *Pax3^{Cre}/Wnt1^{Cre};Dullard$^{Flox/Flox}$* embryos compared to their control couterparts. The pattern of expression of *Sema3c* converges towards the endocardium at distal levels and appears to regionalize with the areas of high NCCs density described in Figure 36.

III.5.2 Overactivation of BMP signaling in NCCs induces asymmetrical differentiation of the distal subpulmonary myocardium

Surprisingly, the gain-of-function of BMP signaling obtained through *Dullard* deletion in the NCCs induced a phenotype of OFT septation that is not only premature but also asymmetric. The increased condensation of NCCs in these embryos, although it explains the premature septation, does not rationalize the asymmetric septation. The localization of the NCCs and the increase in *Sema3c* expression is symmetrically located in between the Ao and Pa sides before endocardium breakdown. Hence, NCCs condensation does not appear be the cause of asymmetric breakdown. Rather, it suggests that a spatial heterogeneity exists in the OFT progenitors responding to increased *Sema3c* signals from the NCCs.

At the distal OFT level of E11.5 embryos, the outer-ring of SHF is differentiating in myocardium and starts expressing Myosin Heavy Chain (MHC, stained by the MF20 antibody) (Figure 38, page 114) (van den Hoff et al., 1999). Yet, there is heterogeneity in this outer-ring of SHF. The presumptive aortic and pulmonary myocardium, positioned respectively in the subpulmonary and subaortic SHF, are developmentally distinct and show different transcriptional signatures (Bajolle et al., 2008; Bertrand et al., 2011; Rochais et al., 2009; Théveniau-Ruissy et al., 2008). *Sema3c* expression characterizes specifically the subpulmonary myocardium.

From there, we noted two remarkable facts about distal SHF differentiation; First, there was a coregionalization of SHF progenitors expressing MHC and Sema3c (compare Figure 37 and Figure 38A), showing that the differentiating myocardium is of subpulmonary lineage (Bajolle et al., 2006; Rana et al., 2014). Second, the MHC^{+} myocardium localization was different in $Pax3^{Cre}/Wnt1^{Cre};Dullard^{flox/flox}$ compared to $Pax3^{Cre}/Wnt1^{Cre};Dullard^{flox/+}$ OFT. In the later, the MHC^{+} myocardium was located medially and symmetrically between the Ao and Pa sides, whereas in the former it was asymmetrically positioned on the pulmonary side (Figure 38B, page 114). These observations highlight that symmetrical septation at the distal OFT level is supported by symmetrical differentiation of the subpulmonary myocardium in between the Ao and Pa poles. As this phenomenon is impaired by *Dullard* deletion in the NCCs, our results suggest that the BMP-dependent regulation of Sema3c expression in the NCCs is crucial for the proper positionning of the differentiating subpulmonary myocardium. This hints towards a preferential paracrine crosstalk between the NCCs and the subpulmonary myocardium rather than with the subaortic myocardium.

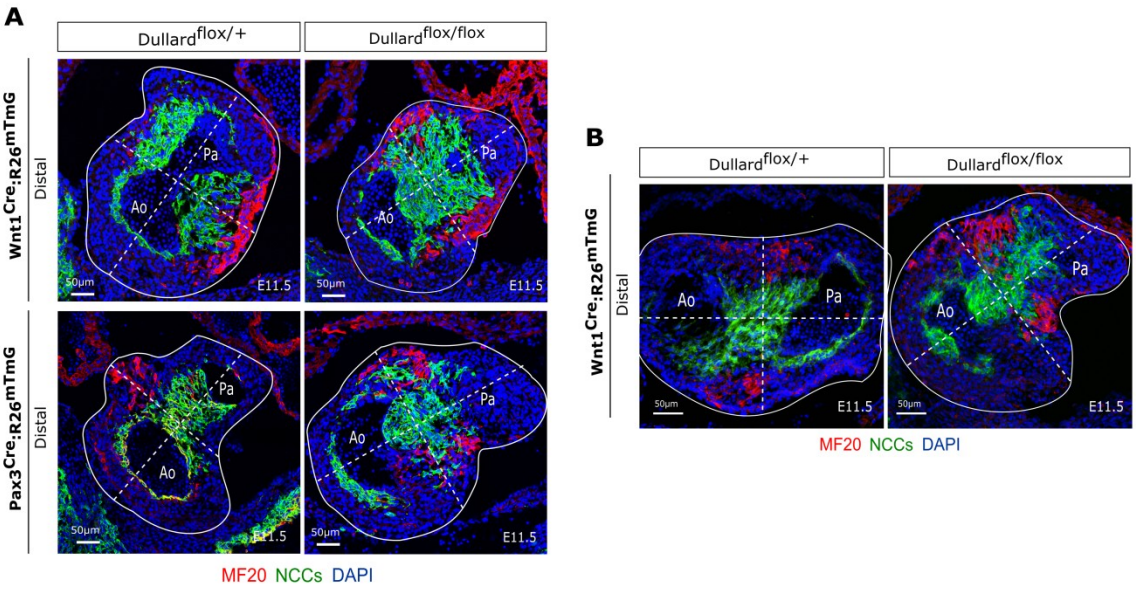

Figure 38 – Asymmetric positioning of the differentiating subpulmonary myocardium at the OFT distal level. **A.** Immunostaining of MHC+ myocardium in *Pax3^{Cre}/Wnt1^{Cre};Dullard$^{+/Flox}$* and *Pax3^{Cre}/Wnt1^{Cre};Dullard$^{Flox/Flox}$* embryos shows a coregionalization with Sema3-positive territories observed at distal OFT levels on the same embryos, pictured in **Figure 37**. As *Sema3c* is a subpulmonary marker, our results suggest that the differentiating myocardium derives from the subpulmonary lineage. **B.** Immunostaining of MHC^{+} myocardium at distal OFT level of *Wnt1^{Cre};Dullard$^{+/Flox}$* and *Wnt1^{Cre};DullarFl$^{lox/Flox}$* show that the positioning of the differentiating myocardium is symmetric in control embryos whereas it is displaced to the Pa side in mutant embryos. Dotted lines represent the Ao-Pa axis of symmetry and its perpendicular.

IV. DISCUSSION

The development of human and mouse hearts is a complex process tightly regulated in time and space during embryonic development. In particular, the septation of the outflow tract (OFT) into the aorta and pulmonary artery is determinant for proper blood circulation and oxygenation of tissues. Impairment of OFT septation is one major cause of congenital heart defects (CHDs) in newborns (Hoffman, 1995; Srivastava and Olson, 2000). The septation of the OFT relies on cells migrating from the neural tube, called the cardiac neural crest cells (NCCs) (Kirby et al., 1983). During evolution, NCCs recruitment to the OFT led to the emergence of separated systemic and pulmonary circulations, which enabled vertebrates' adaptation to terrestrial lifestyles. Yet until now, the central function of NCCs in OFT remodeling and the influence of myocardial BMP on NCCs behavior remains poorly understood. First clues came from impairing BMP signalling in the NCCs, which caused hypoplastic cushions and absence of OFT septation, also called persistent truncus arteriosus (Jia et al., 2007; Stottmann et al., 2004; Tang et al., 2010). However, these approaches did not succeed in unraveling the downstream effectors of BMP signaling that support OFT septation. We thus set out to develop a gain-of-function approach of BMP signaling in the NCCs to dig into its mechanism.

Dullard, a member of the FCP family of phosphatases, was shown to be a negative regulator of BMP signaling in Xenopus, Drosophila and mice (Sakaguchi et al., 2013; Satow et al., 2006; Urrutia et al., 2016). We thus decided to delete Dullard in the NCCs by using mouse transgenic lines and assess if it resulted in an instrumental model of BMP gain-of-function. We used mice carrying floxed versions of *Dullard* allele (Sakaguchi et al., 2013) and expressing the Cre recombinase under either the *Pax3* or *Wnt1* loci, which are active within the pre-delaminating NCC (Danielian et al., 1998; Engleka et al., 2005). We confirmed that Dullard expression was specifically repressed in $Pax3^{Cre}/Wnt1^{Cre};Dullard^{flox/flox}$ NCCs. In these cells, we observed a significant increase in the phosphorylation levels of the downstream BMP effector Smad1,5,8. Our results thus demonstrated that Dullard regulates BMP signaling in the NCCs during arterial pole development, and that *Dullard* deletion is an effective approach for BMP gain-of-function in cardiac NCCs.

We next investigated the phenotypic consequences of *Dullard* deletion in the NCCs on cardiovascular development and more specifically the arterial pole of the heart. *Dullard* knock-out in NCCs led to embryonic death around E12.5, before the 4-chambered heart is fully formed. Our investigation highlighted a striking phenotype in the distal OFT region, where the OFT septation process was strongly impaired. In fact, 3D imaging of $Pax3^{Cre}/Wnt1^{Cre};Dullard^{flox/flox}$ hearts revealed a strong atrophy of the forming pulmonary artery at E11.5-E12. We observed in these embryos that instead of happening centrally the fusion of the cardiac cushions, which is coupled with the breakdown of the endocardium, happened asymmetrically. In fact, the breakdown did not affect the endocardium itself but its point of attachment to a Pecam+ region of the subpulmonary myocardium. More specifically, insights from a recent paper make us believe that the endocardium attaches to

the presumptive pulmonary valve-intercalated cushion PV-IC (Mifflin et al., 2018). In addition to being asymmetrical, the OFT septation process occured prematurely in mutant embryos, as testified by the endocardial breakdown reaching more proximal levels that in controls. Our results, which present the consequences of a gain-of-function of BMP signaling in NCCs, are consistent with previous publications. In fact, while impairing BMP signaling in NCCs prevented the expansion of the cardiac cushions and led to persistent truncus arteriosus (Jia et al., 2007; Stottmann et al., 2004), we show conversely that increasing BMP signaling in NCCs accentuated OFT septation and lead to premature septation.

We next aimed at uncovering the impact of BMP signaling increase in NCCs at the molecular level, and understand why it caused asymmetric septation. To address these questions, we performed single-cell transcriptomic analyses on the progenitors composing *Wnt1*^{Cre}*;Dullard*$^{+/flox}$ and *Wnt1*^{Cre}*;Dullard*$^{flox/flox}$ OFT at E11.5. Our analysis was based on the expression of 44 genes of interest implicated in epithelial-mesenchymal transition (EMT), migration and/or specification of OFT progenitors. Our results revealed that NCCs response to increased BMP signaling is mainly cell-autonomous and consists in (i) a downregulation of mesenchymal markers (*Twist1*, *Snai2*, *Mmp14)* reminiscent of a transition towards epithelial-like states (ii) an increase in expression of a chemokine, called *Sema3c*. Apart from the NCCs, we saw limited effects on the transcriptional signature of the other progenitors composing the OFT niche. We further confirmed on histological sections that *Sema3c* expression was increased in mutants NCCs and was linked to an increased compaction of the NCCs to the sides of the endocardium.

Sema3c is a chemokine involved in cell migration and guidance. It plays a central and intriguing role in OFT septation. In fact, it was first described as being expressed in the subpulmonary myocardium and thought to attract NCCs from the pharyngeal region to the OFT (Bajolle et al., 2006; Feiner et al., 2001; Toyofuku et al., 2008). However, deletion of the Sema3c receptors Nrp1 and Nrp2 in NCCs did not impair their ingression in the OFT (Plein et al., 2015). These results challenged the idea that Sema3c plays the role of a chemoattractant required to drive NCCs ingression to the OFT, at least in mice. Additionally, it was shown that *Sema3c* is expressed by the NCCs themselves and tunes their behavior once they colonized the OFT cushions. It has been shown that indeed Sema3c drives NCCs convergence from lateral cushion positions by the sides of the myocardium, to central positions at the sides of the endocardium (Plein et al., 2015). This convergence enables the breakdown of the endocardium and cardiac cushion fusion (High et al., 2009; Plein et al., 2015). By showing that BMP signaling regulates *Sema3c* expression in the NCCs our results unravel a central role of BMP signaling on NCCs during OFT septation. It demonstrates that BMP signaling is able to regulate the convergence of NCCs to the endocardium by regulating Sema3c expression. Moreover, we show that the upregulation of *Sema3c* in the NCCs correlates with the downregulation of mesenchymal markers at the transcriptional level. In accordance, we observe on cryosections that mutant NCCs are more compacted to the

endocardium. BMP signaling transduction could directly act on the expression of mesenchymal markers, or indirectly, via an autocrine effect of Sema3c signals on NCCs. The results of Kodo *et al.* in 2017, which showed that addition of Sema3c in primary cultures of NCCs triggers their aggregation, suggest that it is the autocrine influence of Sema3c that drives the transition of NCCs to epithelial-like states.

The spatiotemporal progress of OFT septation has been compared to a zipper-like closure because it progressively divides the truncus arteriosus in two, from its distal to proximal end. However, the molecular basis of such a spatiotemporal progression and the relation with the NCCs behavior in the cardiac cushions, remained poorly understood. We show that a gradient of BMP activation exists in the NCCs along the distal to proximal OFT axis and establishes a gradient of Sema3c expression. Besides, *Sema3c* expression territories co-regionalize with areas of NCCs compaction, which converge towards the endocardium as septation proceeds. We thus propose that the gradient of BMP signaling activity established in the NCCs, regulates the progressive spatial convergence of the NCCs to the endocardium, responsible for the zipper-like septation of the OFT (Figure 39, page 119). The establishment of the gradient of BMP signaling in the NCCs is a very intriguing question. To better understand the establishment and duration of such a gradient in the OFT it would be informative to perform a spatial analysis of BMP signaling activity in the NCCs on serial cryosections, similar as the one we did, but at gestational stages spanning the whole duration of great arteries formation. In a complementary manner, a precise analysis of the expression of *Bmp2/4/6/7* along the OFT would be needed to get a better insight in the spatiotemporal evolution of the source of BMP ligands expressed by the OFT myocardium.

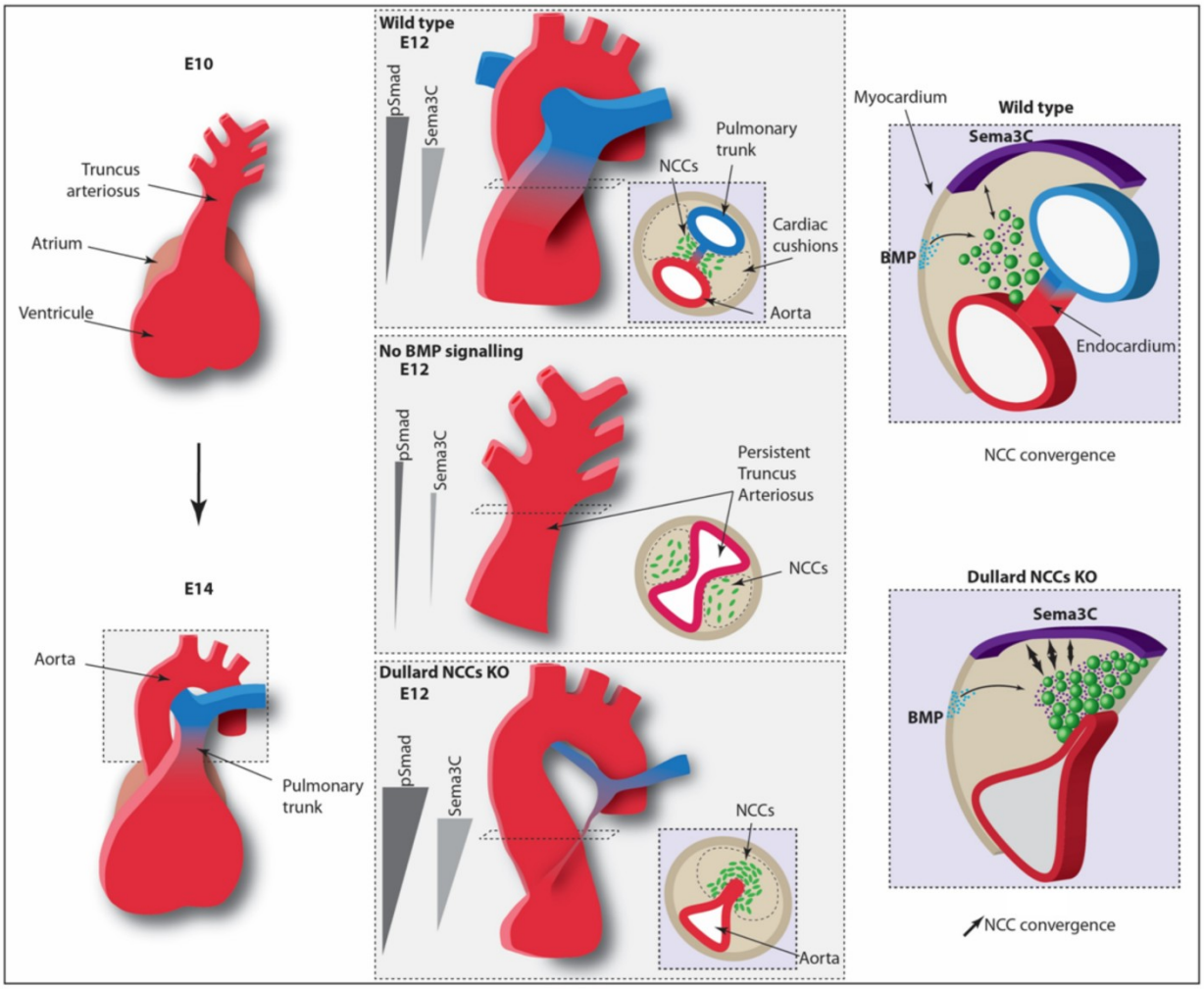

Figure 39 – Proposed model for the molecular cues driving the spatiotemporal septation of the OFT. On the left: Morphological transition between the unseptated *truncus arteriosus* at E10 in mice and the fully formed great arteries (aorta and pulmonary trunk) at E14. **In the middle:** Correlation between the OFT septation phenotype and the establishment of BMP-activity and *Sema3c*-expression gradients in NCCs positionned along the disto-proximal axis of the OFT; Comparison between the wiltype, BMP loss-of-function and BMP gain-of-function conditions. The BMP loss-of-function condition is based on literature (Jia et al., 2007; Stottmann et al., 2004; Tang et al., 2010). We propose that a gradient of BMP activity and *Sema3c* response in the NCCs orchestrates the progressive convergence of the NCCs and breakdown of the endocardium. This mechanism would be the molecular basis for the spatiotemporal zipper-like remodelling of the OFT. **On the right:** Gain-of-function of BMP in the NCCs leads to the premature compaction of the NCCs to the endocardium and the asymmetric differentiation of the subpulmonary myocardium (in purple), which together cause the detachment of the endocardium from the subpulmonary wall, and the obstruction of the pulmonary artery at the tissue level.

Many publications described that the full length of the OFT myocardium expresses BMP4 at E10.5-11.5 and that this expression is maintained through heart arteries formation (Jia et al., 2007; Jiao et al., 2003; Jones et al., 1991; Liu et al., 2004; Zhang et al., 2010). Hence, the establishment of the distal-to-proximal gradient of BMP activity should not derive from the diffusion of BMP signals secreted by a source located at distal OFT levels. However, different regulations could account for the establishment of such a polarized gradient. The competence of NCCs receiving the BMP signals could vary along the OFT axis. Such a spatial heterogeneity of competence could come from inner regulatory feedback loops that differentially integrate BMP signals along the OFT axis. As presented in I.3.3 mechanisms of adaptation (i.e. negative regulatory feedback loops) could downregulate the activity of BMP signaling while BMP signals concentration remains stable along the OFT. According to such an hypothesis, NCCs would start receiving BMP signals at the distal end of the tube, where they first ingress, and would get adapted to BMP signals as reaching proximal levels. As a result, NCCs would present lower levels of Smad phosphorylation at proximal than at distal OFT levels, which is what we describe. The Inhibitory-Smads, Smad6 and Smad7, are negative feedback effectors of BMP signaling that could account for NCCs adaptation to BMP signaling. In fact, BMP signaling promotes the expression of the I-Smads, which in turn inhibit its transduction cascade by acting as decoy proteins that interact with activated BMP receptors and activated R-Smads (Hata et al., 1998; Ishida et al., 2000; Nakao et al., 1997). Very interestingly, E10.5 embryos show prominent expression of *Smad6* specifically localized to the OFT and atrioventricular cushions (Galvin et al., 2000). Its expression is also observed at E15.5 in the great vessels, suggesting that it lasts throughout great arteries formation (Galvin et al., 2000). *Smad6* is thus a very promising candidate, that could take part in the establishment of the BMP activity gradient observed along the OFT axis. Moreover, over-expression of *Smad7* in the NCCs has been shown to recapitulate the phenotype of other approaches of BMP loss-of-function in the NCCs (i.e. defect in NCCs colonization of the OFT resulting in a persistent truncus arteriosus) (Tang et al., 2010). This shows that Smad7 is a potent regulator of BMP signaling in the cardiac NCCs although its pattern of expression is, to our knowledge, not yet described in the developing OFT. Lastly, the BMP gradient could also result from the action of extracellular decoy or trapping proteins that would be secreted by a ventral source, possibly the progenitors of the heart ventricles. Looking at the pattern of expression of proteins acting in such a manner, as Gremlin, Noggin, Chordin or other known antagonists of BMP signaling, could unveil the molecular basis of the gradient establishment.

Interestingly, a publication described another approach of BMP gain-of-function in the NCCs (Komatsu et al., 2013). It was performed by using a constitutively active form of BMPR1a (ca-BMPR1a), crossed to the $P0^{Cre}$ line to target the NCCs. Mutant mice carrying both ca-Bmpr1a and $P0^{Cre}$ transgenes show much milder phenotypes than the $Wnt1^{Cre}/Pax3^{Cre}$; $Dullard^{Flox/Flox}$ mutants. Authors do not describe any increase in embryonic or postnatal death, neither any cardiac malformation. The detailed phenotype is called craniosynostosis

and consists in the premature fusion of skull sutures, which is shown to be caused by increased BMP signaling in cranial tissues derived from the NCCs. The phenotypic discrepancies observed between this approach and ours could be explained by a variety of reasons, although none can be asserted. A lower efficiency of the $P0^{Cre}$ line to target NCCs could be at play, or a lower efficiency in BMP signaling activation, which would be more weakly activated through a constitutively active BMP receptor than by the deletion of a downstream regulator of BMP signaling transduction, as Dullard.

The general view is that OFT septation relies on tightly regulated crosstalks between NCCs, myocardial and endocardial progenitors. We first discuss the relation of NCCs with endocardial progenitors. The results of Plein *et al.* interestingly suggested that Sema3c signals acts on endocardial cells via the Nrp1 receptor and induced endocardial EMT (endoMT) (Plein et al., 2015). EndoMT and NCCs convergence would act synergistically to drive cushion fusion and OFT septation. Unexpectedly, our transcriptional analysis of *Wnt1*^{Cre}*;Dullard*$^{flox/flox}$ OFT progenitors, although it showed in NCCs an increase in *Sema3c* expression, did not show any increase but rather a decrease in the expression of EMT markers, as *Twist1*, in endocardial cells. Our results are thus conflicting with the theory that Sema3c triggers endoMT. We hypothesize that the mechanism depicted by Plein *et al.* might account for the OFT septation process happening at proximal but not distal levels. In fact, it is well known that discrepancies exist between the distal and proximal development of the OFT, respectively called truncus and conus (Délot et al., 2003). At distal levels, the major part of the cushion mesenchyme derives from NCCs, whereas at proximal levels it is mostly generated by endoMT (von Gise and Pu, 2012; Keyte and Hutson, 2012). In accordance with our hypothesis, *Sema3c* deletion in NCCs causes a septation defect with an incomplete penetrance, characterized by a proper septation at the distal OFT levels but impaired at proximal levels (Plein et al., 2015). In addition, our results show that the increase of Sema3c expression in NCCs precipitates OFT septation not by breaking the endocardium structure itself, but by breaking down its attachment to the OFT subpulmonary wall. It suggests that the endocardium is not sensitive to high Sema3c signals at least at distal OFT levels. An attractive hypothesis would be that OFT septation relies at proximal levels on cushion expansion driven by Sema3c dependent endoMT, while at distal levels, where NCCs density is much higher and endoMT sparse, NCCs would drive cushion expansion and OFT septation.

We made the observation that the endocardium attaches on the pulmonary side to a specific region of the myocardium, which express the adhesion molecule Pecam. The alignment of this region with the endocardium and the recent results from Mifflin *et al.* suggest that this region could be the presumptive pulmonary-valve intercalated-leaflet (PV-IC) (Mifflin et al., 2018). In fact Mifflin *et al.* described that the mesenchymal cells forming the PV-IC arise from the OFT subpulmonary wall, from a lineage previously thought to be exclusively myocardial. Accordingly, we observed that at medial OFT levels the OFT wall is

MF20^{+} and thus differentiated in myocardium, whereas the described subpulmonary region is MF20^{-}, Pecam^{+} and Sox9^{+}. MF20 and Sox9 staining point out that these progenitors are not myocardial but mesenchymal, and the Pecam staining, in continuity with the endocardium, suggests that strong adhesion exists between endocardial and PV-IC progenitors. This adhesion would be ruptured in case of BMP signaling increase, because of the asymmetric differentiation of the myocardium at OFT distal levels (discussed later on). Hence, our results suggest that the proper attachment of the endocardium to the PV-IC is crucial for proper OFT septation and formation of the great arteries. Dullard deletion in the NCCs is a good model of rupture of this attachment and shows that it leads to endocardial displacement on the aortic side and pulmonary artery obstruction on the other.

As mentioned above we think that converging NCCs exert a mechanical constraint on the endocardium. In accordance, different conditional knock-out mouse models deleting proteins involved in cell-cell adhesion and cell-matrix adhesion in the NCCs impaired OFT remodelling (Luo et al., 2006; Vallejo-Illarramendi et al., 2009). Relaxed nuclei are spherical and require external forces to become ellipsoid during morphogenetic processes (Panousopoulou and Green, 2016). We observed deformation of NCCs nuclei by the side of the endocardium. In NCCs closest to the endocardium the nuclei are elongated and parallel to the endocardial axis. This suggests that the force applied to these nuclei and to the adjacent endocardium is perpendicular to the endocardial axis. Theoretically, this is would in fact be the most efficient position of the force vector to efficiently breakdown the endocardium centrally. While NCCs converge to the endocardium they presumably apply an increasing force to the endocardium, and concomitantly the extracellular matrix has been shown to undergo transformations. In fact, it was desribed that the proteoglycan Versican go through proteolytic cleavage during OFT septation (Kern et al., 2006; Mifflin et al., 2018). Adamts metalloproteinases and notably Adamts1, are involved in the cleavage of Versican detected by the DPEAAE antibody (Mifflin et al., 2018). Interestingly, the intact and cleaved forms of Versican segregate spatially in the cushion. The cleaved form is detected in the ECM around the endocardium while the rest of the cushion mesenchyme is positive for the intact form of Versican. Authors have shown that this transformation of the ECM composition correlates with changes in mesenchymal cells condensation and shape, the region of high cellular condensation of the septum being positive for the cleaved form of Versican (Kern et al., 2006; Mifflin et al., 2018). These observations, combined with our analysis of NCCs condensation during OFT septation, point out that the proteolytic cleavage of Versican and other proteoglycans might be crucial to trigger cellular condensation and endocardium breakdown. Moreover, Adamts1 is also able to cleave Sema3c, which has been shown to facilitate its release from the ECM and to promote cancer cell migration (Esselens et al., 2010). Hence, we think that investigating the spatiotemporal expression of metalloproteinases, combined to the proteolytic state of proteoglycans and Sema3c, would be key to unravel the molecular cues driving cushions fusion and endocardium breakdown. The proteoglycan composition of the ECM could control the mechanotransduction applied

to the endocardium. For example, we could hypothesize that in *Pax3^{Cre}/Wnt1^{Cre};Dullard$^{flox/flox}$* embryos, the endocardium is unable to breakdown, and thus breaks at its attachment point to the myocardial wall, because proteoglycans of the ECM surrounding the endocardium are not properly cleaved.

Apart from interacting with endocardial cells, NCCs also dialog with the SHF progenitors that compose the OFT myocardium. The current view on the regulation of SHF addition to the OFT, is that a balance exist between FGF pharyngeal signals, which induce SHF proliferation before it ingresses in the OFT, and BMP signals, which induce SHF differentiation in the OFT (Kelly, 2012) (Figure 11, page 52). Fgf8 is considered as the major FGF ligand regulating SHF proliferation by acting on Erk intracellular signaling (Ilagan et al., 2006; Tirosh-Finkel et al., 2010). Conversely, it was shown that NCCs repress FGF signals by secreting a still unknown inhibitor of Fgf8 expression (Hutson et al., 2006). Receiving BMP signals, NCCs would thus favor pro-differentiation BMP signals by inhibiting pro-proliferation FGF signals (Tirosh-Finkel et al., 2010). Because we show that *Sema3c* expression in the NCCs is regulated by BMP signaling, we hypothesize that Sema3c is the unknown paracrine signal secreted by the NCCs that represses Fgf8 in the pharyngeal SHF. In order to test this hypothesis we could quantify in our model, where Sema3c is increased in the NCCs, the levels of phosphorylation of Erk in the SHF ingressing in the OFT. In addition, Fgf8 signals have been shown to prevent Sema3c expression in the NCCs as well as their aggregation (Kodo et al., 2017). Conversely, our results and those of Kodo *et al.* show that the expression of *Sema3c* enhances NCCs aggregation. This highlights that Fgf8 and Sema3c are two cross-repressing paracrine signals. Fgf8 is expressed in the pharyngeal region whereas Sema3c in expressed in the OFT region, which would control not only the deployment of SHF to the developing OFT but also the deployment of the NCCs.

As mentioned, *Sema3c* increase in NCCs surprisingly induced an asymmetric phenotype of septation. However, the expression of *Sema3c* in the cardiac cushions of mutant embryos appeared to be symmetrically located in between the Ao and Pa sides at levels where endocardial rupture had not yet occured. This suggests that, while controlled *Sema3c* expression in the NCCs does not lead to spatial asymmetry, increased *Sema3c* signals would trigger heterogeneous responses of some OFT progenitors, thus discriminating the Ao and Pa poles and causing the asymmetry of remodelling. It has been shown that in the OFT, the presumptive aortic and pulmonary myocardium are developmentally distinct (Bajolle et al., 2008; Bertrand et al., 2011; Théveniau-Ruissy et al., 2008). Prior to addition to the OFT, the SHF localized in the pharyngeal region are pre-patterned in discrete myocardial subdomains that respectively add to the superior and inferior wall of the outflow tract (Keyte et al., 2014). Very interestingly, Rana et al. showed that the future subpulmonary myocardium is characterized by a specific transcriptomic signature by notably expressing Sema3c (Bajolle et al., 2006; Rana et al., 2014). We observe that in the myocardial wall of control embryos, the

distal OFT presents a central differentiation of the Sema3c^{+} myocardium in between the Ao and Pa poles. In contrast, mutant distal OFT levels present an asymmetric differentiation of the Sema3c^{+} myocardium on the pulmonary side. These observations suggest that the correct septation onset at the distal OFT level requires the medial positioning of differentiating subpulmonary myocardium. Hence, Sema3c signals from the NCCs seem to control the symmetrical localization and coupling between myocardial differentiation and cushions fusion. We suppose that, at distal OFT levels, the central differentiation and contraction of the outer myocardium ensure the symmetrical start of endocardial breakdown. At more proximal levels, the overall subpulmonary and subaortic myocardium are already differentiated, and would not provide any spatial correction for an asymmetrical start of septation at the distal level.

This proposed model is informative regarding the etiology of CHDs affecting the arterial pole of the heart, as for DiGeorge syndrome. Tbx1 is the major candidate gene for DiGeorge syndrome and regulates *Sema3c* expression in the subpulmonary myocardium (Théveniau-Ruissy et al., 2008). Tbx1$^{-/-}$ mutant embryos present a missing or reduced subpulmonary contribution to the OFT, leading to failure of OFT septation and defective NCCs contribution to the OFT (Jerome and Papaioannou, 2001; Théveniau-Ruissy et al., 2008). Our results suggest that the subpulmonary myocardium is more sensitive to NCCs-derived Sema3c signals, which enable the proper onset of OFT septation. On an evolutionary perspective, Keyte *et al.* postulated that the emergence of Sema3c expression in the subpulmonary myocardium has represented a turning point in the dialogue between SHF and NCCs, by attracting NCCs to the OFT (although this hypothesis is questionned by the work of Plein *et al*.). It would have enabled the OFT septation and provided birds and mammals awith divided systemic and pulmonary circulations (Keyte et al., 2014). Our results suggest that conversely, NCCs have a favored ability to dialogue with the subpulmonary myocardium compared to the subaortic one through Sema3c, which consolidates the idea of a co-evolution between the NCCs and the pulmonary myocardium to generate a separated pulmonary circulation.

Lastly, NCCs are considered as a good system to study the neo-colonization of tissues by invading cells. After induction, NCCs delaminate from the neural tube by EMT, and quickly form streams targeting different tissues. In a similar manner, metastatic cells undergo EMT and invade tumour surrounding tissues while showing high proliferation. It is believed that a clear characterisation of NCCs induction and migration factors will help to better understand the pathogenesis of tumor invasion. Interestingly, cancer cells grafted into NCCs migration pathways follow identical trajectories and can reprogram to differentiate as NCCs do (Gallik et al., 2017). NCCs and metastatic cells are characterized by opportunistic behaviors and make use of pre-existing structures like basement membranes to spread. Both cell types interact with the environment they invade by responding to and secreting guiding cues, like Semaphorins, and metalloproteinases like Mmps and Adamts (Alfandari et al., 2001;

Christian et al., 2013; Tucker, 2004). The misexpression of these molecules in cancers is often correlated with high invasive potential and poor prognosis (Radisky and Radisky, 2010, 2015). Sema3c in particular, plays an oncogenic role in many types of cancers. It is overexpressed in 85% of glioblastoma and is an indicator of poor prognosis in glioblastoma, prostate cancer, breast cancer, liver cancer, gastric cancer, pancreatic cancer and lung cancer (Hao and Yu, 2018; Rieger et al., 2003). Surprinsingly, while in most cancer types Sema3c stimulates cancer cell invasion, it was shown in neuroblastoma to be a cohesion cue preventing cells detachment from the tumor and metastasis (Delloye-Bourgeois et al., 2017; Hao and Yu, 2018). This last phenotype is quite reminiscent of the NCCs compaction to the endocardium induced by Sema3c in the OFT. Sema3c is also characterized as an angiogenic factor although its regulatory role is incompletely understood.

In addition, BMP signaling dysregulation is linked to cancer cells invasion in many different organs. However, BMPs as well represent a double-edged sword able to act as a tumor suppressor or promoter, depending on the cancer cells type, environment and phenotypic state (Zhang et al., 2016). Therefore the OFT niche, where colonizing NCCs express Sema3c and cause intense vascular remodeling in response to BMP signals, could be a very informative system to investigate the crosstalks at play between invading cells and blood vessels remodelling. Our results suggest that BMP signaling is able to regulate Sema3c expression, which is to our knowledge the first evidences highlighting a regulatory interaction between these two pathways involved in cancer progression. It would thus be very interesting to correlate the dysregulation of BMP and Sema3c signaling in different types and models of cancers.

References

Abercrombie, M., and Dunn, G.A. (1975). Adhesions of fibroblasts to substratum during contact inhibition observed by interference reflection microscopy. Exp. Cell Res. *92*, 57–62.

Abu-Issa, R., and Kirby, M.L. (2007). Heart Field: From Mesoderm to Heart Tube. Annu. Rev. Cell Dev. Biol. *23*, 45–68.

Abu-Issa, R., Smyth, G., Smoak, I., Yamamura, K., and Meyers, E.N. (2002). Fgf8 is required for pharyngeal arch and cardiovascular development in the mouse. Development *129*, 4613–4625.

Aggarwal, V.S., Liao, J., Bondarev, A., Schimmang, T., Lewandoski, M., Locker, J., Shanske, A., Campione, M., and Morrow, B.E. (2006). Dissection of Tbx1 and Fgf interactions in mouse models of 22q11DS suggests functional redundancy. Hum. Mol. Genet. *15*, 3219–3228.

Alarcón, C., Zaromytidou, A.-I., Xi, Q., Gao, S., Yu, J., Fujisawa, S., Barlas, A., Miller, A.N., Manova-Todorova, K., Macias, M.J., et al. (2009). Nuclear CDKs Drive Smad Transcriptional Activation and Turnover in BMP and TGF-β Pathways. Cell *139*, 757–769.

Alfandari, D., Cousin, H., Gaultier, A., Smith, K., White, J.M., Darribère, T., and DeSimone, D.W. (2001). Xenopus ADAM 13 is a metalloprotease required for cranial neural crest-cell migration. Curr. Biol. CB *11*, 918–930.

Alonso, A., Sasin, J., Bottini, N., Friedberg, I., Friedberg, I., Osterman, A., Godzik, A., Hunter, T., Dixon, J., and Mustelin, T. (2004). Protein Tyrosine Phosphatases in the Human Genome. Cell *117*, 699–711.

Anderson, R.H., Mori, S., Spicer, D.E., Brown, N.A., and Mohun, T.J. (2016). Development and Morphology of the Ventricular Outflow Tracts. World J. Pediatr. Congenit. Heart Surg. *7*, 561–577.

Aragón, E., Goerner, N., Zaromytidou, A.-I., Xi, Q., Escobedo, A., Massagué, J., and Macias, M.J. (2011). A Smad action turnover switch operated by WW domain readers of a phosphoserine code. Genes Dev. *25*, 1275–1288.

Aramaki, M., Udaka, T., Kosaki, R., Makita, Y., Okamoto, N., Yoshihashi, H., Oki, H., Nanao, K., Moriyama, N., Oku, S., et al. (2006). Phenotypic spectrum of CHARGE syndrome with CHD7 mutations. J. Pediatr. *148*, 410–414.

Arima, Y., Miyagawa-Tomita, S., Maeda, K., Asai, R., Seya, D., Minoux, M., Rijli, F.M., Nishiyama, K., Kim, K.-S., Uchijima, Y., et al. (2012). Preotic neural crest cells contribute to coronary artery smooth muscle involving endothelin signalling. Nat. Commun. *3*, 1267.

Arnold, T.D., Zang, K., and Vallejo-Illarramendi, A. (2013). Deletion of integrin-linked kinase from neural crest cells in mice results in aortic aneurysms and embryonic lethality. Dis. Model. Mech. *6*, 1205–1212.

Aubin, J., Davy, A., and Soriano, P. (2004). In vivo convergence of BMP and MAPK signaling pathways: impact of differential Smad1 phosphorylation on development and homeostasis. Genes Dev. *18*, 1482–1494.

Ayer-Le Lievre, C.S., and Le Douarin, N.M. (1982). The early development of cranial sensory ganglia and the potentialities of their component cells studied in quail-chick chimeras. Dev. Biol. *94*, 291–310.

Bajolle, F., Zaffran, S., Kelly, R.G., Hadchouel, J., Bonnet, D., Brown, N.A., and Buckingham, M.E. (2006). Rotation of the Myocardial Wall of the Outflow Tract Is Implicated in the Normal Positioning of the Great Arteries. Circ. Res.

Bajolle, F., Zaffran, S., Meilhac, S.M., Dandonneau, M., Chang, T., Kelly, R.G., and Buckingham, M.E. (2008). Myocardium at the base of the aorta and pulmonary trunk is prefigured in the outflow tract of the heart and in subdomains of the second heart field. Dev. Biol. *313*, 25–34.

Baker, R.K., and Antin, P.B. (2003). Ephs and ephrins during early stages of chick embryogenesis. Dev. Dyn. *228*, 128–142.

Belle, M., Godefroy, D., Dominici, C., Heitz-Marchaland, C., Zelina, P., Hellal, F., Bradke, F., and Chédotal, A. (2014). A Simple Method for 3D Analysis of Immunolabeled Axonal Tracts in a Transparent Nervous System. Cell Rep. *9*, 1191–1201.

Bergwerff, M., Verberne, M.E., DeRuiter, M.C., Poelmann, R.E., and Gittenberger-de Groot, A.C. (1998). Neural crest cell contribution to the developing circulatory system: implications for vascular morphology? Circ. Res. *82*, 221–231.

Bertrand, N., Roux, M., Ryckebüsch, L., Niederreither, K., Dollé, P., Moon, A., Capecchi, M., and Zaffran, S. (2011). Hox genes define distinct progenitor sub-domains within the second heart field. Dev. Biol. *353*, 266–274.

Betancur, P., Bronner-Fraser, M., and Sauka-Spengler, T. (2010). Assembling Neural Crest Regulatory Circuits into a Gene Regulatory Network. Annu. Rev. Cell Dev. Biol. *26*, 581–603.

Bettex, D.A., Prêtre, R., and Chassot, P.-G. (2014). Is our heart a well-designed pump? The heart along animal evolution. Eur. Heart J. *35*, 2322–2332.

Bier, E., and Robertis, E.M.D. (2015). BMP gradients: A paradigm for morphogen-mediated developmental patterning. Science *348*, aaa5838.

Bintu, L., Yong, J., Antebi, Y.E., McCue, K., Kazuki, Y., Uno, N., Oshimura, M., and Elowitz, M.B. (2016). Dynamics of epigenetic regulation at the single-cell level. Science *351*, 720–724.

Bockman, D.E., Redmond, M.E., Waldo, K., Davis, H., and Kirby, M.L. (1987). Effect of neural crest ablation on development of the heart and arch arteries in the chick. Am. J. Anat. *180*, 332–341.

Bollenbach, T., Pantazis, P., Kicheva, A., Bökel, C., González-Gaitán, M., and Jülicher, F. (2008). Precision of the Dpp gradient. Development *135*, 1137–1146.

Bondue, A., and Blanpain, C. (2010). Mesp1: A Key Regulator of Cardiovascular Lineage Commitment. Circ. Res. *107*, 1414–1427.

Bondue, A., Lapouge, G., Paulissen, C., Semeraro, C., Iacovino, M., Kyba, M., and Blanpain, C. (2008). Mesp1 Acts as a Master Regulator of Multipotent Cardiovascular Progenitor Specification. Cell Stem Cell *3*, 69–84.

Botto, L.D., May, K., Fernhoff, P.M., Correa, A., Coleman, K., Rasmussen, S.A., Merritt, R.K., O'Leary, L.A., Wong, L.-Y., Elixson, E.M., et al. (2003). A Population-Based Study of the 22q11.2 Deletion: Phenotype, Incidence, and Contribution to Major Birth Defects in the Population. Pediatrics *112*, 101–107.

Bouman, H.G., Broekhuizen, M.L., Baasten, A.M., Gittenberger-De Groot, A.C., and Wenink, A.C. (1995). Spectrum of looping disturbances in stage 34 chicken hearts after retinoic acid treatment. Anat. Rec. *243*, 101–108.

Brickner, M.E., Hillis, L.D., and Lange, R.A. (2000). Congenital heart disease in adults. First of two parts. N. Engl. J. Med. *342*, 256–263.

Brown, C.B., Feiner, L., Lu, M.-M., Li, J., Ma, X., Webber, A.L., Jia, L., Raper, J.A., and Epstein, J.A. (2001). PlexinA2 and semaphorin signaling during cardiac neural crest development. Development *128*, 3071–3080.

Bruce, D.L., and Sapkota, G.P. (2012). Phosphatases in SMAD regulation. FEBS Lett. *586*, 1897–1905.

Bruneau, B.G., Nemer, G., Schmitt, J.P., Charron, F., Robitaille, L., Caron, S., Conner, D.A., Gessler, M., Nemer, M., Seidman, C.E., et al. (2001). A murine model of Holt-Oram syndrome defines roles of the T-box transcription factor Tbx5 in cardiogenesis and disease. Cell *106*, 709–721.

Buckingham, M., Meilhac, S., and Zaffran, S. (2005). Building the mammalian heart from two sources of myocardial cells. Nat. Rev. Genet. *6*, 826–837.

Cai, C.-L., Liang, X., Shi, Y., Chu, P.-H., Pfaff, S.L., Chen, J., and Evans, S. (2003). Isl1 Identifies a Cardiac Progenitor Population that Proliferates Prior to Differentiation and Contributes a Majority of Cells to the Heart. Dev. Cell *5*, 877–889.

Camenisch, T.D., Molin, D.G.M., Person, A., Runyan, R.B., Gittenberger-de Groot, A.C., McDonald, J.A., and Klewer, S.E. (2002). Temporal and Distinct TGFβ Ligand Requirements during Mouse and Avian Endocardial Cushion Morphogenesis. Dev. Biol. *248*, 170–181.

Campione, M., Ros, M.A., Icardo, J.M., Piedra, E., Christoffels, V.M., Schweickert, A., Blum, M., Franco, D., and Moorman, A.F.M. (2001). Pitx2 Expression Defines a Left Cardiac Lineage of Cells: Evidence for Atrial and Ventricular Molecular Isomerism in the iv/iv Mice. Dev. Biol. *231*, 252–264.

Carmichael, S.L., Shaw, G.M., Yang, W., and Lammer, E.J. (2003). Maternal periconceptional alcohol consumption and risk for conotruncal heart defects. Birt. Defects Res. A. Clin. Mol. Teratol. *67*, 875–878.

Carmona-Fontaine, C., Matthews, H.K., Kuriyama, S., Moreno, M., Dunn, G.A., Parsons, M., Stern, C.D., and Mayor, R. (2008). Contact inhibition of locomotion *in vivo* controls neural crest directional migration. Nature *456*, 957–961.

Carmona-Fontaine, C., Theveneau, E., Tzekou, A., Tada, M., Woods, M., Page, K.M., Parsons, M., Lambris, J.D., and Mayor, R. (2011). Complement Fragment C3a Controls Mutual Cell Attraction during Collective Cell Migration. Dev. Cell *21*, 1026–1037.

Chen, B., Bronson, R.T., Klaman, L.D., Hampton, T.G., Wang, J., Green, P.J., Magnuson, T., Douglas, P.S., Morgan, J.P., and Neel, B.G. (2000). Mice mutant for Egfr and Shp2 have defective cardiac semilunar valvulogenesis. Nat. Genet. *24*, 296–299.

Chen, D., Wang, X., Liang, D., Gordon, J., Mittal, A., Manley, N., Degenhardt, K., and Astrof, S. (2015). Fibronectin signals through integrin α5β1 to regulate cardiovascular development in a cell type-specific manner. Dev. Biol. *407*, 195–210.

Chen, H.B., Shen, J., Ip, Y.T., and Xu, L. (2006). Identification of phosphatases for Smad in the BMP/DPP pathway. Genes Dev. *20*, 648–653.

Chen, L., Fulcoli, F.G., Tang, S., and Baldini, A. (2009). Tbx1 Regulates Proliferation and Differentiation of Multipotent Heart Progenitors. Circ. Res. *105*, 842–851.

Chiapparo, G., Lin, X., Lescroart, F., Chabab, S., Paulissen, C., Pitisci, L., Bondue, A., and Blanpain, C. (2016). Mesp1 controls the speed, polarity, and directionality of cardiovascular progenitor migration. J Cell Biol *213*, 463–477.

Chin, A.J., Saint-Jeannet, J.-P., and Lo, C.W. (2012). How insights from cardiovascular developmental biology have impacted the care of infants and children with congenital heart disease. Mech. Dev. *129*, 75–97.

Christian, L., Bahudhanapati, H., and Wei, S. (2013). Extracellular metalloproteinases in neural crest development and craniofacial morphogenesis. Crit. Rev. Biochem. Mol. Biol. *48*, 544–560.

Christoffels, V.M., and Moorman, A.F.M. (2009). Development of the Cardiac Conduction System: Why Are Some Regions of the Heart More Arrhythmogenic Than Others? Circ. Arrhythm. Electrophysiol. *2*, 195–207.

Clay, M.R., and Halloran, M.C. (2010). Control of neural crest cell behavior and migration. Cell Adhes. Migr. *4*, 586–594.

Coles, E.G., Taneyhill, L.A., and Bronner-Fraser, M. (2007). A critical role for Cadherin6B in regulating avian neural crest emigration. Dev. Biol. *312*, 533–544.

Combs, M.D., and Yutzey, K.E. (2009). Heart Valve Development. Circ. Res. *105*, 408–421.

Copp, A.J., Greene, N.D.E., and Murdoch, J.N. (2003). The genetic basis of mammalian neurulation. Nat. Rev. Genet. *4*, 784–793.

Creuzet, S., Couly, G., Vincent, C., and Douarin, N.M.L. (2002). Negative effect of Hox gene expression on the development of the neural crest-derived facial skeleton. Development *129*, 4301–4313.

de la Cruz, M.V., Sánchez Gómez, C., Arteaga, M.M., and Argüello, C. (1977). Experimental study of the development of the truncus and the conus in the chick embryo. J. Anat. *123*, 661–686.

Danielian, P.S., Muccino, D., Rowitch, D.H., Michael, S.K., and McMahon, A.P. (1998). Modification of gene activity in mouse embryos in utero by a tamoxifen-inducible form of Cre recombinase. Curr. Biol. *8*, S1–S2.

David, R., Brenner, C., Stieber, J., Schwarz, F., Brunner, S., Vollmer, M., Mentele, E., Müller-Höcker, J., Kitajima, S., Lickert, H., et al. (2008). MesP1 drives vertebrate cardiovascular differentiation through Dkk-1-mediated blockade of Wnt-signalling. Nat. Cell Biol. *10*, 338–345.

Davidson, L.A., and Keller, R.E. (1999). Neural tube closure in Xenopus laevis involves medial migration, directed protrusive activity, cell intercalation and convergent extension. Development *126*, 4547–4556.

Davis, B.N., Hilyard, A.C., Lagna, G., and Hata, A. (2008). SMAD proteins control DROSHA-mediated microRNA maturation. Nature *454*, 56–61.

Debby-Brafman, A., Burstyn-Cohen, T., Klar, A., and Kalcheim, C. (1999). F-Spondin, Expressed in Somite Regions Avoided by Neural Crest Cells, Mediates Inhibition of Distinct Somite Domains to Neural Crest Migration. Neuron *22*, 475–488.

Delloye-Bourgeois, C., Bertin, L., Thoinet, K., Jarrosson, L., Kindbeiter, K., Buffet, T., Tauszig-Delamasure, S., Bozon, M., Marabelle, A., Combaret, V., et al. (2017). Microenvironment-Driven Shift of Cohesion/Detachment Balance within Tumors Induces a Switch toward Metastasis in Neuroblastoma. Cancer Cell *32*, 427-443.e8.

DeLong, K.T. (1962). Quantitative Analysis of Blood Circulation through the Frog Heart. Science *138*, 693–694.

Délot, E.C., Bahamonde, M.E., Zhao, M., and Lyons, K.M. (2003). BMP signaling is required for septation of the outflow tract of the mammalian heart. Development *130*, 209–220.

Devine, W.P., Wythe, J.D., George, M., Koshiba-Takeuchi, K., and Bruneau, B.G. (2014). Early patterning and specification of cardiac progenitors in gastrulating mesoderm. ELife *3*, e03848.

Dijke, P. ten, Egorova, A.D., Goumans, M.-J.T.H., Poelmann, R.E., and Hierck, B.P. (2012). TGF-β Signaling in Endothelial-to-Mesenchymal Transition: The Role of Shear Stress and Primary Cilia. Sci Signal *5*, pt2–pt2.

Diller, G.-P., Breithardt, G., and Baumgartner, H. (2011). Congenital Heart Defects in Adulthood. Dtsch. Ärztebl. Int. *108*, 452–459.

Domínguez, J.N., Meilhac, S.M., Bland, Y.S., Buckingham, M.E., and Brown, N.A. (2012). Asymmetric Fate of the Posterior Part of the Second Heart Field Results in Unexpected Left/Right Contributions to Both Poles of the HeartNovelty and Significance. Circ. Res. *111*, 1323–1335.

Douarin, N.L., and Kalcheim, C. (1999). The Neural Crest (Cambridge University Press).

Douarin, N.M.L., Creuzet, S., Couly, G., and Dupin, E. (2004). Neural crest cell plasticity and its limits. Development *131*, 4637–4650.

Duan, X., Liang, Y.-Y., Feng, X.-H., and Lin, X. (2006). Protein Serine/Threonine Phosphatase PPM1A Dephosphorylates Smad1 in the Bone Morphogenetic Protein Signaling Pathway. J. Biol. Chem. *281*, 36526–36532.

Duband, J.-L. (2010). Diversity in the molecular and cellular strategies of epithelium-to-mesenchyme transitions: Insights from the neural crest. Cell Adhes. Migr. *4*, 458–482.

Dubois, C.M., Laprise, M.H., Blanchette, F., Gentry, L.E., and Leduc, R. (1995). Processing of transforming growth factor beta 1 precursor by human furin convertase. J. Biol. Chem. *270*, 10618–10624.

Dupin, E., and Sommer, L. (2012). Neural crest progenitors and stem cells: From early development to adulthood. Dev. Biol. *366*, 83–95.

Dutt, S., Kléber, M., Matasci, M., Sommer, L., and Zimmermann, D.R. (2006). Versican V0 and V1 Guide Migratory Neural Crest Cells. J. Biol. Chem. *281*, 12123–12131.

Dyer, L.A., Makadia, F.A., Scott, A., Pegram, K., Hutson, M.R., and Kirby, M.L. (2010). BMP signaling modulates hedgehog-induced secondary heart field proliferation. Dev. Biol. *348*, 167–176.

Egorova, A.D., Heiden, K.V. der, Pas, S.V. de, Vennemann, P., Poelma, C., DeRuiter, M.C., Goumans, M.-J.T.H., Groot, A.C.G., Dijke, P. ten, Poelmann, R.E., et al. (2011). Tgfβ/Alk5 signaling is required for shear stress induced klf2 expression in embryonic endothelial cells. Dev. Dyn. *240*, 1670–1680.

Eickholt, B.J. (2008). Functional diversity and mechanisms of action of the semaphorins. Development *135*, 2689–2694.

Eisenberg, L.M., and Markwald, R.R. (1995). Molecular regulation of atrioventricular valvuloseptal morphogenesis. Circ. Res. *77*, 1–6.

Engleka, K.A., Gitler, A.D., Zhang, M., Zhou, D.D., High, F.A., and Epstein, J.A. (2005). Insertion of Cre into the Pax3 locus creates a new allele of Splotch and identifies unexpected Pax3 derivatives. Dev. Biol. *280*, 396–406.

Erickson, C.A., and Weston, J.A. (1983). An SEM analysis of neural crest migration in the mouse. Development *74*, 97–118.

Esselens, C., Malapeira, J., Colomé, N., Casal, C., Rodríguez-Manzaneque, J.C., Canals, F., and Arribas, J. (2010). The Cleavage of Semaphorin 3C Induced by ADAMTS1 Promotes Cell Migration. J. Biol. Chem. *285*, 2463–2473.

Feiner, L., Webber, A.L., Brown, C.B., Lu, M.M., Jia, L., Feinstein, P., Mombaerts, P., Epstein, J.A., and Raper, J.A. (2001). Targeted disruption of semaphorin 3C leads to persistent truncus arteriosus and aortic arch interruption. Development *128*, 3061–3070.

Foletta, V.C., Lim, M.A., Soosairajah, J., Kelly, A.P., Stanley, E.G., Shannon, M., He, W., Das, S., Massagué, J., and Bernard, O. (2003). Direct signaling by the BMP type II receptor via the cytoskeletal regulator LIMK1. J. Cell Biol. *162*, 1089–1098.

Frank, D.U., Fotheringham, L.K., Brewer, J.A., Muglia, L.J., Tristani-Firouzi, M., Capecchi, M.R., and Moon, A.M. (2002). An Fgf8 mouse mutant phenocopies human 22q11 deletion syndrome. Development *129*, 4591–4603.

Fuentealba, L.C., Eivers, E., Ikeda, A., Hurtado, C., Kuroda, H., Pera, E.M., and De Robertis, E.M. (2007). Integrating Patterning Signals: Wnt/GSK3 Regulates the Duration of the BMP/Smad1 Signal. Cell *131*, 980–993.

Fulcoli, F.G., Huynh, T., Scambler, P.J., and Baldini, A. (2009). Tbx1 Regulates the BMP-Smad1 Pathway in a Transcription Independent Manner. PLOS ONE *4*, e6049.

Galli, D., Domínguez, J.N., Zaffran, S., Munk, A., Brown, N.A., and Buckingham, M.E. (2008). Atrial myocardium derives from the posterior region of the second heart field, which acquires left-right identity as Pitx2c is expressed. Development *135*, 1157–1167.

Gallik, K.L., Treffy, R.W., Nacke, L.M., Ahsan, K., Rocha, M., Green-Saxena, A., and Saxena, A. (2017). Neural Crest and Cancer: Divergent Travelers on Similar Paths. Mech. Dev. *148*, 89–99.

Galvin, K.M., Donovan, M.J., Lynch, C.A., Meyer, R.I., Paul, R.J., Lorenz, J.N., Fairchild-Huntress, V., Dixon, K.L., Dunmore, J.H., Gimbrone, M.A., et al. (2000). A role for Smad6 in development and homeostasis of the cardiovascular system. Nat. Genet. *24*, 171–174.

Gammill, L.S., Gonzalez, C., Gu, C., and Bronner-Fraser, M. (2006). Guidance of trunk neural crest migration requires neuropilin 2/semaphorin 3F signaling. Development *133*, 99–106.

Gammill, L.S., Gonzalez, C., and Bronner-Fraser, M. (2007). Neuropilin 2/semaphorin 3F signaling is essential for cranial neural crest migration and trigeminal ganglion condensation. Dev. Neurobiol. *67*, 47–56.

Gans, C., and Northcutt, R.G. (1983). Neural Crest and the Origin of Vertebrates: A New Head. Science *220*, 268–273.

Garcia-Martinez, V., and Schoenwolf, G.C. (1993). Primitive-streak origin of the cardiovascular system in avian embryos. Dev. Biol. *159*, 706–719.

Garg, V., Yamagishi, C., Hu, T., Kathiriya, I.S., Yamagishi, H., and Srivastava, D. (2001). Tbx1, a DiGeorge Syndrome Candidate Gene, Is Regulated by Sonic Hedgehog during Pharyngeal Arch Development. Dev. Biol. *235*, 62–73.

Garrec, J.-F.L., Domínguez, J.N., Desgrange, A., Ivanovitch, K.D., Raphaël, E., Bangham, J.A., Torres, M., Coen, E., Mohun, T.J., and Meilhac, S.M. (2017). A predictive model of asymmetric morphogenesis from 3D reconstructions of mouse heart looping dynamics. ELife *6*, e28951.

Garside, V.C., Chang, A.C., Karsan, A., and Hoodless, P.A. (2013). Co-ordinating Notch, BMP, and TGFβ Signalling During Heart Valve Development. Cell. Mol. Life Sci. CMLS *70*, 2899–2917.

von Gise, A., and Pu, W.T. (2012). Endocardial and epicardial epithelial to mesenchymal transitions in heart development and disease. Circ. Res. *110*, 1628–1645.

Gitler, A.D., Lu, M.M., and Epstein, J.A. (2004). PlexinD1 and Semaphorin Signaling Are Required in Endothelial Cells for Cardiovascular Development. Dev. Cell *7*, 107–116.

Gopalakrishnan, S., Comai, G., Sambasivan, R., Francou, A., Kelly, R.G., and Tajbakhsh, S. (2015). A Cranial Mesoderm Origin for Esophagus Striated Muscles. Dev. Cell *34*, 694–704.

Grimes, A.C., Durán, A.C., Sans-Coma, V., Hami, D., Santoro, M.M., and Torres, M. (2010). Phylogeny informs ontogeny: a proposed common theme in

the arterial pole of the vertebrate heart. Evol. Dev. *12*, 552–567.

Groves, A.K., and LaBonne, C. (2014). Setting appropriate boundaries: Fate, patterning and competence at the neural plate border. Dev. Biol. *389*, 2–12.

Hall, B.K. (2000). The neural crest as a fourth germ layer and vertebrates as quadroblastic not triploblastic. Evol. Dev. *2*, 3–5.

Hao, J., and Yu, J.S. (2018). Semaphorin 3C and Its Receptors in Cancer and Cancer Stem-Like Cells. Biomedicines *6*.

Hassler, J.A., and Moran, D.J. (1986). Effects of ethanol on the cytoskeleton of migrating and differentiating neural crest cells: possible role in teratogenesis. J. Craniofac. Genet. Dev. Biol. Suppl. *2*, 129–136.

Hata, A., Lagna, G., Massagué, J., and Hemmati-Brivanlou, A. (1998). Smad6 inhibits BMP/Smad1 signaling by specifically competing with the Smad4 tumor suppressor. Genes Dev. *12*, 186–197.

Hayata, T., Ezura, Y., Yoichi, E., Asashima, M., Nishinakamura, R., and Noda, M. (2015). Dullard/Ctdnep1 regulates endochondral ossification via suppression of TGF-β signaling. J. Bone Miner. Res. Off. J. Am. Soc. Bone Miner. Res. *30*, 318–329.

Hayata, T., Chiga, M., Ezura, Y., Asashima, M., Katabuchi, H., Nishinakamura, R., and Noda, M. (2018). Dullard deficiency causes hemorrhage in the adult ovarian follicles. Genes Cells *23*, 345–356.

Helms, J.A., Cordero, D., and Tapadia, M.D. (2005). New insights into craniofacial morphogenesis. Development *132*, 851–861.

Higashihori, N., Song, Y., and Richman, J.M. (2008). Expression and regulation of the decoy bone morphogenetic protein receptor BAMBI in the developing avian face. Dev. Dyn. *237*, 1500–1508.

High, F.A., and Epstein, J.A. (2008). The multifaceted role of Notch in cardiac development and disease. Nat. Rev. Genet. *9*, 49–61.

High, F.A., Zhang, M., Proweller, A., Tu, L., Parmacek, M.S., Pear, W.S., and Epstein, J.A. (2007). An essential role for Notch in neural crest during cardiovascular development and smooth muscle differentiation. J. Clin. Invest. *117*, 353–363.

High, F.A., Jain, R., Stoller, J.Z., Antonucci, N.B., Lu, M.M., Loomes, K.M., Kaestner, K.H., Pear, W.S., and Epstein, J.A. (2009). Murine Jagged1/Notch signaling in the second heart field orchestrates Fgf8 expression and tissue-tissue interactions during outflow tract development. J. Clin. Invest. *119*, 1986–1996.

Hill, C.S. (2009). Nucleocytoplasmic shuttling of Smad proteins. Cell Res. *19*, 36–46.

van den Hoff, M.J.B., and Moorman, A.F.M. (2005). Wnt, a driver of myocardialization? Circ. Res. *96*, 274–276.

van den Hoff, M.J.B., Moorman, A.F.M., Ruijter, J.M., Lamers, W.H., Bennington, R.W., Markwald, R.R., and Wessels, A. (1999). Myocardialization of the Cardiac Outflow Tract. Dev. Biol. *212*, 477–490.

Hoffman, J.I.E. (1995). Incidence of congenital heart disease: I. Postnatal incidence. Pediatr. Cardiol. *16*, 103–113.

Hoffman, J.I.E., and Kaplan, S. (2002). The incidence of congenital heart disease. J. Am. Coll. Cardiol. *39*, 1890–1900.

Hosseini, H.S., Garcia, K.E., and Taber, L.A. (2017). A new hypothesis for foregut and heart tube formation based on differential growth and actomyosin contraction. Development *144*, 2381–2391.

Hsu, D.R., Economides, A.N., Wang, X., Eimon, P.M., and Harland, R.M. (1998). The Xenopus Dorsalizing Factor Gremlin Identifies a Novel Family of Secreted Proteins that Antagonize BMP Activities. Mol. Cell *1*, 673–683.

Huminiecki, L., Goldovsky, L., Freilich, S., Moustakas, A., Ouzounis, C., and Heldin, C.-H. (2009). Emergence, development and diversification of the TGF-β signalling pathway within the animal kingdom. BMC Evol. Biol. *9*, 28.

Hutson, M.R., and Kirby, M.L. (2007). Seminars in Cell and Developmental Biology Model Systems for the Study of Heart Development and Disease Cardiac Neural Crest and Conotruncal Malformations. Semin. Cell Dev. Biol. *18*, 101–110.

Hutson, M.R., and Kirby, M.L. (2010). Chapter 7.2 - Role of Cardiac Neural Crest in the Development of

the Caudal Pharyngeal Arches, the Cardiac Outflow and Disease. In Heart Development and Regeneration, (Boston: Academic Press), pp. 441–462.

Hutson, M.R., Zhang, P., Stadt, H.A., Sato, A.K., Li, Y.-X., Burch, J., Creazzo, T.L., and Kirby, M.L. (2006). Cardiac arterial pole alignment is sensitive to FGF8 signaling in the pharynx. Dev. Biol. *295*, 486–497.

Hutson, M.R., Zeng, X.L., Kim, A.J., Antoon, E., Harward, S., and Kirby, M.L. (2010). Arterial pole progenitors interpret opposing FGF/BMP signals to proliferate or differentiate. Development *137*, 3001–3011.

Ieda, M., Fu, J.-D., Delgado-Olguin, P., Vedantham, V., Hayashi, Y., Bruneau, B.G., and Srivastava, D. (2010). Direct reprogramming of fibroblasts into functional cardiomyocytes by defined factors. Cell *142*, 375–386.

Ilagan, R., Abu-Issa, R., Brown, D., Yang, Y.-P., Jiao, K., Schwartz, R.J., Klingensmith, J., and Meyers, E.N. (2006). Fgf8 is required for anterior heart field development. Development *133*, 2435–2445.

Ishida, W., Hamamoto, T., Kusanagi, K., Yagi, K., Kawabata, M., Takehara, K., Sampath, T.K., Kato, M., and Miyazono, K. (2000). Smad6 Is a Smad1/5-induced Smad Inhibitor CHARACTERIZATION OF BONE MORPHOGENETIC PROTEIN-RESPONSIVE ELEMENT IN THE MOUSE Smad6 PROMOTER. J. Biol. Chem. *275*, 6075–6079.

Jain, R., Engleka, K.A., Rentschler, S.L., Manderfield, L.J., Li, L., Yuan, L., and Epstein, J.A. (2011). Cardiac neural crest orchestrates remodeling and functional maturation of mouse semilunar valves. J. Clin. Invest. *121*, 422–430.

Jerome, L.A., and Papaioannou, V.E. (2001). DiGeorge syndrome phenotype in mice mutant for the T-box gene, *Tbx1*. Nat. Genet. *27*, 286–291.

Jia, Q., McDill, B.W., Li, S.-Z., Deng, C., Chang, C.-P., and Chen, F. (2007). Smad signaling in the neural crest regulates cardiac outflow tract remodeling through cell autonomous and non-cell autonomous effects. Dev. Biol. *311*, 172–184.

Jiang, X., Rowitch, D.H., Soriano, P., McMahon, A.P., and Sucov, H.M. (2000). Fate of the mammalian cardiac neural crest. Development *127*, 1607–1616.

Jiao, K., Kulessa, H., Tompkins, K., Zhou, Y., Batts, L., Baldwin, H.S., and Hogan, B.L.M. (2003). An essential role of Bmp4 in the atrioventricular septation of the mouse heart. Genes Dev. *17*, 2362–2367.

Jones, C.M., Lyons, K.M., and Hogan, B.L. (1991). Involvement of Bone Morphogenetic Protein-4 (BMP-4) and Vgr-1 in morphogenesis and neurogenesis in the mouse. Development *111*, 531–542.

Jongmans, M.C.J., Admiraal, R.J., Donk, K.P. van der, Vissers, L.E.L.M., Baas, A.F., Kapusta, L., Hagen, J.M. van, Donnai, D., Ravel, T.J. de, Veltman, J.A., et al. (2006). CHARGE syndrome: the phenotypic spectrum of mutations in the CHD7 gene. J. Med. Genet. *43*, 306–314.

Kaartinen, V., Dudas, M., Nagy, A., Sridurongrit, S., Lu, M.M., and Epstein, J.A. (2004). Cardiac outflow tract defects in mice lacking ALK2 in neural crest cells. Development *131*, 3481–3490.

Kalcheim, C., and Burstyn-Cohen, T. (2003). Early stages of neural crest ontogeny: formation and regulation of cell delamination. Int. J. Dev. Biol. *49*, 105–116.

Kelly, R.G. (2012). Chapter two - The Second Heart Field. In Current Topics in Developmental Biology, B.G. Bruneau, ed. (Academic Press), pp. 33–65.

Kelly, R.G., and Buckingham, M.E. (2002). The anterior heart-forming field: voyage to the arterial pole of the heart. Trends Genet. *18*, 210–216.

Kelly, R.G., Brown, N.A., and Buckingham, M.E. (2001). The Arterial Pole of the Mouse Heart Forms from Fgf10-Expressing Cells in Pharyngeal Mesoderm. Dev. Cell *1*, 435–440.

Kelly, R.G., Buckingham, M.E., and Moorman, A.F. (2014). Heart Fields and Cardiac Morphogenesis. Cold Spring Harb. Perspect. Med. *4*, a015750.

Kern, C.B., Twal, W.O., Mjaatvedt, C.H., Fairey, S.E., Toole, B.P., Iruela-Arispe, M.L., and Argraves, W.S. (2006). Proteolytic Cleavage of Versican During Cardiac Cushion Morphogenesis. Dev. Dyn. Off. Publ. Am. Assoc. Anat. *235*, 2238–2247.

Keyte, A., and Hutson, M.R. (2012). The Neural Crest in Cardiac Congenital Anomalies. Differ. Res. Biol. Divers. *84*, 25–40.

Keyte, A.L., Alonzo-Johnsen, M., and Hutson, M.R. (2014). Evolutionary and Developmental Origins of the Cardiac Neural Crest: Building a Divided Outflow Tract. Birth Defects Res. Part C Embryo Today Rev. *102*, 309–323.

Khudyakov, J., and Bronner-Fraser, M. (2009). Comprehensive spatiotemporal analysis of early chick neural crest network genes. Dev. Dyn. Off. Publ. Am. Assoc. Anat. *238*, 716–723.

Kim, R.Y., Robertson, E.J., and Solloway, M.J. (2001). Bmp6 and Bmp7 Are Required for Cushion Formation and Septation in the Developing Mouse Heart. Dev. Biol. *235*, 449–466.

Kim, Y., Gentry, M.S., Harris, T.E., Wiley, S.E., Lawrence, J.C., and Dixon, J.E. (2007). A conserved phosphatase cascade that regulates nuclear membrane biogenesis. Proc. Natl. Acad. Sci. *104*, 6596–6601.

Kirby, M.L. (1989). Plasticity and predetermination of mesencephalic and trunk neural crest transplanted into the region of the cardiac neural crest. Dev. Biol. *134*, 402–412.

Kirby, M.L., Gale, T.F., and Stewart, D.E. (1983). Neural crest cells contribute to normal aorticopulmonary septation. Science *220*, 1059–1061.

Kitajima, S., Takagi, A., Inoue, T., and Saga, Y. (2000). MesP1 and MesP2 are essential for the development of cardiac mesoderm. Dev. Camb. Engl. *127*, 3215–3226.

Kitajima, S., Miyagawa-Tomita, S., Inoue, T., Kanno, J., and Saga, Y. (2006). Mesp1-nonexpressing cells contribute to the ventricular cardiac conduction system. Dev. Dyn. Off. Publ. Am. Assoc. Anat. *235*, 395–402.

Kloesel, B., DiNardo, J.A., and Body, S.C. (2016). Cardiac Embryology and Molecular Mechanisms of Congenital Heart Disease – A Primer for Anesthesiologists. Anesth. Analg. *123*, 551–569.

Knockaert, M., Sapkota, G., Alarcón, C., Massagué, J., and Brivanlou, A.H. (2006). Unique players in the BMP pathway: Small C-terminal domain phosphatases dephosphorylate Smad1 to attenuate BMP signaling. Proc. Natl. Acad. Sci. *103*, 11940–11945.

Kodo, K., Nishizawa, T., Furutani, M., Arai, S., Yamamura, E., Joo, K., Takahashi, T., Matsuoka, R., and Yamagishi, H. (2009). GATA6 mutations cause human cardiac outflow tract defects by disrupting semaphorin-plexin signaling. Proc. Natl. Acad. Sci. *106*, 13933–13938.

Kodo, K., Shibata, S., Miyagawa-Tomita, S., Ong, S.-G., Takahashi, H., Kume, T., Okano, H., Matsuoka, R., and Yamagishi, H. (2017). Regulation of Sema3c and the Interaction between Cardiac Neural Crest and Second Heart Field during Outflow Tract Development. Sci. Rep. *7*.

Kokabu, S., Nojima, J., Kanomata, K., Ohte, S., Yoda, T., Fukuda, T., and Katagiri, T. (2010). Protein phosphatase magnesium-dependent 1A–mediated inhibition of BMP signaling is independent of Smad dephosphorylation. J. Bone Miner. Res. *25*, 653–660.

Komatsu, Y., Yu, P.B., Kamiya, N., Pan, H., Fukuda, T., Scott, G.J., Ray, M.K., Yamamura, K., and Mishina, Y. (2013). Augmentation of Smad-dependent BMP signaling in neural crest cells causes craniosynostosis in mice. J. Bone Miner. Res. Off. J. Am. Soc. Bone Miner. Res. *28*, 1422–1433.

Kulesa, P.M., and Fraser, S.E. (1998). Neural Crest Cell Dynamics Revealed by Time-Lapse Video Microscopy of Whole Embryo Chick Explant Cultures. Dev. Biol. *204*, 327–344.

Kuratani, S.C., and Kirby, M.L. (1992). Migration and distribution of circumpharyngeal crest cells in the chick embryo. Anat. Rec. *234*, 263–280.

Kuriyama, S., and Mayor, R. (2008). Molecular analysis of neural crest migration. Philos. Trans. R. Soc. B Biol. Sci. *363*, 1349–1362.

Kurosaka, S., and Kashina, A. (2008). Cell Biology of Embryonic Migration. Birth Defects Res. Part C Embryo Today Rev. *84*, 102–122.

de Lange, F.J., Moorman, A.F.M., Anderson, R.H., Männer, J., Soufan, A.T., Vries, C. de G., Schneider, M.D., Webb, S., van den Hoff, M.J.B., and Christoffels, V.M. (2004). Lineage and Morphogenetic Analysis of the Cardiac Valves. Circ. Res. *95*, 645–654.

Le Douarin, N.M., and Dupin, E. (2012). The neural crest in vertebrate evolution. Curr. Opin. Genet. Dev. *22*, 381–389.

Le Douarin, N.M., and Teillet, M.-A.M. (1974). Experimental analysis of the migration and

differentiation of neuroblasts of the autonomic nervous system and of neurectodermal mesenchymal derivatives, using a biological cell marking technique. Dev. Biol. *41*, 162–184.

Lee, Y.-H., and Saint-Jeannet, J.-P. (2011). Cardiac neural crest is dispensable for outflow tract septation in Xenopus. Development *138*, 2025–2034.

Lepore, J.J., Mericko, P.A., Cheng, L., Lu, M.M., Morrisey, E.E., and Parmacek, M.S. (2006). GATA-6 regulates semaphorin 3C and is required in cardiac neural crest for cardiovascular morphogenesis. J. Clin. Invest. *116*, 929–939.

Lescroart, F., Kelly, R.G., Garrec, J.-F.L., Nicolas, J.-F., Meilhac, S.M., and Buckingham, M. (2010). Clonal analysis reveals common lineage relationships between head muscles and second heart field derivatives in the mouse embryo. Development *137*, 3269–3279.

Lescroart, F., Chabab, S., Lin, X., Rulands, S., Paulissen, C., Rodolosse, A., Auer, H., Achouri, Y., Dubois, C., Bondue, A., et al. (2014). Early lineage restriction in temporally distinct populations of *Mesp1* progenitors during mammalian heart development. Nat. Cell Biol. *16*, 829–840.

Lescroart, F., Wang, X., Lin, X., Swedlund, B., Gargouri, S., Sànchez-Dànes, A., Moignard, V., Dubois, C., Paulissen, C., Kinston, S., et al. (2018). Defining the earliest step of cardiovascular lineage segregation by single-cell RNA-seq. Science *359*, 1177–1181.

Liang, X., Wang, G., Lin, L., Lowe, J., Zhang, Q., Bu, L., Chen, Y., Chen, J., Sun, Y., and Evans, S.M. (2013). HCN4 Dynamically Marks the First Heart Field and Conduction System PrecursorsNovelty and Significance. Circ. Res. *113*, 399–407.

Linask, K.K., Han, M.-D., Artman, M., and Ludwig, C.A. Sodium-calcium exchanger (NCX-1) and calcium modulation: NCX protein expression patterns and regulation of early heart development. Dev. Dyn. *221*, 249–264.

Lincoln, J., Alfieri, C.M., and Yutzey, K.E. (2004). Development of heart valve leaflets and supporting apparatus in chicken and mouse embryos. Dev. Dyn. *230*, 239–250.

Lincoln, J., Alfieri, C.M., and Yutzey, K.E. (2006). BMP and FGF regulatory pathways control cell lineage diversification of heart valve precursor cells. Dev. Biol. *292*, 290–302.

Lindsley, R.C., Gill, J.G., Kyba, M., Murphy, T.L., and Murphy, K.M. (2006). Canonical Wnt signaling is required for development of embryonic stem cell-derived mesoderm. Development *133*, 3787–3796.

Lindsley, R.C., Gill, J.G., Murphy, T.L., Langer, E.M., Cai, M., Mashayekhi, M., Wang, W., Niwa, N., Nerbonne, J.M., Kyba, M., et al. (2008). Mesp1 Coordinately Regulates Cardiovascular Fate Restriction and Epithelial-Mesenchymal Transition in Differentiating ESCs. Cell Stem Cell *3*, 55–68.

Liu, C., Liu, W., Palie, J., Lu, M.F., Brown, N.A., and Martin, J.F. (2002). Pitx2c patterns anterior myocardium and aortic arch vessels and is required for local cell movement into atrioventricular cushions. Development *129*, 5081–5091.

Liu, J.A.J., Wu, M.-H., Yan, C.H., Chau, B.K.H., So, H., Ng, A., Chan, A., Cheah, K.S.E., Briscoe, J., and Cheung, M. (2013). Phosphorylation of Sox9 is required for neural crest delamination and is regulated downstream of BMP and canonical Wnt signaling. Proc. Natl. Acad. Sci. U. S. A. *110*, 2882–2887.

Liu, W., Selever, J., Wang, D., Lu, M.-F., Moses, K.A., Schwartz, R.J., and Martin, J.F. (2004). Bmp4 signaling is required for outflow-tract septation and branchial-arch artery remodeling. Proc. Natl. Acad. Sci. U. S. A. *101*, 4489–4494.

Lomonico, M.P., Moore, G.W., and Hutchins, G.M. (1986). Rotation of the junction of the outflow tract and great arteries in the embryonic human heart. Anat. Rec. *216*, 544–549.

Luo, Y., High, F.A., Epstein, J.A., and Radice, G.L. (2006). N-cadherin is required for neural crest remodeling of the cardiac outflow tract. Dev. Biol. *299*, 517–528.

Lwigale, P.Y., Conrad, G.W., and Bronner-Fraser, M. (2004). Graded potential of neural crest to form cornea, sensory neurons and cartilage along the rostrocaudal axis. Development *131*, 1979–1991.

Ma, Q., Zhou, B., and Pu, W.T. (2008). Reassessment of Isl1 and Nkx2-5 cardiac fate maps using a Gata4-based reporter of Cre activity. Dev. Biol. *323*, 98–104.

Macatee, T.L., Hammond, B.P., Arenkiel, B.R., Francis, L., Frank, D.U., and Moon, A.M. (2003). Ablation of specific expression domains reveals discrete functions of ectoderm- and endoderm-derived FGF8 during cardiovascular and pharyngeal development. Development *130*, 6361–6374.

Macias, M.J., Martin-Malpartida, P., and Massagué, J. (2015). Structural determinants of Smad function in TGF-β signaling. Trends Biochem. Sci. *40*, 296–308.

Marguerie, A., Bajolle, F., Zaffran, S., Brown, N.A., Dickson, C., Buckingham, M.E., and Kelly, R.G. (2006). Congenital heart defects in Fgfr2-IIIb and Fgf10 mutant mice. Cardiovasc. Res. *71*, 50–60.

Martik, M.L., and Bronner, M.E. (2017). Regulatory Logic Underlying Diversification of the Neural Crest. Trends Genet. *33*, 715–727.

Martin-Puig, S., Wang, Z., and Chien, K.R. (2008). Lives of a Heart Cell: Tracing the Origins of Cardiac Progenitors. Cell Stem Cell *2*, 320–331.

Massagué, J. (2012). TGFβ signalling in context. Nat. Rev. Mol. Cell Biol. *13*, 616–630.

Massagué, J., Seoane, J., and Wotton, D. (2005). Smad transcription factors. Genes Dev. *19*, 2783–2810.

McCulley, D.J., Kang, J.-O., Martin, J.F., and Black, B.L. (2008). BMP4 is required in the anterior heart field and its derivatives for endocardial cushion remodeling, outflow tract septation, and semilunar valve development. Dev. Dyn. *237*, 3200–3209.

McLennan, R., Teddy, J.M., Kasemeier-Kulesa, J.C., Romine, M.H., and Kulesa, P.M. (2010). Vascular endothelial growth factor (VEGF) regulates cranial neural crest migration in vivo. Dev. Biol. *339*, 114–125.

Meilhac, S.M., Esner, M., Kelly, R.G., Nicolas, J.-F., and Buckingham, M.E. (2004). The Clonal Origin of Myocardial Cells in Different Regions of the Embryonic Mouse Heart. Dev. Cell *6*, 685–698.

Meilhac, S.M., Lescroart, F., Blanpain, C., and Buckingham, M.E. (2014). Cardiac Cell Lineages that Form the Heart. Cold Spring Harb. Perspect. Med. *4*, a013888.

Mellott, D.O., and Burke, R.D. (2008). Divergent roles for Eph and Ephrin in Avian Cranial Neural Crest. BMC Dev. Biol. *8*, 56.

Mesbah, K., Rana, M.S., Francou, A., van Duijvenboden, K., Papaioannou, V.E., Moorman, A.F., Kelly, R.G., and Christoffels, V.M. (2012). Identification of a Tbx1/Tbx2/Tbx3 genetic pathway governing pharyngeal and arterial pole morphogenesis. Hum. Mol. Genet. *21*, 1217–1229.

Meulemans, D., and Bronner-Fraser, M. (2004). Gene-Regulatory Interactions in Neural Crest Evolution and Development. Dev. Cell *7*, 291–299.

Mifflin, J.J., Dupuis, L.E., Alcala, N.E., Russell, L.G., and Kern, C.B. (2018). Intercalated cushion cells within the cardiac outflow tract are derived from the myocardial troponin T type 2 (Tnnt2) Cre lineage. Dev. Dyn. *247*, 1005–1017.

Milgrom-Hoffman, M., Harrelson, Z., Ferrara, N., Zelzer, E., Evans, S.M., and Tzahor, E. (2011). The heart endocardium is derived from vascular endothelial progenitors. Development *138*, 4777–4787.

Minoux, M., Antonarakis, G.S., Kmita, M., Duboule, D., and Rijli, F.M. (2009). Rostral and caudal pharyngeal arches share a common neural crest ground pattern. Development *136*, 637–645.

Mjaatvedt, C.H., Nakaoka, T., Moreno-Rodriguez, R., Norris, R.A., Kern, M.J., Eisenberg, C.A., Turner, D., and Markwald, R.R. (2001). The Outflow Tract of the Heart Is Recruited from a Novel Heart-Forming Field. Dev. Biol. *238*, 97–109.

Molin, D.G.M., Bartram, U., Van der Heiden, K., Van Iperen, L., Speer, C.P., Hierck, B.P., Poelmann, R.E., and Gittenberger-de-Groot, A.C. (2003). Expression patterns of Tgfβ1–3 associate with myocardialisation of the outflow tract and the development of the epicardium and the fibrous heart skeleton. Dev. Dyn. *227*, 431–444.

Monahan-Earley, R., Dvorak, A.M., and Aird, W.C. (2013). Evolutionary origins of the blood vascular system and endothelium. J. Thromb. Haemost. JTH *11*, 46–66.

Moon, A. (2008). Chapter 4 Mouse Models of Congenital Cardiovascular Disease. In Current Topics in Developmental Biology, (Academic Press), pp. 171–248.

Morikawa, M., Koinuma, D., Tsutsumi, S., Vasilaki, E., Kanki, Y., Heldin, C.-H., Aburatani, H., and Miyazono, K. (2011). ChIP-seq reveals cell type-specific binding patterns of BMP-specific Smads and a novel binding motif. Nucleic Acids Res. *39*, 8712–8727.

Morikawa, M., Koinuma, D., Miyazono, K., and Heldin, C.-H. (2013). Genome-wide mechanisms of Smad binding. Oncogene *32*, 1609–1615.

Muzumdar, M.D., Tasic, B., Miyamichi, K., Li, L., and Luo, L. (2007). A global double-fluorescent Cre reporter mouse. Genesis *45*, 593–605.

Nakajima, Y., Morishima, M., Nakazawa, M., and Momma, K. (1996). Inhibition of outflow cushion mesenchyme formation in retinoic acid-induced complete transposition of the great arteries. Cardiovasc. Res. *31 Spec No*, E77-85.

Nakamura, H., and Lievre, C.S.A.-L. (1982). Mesectodermal capabilities of the trunk neural crest of birds. Development *70*, 1–18.

Nakamura, T., Colbert, M.C., and Robbins, J. (2006). Neural Crest Cells Retain Multipotential Characteristics in the Developing Valves and Label the Cardiac Conduction System. Circ. Res. *98*, 1547–1554.

Nakao, A., Afrakhte, M., Morn, A., Nakayama, T., Christian, J.L., Heuchel, R., Itoh, S., Kawabata, M., Heldin, N.-E., Heldin, C.-H., et al. (1997). Identification of Smad7, a TGFβ-inducible antagonist of TGF-β signalling. Nature *389*, 631–635.

Nathan, E., Monovich, A., Tirosh-Finkel, L., Harrelson, Z., Rousso, T., Rinon, A., Harel, I., Evans, S.M., and Tzahor, E. (2008). The contribution of Islet1-expressing splanchnic mesoderm cells to distinct branchiomeric muscles reveals significant heterogeneity in head muscle development. Development *135*, 647–657.

Nichane, M., de Crozé, N., Ren, X., Souopgui, J., Monsoro-Burq, A.H., and Bellefroid, E.J. (2008). Hairy2–Id3 interactions play an essential role in Xenopus neural crest progenitor specification. Dev. Biol. *322*, 355–367.

Nomura-Kitabayashi, A., Phoon, C.K.L., Kishigami, S., Rosenthal, J., Yamauchi, Y., Abe, K., Yamamura, K., Samtani, R., Lo, C.W., and Mishina, Y. (2009). Outflow tract cushions perform a critical valve-like function in the early embryonic heart requiring BMPRIA-mediated signaling in cardiac neural crest. Am. J. Physiol. - Heart Circ. Physiol. *297*, H1617–H1628.

Oda, T., Elkahloun, A.G., Pike, B.L., Okajima, K., Krantz, I.D., Genin, A., Piccoli, D.A., Meltzer, P.S., Spinner, N.B., Collins, F.S., et al. (1997). Mutations in the human Jagged1 gene are responsible for Alagille syndrome. Nat. Genet. *16*, 235–242.

Odelin, G., Faure, E., Coulpier, F., Bonito, M.D., Bajolle, F., Studer, M., Avierinos, J.-F., Charnay, P., Topilko, P., and Zaffran, S. (2018). Krox20 defines a subpopulation of cardiac neural crest cells contributing to arterial valves and bicuspid aortic valve. Development *145*, dev151944.

Oosterveen, T., Kurdija, S., Ensterö, M., Uhde, C.W., Bergsland, M., Sandberg, M., Sandberg, R., Muhr, J., and Ericson, J. (2013). SoxB1-driven transcriptional network underlies neural-specific interpretation of morphogen signals. Proc. Natl. Acad. Sci. U. S. A. *110*, 7330–7335.

Osborne, N.J., Begbie, J., Chilton, J.K., Schmidt, H., and Eickholt, B.J. (2005). Semaphorin/neuropilin signaling influences the positioning of migratory neural crest cells within the hindbrain region of the chick. Dev. Dyn. *232*, 939–949.

Panchision, D.M., Pickel, J.M., Studer, L., Lee, S.-H., Turner, P.A., Hazel, T.G., and McKay, R.D.G. (2001). Sequential actions of BMP receptors control neural precursor cell production and fate. Genes Dev. *15*, 2094–2110.

Panousopoulou, E., and Green, J.B.A. (2016). Invagination of Ectodermal Placodes Is Driven by Cell Intercalation-Mediated Contraction of the Suprabasal Tissue Canopy. PLoS Biol. *14*.

Perchet, T., Petit, M., Banchi, E.-G., Meunier, S., Cumano, A., and Golub, R. (2018). The Notch Signaling Pathway Is Balancing Type 1 Innate Lymphoid Cell Immune Functions. Front. Immunol. *9*.

Person, A.D., Klewer, S.E., and Runyan, R.B. (2005). Cell Biology of Cardiac Cushion Development. In International Review of Cytology, (Academic Press), pp. 287–335.

Phillips, H.M., Murdoch, J.N., Chaudhry, B., Copp, A.J., and Henderson, D.J. (2005). Vangl2 Acts via RhoA Signaling to Regulate Polarized Cell Movements During Development of the Proximal Outflow Tract. Circ. Res. *96*, 292–299.

Phillips, H.M., Mahendran, P., Singh, E., Anderson, R.H., Chaudhry, B., and Henderson, D.J. (2013). Neural crest cells are required for correct positioning of the developing outflow cushions and pattern the arterial valve leaflets. Cardiovasc. Res. *99*, 452–460.

Piccolo, S., Sasai, Y., Lu, B., and De Robertis, E.M. (1996). Dorsoventral Patterning in Xenopus: Inhibition of Ventral Signals by Direct Binding of Chordin to BMP-4. Cell *86*, 589–598.

Platt, J.B. (1894). Ectodermic Origin of the Cartilages of the Head (Mass.).

Plein, A., Calmont, A., Fantin, A., Denti, L., Anderson, N.A., Scambler, P.J., and Ruhrberg, C. (2015). Neural crest–derived SEMA3C activates endothelial NRP1 for cardiac outflow tract septation. J. Clin. Invest. *125*, 2661–2676.

Plouhinec, J.-L., Zakin, L., Moriyama, Y., and De Robertis, E.M. (2013). Chordin forms a self-organizing morphogen gradient in the extracellular space between ectoderm and mesoderm in the Xenopus embryo. Proc. Natl. Acad. Sci. U. S. A. *110*, 20372–20379.

Poelmann, R.E., and Gittenberger-de Groot, A.C. (2005). Apoptosis as an instrument in cardiovascular development. Birth Defects Res. Part C Embryo Today Rev. *75*, 305–313.

Poelmann, R.E., Mikawa, T., and Groot, A.C.G.-D. (1998). Neural crest cells in outflow tract septation of the embryonic chicken heart: Differentiation and apoptosis. Dev. Dyn. *212*, 373–384.

Powell, D.R., Blasky, A.J., Britt, S.G., and Artinger, K.B. (2013). Riding the crest of the wave: parallels between the neural crest and cancer in epithelial-to-mesenchymal transition and migration. Wiley Interdiscip. Rev. Syst. Biol. Med. *5*, 511–522.

Prall, O.W.J., Menon, M.K., Solloway, M.J., Watanabe, Y., Zaffran, S., Bajolle, F., Biben, C., McBride, J.J., Robertson, B.R., Chaulet, H., et al. (2007). An Nkx2-5/Bmp2/Smad1 Negative Feedback Loop Controls Heart Progenitor Specification and Proliferation. Cell *128*, 947–959.

Radisky, E.S., and Radisky, D.C. (2010). Matrix Metalloproteinase-Induced Epithelial-Mesenchymal Transition in Breast Cancer. J. Mammary Gland Biol. Neoplasia *15*, 201–212.

Radisky, E.S., and Radisky, D.C. (2015). Matrix metalloproteinases as breast cancer drivers and therapeutic targets. Front. Biosci. Landmark Ed. *20*, 1144–1163.

Rana, M.S., Théveniau-Ruissy, M., Bono, C.D., Mesbah, K., Francou, A., Rammah, M., Domínguez, J.N., Roux, M., Laforest, B., Anderson, R.H., et al. (2014). Tbx1 Coordinates Addition of Posterior Second Heart Field Progenitor Cells to the Arterial and Venous Poles of the HeartNovelty and Significance. Circ. Res. *115*, 790–799.

Rawles, M.E. (1943). The Heart-Forming Areas of the Early Chick Blastoderm. Physiol. Zool. *16*, 22–43.

Richarte, A.M., Mead, H.B., and Tallquist, M.D. (2007). Cooperation between the PDGF receptors in cardiac neural crest cell migration. Dev. Biol. *306*, 785–796.

Rieger, J., Wick, W., and Weller, M. (2003). Human malignant glioma cells express semaphorins and their receptors, neuropilins and plexins. Glia *42*, 379–389.

Roberts, C., Ivins, S.M., James, C.T., and Scambler, P.J. (2005). Retinoic acid down-regulates Tbx1 expression in vivo and in vitro. Dev. Dyn. *232*, 928–938.

Rochais, F., Mesbah, K., and Kelly, R.G. (2009). Signaling Pathways Controlling Second Heart Field Development. Circ. Res. *104*, 933–942.

Rothstein, M., Bhattacharya, D., and Simoes-Costa, M. (2018). The molecular basis of neural crest axial identity. Dev. Biol.

Ryckebusch, L., Wang, Z., Bertrand, N., Lin, S.-C., Chi, X., Schwartz, R., Zaffran, S., and Niederreither, K. (2008). Retinoic acid deficiency alters second heart field formation. Proc. Natl. Acad. Sci. U. S. A. *105*, 2913–2918.

Saga, Y., Hata, N., Kobayashi, S., Magnuson, T., Seldin, M.F., and Taketo, M.M. (1996). MesP1: a novel basic helix-loop-helix protein expressed in the nascent mesodermal cells during mouse gastrulation. Development *122*, 2769–2778.

Saga, Y., Miyagawa-Tomita, S., Takagi, A., Kitajima, S., Miyazaki, J. i, and Inoue, T. (1999). MesP1 is expressed in the heart precursor cells and required for the formation of a single heart tube. Development *126*, 3437–3447.

Sagner, A., and Briscoe, J. (2017). Morphogen interpretation: concentration, time, competence, and signaling dynamics. Wiley Interdiscip. Rev. Dev. Biol. *6*, e271.

Sakaguchi, M., Sharmin, S., Taguchi, A., Ohmori, T., Fujimura, S., Abe, T., Kiyonari, H., Komatsu, Y., Mishina, Y., Asashima, M., et al. (2013). The phosphatase Dullard negatively regulates BMP signalling and is essential for nephron maintenance after birth. Nat. Commun. *4*, 1398.

Sanvitale, C.E., Kerr, G., Chaikuad, A., Ramel, M.-C., Mohedas, A.H., Reichert, S., Wang, Y., Triffitt, J.T., Cuny, G.D., Yu, P.B., et al. (2013). A new class of small molecule inhibitor of BMP signaling. PloS One *8*, e62721.

Sato, A., Scholl, A.M., Kuhn, E., Stadt, H.A., Decker, J.R., Pegram, K., Hutson, M.R., and Kirby, M.L. (2011). FGF8 Signaling is Chemotactic for Cardiac Neural Crest Cells. Dev. Biol. *354*, 18–30.

Satow, R., Chan, T., and Asashima, M. (2002). Molecular cloning and characterization of dullard: a novel gene required for neural development. Biochem. Biophys. Res. Commun. *295*, 85–91.

Satow, R., Kurisaki, A., Chan, T., Hamazaki, T.S., and Asashima, M. (2006). Dullard Promotes Degradation and Dephosphorylation of BMP Receptors and Is Required for Neural Induction. Dev. Cell *11*, 763–774.

Sauka-Spengler, T., and Bronner-Fraser, M. (2008). A gene regulatory network orchestrates neural crest formation. Nat. Rev. Mol. Cell Biol. *9*, nrm2428.

Scarpa, E., and Mayor, R. (2016). Collective cell migration in development. J Cell Biol *212*, 143–155.

Schindelin, J., Arganda-Carreras, I., Frise, E., Kaynig, V., Longair, M., Pietzsch, T., Preibisch, S., Rueden, C., Saalfeld, S., Schmid, B., et al. (2012). Fiji: an open-source platform for biological-image analysis. Nat. Methods *9*, 676–682.

Schleiffarth, J.R., Person, A.D., Martinsen, B.J., Sukovich, D.J., Neumann, A., Baker, C.V.H., Lohr, J.L., Cornfield, D.N., Ekker, S.C., and Petryk, A. (2007). Wnt5a Is Required for Cardiac Outflow Tract Septation in Mice. Pediatr. Res. *61*, 386–391.

Simões-Costa, M., and Bronner, M.E. (2015). Establishing neural crest identity: a gene regulatory recipe. Development *142*, 242–257.

Simoes-Costa, M., and Bronner, M.E. (2016). Reprogramming of avian neural crest axial identity and cell fate. Science *352*, 1570–1573.

Simões-Costa, M.S., Vasconcelos, M., Sampaio, A.C., Cravo, R.M., Linhares, V.L., Hochgreb, T., Yan, C.Y.I., Davidson, B., and Xavier-Neto, J. (2005). The evolutionary origin of cardiac chambers. Dev. Biol. *277*, 1–15.

Simões-Costa, M.S., McKeown, S.J., Tan-Cabugao, J., Sauka-Spengler, T., and Bronner, M.E. (2012). Dynamic and Differential Regulation of Stem Cell Factor FoxD3 in the Neural Crest Is Encrypted in the Genome. PLOS Genet. *8*, e1003142.

Sirbu, I.O., Zhao, X., and Duester, G. Retinoic acid controls heart anteroposterior patterning by down-regulating Isl1 through the Fgf8 pathway. Dev. Dyn. *237*, 1627–1635.

Smith, M.M. (1991). Putative Skeletal Neural Crest Cells in Early Late Ordovician Vertebrates from Colorado. Science *251*, 301–303.

Smith, M.M., and Hall, B.K. (1990). Development and evolutionary origins of vertebrate skeletogenic and odontogenic tissues. Biol. Rev. Camb. Philos. Soc. *65*, 277–373.

Smith, A., Robinson, V., Patel, K., and Wilkinson, D.G. (1997). The EphA4 and EphB1 receptor tyrosine kinases and ephrin-B2 ligand regulate targeted migration of branchial neural crest cells. Curr. Biol. *7*, 561–570.

Snider, P., Olaopa, M., Firulli, A.B., and Conway, S.J. (2007). Cardiovascular Development and the Colonizing Cardiac Neural Crest Lineage. Sci. World J. *7*, 1090–1113.

Šolc, D. (2007). The heart and heart conducting system in the kingdom of animals: A comparative approach to its evolution. Exp. Clin. Cardiol. *12*, 113–118.

Sorre, B., Warmflash, A., Brivanlou, A.H., and Siggia, E.D. (2014). Encoding of Temporal Signals by the TGF-β Pathway and Implications for Embryonic Patterning. Dev. Cell *30*, 334–342.

Später, D., Abramczuk, M.K., Buac, K., Zangi, L., Stachel, M.W., Clarke, J., Sahara, M., Ludwig, A.,

and Chien, K.R. (2013). A HCN4+ cardiomyogenic progenitor derived from the first heart field and human pluripotent stem cells. Nat. Cell Biol. *15*, 1098–1106.

Srivastava, D., and Olson, E.N. (2000). A genetic blueprint for cardiac development. Nature *407*, 221–226.

Stankunas, K., Ma, G.K., Kuhnert, F.J., Kuo, C.J., and Chang, C.-P. (2010). VEGF signaling has distinct spatiotemporal roles during heart valve development. Dev. Biol. *347*, 325–336.

Stolfi, A., Gainous, T.B., Young, J.J., Mori, A., Levine, M., and Christiaen, L. (2010). Early Chordate Origins of the Vertebrate Second Heart Field. Science *329*, 565–568.

Stottmann, R.W., Choi, M., Mishina, Y., Meyers, E.N., and Klingensmith, J. (2004). BMP receptor IA is required in mammalian neural crest cells for development of the cardiac outflow tract and ventricular myocardium. Dev. Camb. Engl. *131*, 2205–2218.

Sugi, Y., Yamamura, H., Okagawa, H., and Markwald, R.R. (2004). Bone morphogenetic protein-2 can mediate myocardial regulation of atrioventricular cushion mesenchymal cell formation in mice. Dev. Biol. *269*, 505–518.

Sulik, K.K., Johnston, M.C., Daft, P.A., Russell, W.E., and Dehart, D.B. (1986). Fetal alcohol syndrome and DiGeorge anomaly: critical ethanol exposure periods for craniofacial malformations as illustrated in an animal model. Am. J. Med. Genet. Suppl. *2*, 97–112.

Sun, Y., Liang, X., Najafi, N., Cass, M., Lin, L., Cai, C., Chen, J., and Evans, S. (2007). Islet 1 is Expressed in Distinct Cardiovascular Lineages, Including Pacemaker and Coronary Vascular Cells. Dev. Biol. *304*, 286–296.

Szabó, A., Melchionda, M., Nastasi, G., Woods, M.L., Campo, S., Perris, R., and Mayor, R. (2016). In vivo confinement promotes collective migration of neural crest cells. J. Cell Biol. *213*, 543–555.

Takeuchi, J.K., and Bruneau, B.G. (2009). Directed transdifferentiation of mouse mesoderm to heart tissue by defined factors. Nature *459*, 708–711.

Tam, P.P., Loebel, D.A., and Tanaka, S.S. (2006). Building the mouse gastrula: signals, asymmetry and lineages. Curr. Opin. Genet. Dev. *16*, 419–425.

Tanaka, S.S., Nakane, A., Yamaguchi, Y.L., Terabayashi, T., Abe, T., Nakao, K., Asashima, M., Steiner, K.A., Tam, P.P.L., and Nishinakamura, R. (2013). Dullard/Ctdnep1 Modulates WNT Signalling Activity for the Formation of Primordial Germ Cells in the Mouse Embryo. PLoS ONE *8*, e57428.

Tang, S., Snider, P., Firulli, A.B., and Conway, S.J. (2010). Trigenic neural crest-restricted Smad7 over-expression results in congenital craniofacial and cardiovascular defects. Dev. Biol. *344*, 233–247.

Teddy, J.M., and Kulesa, P.M. (2004). In vivo evidence for short- and long-range cell communication in cranial neural crest cells. Development *131*, 6141–6151.

Theveneau, E., and Mayor, R. (2012). Neural crest delamination and migration: From epithelium-to-mesenchyme transition to collective cell migration. Dev. Biol. *366*, 34–54.

Théveniau-Ruissy, M., Dandonneau, M., Mesbah, K., Ghez, O., Mattei, M.-G., Miquerol, L., and Kelly, R.G. (2008). The del22q11.2 Candidate Gene Tbx1 Controls Regional Outflow Tract Identity and Coronary Artery Patterning. Circ. Res. *103*, 142–148.

Tirosh-Finkel, L., Zeisel, A., Brodt-Ivenshitz, M., Shamai, A., Yao, Z., Seger, R., Domany, E., and Tzahor, E. (2010). BMP-mediated inhibition of FGF signaling promotes cardiomyocyte differentiation of anterior heart field progenitors. Development *137*, 2989–3000.

Toyofuku, T., Yoshida, J., Sugimoto, T., Yamamoto, M., Makino, N., Takamatsu, H., Takegahara, N., Suto, F., Hori, M., Fujisawa, H., et al. (2008). Repulsive and attractive semaphorins cooperate to direct the navigation of cardiac neural crest cells. Dev. Biol. *321*, 251–262.

Tozer, S., Dréau, G.L., Marti, E., and Briscoe, J. (2013). Temporal control of BMP signalling determines neuronal subtype identity in the dorsal neural tube. Development *140*, 1467–1474.

Trainor, P., and Krumlauf, R. (2000). Plasticity in mouse neural crest cells reveals a new patterning role for cranial mesoderm. Nat. Cell Biol. *2*, 96–102.

Trokovic, N., Trokovic, R., and Partanen, J. (2004). Fibroblast growth factor signalling and regional

specification of the pharyngeal ectoderm. Int. J. Dev. Biol. *49*, 797–805.

Trompouki, E., Bowman, T.V., Lawton, L.N., Fan, Z.P., Wu, D.-C., DiBiase, A., Martin, C.S., Cech, J.N., Sessa, A.K., Leblanc, J.L., et al. (2011). Lineage Regulators Direct BMP and Wnt Pathways to Cell-Specific Programs during Differentiation and Regeneration. Cell *147*, 577–589.

Tucker, R.P. (2004). Neural crest cells: a model for invasive behavior. Int. J. Biochem. Cell Biol. *36*, 173–177.

Ueno, S., Weidinger, G., Osugi, T., Kohn, A.D., Golob, J.L., Pabon, L., Reinecke, H., Moon, R.T., and Murry, C.E. (2007). Biphasic role for Wnt/β-catenin signaling in cardiac specification in zebrafish and embryonic stem cells. Proc. Natl. Acad. Sci. *104*, 9685–9690.

Urist, M.R. (1965). Bone: Formation by Autoinduction. Science *150*, 893–899.

Urrutia, H., Aleman, A., and Eivers, E. (2016). Drosophila Dullard functions as a Mad phosphatase to terminate BMP signaling. Sci. Rep. *6*, 32269.

Valdimarsdottir, G., Goumans, M.-J., Itoh, F., Itoh, S., Heldin, C.-H., and Dijke, P. ten (2006). Smad7 and protein phosphatase 1α are critical determinants in the duration of TGF-β/ALK1 signaling in endothelial cells. BMC Cell Biol. *7*, 16.

Vallejo-Illarramendi, A., Zang, K., and Reichardt, L.F. (2009). Focal adhesion kinase is required for neural crest cell morphogenesis during mouse cardiovascular development. J. Clin. Invest. *119*, 2218–2230.

Vermeren, M., Maro, G.S., Bron, R., McGonnell, I.M., Charnay, P., Topilko, P., and Cohen, J. (2003). Integrity of Developing Spinal Motor Columns Is Regulated by Neural Crest Derivatives at Motor Exit Points. Neuron *37*, 403–415.

Verzi, M.P., McCulley, D.J., De Val, S., Dodou, E., and Black, B.L. (2005). The right ventricle, outflow tract, and ventricular septum comprise a restricted expression domain within the secondary/anterior heart field. Dev. Biol. *287*, 134–145.

Virágh, S., and Challice, C.E. (1973). Origin and differentiation of cardiac muscle cells in the mouse. J. Ultrastruct. Res. *42*, 1–24.

Vitelli, F., Morishima, M., Taddei, I., Lindsay, E.A., and Baldini, A. (2002). Tbx1 mutation causes multiple cardiovascular defects and disrupts neural crest and cranial nerve migratory pathways. Hum. Mol. Genet. *11*, 915–922.

Wagner, G.P. (1990). Hall, B. K. and S. Hörstadius 1988. The Neural Crest. Oxford University Press, London, New York, Tokyo, Toronto, viii + 302 pp. J. Evol. Biol. *3*, 482–483.

Waldo, K., Miyagawa-Tomita, S., Kumiski, D., and Kirby, M.L. (1998). Cardiac Neural Crest Cells Provide New Insight into Septation of the Cardiac Outflow Tract: Aortic Sac to Ventricular Septal Closure. Dev. Biol. *196*, 129–144.

Waldo, K.L., Kumiski, D.H., Wallis, K.T., Stadt, H.A., Hutson, M.R., Platt, D.H., and Kirby, M.L. (2001). Conotruncal myocardium arises from a secondary heart field. Development *128*, 3179–3188.

Waldo, K.L., Hutson, M.R., Stadt, H.A., Zdanowicz, M., Zdanowicz, J., and Kirby, M.L. (2005). Cardiac neural crest is necessary for normal addition of the myocardium to the arterial pole from the secondary heart field. Dev. Biol. *281*, 66–77.

Wang, X., and Astrof, S. (2016). Neural crest cell-autonomous roles of fibronectin in cardiovascular development. Development *143*, 88–100.

Wang, Y.-C., and Ferguson, E.L. (2005). Spatial bistability of Dpp–receptor interactions during *Drosophila* dorsal–ventral patterning. Nature *434*, 229–234.

Wang, R.N., Green, J., Wang, Z., Deng, Y., Qiao, M., Peabody, M., Zhang, Q., Ye, J., Yan, Z., Denduluri, S., et al. (2014). Bone Morphogenetic Protein (BMP) signaling in development and human diseases. Genes Dis. *1*, 87–105.

Watanabe, Y., Miyagawa-Tomita, S., Vincent, S.D., Kelly, R.G., Moon, A.M., and Buckingham, M.E. (2010). Role of Mesodermal FGF8 and FGF10 Overlaps in the Development of the Arterial Pole of the Heart and Pharyngeal Arch Arteries. Circ. Res. *106*, 495–503.

Xavier-Neto, J., Trueba, S.S., Stolfi, A., Souza, H.M., Sobreira, T.J.P., Schubert, M., and Castillo, H.A. (2012). Chapter three - An Unauthorized Biography of the Second Heart Field and a Pioneer/Scaffold Model for Cardiac Development. In Current Topics in Developmental Biology, B.G. Bruneau, ed. (Academic Press), pp. 67–105.

Xie, L., Hoffmann, A.D., Burnicka-Turek, O., Friedland-Little, J.M., Zhang, K., and Moskowitz, I.P. (2012). Tbx5-Hedgehog Molecular Networks Are Essential in the Second Heart Field for Atrial Septation. Dev. Cell *23*, 280–291.

Xu, H., Morishima, M., Wylie, J.N., Schwartz, R.J., Bruneau, B.G., Lindsay, E.A., and Baldini, A. (2004). Tbx1 has a dual role in the morphogenesis of the cardiac outflow tract. Development *131*, 3217–3227.

Xu, M., Kirov, N., and Rushlow, C. (2005). Peak levels of BMP in the Drosophila embryo control target genes by a feed-forward mechanism. Development *132*, 1637–1647.

Yang, L., Cai, C.-L., Lin, L., Qyang, Y., Chung, C., Monteiro, R.M., Mummery, C.L., Fishman, G.I., Cogen, A., and Evans, S. (2006). Isl1Cre reveals a common Bmp pathway in heart and limb development. Development *133*, 1575–1585.

Yelin, R., Ben-Haroush Schyr, R., Kot, H., Zins, S., Frumkin, A., Pillemer, G., and Fainsod, A. (2005). Ethanol exposure affects gene expression in the embryonic organizer and reduces retinoic acid levels. Dev. Biol. *279*, 193–204.

Yokomizo, T., Yamada-Inagawa, T., Yzaguirre, A.D., Chen, M.J., Speck, N.A., and Dzierzak, E. (2012). Whole-mount three-dimensional imaging of internally localized immunostained cells within mouse embryos. Nat. Protoc. *7*, 421–431.

Yu, H.-H., and Moens, C.B. (2005). Semaphorin signaling guides cranial neural crest cell migration in zebrafish. Dev. Biol. *280*, 373–385.

Yu, J.-K., Meulemans, D., McKeown, S.J., and Bronner-Fraser, M. (2008). Insights from the amphioxus genome on the origin of vertebrate neural crest. Genome Res. *18*, 1127–1132.

Zachman, R.D., and Grummer, M.A. (1998). The Interaction of Ethanol and Vitamin A as a Potential Mechanism for the Pathogenesis of Fetal Alcohol Syndrome. Alcohol. Clin. Exp. Res. *22*, 1544–1556.

Zaffran, S., Kelly, R.G., Meilhac, S.M., Buckingham, M.E., and Brown, N.A. (2004). Right Ventricular Myocardium Derives From the Anterior Heart Field. Circ. Res. *95*, 261–268.

Zaret, K.S., and Carroll, J.S. (2011). Pioneer transcription factors: establishing competence for gene expression. Genes Dev. *25*, 2227–2241.

Zhang, J., Chang, J.Y.F., Huang, Y., Lin, X., Luo, Y., Schwartz, R.J., Martin, J.F., and Wang, F. (2010). The FGF-BMP Signaling Axis Regulates Outflow Tract Valve Primordium Formation by Promoting Cushion Neural Crest Cell DifferentiationNovelty and Significance. Circ. Res. *107*, 1209–1219.

Zhang, L., Ye, Y., Long, X., Xiao, P., Ren, X., and Yu, J. (2016). BMP signaling and its paradoxical effects in tumorigenesis and dissemination. Oncotarget *7*, 78206–78218.

Zhang, Y., Singh, M.K., Degenhardt, K.R., Lu, M.M., Bennett, J., Yoshida, Y., and Epstein, J.A. (2009). Tie2Cre-mediated inactivation of plexinD1 results in congenital heart, vascular and skeletal defects. Dev. Biol. *325*, 82–93.

Zhao, B., Etter, L., Hinton, R.B., and Benson, D.W. (2007). BMP and FGF regulatory pathways in semilunar valve precursor cells. Dev. Dyn. *236*, 971–980.

Zhou, W., Lin, L., Majumdar, A., Li, X., Zhang, X., Liu, W., Etheridge, L., Shi, Y., Martin, J., Van de Ven, W., et al. (2007). Modulation of morphogenesis by noncanonical Wnt signaling requires ATF/CREB family–mediated transcriptional activation of TGFβ2. Nat. Genet. *39*, 1225–1234.